
This item was submitted to [Loughborough's Research Repository](#) by the author.
Items in Figshare are protected by copyright, with all rights reserved, unless otherwise indicated.

Analysis and control of rotary drilling rigs

PLEASE CITE THE PUBLISHED VERSION

PUBLISHER

© Fesmi Abdul Majeed

LICENCE

CC BY-NC-ND 4.0

REPOSITORY RECORD

Majeed, Fesmi Abdul. 2019. "Analysis and Control of Rotary Drilling Rigs". figshare.
<https://hdl.handle.net/2134/12559>.

This item was submitted to Loughborough University as a PhD thesis by the author and is made available in the Institutional Repository (<https://dspace.lboro.ac.uk/>) under the following Creative Commons Licence conditions.



For the full text of this licence, please go to:
<http://creativecommons.org/licenses/by-nc-nd/2.5/>

ANALYSIS AND CONTROL OF VIBRATIONS IN ROTARY DRILLING RIGS

A Doctoral Thesis

Submitted in partial fulfillment of the requirements

for the award of

PhD of Loughborough University

©by Fesmi Abdul Majeed (2012)

CERTIFICATE OF ORIGINALITY

This is to certify that I am responsible for the work submitted in this thesis, that the original work is my own except as specified in acknowledgments or in footnotes, and that neither the thesis nor the original work contained therein has been submitted to this or any other institution for a degree.

Fesmi Abdul Majeed

..... (Signed)

.....19th April 2012..... (Date)

Table of Contents

TABLE OF CONTENTS.....	III
ABSTRACT.....	XI
ACKNOWLEDGEMENTS.....	XIII
LIST OF TABLES.....	XIV
LIST OF FIGURES.....	XV
CHAPTER 1. INTRODUCTION.....	1
1.1 Major parts of rotary drilling rig.....	2
1.2 Method of rotary drilling	4
1.3 Types of drilling rigs.....	5
1.4 Vibrations and shocks in rotary drilling.....	7
1.4.1 Shocks	8
1.4.2 Vibrations	8
CHAPTER 2. LITERATURE REVIEW-1	12

2.1 Study on drill string vibrations and their causes	12
2.1.1 Torsional vibrations:	13
2.1.2 Axial vibrations:.....	14
2.1.3 Lateral vibrations:	15
2.2 Study on the mathematical modeling of rotary drilling dynamics.....	16
2.3 Study on the unbalanced drill bit dynamics	19
2.4 Study on drill string natural frequency and resonant vibrations	22
 CHAPTER 3. LITERATURE REVIEW – 2.....	 25
3.1 Active and passive vibration minimization techniques	25
3.1.1 Torque feedback.....	25
3.1.2 Soft Torque Rotary System	26
3.1.3 PID-control.....	26
3.1.4 H_{∞} -control	27
3.1.5 Active damping technique.....	27
3.1.6 D-OSKIL.....	28
3.1.7 Smart control	28
3.2 Study on under actuated control solutions.	30
3.2.1 Case study 1:	31

3.2.2 Case study 2:	32
3.3 Control solutions proving vibration mitigation in simulations.....	35
3.4 Experimental and field tests proving vibration mitigation	37
3.5 Adaptive control technology and drill string vibration mitigation	41
 CHAPTER 4. RESEARCH METHODOLOGY	 43
4.1 Literature review inferences	43
4.2 Limitations of current research	44
4.3 Scope of the research	44
4.4 Research plan flow chart.....	45
4.4.1 Mathematical modeling and simulations.....	46
4.4.2 Experimental analysis and controller implementation	48
4.5 Chapter lay out.....	49
4.6 Research objectives	52
 CHAPTER 5. LABORATORY ARRANGEMENT AND LABVIEW™ INTERFACE PROGRAM DEVELOPMENT.....	 53
5.1 The laboratory set up configuration-1 and rotary drilling rig	54
5.2 NI LabVIEW™ program development and dynamic data acquisition.....	60

5.2.1 LabVIEW™	60
5.3 Sensors used in the laboratory set up.....	62
5.3.1 Incremental encoders.....	62
5.3.2 Three-axis vibration detection and logging using Kionix accelerometer	65
 CHAPTER 6. LABORATORY SET-UP CONFIGURATIONS AND ANALYSIS OF DYNAMICS	 69
6.1 Analysis of drill string dynamics when effected by a hard brake	69
6.1.1 Configuration 2: Hard brake implemented on laboratory set up.....	69
6.1.2 Observed dynamics: Configuration 2.....	72
6.2 Analysis of drill string dynamics in presence of borehole friction	73
6.2.1 Configuration 3: Borehole friction.....	73
6.3 Analysis of lateral vibrations & bit whirl	77
6.3.1 Configuration 4: Unbalanced Drill bit	78
6.3.2 Analysis of the nonlinear characteristics presented by laboratory set up configuration 4.	83
 CHAPTER 7. IDENTIFICATION OF MATHEMATICAL MODEL: CONFIGURATION 1	 87
7.1 System identification Method	89
7.2 Ideal drill string dynamics (Configuration 1)	91

7.3 The Black box model identification of rotary drilling process	93
7.4 Collecting useful data from the process.	93
7.5 Selecting a model structure to represent the system.....	98
7.6 Choosing the model parameters.	102
7.6.1 Derivation of least squares estimate	102
7.6.2 Model order selection.....	104
7.6.3 Residual error and residual correlation tests on model	107
7.6.4 Model Prediction tests	108
7.7 Validating the ARMAX model.	109
 CHAPTER 8. MATHEMATICAL MODEL IDENTIFICATION FOR CONFIGURATION 4	
LABORATORY SET UP.	111
8.1 Analyses of the drill string system with unbalanced drill bit	112
8.2 Identifying an ARX model	113
8.3 Identification of a Box Jenkins model.....	120
8.3.1 PZ Map Analysis for Different Model Orders	122
8.4 Model Validation Tests.....	125
8.4.1 Command signal type variation.....	125
8.4.2 Varying operational speeds	127
	VII

8.5 Model robustness analysis.....	129
8.5.1 Residual error and Model error	129
8.5.2 Modelling error	133
8.6 Validation with analytical model.....	136
8.6.1 Analytical model development and simulation.....	136
8.6.2 Single DOF model development	142
8.6.3 Single DOF Model analysis and validation	145
 CHAPTER 9. ANALYZING SOLUTIONS TO MITIGATE DRILL STRING VIBRATIONS	149
9.1 Vibrations and critical speeds.....	149
9.2 Identifying the presence of natural frequencies.....	150
9. 3 Controllability of Bit whirl.....	153
9.3.1 Conclusion on applying under actuated control laws to bend drill string dynamics.....	153
 CHAPTER 10. CONTROL METHODOLOGY AND IMPLEMENTATION.....	155
10.1 Self tuning adaptive control:.....	156
10.2 Controller development and implementation	158
10.3 Simulation of Closed loop control	161
10.4 Closing the loop - Laboratory Data synchronization using LabVIEW™	165

10.4.1 Experimental closed loop configuration 3 observations	167
10.5 Testing controller on configuration 4 laboratory set-up	171
10.6 Comparison to other experimental research.....	173
10.6.1 Conclusions of the comparative study	174
CHAPTER 11. CONCLUSIONS AND FUTURE WORK.....	176
REFERENCES.....	178
APPENDIX 1: MAJOR EQUIPMENT SPECIFICATIONS:	192
APPENDIX 2: DATA SHEETS	198
APPENDIX 3: LIST OF PUBLICATIONS	208
Selected Published Papers	210
1. Identification Of A Box Jenkins Model For Rotary Drilling Laboratory Prototype.	210
2. Modeling by System Identification of a Nonlinear rotor system with an Un Actuated end,	219
3. Nonlinearity And Spectrum Analysis Of Drill Strings With Component Mass Unbalance.	234
APPENDIX 4: LABVIEW™ VIRTUAL INSTRUMENT BLOCK DIAGRAMS.....	242

1. Data acquisition using Incremental encoder	242
2. Closed loop vibration control using adaptive controller.....	244

APPENDIX 5: THE PART OF THE MATLAB® PROGRAM USED FOR PLOTTING THE FFT SPECTRUM.	246
---	------------

APPENDIX 6: 4 DOF ANALYTICAL MODEL DEVELOPMENT AND ONLINE IDENTIFICATION METHOD OF NATURAL FREQUENCY DETECTION FOR MULTI DOF SYSTEM BY WAVELET TRANSFORMS	247
--	------------

Abstract

The objective of this research is to analyze and develop controller to minimize vibrations of the drill string in rotary drilling rigs.

The rotary drilling process is affected by many vibrations which adversely affect the drilling efficiency. The vibrations are mainly classified into three: lateral, torsional and axial. Among the vibrations, lateral vibrations are the most destructive. The research conducted a detailed analysis on lateral vibrations. Bent drill string and unbalanced drill bit was found to be its major causes; and the resultant phenomenon was known as drill bit whirl. Practical demonstration and analysis of the bit whirl phenomenon was done by conducting experiments using an unbalanced drill bit model. Their controllability issues were also discussed and practical solutions suggested. Black box identification methods were applied to develop mathematical models for the system. Box Jenkins structure model was identified and validated by a twofold procedure. Accurate simulations results were obtained with a mere 0.05% residual.

Studies revealed that the vibrations in rotary drilling were aggravated by two major causes: borehole friction and critical operation speeds. This research developed a self tuning adaptive controller which could effectively mitigate the vibration aggravating causes and improve overall drilling efficiency. On practical implementation, the controller automatically detected vibrations, mitigated the vibration aggravating causes, and resumed normal drilling operation in less than 10 seconds. The controller action was proven experimentally in two cases: (1) when affected by borehole friction and (2) in presence of an unbalanced drill bit.

All the experiments and control techniques applied in this research are validated by experimental data. The prototype used in this research is also distinguished from the rest due to a

universal joint, providing an additional two degrees of freedom. Thus, the laboratory set-up provided better dynamic analysis.

Acknowledgements

All praise and thanks to Allah, The Most Gracious, The Most Merciful, by whose favor good things are completed and perfected.

I would like to acknowledge my advisors, Prof. Mike Jackson at Loughborough University, Prof. Mansour Karkoub at Texas A&M , Qatar, Dr. Hamad Karki and Professor Youssef Abdel Magid at The Petroleum Institute, U.A.E, for their immense help, patience and guidance throughout this research.

I would like thank everybody at The Petroleum Institute who have supported me to complete my work directly and indirectly.

LIST OF TABLES

TABLE 1.1: SCHEMATIC OF DRILL BIT VIBRATIONS [SCHLUMBERGER 2011]	9
TABLE 1.2: DRILL STRING VIBRATIONS AND THEIR CONSEQUENCES; SOURCE: SPERRY DRILLING SERVICES, HALLIBURTON, DRILLING EVALUATION AND DIGITAL SOLUTION, 2007	11
TABLE 5.1: PARTS OF THE LABORATORY SET UP.....	57
TABLE 7.1: IDENTIFICATION TEST RESULTS FOR ARMAX MODEL STRUCTURE.....	106
TABLE 7.2: LEAST SQUARES BASED PARAMETER ESTIMATES FOR ARMAX MODEL	106
TABLE 8.1: IDENTIFICATION TEST RESULTS FOR ARX MODEL STRUCTURE	115
TABLE 8.2: LEAST SQUARES BASED PARAMETER ESTIMATES FOR ARX MODEL	116
TABLE 8.3: RESIDUAL TEST AND ESTIMATION CRITERIA FOR ARX AND BJ MODEL ORDERS.....	121
TABLE 8.4: LEAST SQUARES BASED PARAMETER ESTIMATES FOR SELECTED BOX JENKINS MODEL	125

LIST OF FIGURES

FIGURE 1.1: SCHEMATIC OF A ROTARY OIL RIG [HOW STUFF WORKS (2001)]	2
FIGURE 1.2: SCHEMATIC DIAGRAM OF DRILL STRING COMPONENTS AND DRILL BIT	3
FIGURE 1.3: WORLD RIG COUNT FROM 1996 TO 2012; SOURCE: BAKER-HUGHES, ENERGY, INFORMATION ADMINISTRATION (DOE), WTRG ECONOMICS.....	8
FIGURE 2.1: DRILL STRING FAILURES: (A) STEM SEPARATION AND (B) WASHOUT	13
FIGURE 2.2: DRILLING VIBRATIONS AND FREQUENCIES [MARTIN ET AL., (2005)]	23
FIGURE 3.1: SCHEMATIC OF FRONT AND SIDE PERSPECTIVE DRAWINGS OF THE PENDUBOT [JEROME D., (1991)]	31
FIGURE 3.2 (A) AND 3.2 (B): SWING UP TO THE TOP POSITION & SWING UP TO THE MID POSITION [JEROME, D., (1991)]	32
FIGURE 3.3: SCHEMATIC OF TWO DEGREE OF FREEDOM SYSTEM [W. BLAZER ET AL.(2010)].	33
FIGURE 3.4: FIELD TEST RESULTS TO SUPPRESS TORSIONAL VIBRATION. (JANSEN ET AL., 1995)	38

FIGURE 3.5: CLOSED LOOP CONTROL SCHEMATIC USING H INFINITY CONTROLLER.[A.F.A.SERRARENS (1998)]	39
FIGURE 3.6: EXPERIMENTAL OBSERVATIONS USING H-INFINITY CONTROLLER [A.F.A.SERRARENS(1998)].....	40
FIGURE 3.7: ILLUSTRATION OF ACTIVE DAMPING CAPABILITY [PAVKOVIC (2011)]......	41
FIGURE 4.1: SCHEMATIC OF RESEARCH PLAN.....	46
FIGURE 4.2: FLOW DIAGRAM OF MATHEMATICAL MODELING AND SIMULATIONS PART OF RESEARCH.	47
FIGURE 4.3: FLOW DIAGRAM DISPLAYING VARIOUS EXPERIMENTAL ANALYSIS DONE BY THE RESEARCH	48
FIGURE 5.1: LABORATORY SET UP.....	55
FIGURE 5.2: PROCESS FLOW DIAGRAM FOR OPEN LOOP DRILL STRING ANALYSIS	58
FIGURE 5.7: REVOLUTIONS TAKEN BY THE UPPER ROTARY AND DRILL BIT	62
FIGURE 5.8: STEP RESPONSE OF THE UPPER ROTARY TO COMMAND SPEED OF 26RPM.	63
FIGURE 5.11: PLOT OF COMMAND SPEED AND PROCESS RESPONSE FOR VARIOUS SPEEDS (CONFIGURATION 1).....	64

FIGURE 5.12: LABORATORY ARRANGEMENT OF THE ACCELERATION SENSOR MOUNTED ON THE INCREMENTAL ENCODER.	66
FIGURE 5.13: MOUNTING HOLDERS OF THE INCREMENTAL ENCODER.	66
FIGURE 5.14: CONFIGURATION PALETTE FOR THE 3 AXES ACCELERATION SENSOR.	67
FIGURE 5.15: DATA LOGGING PANEL OF THE 3 AXES ACCELEROMETER	68
FIGURE 6.1: APPLIED NORMAL FORCE AT THE DRILL BIT [MIHAJLOVIC ET AL., (2003)].....	70
FIGURE 6.2: SCHEMATIC OF BRAKING ARRANGEMENT.....	70
FIGURE 6.3: LABORATORY ARRANGEMENT OF IMPLEMENTING HARD BRAKE ON LOWER FLYWHEEL.....	71
FIGURE 6.4: RESULTS OF HARD BRAKE TESTS (CONFIGURATION 2).	72
FIGURE 6.5: THE CYLINDRICAL CASING LINED WITH RUBBER SPONGE.....	73
FIGURE 6.6A: CONFIGURATION 3 DRILL BIT EXPERIMENTAL RESPONSE AT 23 RPM.	74
FIGURE 6.6B: CONFIGURATION 3 DRILL BIT EXPERIMENTAL RESPONSE AT 53 RPM.	74
FIGURE 6.6C: CONFIGURATION 3 DRILL BIT EXPERIMENTAL RESPONSE AT 69 RPM.....	75
FIGURE 6.6D: CONFIGURATION 3 DRILL BIT EXPERIMENTAL RESPONSE AT 83 RPM.	75

FIGURE 6.7: LABORATORY SET-UP CONFIGURATION 4 WITH UNBALANCED MASS.	79
FIGURE 6.8A: THE COMMAND SPEEDS AND THE RESPONSES OF THE LABORATORY SET UP CONFIGURATION 4 AT LOW SPEED OF OPERATION.	81
FIGURE 6.8B: THE COMMAND SPEEDS AND THE RESPONSES OF THE LABORATORY SET UP CONFIGURATION 4 AT AVERAGE SPEED OF OPERATION.....	82
FIGURE 6.8C: THE COMMAND SPEEDS AND THE RESPONSES OF THE LABORATORY SET UP CONFIGURATION 4 AT HIGH SPEED OF OPERATION.	82
FIGURE 6.9A: COMMAND SIGNAL APPLIED TO TEST CONFIGURATION 4 LABORATORY SET-UP FOR NONLINEAR CHARACTERISTICS. (CASE 1).....	83
FIGURE 6.9B: RESIDUAL SIGNAL UNDER ZERO UNBALANCED MASS ON DRILL BIT.(CASE 1). 84	
FIGURE 6.9C: RESIDUAL SIGNAL OBTAINED WITH 2.6% UNBALANCED MASS ON DRILL BIT. (CASE 1).....	84
FIGURE 6.10A: COMMAND SIGNAL APPLIED TO TEST CONFIGURATION 4 LABORATORY SET UP FOR ANALYZING NONLINEAR CHARACTERISTICS (CASE 2).....	85
FIGURE 6.10B: RESIDUAL SIGNAL OBTAINED UNDER ZERO UNBALANCED MASS CONDITION (CASE 2).....	86
FIGURE 6.10C: RESIDUAL SIGNAL OBTAINED UNDER 2.6% UNBALANCED MASS CONDITION (CASE 2).....	86

FIGURE 8.1: SCHEMATIC OF DRILL STRING WITH UNBALANCED DRILL BIT	112
FIGURE 8.2: RAW INPUT AND OUTPUT DATA OBTAINED FROM SYSTEM(RED).	113
FIGURE 8.3: MEAN REMOVED AND DETRENDED SYSTEM INPUT AND OUTPUT DATA.	114
FIGURE 8.4: CORRELATION TEST RESULTS AND PREDICTION ERROR GRAPH FOR ARX MODEL.	117
FIGURE 8.5: ONE STEP AHEAD PREDICTED OUTPUTS AND MEASURED OUTPUT. (MSE 0.00197).....	118
FIGURE 8.6: 100 STEP AHEAD PREDICTED OUTPUTS AND MEASURED OUTPUT. (MSE 0.00810).....	118
FIGURE 8.7: CORRELATION TESTS RESULTS AND PREDICTION ERROR GRAPH FOR THE BJ MODEL.	121
FIGURE 8.8: POLE ZERO PLOT OF ARX MODEL WITH ORDERS A=3, B=2, DELAY=0.....	123
FIGURE 8.9: POLE ZERO PLOT FOR ARX MODEL WITH ORDERS A=4, B=3, DELAY =0.	123
FIGURE 8.10: POLE ZERO PLOT FOR BJ MODEL WITH ORDERS B=2, F=3, C=2, D=2, DELAY = 0.	124
FIGURE 8.11: POLE ZERO PLOT FOR BJ MODEL WITH ORDERS B= 3, F=4,C=3,D=3,DELAY =0.	124

FIGURE 8.12A: ARX AND BJ MODEL VALIDATION WITH SQUARE INPUT.	126
FIGURE 8.12B: ARX AND BJ MODEL VALIDATION WITH SINUSOIDAL INPUT.....	126
FIGURE 8.12C: ARX AND BJ MODEL VALIDATION WITH RAMP INPUT.....	127
FIGURE 8.13A: BJ MODEL VALIDATION AT LOW SPEED OPERATION.....	128
FIGURE 8.13B: BJ MODEL VALIDATION AT AVERAGE SPEED OPERATION.	128
FIGURE 8.13C: BJ MODEL VALIDATION AT HIGH SPEED OPERATION.	129
FIGURE 8.14: PROCESS RESPONSE AND MODEL RESPONSE FOR LOW DRILLING SPEED.....	130
FIGURE 8.15: PROCESS RESPONSE AND MODEL RESPONSE AT AVERAGE DRILLING SPEED.	130
FIGURE 8.16: RESIDUAL SIGNAL FOR LOW SPEED ANALYSIS.....	131
FIGURE 8.17: RESIDUAL SIGNAL FOR AVERAGE SPEED ANALYSIS.....	131
FIGURE 8.18: EXPERIMENTAL AND SIMULATED RESPONSE AT 38 RPM.....	131
FIGURE 8.19: BODE PLOT OF THE MODEL WITH LOWER (GREEN) AND UPPER (RED) BOUNDS.	132
FIGURE 8.20: FREQUENCY RESPONSE MAGNITUDE PLOT FOR SMALL MASS UNBALANCE....	135

FIGURE 8.21: FREQUENCY RESPONSE MAGNITUDE PLOT FOR LARGE MASS UNBALANCE....	135
FIGURE 8.22: SCHEMATIC OF LABORATORY ARRANGEMENT (FRONT AND SIDE PERSPECTIVES) DISPLAYING DEGREES-OF-FREEDOM.....	138
FIGURE 8.23: MATLAB® SIMULINK BLOCK DIAGRAM DEVELOPED FOR SIMULATING THE SDOF MODEL.	146
FIGURE 8.24: ANALYTICAL MODEL VALIDATION.....	147
FIGURE 8.25: COMPARING BJ MODEL AND ANALYTICAL MODEL SIMULATIONS.....	148
FIGURE 9.1: FFT SPECTRUM FOR CONFIGURATION 4 LABORATORY SET UP.	151
FIGURE 9.2: FFT SPECTRUM FOR LABORATORY SET UP CONFIGURATION 3 AND 4.....	152
FIGURE 10.1: ESTIMATED MODEL AND OPEN LOOP MODEL SIMULATIONS.	163
FIGURE 10.2: OPEN LOOP AND CLOSED SIMULATION RESULTS.	164
FIGURE 10.3: SCHEMATIC OF FLOW OF DATA DURING SYNCHRONIZATION OF THE OPERATING COMMAND SIGNAL AND ADAPTIVE CONTROL SIGNAL.	166
FIGURE 10.4: EXPERIMENTAL OPEN AND CLOSED LOOP OBSERVATIONS AT 54 RPM OPERATION.....	168

FIGURE 10.5: THREE AXES ACCELERATION DATA OF THE DRILL BIT WHIRL CONTROL IN OPEN LOOP.....	169
FIGURE 10.6: THREE AXES ACCELERATION DATA OF THE DRILL BIT WHIRL CONTROL IN CLOSED LOOP.....	169
FIGURE 10.7: EXPERIMENTAL OPEN AND CLOSED LOOP OBSERVATIONS AT 84 RPM.	170
FIGURE 10.8: DRILL BIT ANGULAR VELOCITY IN OPEN AND CLOSED LOOP CONFIGURATION 4 OPERATION.....	171
FIGURE 10.9: RESIDUAL SIGNALS IN OPEN AND CLOSED LOOP OPERATION.....	172

Chapter 1. Introduction

Rotary drilling rigs are the most common method of extracting petroleum oil and its by-products from an oil reservoir. Since the early 19th century, petroleum oil and its by-products have become an important and major source of energy. The task of finding oil is done by geologists and seismologists who survey and interpret the earth for source rocks and use satellite images to detect oil wells. An oil well is the term used for a boring through the earth's surface, designed for finding and acquiring petroleum oil hydrocarbons. The oil wells differ in depth from region to region and can vary from 1 to 12 kms.

Rotary drilling is affected by three major types of vibrations: lateral, axial and torsional. These vibrations can exist individually or coupled during drilling. They cause various nonlinear phenomena such as drill bit whirl, stick slip, bit bounce, etc., in addition to in-homogenous borehole, bent drill strings and drill bit damages. Borehole friction and critical speeds of operation are the major vibration aggravating causes leading to drilling failure. The research aims to understand, analyze and minimize the vibrations in rotary drilling rigs by applying modern control techniques.

This chapter introduces the drilling rig used to extract oil from the oil wells. The drilling rig is the apparatus placed at the site of the oil reservoir to extract oil. The following sections describe the major parts of the drilling rig, the method of rotary drilling and the vibrations associated with it.

1.1 Major parts of rotary drilling rig

Rotary drilling is the method by which oil or gas is extracted by creating a borehole in the earth's surface by rotating a drill tool called the drill bit. Figure 1.1 is a simple schematic displaying the major components of the rotary oil rig. The rig is the structure placed at the site of the reservoir consisting of various components: derrick, hoisting system, power system, etc. These components are explained below.

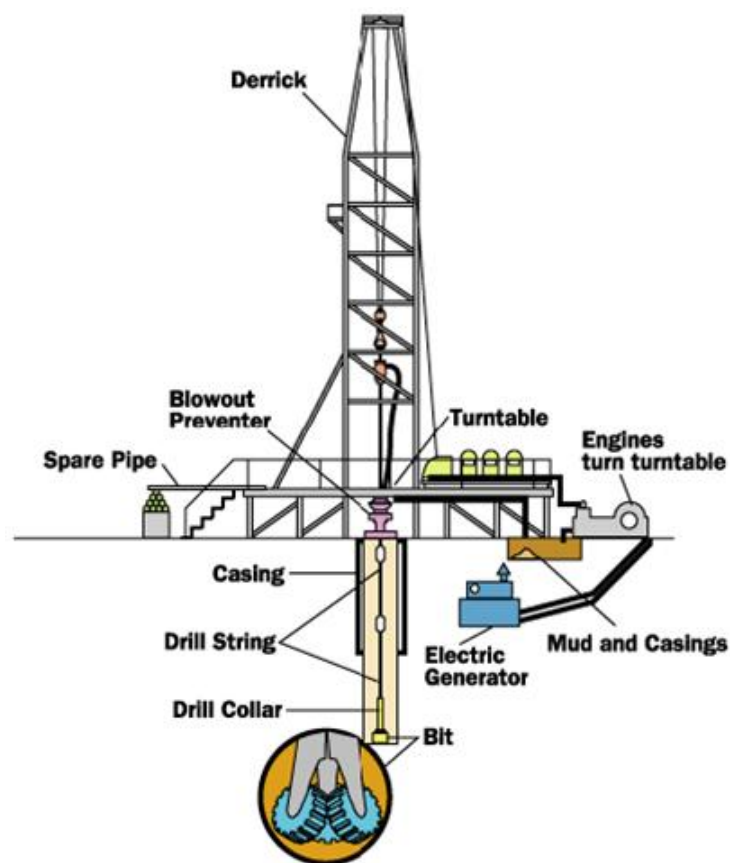


Figure 1.1: Schematic of a rotary oil rig [How Stuff Works (2001)]

Derrick: It is a tall (approximately 100 m) support structure that holds the drilling apparatus. It is classified based on the number of sections of drill pipe it can hold. Drill pipes are held by the derrick to be added to the drilling apparatus as drilling progresses.

Hoisting system: The hoisting system is attached to the derrick at the top. It consists of the tools required for lifting and lowering heavy loads and equipment into the well, and holding the drill pipes which are to be attached together as the drilling well gets deeper.

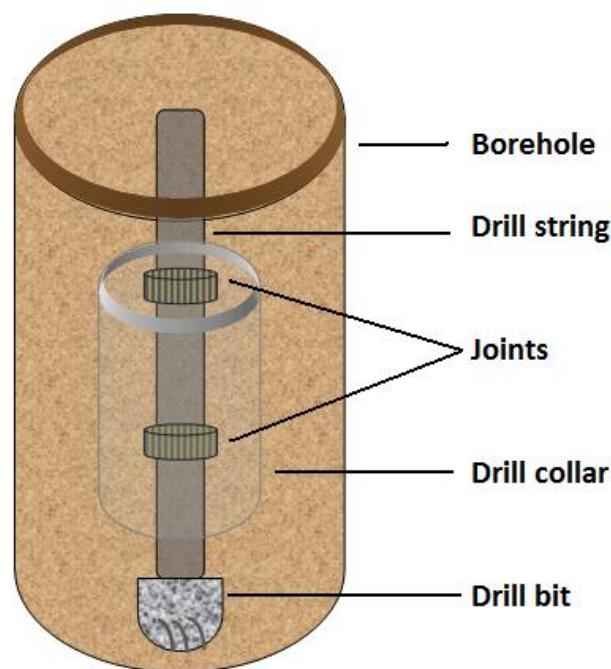


Figure 1.2: Schematic diagram of drill string components and drill bit

Rotating equipment: The rig consists of many pieces of rotating equipment. Figure 1.2 shows a schematic of the major rotating components in a rotary drilling rig. The turntable which is placed at the surface is not depicted in the schematic. The turntable is also called the rotary table. It drives the entire drill string using power from electric motors. The drill strings are attached to the turntable, and consists of drill pipes and drill collars. The drill pipes (around 30 m long sections of high grade carbon steel) are connected together by tool joints and are attached as the

drill gets deeper. The drill collars are large heavy tubular sections which fit around the drill pipe and are used for providing the weight on bit (WOB) required, ensuring the drill bit stays down and centered during the drilling process. The drill bit is attached at the end of the drill string and it is the tool which cuts the rock and drills the borehole.

Casing: It is a large diameter concrete pipe that lines the drill hole. It prevents the hole from collapsing onto the drill string.

Circulation system: It is used for pumping the drilling mud (a mixture of water, clay, weighting material, and chemicals used to lift rock cuttings from the drill bit to the surface) under pressure through the kelly, rotary table, drill pipes, and drill collars. It also serves as lubricant and coolant for the process. The circulation system consists of pumps, pipes, hoses, etc.

Power system: Usually rigs are set-up at remote places and may be isolated from sources of power. Power system consists of large diesel engines which are used to power electrical generators. These generators provide electrical power to run the entire rig.

1.2 Method of rotary drilling

In the rotary method of drilling, the hole is drilled by a rotating bit to which a downward force is applied. The bit is fastened to, and rotated by, a drill string, composed of drill pipe and drill collars. New sections or joints are added as drilling progresses. The drill bit is located at the bottom end of the drill string, and it is the part which makes contact with the subsurface layers. The drill bit is responsible for breaking up and dislodging rock, sediment, and anything else that may be encountered while drilling. As the well gets deeper, additional sections of pipe are connected at the top of the hole. The taller the derrick, the longer the sections of drill pipe that it can hold.

The whole length of pipe, or drill string, is twisted by a rotating turntable that sits on the floor of the derrick. When the drill bit is worn, or when a different type of drill bit is needed, the whole drill string must be pulled out of the hole to change the bit. Each piece of pipe is unscrewed and stacked on the derrick. When the oil-bearing formation is reached, the hole is lined with a pipe called a casing, and finally the well is completed or made ready for production.

Throughout the rotary drilling process, a stream of fluid called drilling mud is continuously forced to the bottom of the hole, through the bit, and back up to the surface. This special mud contains clay and chemicals mixed with water, lubricate the bit and keep it from getting too hot. The drilling mud also carries rock cuttings up out of the hole and clears the way for the bit. Thus it helps the drilling crew's geologists to study the rock to learn more about the formations underground. The mud also helps prevent cave-ins by shoring up the sides of the hole and functions as a coolant for the process. The next section discusses the major types of drilling rigs and their classification.

1.3 Types of drilling rigs

There are many types and designs of drilling rigs, with many drilling rigs capable of switching or combining different drilling technologies as needed. Drilling rigs can be described using any of the following attributes:

By power used

- Mechanical — the rig uses torque converters, clutches, and transmissions powered by its own engines, often diesel
- Electric — the major items of machinery are driven by electric motors, usually with power generated on-site using internal combustion engines

- Hydraulic — the rig primarily uses hydraulic power
- Pneumatic — the rig is primarily powered by pressurized air
- Steam — the rig uses steam-powered engines and pumps (obsolete after the middle of the 20th Century)

By pipe used

- Cable — a cable is used to raise and drop the drill bit
- Conventional — uses metal or plastic drill pipe of varying types
- Coil tubing — uses a giant coil of tube and a down hole drilling motor

By the drilling method

- No-rotation includes direct push rigs and most service rigs. Service rigs are equipments used for cleaning and maintenance of drilled rigs.
- Rotary table — rotation is achieved by turning a square or hexagonal pipe (known as the "Kelly") at drill floor level.
- Top drive — rotation and circulation is done at the top of the drill string, on a motor that moves in a track along the derrick.
- Sonic — uses primarily vibratory energy to advance the drill string

By position of derrick

- Conventional — derrick is vertical
- Slant — derrick is slanted at a 45 degree angle to facilitate horizontal drilling

The laboratory prototype used in this research is of a conventional rotary drilling system driven by an electric motor. The next section discusses the factors affecting an ideal rotary drilling system, namely the shocks and vibrations.

1.4 Vibrations and shocks in rotary drilling

Increase in the demand for oil and gas has lead to an increase in their production and drilling activities. Figure 1.3 displays a count of the rotary rigs. The number of rotary rigs has increased steadily now reaching near 4000. Hence efficiency of rotary drilling is a very crucial aspect affecting the oil prices. It can be observed from the figure that oil prices were very high in the 2008's, but have decreased lately and this could indicate an increase of efficiency of drilling. Poor drilling performance and drill string failures cost oil and gas companies hundreds of millions of dollars every year and became a significant factor in the rise of production costs. A major cause of poor drilling performance is drill-string vibrations and high shock loads. Significant improvements in overall drilling performance can be achieved by taking a proactive approach to the prevention or reduction of destructive down hole mechanical forces; i.e., shocks and vibrations. By definition, they are dynamic mechanical excitations that may cause a dynamic response of a physical system that is exposed to that excitation.

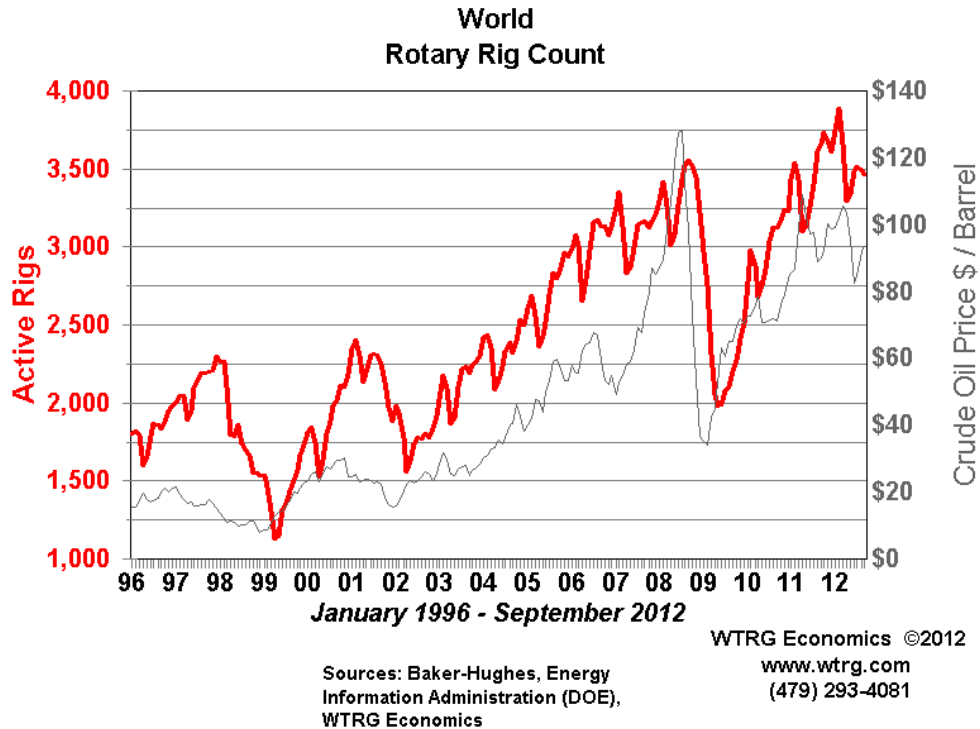


Figure 1.3: World rig count from 1996 to 2012; Source: Baker-Hughes, Energy, Information Administration (DOE), WTRG Economics.

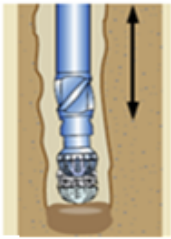
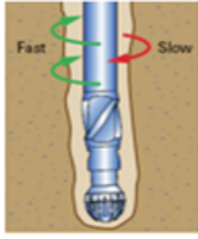
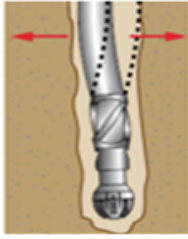
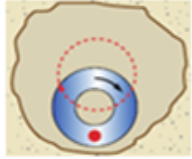
1.4.1 Shocks

Shocks are mechanical excitations over a relatively short duration. They lead to direct equipment failures. They also contribute to drill string fatigue and cause energy dissipation away from drilling. They also create tortuosity and spiraling to wellbore.

1.4.2 Vibrations

Vibrations are excitations over a relatively long duration. Vibrations in rotary drilling are mainly divided into three categories: axial, torsional and lateral. These vibrations individually produce different damages and complex phenomena destructive to the drilling process. These vibrations are briefly explained below and further detailed in chapter 2. Each of torsional, axial, lateral, or combined vibration modes are caused by a specific phenomena/mechanism.

Table 1.1: Schematic of drill bit vibrations [Schlumberger 2011]

Axial Vibration	Torsional vibration	Lateral vibration	Bit Whirl
			

Axial vibrations: Axial/longitudinal vibrations arise due to interaction between the drilling bit and the borehole is displayed in the schematic in Table 1.1. Drill strings are subjected to both static and dynamic axial loadings. Dynamic axial loads on the drilling assembly are caused by bit-formation interactions. They give rise to time-dependent fluctuations of the weight applied to the bit. Due to this, the bit bounces from the surface of the well. Bit bounce leads to damage of drill bit cutters and bearings.

Torsional vibrations: Torsional vibrations results from a difference in angular velocities of the top and bottom portion of the drill string, causing irregular rotation of the drill bit. Table 1.1 displays a simple schematic of torsional vibration. Stick slip is a common phenomenon associated with torsional vibrations in which the drill bit gets stuck in the borehole at near zero RPM and releases at very high RPM intermittently. Torsional vibrations cause damage to drill collar connections and drill bits.

Stick Slip is identified by the following characteristics:

- Drill Bit stalling
- Intermittent rotation of drill bit
- May be seen on surface as surface RPM variation or as surface torque variation

- Drill bit or the bottom hole assembly (BHA) may stop rotating.

Lateral vibrations: These are also called bending vibrations. They cause the drill string to bend or break, resulting in severe damage to the drill bit and well borehole enlargement. Table 1.1 displays a schematic of how lateral vibrations cause the drill string to bend. Lateral vibrations are the most destructive vibrations affecting the drill string in rotary drilling. Bit whirl is a popular phenomenon resulting from lateral vibrations.

BHA whirl, popularly known as ‘bit whirl’ is an eccentric motion of the drill bit, together with down-hole components in the borehole. Schematic of Bit whirl is depicted in Table 1.1. It is identified by the following characteristics:

- Large frequent shocks
- BHA hits borehole and is flung across by rotation of pipe.
- Drill bit whirl may be forward (synchronous with operational direction) or backward (in opposite direction to operation).
- Energy imparted to the drill bit during the BHA whirl is dependent on friction and restitution of borehole wall.
- Increased bending stress in the drill string.

The three types of vibrations may be coupled or occur individually. Parametric resonance, bit chatter and modal coupling are some phenomena resulting from coupled vibrations acting on the drill string. A detailed layout of the types and consequences of vibrations affecting drill strings is presented in Table 1.2.

Table 1.2: Drill string vibrations and their consequences; Source: Sperry Drilling Services, Halliburton, drilling evaluation and digital solution, 2007

Mechanism	Mode of vibration	Frequency	Consequences
Stick-slip	Torsional	0.1-5 Hz	PDC bit damage, lower ROP, back-off and drilling twist offs ...
Bit bounce	Axial	1-10 Hz	Damage to the drill bit cutting structure, bearings and seals. Hoisting equipment may be damaged in shallow wells
Bit whirl	Lateral/Torsional	10-50 Hz	Damage to the bit cutting structure. Creates ledges as the weaker rock will be enlarged to a greater diameter than the stronger rock.
BHA forward and backward whirl	Lateral/Torsional	5-20 Hz	Causes BHA and down hole tool failure. Increases fatigue rates of these components. Damages drill collar and down hole electronic.
Lateral shocks	Lateral	Irregular Impacts	Causes MWD (Measurement While Drilling) component failures (motor, MWD tool, etc.); localized tool joint and/or stabilizer wear; washout or twist offs (see Figure 2.1), increases average torque.
Torsional resonance	Torsional	20-350 Hz	Backwards turning of the bit and cutter damage; Damage to down hole electronics.
Parametric resonance	Axial/Lateral	0.1-10 Hz	Create the opportunity for borehole enlargement; Poor directional control; Whirling
Bit chatter	Lateral/Torsional	20-250 Hz	Bit cutter impact damage, Electronics failure; Bit dysfunction that can lead to bit whirl.
Modal coupling	Lateral/Torsional/ Axial	0.1-20 Hz	Causes BHA and down hole tool failure. Increases fatigue rates of these components. Damages drill collar and down hole electronic failure.

The next two chapters discuss the literature review studies conducted to derive the research objectives.

Chapter 2. Literature review- Analysis of vibrations in rotary drilling

Literature review was conducted to understand and analyze the scope of the research and to draw research objectives. Due to the wide research areas found within the field of rotary drilling, the study was categorized to ease the analysis. The observations in the major categories studied and analyzed are detailed in the following sections:

1. Drill string vibrations and their causes
2. Mathematical models of rotary drilling representing drill string dynamics.
3. The causes of bit whirl :Bend drill string and Bit imbalance
4. Drill string natural frequency and resonant vibrations
5. The drill string vibration minimizing solutions.

The literature review is followed up with a chapter on research methodology discussing sections on the scope of research, chapter lay out and Research Contributions.

2.1 Study on drill string vibrations and their causes

Drill string (made of high graded carbon steel) failure prevention has become the focus of numerous research studies in the past few decades. The nonlinear dynamics of this system are not well understood given that the drill string can undergo axial, torsional, and lateral vibrations and operational difficulties include sticking, buckling, and fatiguing of strings. There are many factors affecting the vibration of drill-strings and these include bore-hole angle, drilling fluid types, heave, bit type, bit-lithology interaction, lithology, borehole size, BHA stabilization, and back

reaming with excessively high rotational speed. Two examples of failures are shown in Figure 2.1. Stem separation is breaking of the drill string due to high torsional vibrations. Drill string washout is a hole or crack in the drill string (made of high grade carbon steel) caused by severe lateral shocks or corrosion.

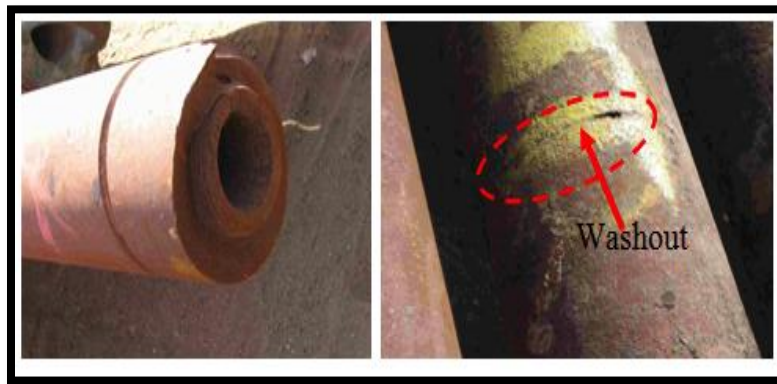


Figure 2.1: Drill string failures: (a) Stem separation and (b) Washout

2.1.1 Torsional vibrations:

Torsional vibrations are caused due to the presence of the torsion in the drill string. Torsional vibration arises when the upper rotary angular speed and position is not synchronized with the angular velocity and position of the drill bit [Dareing et al., (1997)]. The nonlinear interactions between the drill bit and the rock or the drill string with the borehole cause an increase in torsion. As the drilling progresses, the drill pipe stores torsional energy. The piling up of inertial energy within the drill pipe causes sudden backward/forward movement of the drill bit incurring damage to the drill bit, cutter, and down hole electronics. This phenomenon resulting from high torsional vibrations, is also known as torsional resonance. Torsional vibration can be classified into two categories; transient and stationary. Transient vibrations correlate with variations in drilling

conditions, for instance, heterogeneity in the rock. On the other hand, stationary vibrations are caused by the natural resonance of the drill string. This is the most common type of torsional vibration. The most recognizable manifestation of stationary torsional vibration during rotary drilling operation is stick-slip [Suleiman A.H, (2006)].

Stick slip is another reason for drill pipe damage during which the BHA sticks to the borehole. The stick-slip phenomenon is also defined as a self-excited torsional vibration induced by the nonlinear relationship between the torque and the angular velocity at the bit [Jansen et al. (1993)]. As mentioned earlier, the drill pipe stores torsional energy. During operation, when the static friction becomes higher than the dynamic friction, the stored energy in the drill pipe is converted to inertial energy in the BHA. The BHA will then accelerate at a speed faster than the steady-state rotational speed. Consequently, the drill bit revolves in the drill bore hole, sticking at the borehole wall and slipping thus causing a sudden decrease in the lower ROP (rate of penetration), stalling and damaging the drill bit [Elsayed and Dareing, (1994) and Leine et al.,(2002)]. Discussions on the field investigation of the effects of stick slip lateral and whirl vibrations was made by Chen et al., (2002). They tested the effect of these vibrations on roller cone drill bit performance. Juloski et al. (2006) and Mihjlovic et al., (2004) used laboratory set-ups to investigate stick slip phenomenon by applying nonlinear control methods to control or suppress the vibrations.

2.1.2 Axial vibrations:

Axial/longitudinal vibrations arise due to interactions between the drilling bit and borehole [Melakhessou et al., (2003) and Theron et al., (2001)]. These interactions are also known as precession. Precession limits the performance of drilling and often endangers the safety of the

operation. Drill strings are subjected to both static and dynamic axial loadings. Dynamic axial loads on the drilling assembly are caused by bit-formation interactions. They give rise to time-dependent fluctuations of the weight applied to the bit. Bit bounce is the common phenomenon resulting from axial vibrations. It causes damage to the drill bit cutting structure, bearings, and seals.

2.1.3 Lateral vibrations:

Bending/ lateral vibration occurs due to pipe eccentricity; it is also known as drill string whirl (particularly forward and backward whirl) [R.I. Liene et al., (2002)]. Bit whirl leads to ledges in the bore hole as the soft rocks will be enlarged to a greater diameter than the hard rocks. It is the most destructive drill string vibration because there may be no indication at the surface. Moreover, the collisions with the borehole wall and the shocks generated can damage components of the BHA. Lateral vibrations have higher frequencies than their torsional counterpart and are more difficult to predict or anticipate based solely on surface measurements. Lateral shocks leading to washouts (Figure 2.1) and parametric resonance causing borehole enlargement are common phenomena associated with lateral vibration.

The coupling of axial and lateral vibrations result in two types of bending: linear and parametric coupling. Parametric coupling between axial forces in the drill string and bending vibrations is discussed in Duneyevsky et al., (1993). Linear coupling is easily visualized and does not occur in any perfectly straight beam with axial loads. The main source of linear coupling is the initial curvature of the BHA. Modal coupling is another effect of the three major vibrations resulting in BHA and down hole tool failure. A detailed study of drill collar whirling and the

linear coupling between the weight on bit fluctuations and bending vibration of an initially curved BHA are discussed in Liene et al., (2002), Vandiver et al., (1990) and Berlioz et al., (1996).

The lateral vibrations are the most destructive form of vibrations, and drill bit whirl is the most drill pipe damaging phenomena associated with it. Hence, this research simulates, analyzes and applies modern control technology to understand bit whirl dynamics and stabilize the drill bit.

2.2 Study on the mathematical modeling of rotary drilling dynamics

Drill string dynamics is affected by various vibrations as discussed in the last section. Hence to develop a well defined mathematical model which captures all the dynamics is complex and challenging. However, it is necessary as it provides a thorough understanding of the drill string behavior. Many researchers have used laboratory prototypes and mathematical models to analyze the dynamics and vibrations affecting the drill strings during rotary drilling [Dykstra et al., (1996); Leine et al., (2002); Melakhessou et al., (2003); Mihajlovic et al.,(2004a,2004b); Navarro and Suarez, (2004); Liao et al., (2008); Germy et al., (2009)]. The vibrations are also required to be modeled to analyze and understand the important and severe phenomena like stick-slip, bit bounce, and drill bit whirl experienced in the drilling process. Various modeling techniques were applied to develop models to analyze drill string vibrations including lateral vibrations (whirl) and mode coupling [Elsayed and Dareing, (1994); Christoforou and Yigit, (1997); Leine et al., (2002); Mihajlovic et al., (2004); Liao et al., (2010)].

Some of the recent modeling approaches in drill string dynamics modeling are discussed briefly here. Detailed discussion is presented in Chapter 7. Navarro Lopez and Suarez, (2004) modeled the drill string torsional behavior using analytical modeling principles and state space

representations. They used a lumped parameter differential equation based models to model the drill string as a two degrees of freedom (DOF) torsional pendulum. Mihajlovic et al., (2004) used experimental prototypes to analyze stick-slip vibrations and limit cycling. They have used analytical modeling from first principles and then used parameter estimation to estimate the drill string model coefficients and separate friction model for the well borehole friction. The nonlinear properties are analyzed using bifurcation diagrams (plot of trajectory of drill bit) and a constant brake is applied to the set-up. However the type of model obtained or the procedures of model selection are not discussed. It is also interesting to note that they have operated the setup at very low velocities. Elsayed, (2007) presents a method of modeling drill strings by using the frequency response and stability diagrams to validate the developed model. A model based on a servo hydraulic controller is used for the simulation of drill bit dynamics in Raymond et al., (2008). Liao et al., (2008) have developed drill string mass with an unbalanced mass experimental set-up, and have developed reduced order models from analytical principles.

Silveira and Wiercigroch, (2009) presented low dimensional non linear models of the BHA. Torsional 3 DOF models were developed using friction models (Coulomb friction law) and 3 DOF torsional pendulum models developed using analytical equations. Simulation results of the model are also presented using bifurcation diagrams. Germay et al., (2009) have also used lumped parameter model to represent the drill string. Their contribution is a new approach to modeling the stick slip phenomenon as a result of axial and torsional vibration coupling.

Researchers have also used experimental prototypes of the oil rig to simulate torsional/lateral vibrations and have suggested methods to avoid stick-slip behavior [Germay et al., (2009) and Mihajlovic et al., (2004)]. Mihajlovic et al., (2004) used experimental prototypes to analyze stick-slip vibrations and limit cycling. This research has used a similar experimental prototype.

However, there are some major differences between the prototypes used. The prototype used for this research stands out due to the presence of a universal joint connecting the drill string to the upper rotary disk. The joint provides an additional 2 degrees of freedom movement to the drill string and the lower rotating components. Hence, the set-up is more similar in dynamics and degrees of freedom to the actual drilling process. This research also analyzes the drill string dynamics using an unbalanced mass model for the drill bit (detailed in section 6.1)

To facilitate research, the important features of the oil rig are incorporated in a laboratory prototype. A mathematical model is identified using the Black box identification method. The Least Squares method of parameter estimation is also applied to ensure the uniqueness of the model coefficient estimates and the non biased nature of the estimates. A good model estimate will help to design better controllers to control the vibrations, buckling, and fatigue of the drill string. This will in turn increase the efficiency and lifetime of the drill string and BHA, which is one of the most sought after solutions in the drilling field.

2.3 Study on the unbalanced drill bit dynamics

Bit whirl Causes

Bit whirl is a common phenomenon in the rotary drilling industry with few solutions. Lateral vibrations of the drill bit are the major cause of bit whirl. Bit whirl is an important cause of reducing drilling efficiency and it causes drill pipe bending and well bore hole enlargement.

Leine et al., (2002) suggests that the lateral or bending vibrations are caused by pipe eccentricity leading to centripetal forces during rotation causing bit whirl. They also suggest the fluid forces down hole could cause the vibrations. They have analyzed the stick slip and bit whirl phenomenon using a low dimensional model with lateral and torsional degrees of freedom in a fluid. They observed that whirl and stick slip occur in a particular angular velocity range but they do not co exist. The transition from stick-slip to whirl is presumably caused by an interaction between bending and torsion which destabilizes the concentric position of the drill string for high values of angular velocity of rotation of the drill bit. Possible ways of interaction can be caused by drill string eccentricity, gyroscopic effects or fluid mud forces. No control methods are suggested.

Thomas J. Warren, (1990) explained that a high graded commercial bit will have a minimal 2% imbalance while a 10% imbalance is more typical. During rotary drilling, the imbalance of the bit or an inhomogeneous hole will cause the bit to stray away from its center of rotation. This will lead to the development of high centrifugal force which increases the side loading of the bit. This in turn, causes hole enlargement and bit whirling. The paper also describes efforts to control bit whirl by drill string stabilization as unsuccessful and suggests low friction bit models be used to eliminate whirl. The trend in research is also to eliminate the whirling by designing new drill bit models.

Brett et al., (1990) demonstrated that bit-whirl is the major cause of impact loading. They also presented that bit whirl increases at high rotational speeds while stick slip is noticed at lower ranges of angular velocity.

Martin E. Cobern & Mark E. Wassell, (2005) discussed an active vibration damper to minimize the vibrations caused by bit whirl and bit bounce. They proved during laboratory tests that the damper was capable of providing variable damping required to control bit bounce and maintain uniform WOB (weight –on-bit).

H. Santos et al., (1999) presented two interesting historical cases showing a relationship between drill string vibration and wellbore enlargement. Drilling bits perform their duty either by crushing the rock through a number of successive percussions, or by shearing the rock. In both cases, only part of the energy provided by the rotary table or top drive is used in this process. Another part is reflected to the drill string in the form of vibrations, which can reach the surface. Friction and viscous forces dissipate the remaining part. Drill string kinetic energy due to dynamic behavior can be dissipated either by heat or by impact against the wellbore wall. This last form is responsible for the greatest amount of damage suffered by the wall.

Due to lateral vibrations being the most destructive vibrations affecting the drill string, the experimental prototype was configured to analyze the effects of drill bit whirling. Drill bit whirling is popularly known as ‘bit whirl’ and is the most prominent display of the presence of lateral vibrations. Literature review proved drill bit imbalance as the major cause of bit whirl. Hence, an unbalanced mass is added to the disc representing the drill bit in the laboratory set-up.

The unbalanced mass model was first proposed by Jansen, (1991) where self excited vibrations were studied. Similar models were also studied by other researchers; for example, Melakhessou et

al., (2003) modeled the drill string as an unbalanced rotor supported by two bearings and research was concentrated on a contact zone between the drill string and the borehole wall. Dykstra et al., (1996) explained that the source of vibration is the bit and hence the centrifugal forces developed when an unbalanced drill string is rotated can be one of the major sources of vibrations. The tests were focused on drill collars and studies on lateral shocks and backward whirl were analyzed. Liao et al., (2008) developed a reduced order model for a drill string system with a mass imbalance on the rotor. The trajectory of the bit for various mass and angular velocities was determined displaying bit whirl and stick slip characteristics.

The research has been able to demonstrate bit whirl and analyze the vibrations associated with it. Further analysis results are discussed in chapter 6.

2.4 Study on drill string natural frequency and resonant vibrations

This study analyzes some important research work into the causes of high vibrations affecting the drill strings.

Dareing, (1984) found that the drill collar length plays a key role in the BHA vibration problem. Their research used equations for the vibrating bars and shafts for deriving the relation between the natural frequency of vibration and the critical speeds of operation with the length of the drill collars. The tests proved a directly proportional relationship and it was also noted that the axial and torsional vibration modes can be excited separately. Dareing's research proved that it is imperative that the drill collar resonance critical speeds should be known and identified well before to avoid the heavy damage due to large vibrations. They suggested shock absorbers and increasing the drill collar length to minimize the effect of vibrations.

Vibrations in rotary drilling are enhanced when operated near one of the system resonance frequencies, causing a fast destruction of drill string elements. H. Santos et al., (1999) found that operation at critical speeds caused destructive harmonics generating high stresses, reaching 8×10^4 psi and drastically shortening the fatigue life. According to these authors, a great percentage of fatigue failures are related to harmonic lateral vibrations. Drill string vibrations have been studied mainly with the objective of reducing drill pipe fatigue failure. Several vibration analysis models have been developed considering drill string composition, weight on bit, wellbore diameter, distances from the bit, well geometry, and drilling fluid properties [M.W. Dykstra et al., (1995), A.A. Besaisaw et al., (1988), B.S. Aadnoy, (1986), T.V. Aarrestad, (1989)]. These models estimate drill string stresses and lateral displacements as well as vibration critical frequencies. These works suggest that drill string rotational speeds, which generate resonance, ought to be avoided. Lateral displacements larger than 0.025 m have also been estimated by the modeling of

mass unbalanced effects on bottom hole vibrations and have been confirmed by experiments. It can be noticed from Figure 2.2, that the majority of vibrations during drilling occurs in the range of 1 Hz and 10 Hz. This project analyzes Bit whirl dynamics due to it being the most destructive (refer section 2.1.3). It can be noticed from the Figure 2.2, that the most probable frequency range of these vibrations is 1 Hz to 10 Hz, out of which only Backward whirl can be expected. The natural frequencies of the drill string also fall in this frequency range and depend on the BHA and length of the drill string [Martin E. Cobern & Mark E. Wassell, (2005)].

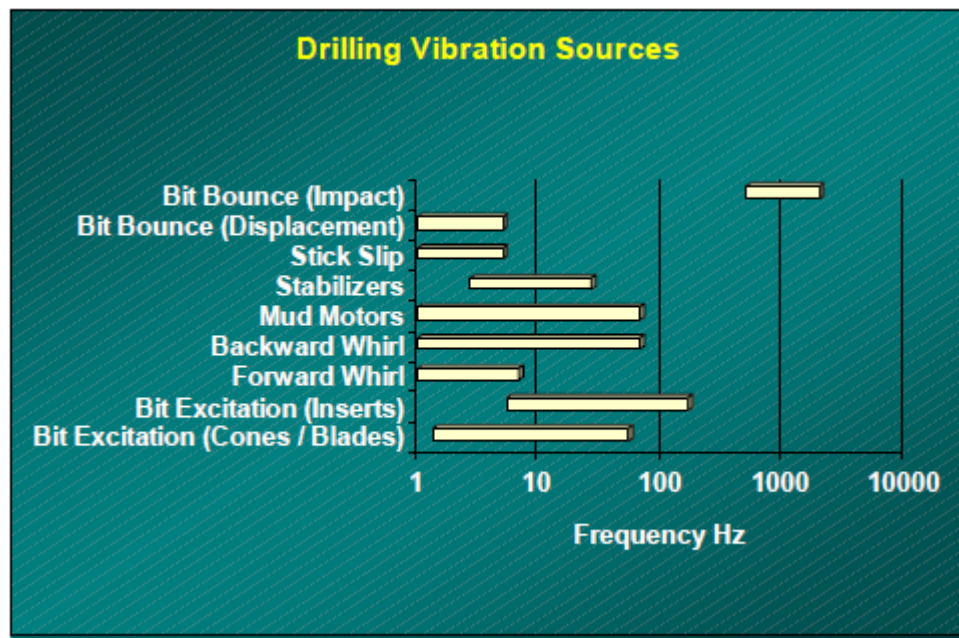


Figure 2.2: Drilling vibrations and frequencies [Martin et al., (2005)]

Cobern, (2007) detailed that the drill strings have relatively low resonance frequencies due to their huge lengths. They discussed the current drilling operations where the drill is operated below the resonant frequency. Optimal drilling cannot be achieved while drilling at this rate and the vibrations could be reduced also when the drill is operated above the resonant frequency.

Bailey, (2008) developed a BHA dynamic modeling tool and have designed the model such that for a particular operating range the critical modes causing resonance are avoided. The drill string vibration and resonant frequencies are still a major research topic in the discussion of vibration minimizing procedures.

Chapter 3. Literature review – Vibration control in rotary drilling

This chapter discusses control efforts applied to minimize vibrations in the field of rotary drilling. The literature review is divided into the following sections:

1. Active and passive techniques developed to minimize drill string vibration.
2. Applicability of under actuated control solutions to minimize vibrations in rotary drilling
3. Control solutions proving rotary drilling vibration mitigation by simulations.
4. Experimental and field tests proving vibration mitigation in rotary drilling

3.1 Active and passive vibration minimization techniques

This section details the available research on recent control laws applied to minimize torsional vibrations. Majority of recent research advancements applying control techniques is directed to minimize torsional vibrations. Hence this sections contains only control techniques used to suppress torsional vibrations, however the objective of this study is to understand the various control techniques applied to the field of vibration suppression in rotary drilling.

3.1.1 Torque feedback

One of the first methods applied to minimize drill string vibrations in rotary drilling used torque feedback from the applied string torque [Halsey, Kyllingstad & Kylling, (1988)]. They suggest that with a torque feedback, the stick-slip oscillations can be prevented by allowing the rotary table speed to respond to dynamic torque variations. Since the torque is used as feedback in

the control loop, a compromise between two contradictory requirements will be required; namely; the control loop needs to maintain the speed set point while also maintaining a constant torque. This is difficult due to presence of well bore hole friction. To prevent stick-slip oscillations the speed was adjusted so the torsional waves were dampened at the rotary table instead of being reflected back to the drill string. A drawback with this method was that it required a good measurement of the drill string torque, which is practically very difficult.

3.1.2 Soft Torque Rotary System

Shell Research was aware of the problems with the measurement of drill string torque so focused their research on improving the torque feedback in the 1990s. They observed two major drawbacks with the torque feedback; the measurement of drill string torque and the control algorithm which was based on zero reflection of the torsional waves. By using the motor current, they computed the torque applied and used this in the feedback loop. By tuning the controller (which could be considered as an active damper), the system dampened stick-slip oscillations in an effective manner. This made the system behave as a tuned damper. This system was called the Soft Torque Rotary System (STRS) and field testing has shown that the system dampens stick-slip oscillations effectively, that ROP is increased, and down-hole equipment failures are reduced. The system has been commercially available for many years and is used at different locations around the world.

3.1.3 PID-control

A simple method for curing stick-slip was presented by Pavone and Desplans, (1994). By doing thorough analyses of data obtained by TRAFOR, a Measurement While Drilling (MWD) system operated by the Institut Français du Pe'trole, they found that by using stability analysis they could avoid stick-slip. They derived parameters for a proportional-integral-derivative (PID)

controller to control the rotary table speed that cured stick-slip. However, the drilling had high vibrations and the controller could not control the drill bit speed. Their main focus was on using the data from TRAFOR to derive a model of the drill string which could simulate stick-slip.

3.1.4 H_∞ -control

In 1998, Serrarens, van de Molengraft and van den Steen proposed a H_∞ -control method to suppress stick-slip oscillations on a contemplated system. H_∞ -control has been a widely used solution for controlling vibration problems, such as in cutting processes where it is used to suppress machine tool chatter. The H_∞ -controller could suppress the stick-slip oscillations in spite of the controller being linear and time-invariant. They have also modeled a two degree-of-freedom mathematical model of the drill string, which captures the torsional dynamics. However, analysis of the lateral and axial dynamics of the drill string was not made because; the model captured only the linear torsional dynamics.

3.1.5 Active damping technique

Navarro Lopez et al., (2004) used an active damping technique for minimizing drill string torsional vibrations. They have presented a twofold solution to mitigate drill string vibrations: by the variation of the weight-on-bit (WOB) and by the introduction of a shock sub (passive damper) at the top of the BHA. The control strategy was set to achieve two main goals:

- (1) The velocity at the top end of the drill string is to be maintained to a reference value, and
- (2) The bit velocity should track the surface velocity with a reduction of the BHA sticking.

They have achieved rotary speed control but tracking of the rotary speed by the drill bit was not achieved.

3.1.6 D-OSKIL

Another method to suppress stick-slip oscillations is to use the WOB as an additional control variable. This method, called Drilling Oscillation KILLer (D-OSKIL), was introduced by Canudas-de-Wit et al. (2005). Their analysis revealed that a major reason for the stick-slip oscillations is the friction torque produced by the contact between the rock cutting tool and the rock. Hence, they conclude that it is required to keep the value of the WOB large to get a good ROP (rate of penetration). However, as the WOB increases it will enhance the possibility of stick-slip to occur. Realizing this D-OSKILL uses a control strategy that manipulates the WOB. The controller works such that when stick-slip oscillations occur, the WOB is decreased by manipulating the force from the hook lifting the drill string at the rig, i.e., the drill string is pulled upwards to reduce the WOB. The proposed controller could effectively minimize stick slip vibrations in simulations.

3.1.7 Smart control

Kyllingstad, A. , (2009) presented a new system for preventing stick slip motion by applying smart (active) control of the drive. They have applied a proportional-integral (PI) type speed controller that is tuned to effectively dampen torsional vibrations. They have used automatic tuning of the speed controller the system including, automatic determination of the stick-slip frequency, estimation of the instantaneous bit rotation speed and calculation of the stick-slip severity.

Many others have focused on controlling the oscillations by operational means such as adding friction reducers to the mud, increasing the rotation speed, or reducing the weight on bit. It is concluded that all these papers concentrate on developing controllers for experimenting on the

mathematical model of the drill strings. Some real field facts on torsional vibrations and stick slip oscillations are presented and their control is discussed in Jerome and Tennyson, (2003), Eva and Rodolfo, (2004), Carlos et al., (2005) and Khuleif and Naser, (2005). A few of the experimental and field demonstrations on practical vibration control are discussed in section 3.4. The next section discusses the research objectives derived from the presented literature review, the thesis chapter lay out and the proposed research contributions.

3.2 Study on under actuated control solutions.

Closer analysis of the rotary drilling process revealed that the upper rotor/ turntable is the only actuated part of the rotary drill rig. The drill pipes are connected together by joints which are not completely rigid. The drill bit is the part which is in contact with the borehole. The joints at the drill pipes lead to the driving force at the turntable in not being fully transmitted to the drill bit. Hence, affecting a change in the upper rotary will not affect a similar change at the drill bit. This situation can be partly overcome by using the borehole casing to hold the drill pipes in the borehole and decreasing the degree of freedom at the tool joints.

The drill bit is not directly energized and hence there is lesser number of actuated elements when compared to the degrees of freedom for the system. Thus the drill string system is an example of an under actuated system.

The subject of under actuated systems and their control is complex and popular. Their control issues arise from the fact that they have more degrees of freedom than the number of actuating inputs. The next section discusses two different approaches of achieving under actuated system control. They have applied control techniques to achieve trajectory following and equilibrium positioning of the under actuated part.

3.2.1 Case study 1:

D. Jerome, (1991) discusses the Pendubot, popular in under actuated systems. It is a two link , under actuated robotic mechanism (Figure 3.1). Link 1 is directly mounted on a motor shaft, and link 2 is coupled to link 1 by needle joint bearings. Both the links have full 360 degree freedom of rotational motion. The research tries to develop a controller to swing the mechanism from its open loop stable configuration to the unstable equilibrium points and then to catch the unactuated link (link2) and balance it there. This control is divided into two parts; swing up control and balancing control.

The swing up control uses the method of partial feedback linearization. The balancing control uses linearizing the system and designing a full state feedback controller for that linearized model.

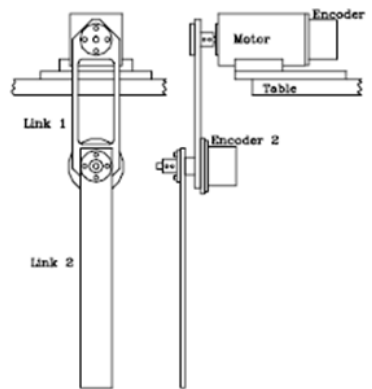


Figure 3.1: Schematic of Front and side perspective drawings of the Pendubot [Jerome D., (1991)]

The equations of motion for the Pendubot can be found using Lagrangian dynamics. In matrix form the equations are:

$$D(q)\ddot{q} + C(q, \dot{q})\dot{q} + g(q) = \tau$$

where \dot{q} is the vector of torque applied to the links and q is the vector of joint angle positions.

Partial Feedback Linearization needs position feedback from both link one and link two but takes into account the nonlinear effects of the linkage. Due to the under actuation of link two, only one DOF was linearized. Jerome had chosen to linearize about the collocated degree of freedom (link1). An outer loop control was designed to track a given trajectory for the linearized degree of freedom to achieve swing up control (Figure 3.2a). For balancing control, the pendubot is balanced at equilibrium points at upright and mid balancing positions (Figure 3.2b). The Taylor series approximation was used to linearize the plant. The partial derivative matrices are evaluated at the equilibrium points to obtain linear models. LQR and pole placement techniques were used to design full state feedback controllers, $u=-Kx$ to achieve balancing control.

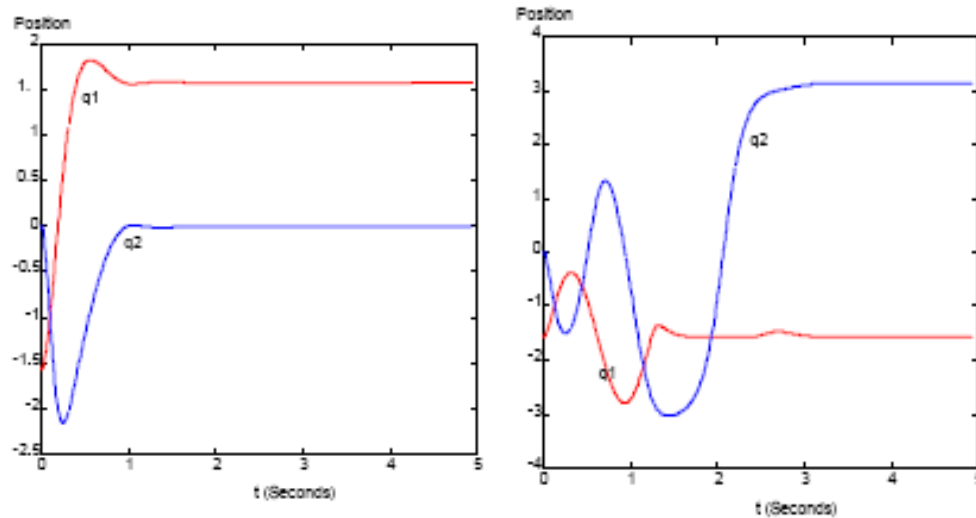


Figure 3.2 (a) and 3.2 (b): Swing Up to the Top Position & Swing Up to the Mid Position [Jerome, D., (1991)].

3.2.2 Case study 2:

W. Blazer et al; (2010) conducted under actuated system research on a system consisting of two rotating discs connected horizontally by a torsional string with the disc 2 as the under actuated element (Figure 3.3). Here disc 2 is taken from rest to a 360 degrees movement and then rest/stops the movement.

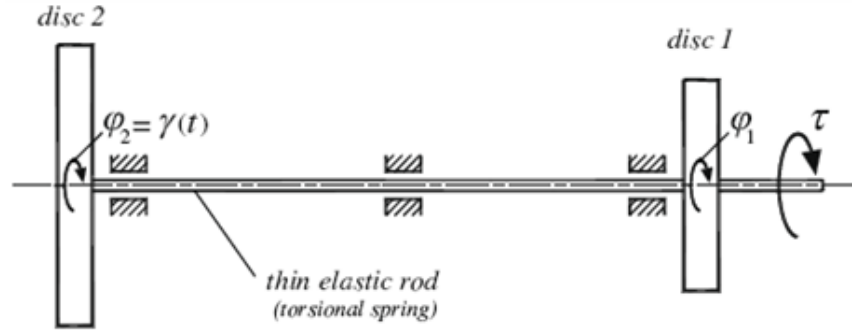


Figure 3.3: Schematic of Two degree of freedom system [W. Blazer et al.(2010)].

They defined a function $s(t)$ to be an appropriately smooth reference function that models a rest-to-rest maneuver. Generally, for an n -degree-of-freedom under actuated system, described by a set of generalized coordinates $q = [q_1 \dots q_n]^T$ and actuated by m control inputs

$$u = [u_1 \dots u_m]^T, \text{ where } m < n.$$

A motion or servo-constraint can be defined as,

$c(q, t) \equiv \phi(q) - v_d(t)$, which force the under actuated system to complete a partly specified motion or performance goals $v_d(t)$.

In the case studied, the specified motion $\phi_2 = v(t)$ of disc 2 is actuated by the torque τ applied to disc 1, and as such $n = 2$ and $m = 1$. The dynamic equations of the system are:

$$J_1 \ddot{\phi}_1 = c_s (\dot{\phi}_2 - \dot{\phi}_1) + k_s (\phi_2 - \phi_1) - \tau_{1res} (\dot{\phi}_1) + \tau$$

$$J_2 \ddot{\phi}_2 = -c_s (\dot{\phi}_2 - \dot{\phi}_1) - k_s (\phi_2 - \phi_1) - \tau_{2res} (\dot{\phi}_2)$$

where J_1 and J_2 are the disc mass moments of inertia, k_s and c_s are the coefficients of rod stiffness and damping, and τ_{1res} and τ_{2res} are the resistance torques caused by friction and damping effects in the bearings. It is assumed that for the system the inputs affect the system dynamics linearly.

A flatness based solution is proposed here on the condition that friction and damping effects are neglected, i.e. $c_s = 0$ and $\tau_{1res} = \tau_{2res} = 0$ and the servo constraint is modeled to allow a specified motion in which a rest to rest maneuver is performed.

The conclusions derived from above study are presented in chapter 4. The next section discusses the control solutions available in literature with proven vibration mitigating capabilities.

3.3 Control solutions proving vibration mitigation in simulations.

This section presents a discussion on the applied control technologies to analyze and control rotary drilling vibrations proven by simulations. Pavone et al. (1994) presented two solutions to avoid stick-slip. The first solution used a PID to servo control the rotary speed. PID controller could suppress stick-slip but the damping of the disturbances was poor and a more powerful servo-control system was required. The second solution suggested using a down hole ‘anti stick-slip’ tool. It created an additional friction with a positive slope that could counteract the negative slope of the bit-rock formation. The solutions were proven by simulations of drilling by adjusting PID controller.

Eva Lopez et al. (2004) suggested two main solutions for mitigating stick slip vibration. Varying the WOB and introducing a shock sub at the top of the BHA. The above suggestions are simulated on the drill string model by an added mass term for the weight on bit and representing the shock sub by a spring and damper system. The simulated control strategy achieved two main goals: (1) the velocity at the top end of the drill string is maintained to a reference value, (2) the bit velocity tracks the surface velocity with a reduction of the BHA sticking.

F.Abdul Galil and H. Siguerdidjne (2005) developed a back-stepping control strategy to eliminate stick-slip vibrations. The stability of the controller is shown through Lyapunov functions. The main advantages of the proposed nonlinear controller lie in the fact that it may provide the control performance with a fast response time (less than three seconds). Sufficient robustness of the controller is verified in opposition to the uncertainties of drill string length and the lumped damping.

Vigue et al. (2009) investigated the possibility of passively mitigating friction-induced vibrations in drill-string systems. They used a nonlinear absorber, Non linear Energy Sink (NES) characterized by essential stiffness nonlinearity. The addition of the NES to the drill-string system improved the global dynamical behavior of the system and substantially extended its domain of operation. It could eliminate completely the instabilities in a relatively wide range of input voltages at the DC-motor generating the driving torque. It is interesting to note that they concluded that an experimental demonstration is necessary to validate the developments proven by simulations.

Eva Lopez et al. (2009) proposed a dynamical sliding-mode control for stick slip vibration control. On the new surface, the bit speed followed the top-rotary-system speed after a reasonable time, without bit sticking phenomena. In the closed-loop system, the angular velocities were driven to a desired reference value in spite of weight-on-bit variations and the presence of a dry friction modeling of the bit-rock contact. The key idea of the controller is to introduce in the system a sliding surface in which the desired dynamics are accomplished. The stick-slip motion was still present in the controlled system; however, the velocities values for which this phenomenon is avoided were identified.

Most of the research in drill string vibrations using applied control technology is concentrated on mitigating torsional vibrations. Some researchers have noted that an experimental procedure is necessary to verify the simulation results. The next section discusses the recent experimental or field applications in rotary drilling vibration mitigation.

3.4 Experimental and field tests proving vibration mitigation

This section presents the recent advancements of successful vibration mitigation in rotary drilling proven using experimental or field tests.

J.Gallagher et al. (1994) suggested using contemporary mud motor technology to reduce vibrations by providing the bit with the operating conditions for which it was designed, rather than the harsh and destructive environment imposed by rotary drill string vibration. They suggested use of Performance Drilling, namely the predictability of both ROP (Rate of Penetration) and bit life when a suitable motor is used. They concluded by suggesting use of a system incorporating high torque motors, anti-whirl bits, hydraulic thrusters (to absorb axial movement and permit a shorter BHA) and soft-torque rotary controls. The net result would benefit a wide spectrum of vibration-related problems and the drilling process would be optimized.

Jansen et al. (1995) developed an active-damping system to eliminate “stick/slip” torsional drill string vibrations. The effect of increasing the rotary speed at surface is to increase the damping of the vibrations that were caused by friction between the rotating string and the mud or the borehole wall. When the rotary speed became high enough, the damping became so large that the energy stored during the time that the bit was stuck did not make up for the energy lost during the time that it rotated. In that case, the stick/slip vibration would stop. In practice, this rotary speed threshold was often so high that it cannot be reached. A way suggested to reduce the threshold was to increase the damping at the top of the drill string. The active damping system developed controlled the energy flow through a hydraulic top drive and made the top drive react as a tuned vibration damper. The control algorithm was implemented in software in the electronic control system for the pump unit of the top drive. The system was field tested in a deep

exploration well in the Barents Sea and contributed to excellent coring performance by eliminating torsional vibrations while coring hard limestone (Figure 3.4).

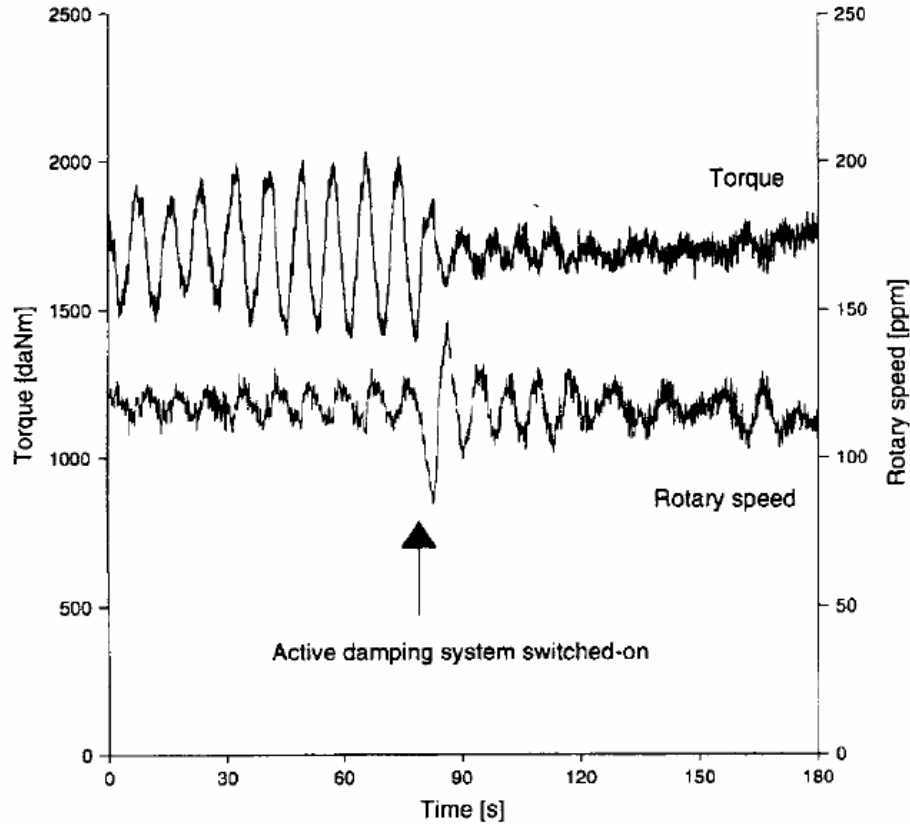


Figure 3.4: Field test results to suppress torsional vibration. (Jansen et al., 1995)

A.F.A Serrarens *et al.*, (1998), applied the H-infinity (H^∞) control technique for suppressing stick-slip in oil well drill strings. The H infinity controller tried to find a controller C that minimized the maximum normed size of the transfer from the norm bounded worst case disturbance w^* to the norm bounded to be controlled output z^* . The infinity norm which was to be minimized was defined as

$\|M(s)\|_{\infty} := \sup_{w^*(t) \in L_2} \frac{\|z^*(t)\|_2}{\|w^*(t)\|_2}$. However, due to the difficulty in finding this closed form, the

authors chose to solve the suboptimal H_{∞} control problem which stated that a stabilizing controller C has to be found that makes the infinity norm of the closed loop H smaller than a predefined value, γ . The value of γ was chosen as 1, from robust stability considerations. The schematic of the closed loop controller is shown in Figure 3.5.

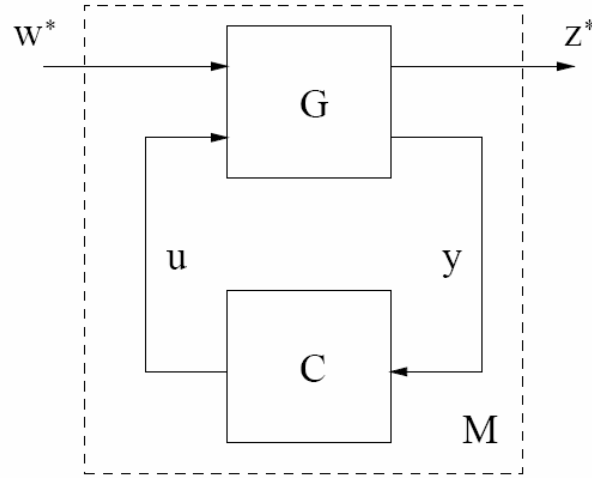


Figure 3.5: Closed loop control schematic using H infinity controller.[A.F.A.Serrarens (1998)]

The experimental system was run at about 5rad/s. The controller exhibited fast response and the stick slip oscillations were controlled and resumed normal operation in about 15 seconds (Figure 3.6). Some sustained oscillations were still present which the authors attributed to a problem with the power controller of the electric motor drive. The controller however was not designed to be robust to changes in the length of the drill string during rotary drilling.

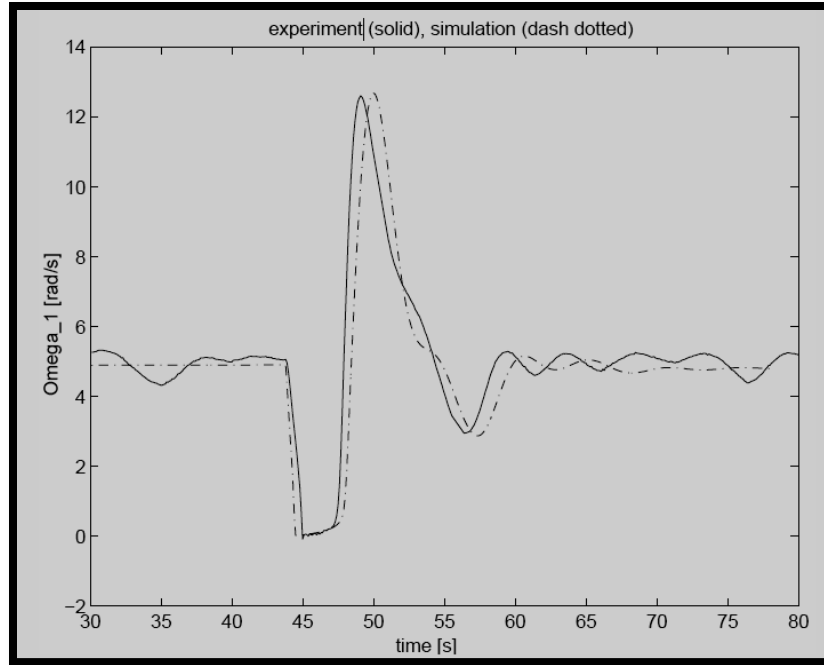


Figure 3.6: Experimental observations using H-infinity controller [A.F.A.Serrarens(1998)].

D.Pavkovic et al. (2011) developed and implemented a drill-string drive control strategy on a hardware-in-the-loop (HIL) experimental drill string set-up. The setup consisted of an induction motor (IM) equipped with an incremental encoder, which was used as a drill-string driving motor, and a permanent-magnet synchronous servomotor (PMSM) used as a loading machine (programmable load). The motors were coupled via a belt drive, and they were driven by power converters configured in current (torque) control mode and tuned for fast response.

A linear active damping control strategy based on the estimation of the drill-string torque was applied for suppressing torsional vibrations. They developed a core proportional-integral (PI) controller. It was then extended by an additional drill-string torque feedback control loop based on the estimated drill-string torque referred to the motor shaft (called the, PIm speed controller). The effectiveness of the proposed control strategy was illustrated by the HIL experimental responses (Figure 3.7) which emulate the case when the tool was located at the bottom of the well. The

figure illustrates switching between fast PI controller and active damping PIm controller (HIL test).

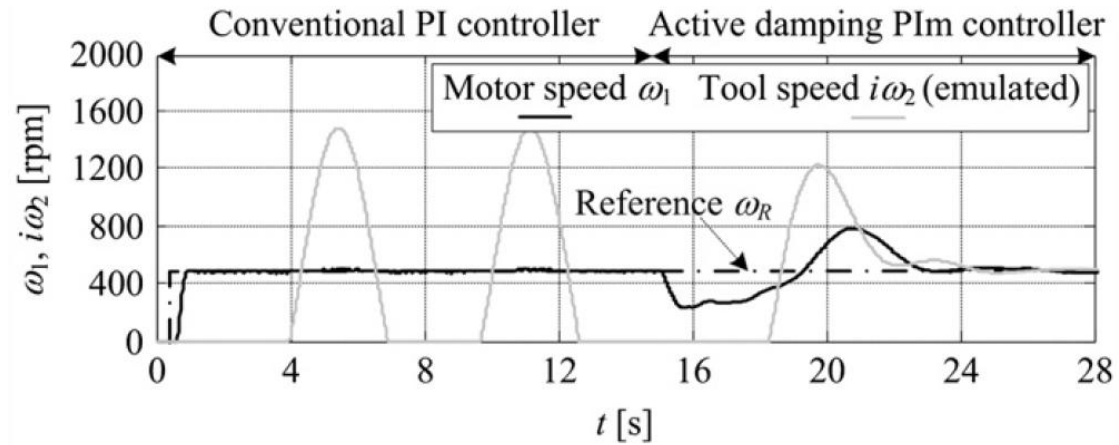


Figure 3.7: Illustration of active damping capability [Pavkovic (2011)].

The major disadvantage of the proposed control strategy is the tool requires to be lifted from the bottom of the well during the auto-tuning execution in order to avoid nonlinear tool friction effects.

3.5 Adaptive control technology and drill string vibration mitigation

Some recent applications of adaptive control used to mitigate rotary drilling vibrations are discussed below. Shi Fubin, et al., (2010) have developed an adaptive PID control strategy of the drilling rotary system to eliminate the stick-slip oscillation of the bit. The main objective of the adaptive PID controller was to improve system characteristics of output-to-input following and dynamic response. The results of the controller were proven only in simulations. Jijo'n R.B., et al., (2010) have developed a design for an adaptive observer. They have analyzed the Drilling-

Oscillation Killer (D-OSKIL) control law proposed by C. Canudas-de Wit et al. (2008). The D-OSKIL controller uses a vertical force WOB as an additional variable to eliminate stick-slip effects. However, they have attempted to improve the control law by aiding it with an additional adaptive observer so that the unknown states of the system could be estimated. Smoother estimates are obtained, however no different control law has been proposed. Li. L et al., (2011) have developed a time varying sliding mode adaptive controller for the mathematical model of a rotary drilling system. The controller used is PID and the simulation results prove a good time response for the bit. However the vibrations of the upper and lower rotary and their magnitudes are not clear. The simulations prove good tracking performance but they are not validated by experimental results. The drill bit being an under actuated part of the rotary drilling system, its accurate movements cannot be completely predicted or demonstrated by simulations [F. Abdul Majeed, et al. (2011)]. However, none of the researchers were successful in developing an adaptive control law for minimizing drill bit vibrations and practically demonstrating the results. Hence it is imperative to develop a control law which can efficiently minimize the vibrations of the drill string resume the normal drilling operation in the least time possible.

This section completes the literature review discussion. The conclusions derived from literature review and the research objectives are discussed in the next chapter.

Chapter 4. Research methodology

The scope of the research is formed from the following inferences drawn from the literature review, and identifying the limitations of current research.

4.1 Literature review inferences

1. Lateral vibration is the most destructive.
2. Bit whirl is the phenomenon associated with it.
3. Most of the research in drill string vibrations had derived models based on analytical principles.
4. Analytical model derivation from analytical principles is based on many assumptions and approximations.
5. A new modeling approach relying less on approximations and more on experimental data is wanting.
6. An unbalanced mass on the drill bit could represent dynamics of a bent drill string and an imbalanced drill bit.
7. The experiments on unbalanced drill bit should conform to the unbalance limits in literature, i.e.; 2-10%.
8. Majority of research concluded effective control using simulations with no experimental backing.
9. Most of the research using advanced control technology was directed to mitigate stick-slip, a popular phenomenon arising from torsional vibrations.

10. Advanced Control technology has never been applied to minimize drill bit whirl.
11. Resonant frequencies are identified to be a major vibration aggravating source.

4.2 Limitations of current research

1. Major part of research concentrated on minimizing torsional vibrations, however, lateral vibrations are the most destructive.
2. Majority of research concluded effective control using simulations with no experimental backing.
3. Research trend is to overcome drill bit whirling by applying passive control methods like designing new drill bits or placing dampers near the BHA.
4. Active control using Advanced Control techniques has never been applied to overcome drill bit whirl.

4.3 Scope of the research

1. The research has concentrated on experimental analyzing of lateral vibrations, bit whirl in particular.
2. The research has introduced a new modeling perspective in the field of drill string vibrations.
3. The research has developed an active vibration controller with three major advantages:
 - a. Advanced control technology
 - b. Mitigates the vibration aggravating causes, rather than a specific phenomenon
 - c. Can be applied practically in the industry

4.4 Research plan flow chart

Figure 4.1 details a schematic of the research plan. The research initiated with an exhaustive literature review covering the topics:

1. Drill string vibrations and their causes
2. Mathematical models of rotary drilling representing drill string dynamics.
3. The causes of bit whirl :Bend drill string and Bit imbalance
4. Drill string natural frequency and resonant vibrations
5. The drill string vibration minimizing solutions.
6. Under actuated control solutions
7. Control solutions proving rotary drilling vibration mitigation
8. Experimental and field tests proving vibration mitigation in rotary drilling

The literature review helped to identify the limitations of current research in vibration mitigation in rotary drilling, as detailed in section 4.2. The literature review also helped to understand the challenges faced by the rotary drilling industry (section 4.3). The research was thenceforth divided into two branches which complement each other:

1. Mathematical modeling and simulations
2. Experimental analysis and implementation.

Experimental analysis included both analyzing dynamics under external influences and controller design and implementation.

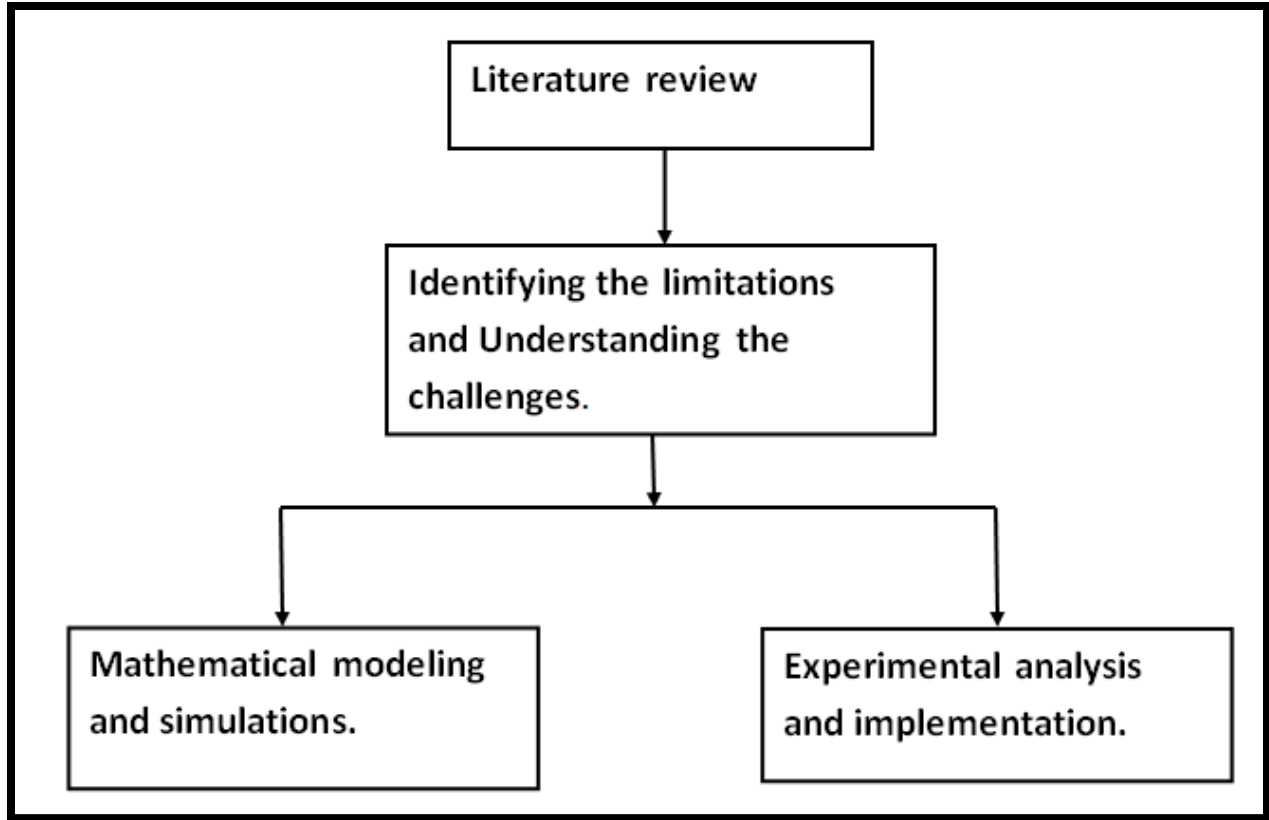


Figure 4.1: Schematic of research plan

4.4.1 Mathematical modeling and simulations

Figure 4.2 details a flow chart of the major sections completed in the mathematical model development and simulations part of the project. In this part of the research, mathematical model of the laboratory set up was identified using the Black Box method of System Identification. The data required for the identification procedure was acquired directly from the test rig by suitable excitation.

Initially an ARMAX model was identified for the linear system represented by test rig configuration 1 in Chapter 5.

In the second stage, an unbalanced mass was added on the drill bit and a Box Jenkins model was identified for the system. This is represented by the test rig configuration 4 in chapter 6. A model was also developed for the same test rig configuration 4 using analytical principles. The Box Jenkins model and the analytical model responses were compared and validated.

The identified mathematical models were used for simulations to test the designed controller effectiveness.

The detailed procedures followed in the model identification procedure are discussed in Chapter 6.

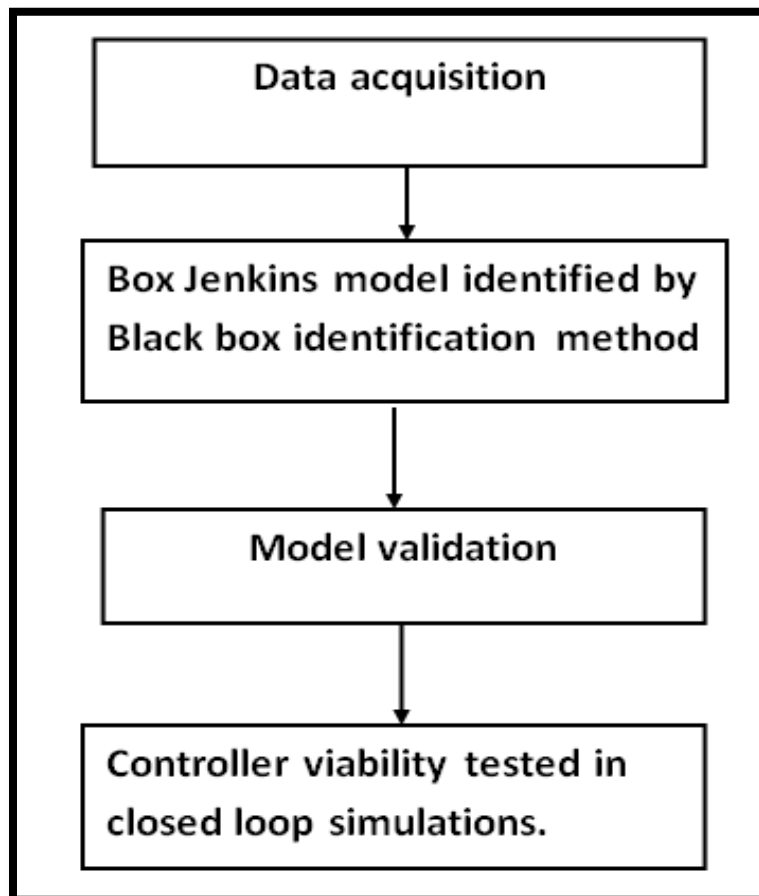


Figure 4.2: Flow diagram of mathematical modeling and simulations part of research.

4.4.2 Experimental analysis and controller implementation

Figure 4.3 displays a flow diagram of the experimental analysis of the various dynamics in rotary drilling and the controller implementation. The research experimentally analyzed various dynamics like effect of hard brake, resonant speeds, drill bit whirl due to unbalanced mass and drill bit whirl due to borehole effect. Resonant speeds and borehole influence were recognized and confirmed experimentally to be a major source of vibration aggravation. The research also developed an active control law and practically implemented it on the test rig.

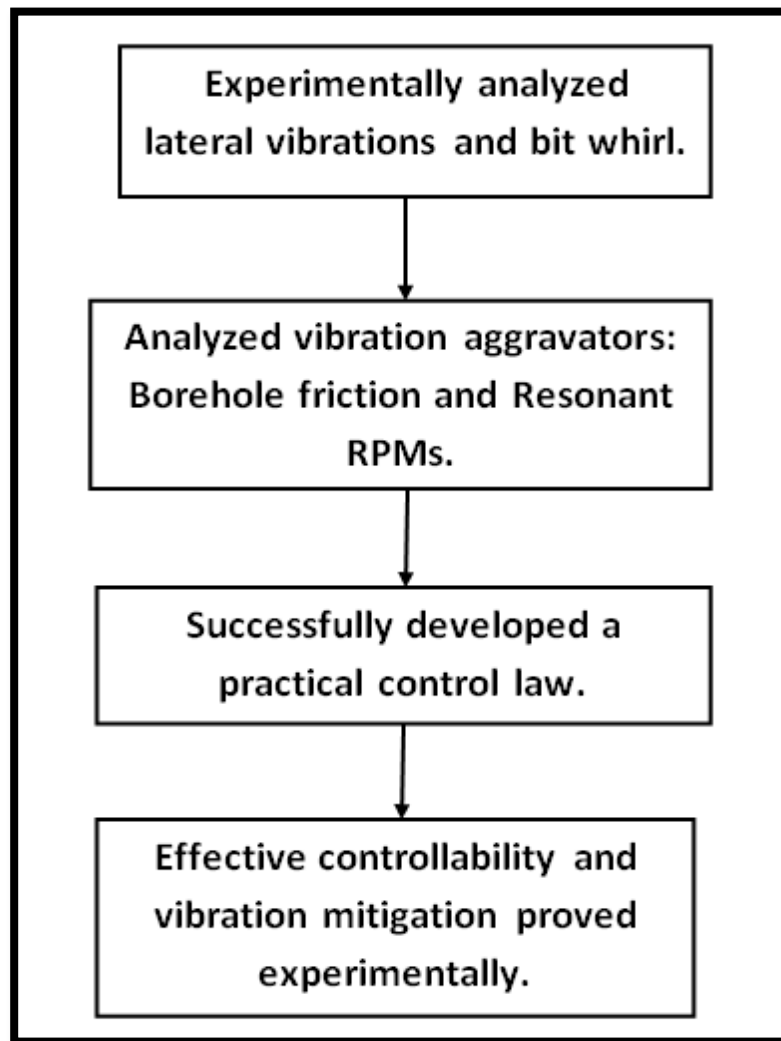


Figure 4.3: Flow diagram displaying various experimental analyses done by the research

4.5 Chapter lay out

The chapters are laid out in this thesis to reflect the above conclusions.

Initially it was realized that a study on drill string vibrations, especially with control objectives, would not be complete without a good experimental set-up which captures the salient features of rotary drilling. Based on research prototypes used by many researchers [J.D.Jansen et al., (1995), N. Mihajlovic et al., (2004), J.C.A. de Bruin et al., (2007)], an experimental set-up was built at the Vibrations lab.

An introduction to the rotary drilling rig and its major parts were discussed in Chapter 1. Chapter 2 and 3 discusses the literature review findings in various topics related to the research. Chapter 4 discusses the findings on the inferences from literature review, limitations, scope of research and the chapter lay out in the thesis.

Chapter 5 details the description of the laboratory set-up configuration 1, its major parts, the data acquisition procedure using LabVIEW™ programs and the sensors used in the project for data acquisition.

Three new configurations of the laboratory set up are also introduced in Chapter 6. These configurations are introduced to analyze various dynamics of the drill string. Configurations 2 and 3 tested external effects like the effect of hard brake, borehole friction and configuration 4 analyzed internal physical or inherent effects like unbalanced drill bit and critical speeds on the rotary drilling dynamics.

Configuration 2 represented the implementation of the hard brake which induced limit cycling dynamics. Configuration 3 introduced the effect of borehole friction which was simulated by a

rubber sponge lining added to the metal casing outside the drill bit. A short analysis of the configuration 3 analysis is also presented in this chapter.

Configuration 4 is used to present the dynamics of rotary drilling when affected by physical internal cause; an unbalanced drill bit or a bent drill string. These dynamics are practically analyzed and demonstrated using configuration 4. An analysis of the nonlinear characteristics presented by laboratory set up configuration 4 is also presented in the chapter 6.

In order to investigate the controllability of vibrations in rotary drilling, the first step was to develop a mathematical model of the experimental set up for use in simulations. Most of the models available in literature used pure analytically derived models while some models used a combination of analytical equations and parameter estimation. Due to the complex vibrations and dynamics of rotary drilling, this research selected a system identification approach to identify the mathematical model for the process. Chapter 7 discusses the identification of an auto regressive moving average exogenous (ARMAX) model of the configuration 1 set up by the least squares based parameter estimation approach of black box model system identification method. The model analysis and validation are also presented in the chapter.

Chapter 8 is an extension of the mathematical modeling to identify a model for the configuration 4 laboratory set up. A Box Jenkins model was identified to represent these dynamics and validated experimentally. The details of the identification procedure, validation and discussion on model robustness are also detailed in the chapter. An analytical model is developed for the configuration 4 laboratory set up in chapter 9. The simulations of the Box Jenkins model and analytical model are compared and verified.

Chapter 10 analyzes the controllability of the drill string vibrations in the presence of the unbalanced drill bit represented by configuration 4. It also discusses two major causes aggravating drill string vibrations: well borehole effect and the critical speeds of operation using configuration 3 of the laboratory set up. The effects of these causes on the dynamics of rotary drilling are demonstrated in the chapter.

This research developed a self tuning adaptive controller for three axes vibration mitigation in rotary drilling systems. The control law developed is a practical solution to minimize and mitigate the effect caused by the boreholes and critical operation speeds on vibration aggravation in rotary drilling. Practical demonstration of the effectiveness of the controller is also a major achievement of the research. They are explained in detail in Chapter 11.

Chapter 12 presents the conclusions of the research work and suggestions on future work.

4.6 Research objectives

1. The research will attempt to identify a mathematical model of the rotary drilling process under various conditions such as ideal drilling, unbalanced drill bit, etc., by the black box identification method.
2. For the rotary drilling with unbalanced drill bit problem, due to the nonlinearity addition near the output end of the process, a Box Jenkins model structure will be used and the model will be validated experimentally.
3. A four degree of freedom analytical model will also be developed for the unbalanced mass system to verify and validate the identified model.
4. The research will analyze the dynamics presented by the rotary drilling under various conditions: presence of unbalanced drill bit, hard brake inducing limit cycling, borehole friction, critical operational speeds, etc.
5. The research intends to offer a practical control solution to mitigate rotary drilling vibrations. A control law using a self tuning adaptive controller with an online identifier will be developed. The controller will be implemented practically and experimental closed loop results will be presented.
6. All the major programs for software and hardware interfacing, model identification, and controller development will be developed using the National Instruments LabVIEWTM software.

Chapter 5. Laboratory Arrangement and LabVIEWTM interface program development

This chapter details the description of the laboratory set-up, its major parts, the data acquisition procedure using LabVIEWTM programs and the sensors used for data acquisition. Section 5.1 discusses the laboratory set up and it's working. Section 5.2 explains the software used for data acquisition, the developed program interface and raw data generation. The data sheets of all the hardware devices used are attached as Appendix 3. The developed LabVIEWTM programs are explained in detail and the synchronization of events and data flow between hardware and software is explained. Section 5.3 discusses the sensors used for data communication in the laboratory set up.

Many researchers have used experimental prototypes of the oil rig to simulate torsional/lateral vibrations [Germy et al., (2009) and Mihajlovic et al., (2004)]. Mihajlovic et al., (2004) used experimental prototypes to analyze stick-slip vibrations and limit cycling. This research has used an experimental prototype to analyze rotary drilling dynamics under various external influences. The prototype used for this research stands out from others by the presence of a universal joint connecting the drill string to the upper rotary disk (Figure 5.1). The joint provides an additional 2 degrees of freedom movement to the drill string and the lower rotating components. Hence, the set-up is more similar in dynamics and degrees of freedom to the actual drilling process.

5.1 The laboratory set up configuration-1 and rotary drilling rig

In order to understand and analyze the vibrations due to the bend drill string, experiments were conducted. The salient features of the rotary drilling rig (Figure 5.1) are captured in the laboratory by a simple experimental set-up. This part of the mechanical design was conducted by Dr.Karkoub's group at the Petroleum Institute (PI). The main focus during this stage was to concentrate on the study of the dynamics of an individual section of the drill string (assuming all the sections of the drill string experience similar forces). The experimental set-up is as shown below in Figure 5.1. Similar prototypes have been used by other researchers for analyzing drilling vibrations. The prototype used for this research stands out due to the presence of a universal joint connecting the drill string to the upper rotary disk. The joint provides an additional 2 degrees of freedom movement to the drill string and the lower rotating components. Hence, the set-up is more similar in dynamics and degrees of freedom to the actual drilling process.

As explained previously in chapter 1, the electric generator provides the driving energy for the entire drilling. This energy is transmitted to the drill string and BHA through a large turntable at the surface of the well. The drill strings are connected by tool joints and they are joined together as the well deepens. A casing is also inserted into the well to keep the mud and rocks from falling into the borehole. The drill collars provide the weight required to keep the drill bit on the drilling end. The drill bit is the part which actually comes in contact with the rocks.

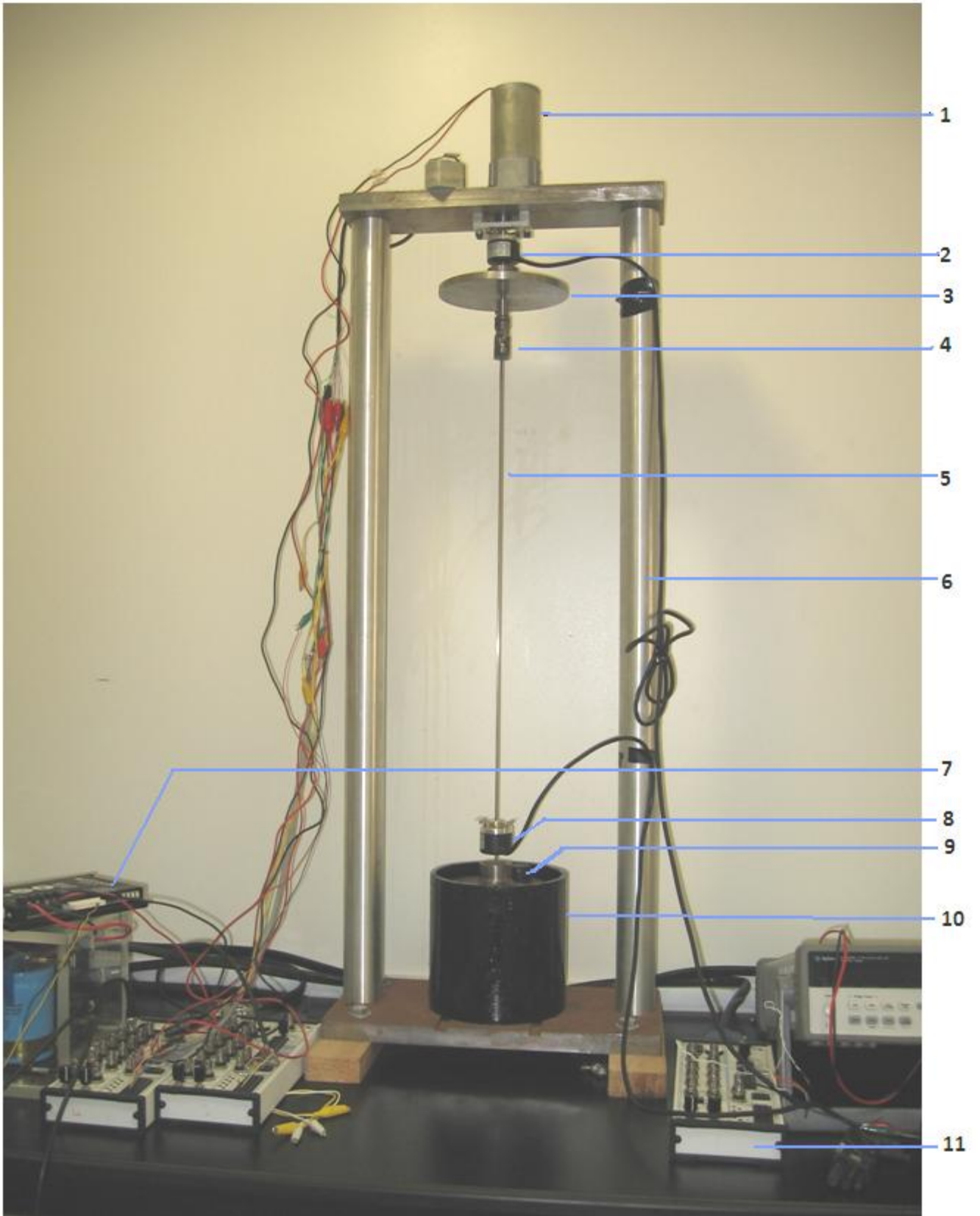


Figure 5.1: Laboratory set up.

The various parts of the laboratory set up as labeled in Figure 5.1 are laid out in Table 5.1, and the number in parentheses in the text below refer to the table. The laboratory set-up in Figure 5.1 operates by energizing a DC power source and a PWM amplifier. The output of the PWM amplifier (7) is used to operate a DC motor (1), which rotates a large flywheel (3), coupled to the motor shaft. The fly wheel (weighing approx. 2 Kg, hereafter also referred to as the upper rotary) serves to represent the large rotary table found at the surface in rotary drilling. In rotary drilling, the rotary table (approx. 20,000 Kg) provides the driving torque necessary to rotate the drill string and drill collars. In the laboratory set up a 1m long string (made of carbon steel) is attached to the upper flywheel by a universal joint (4) to represent the drill string (5). The drill string in a rotary drill rig (Figure 1.1) is made up of high grade carbon steel drill pipes (approx. 10 m long) attached together, and could be anywhere from 8 to 10 km depending on the length of the well. This joint provides two degree of rotational freedom (x and y axes).The motor rotation provides the set-up with one DOF of rotation about the z axis. The entire set up is supported by a metal frame (6).

Two incremental encoders (2 & 8) are used to sense the angular velocity of the upper rotary and drill bit. The lower flywheel (weighs approx. 1.1 Kg, hereafter also referred to as the drill bit) in the laboratory set up represents the rotating mass of the BHA (Bottom hole assembly: drill collars and other equipment) and drill bit (referred to as drill bit in this thesis) (9). In practice, the BHA could weigh anywhere from 500 to 2000 Kg depending on the bore hole size and equipments used. A metal cylindrical casing (10) is fixed to the frame around the lower flywheel. It is used to represent the well bore hole. Two of NI DAQ BNC 2120 are used to communicate data between the NI Lab VIEW™ program and the encoders (11).

Table 5.1: Parts of the laboratory set up

Part number from Figure 5.1	Name of the part
1	DC Motor
2	Upper incremental Encoder
3	Upper rotary table
4	Universal Joint
5	Drill string
6	Metal frame
7	PWM Amplifier
8	Lower incremental encoder
9	Drill bit
10	Metal casing
11	NI DAQ BNC 2120

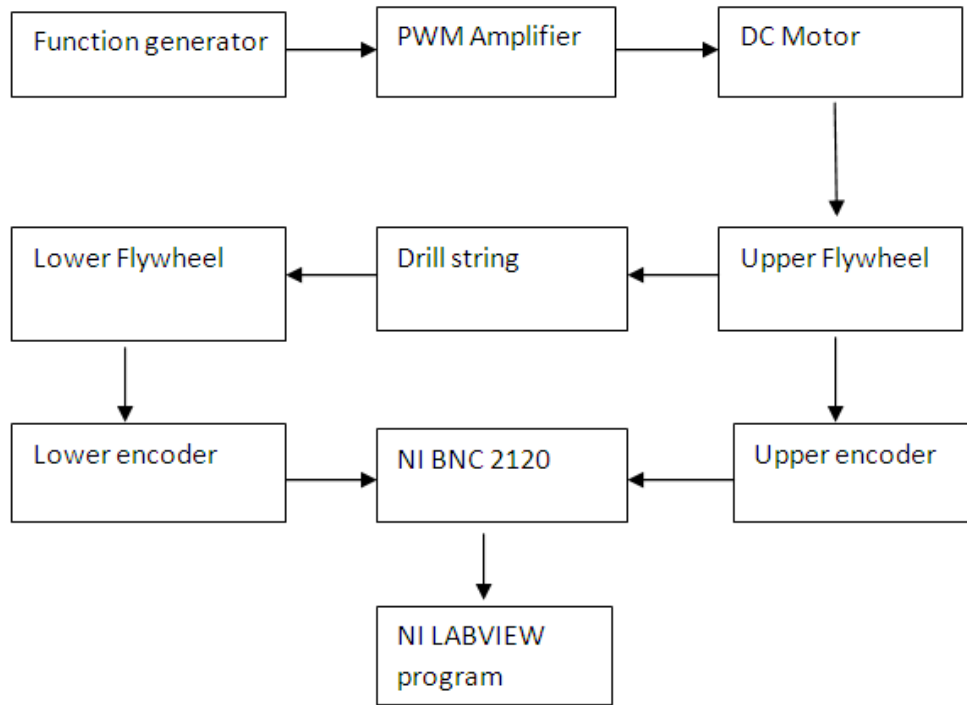


Figure 5.2: Process flow diagram for open loop drill string analysis

The flow of data between hardware and software for operating the laboratory set-up and data logging is as per the schematic in Figure 5.2. A power supply unit is connected to the Motor to drive it. A function generator and amplifier are connected to the power unit to provide required triggering /reference signal to the drill system. This type of desired function generation is very crucial. It helps in generating desired excitation signals to the drill system to excite all the system states and extract the required system information from the data. The PWM amplifier is essential to provide the necessary current for the motor to run.

The purpose of the encoder in this experiment is to analyze the angular velocity of the upper and lower flywheels and compare them; here incremental encoders are used for the purpose. Incremental encoders will provide angular velocity data quite accurately. However they may also

have some approximation or errors due to shaft movement etc, but if two similar encoders are used and the objective is comparison of two data, incremental encoders will work well. Moreover, this is an experimental setup and the size of the setup and the accuracy requirements allow the use of tethered encoders to read the speed signals to a good accuracy. However, in the field there are many tools that were developed and others in the development process to read drilling data (tethered and un-tethered). This is known to the research community as MWD (measurement while drilling). The tools used to perform in situ measurements and relay information to the surface through wires, wireless, or other means such as acoustic waves. The drilling speeds are relatively low (~ 100 rpm) and therefore the encoders are expected to read the speeds fairly accurately. Also, IMUs (inertial measurement units) are used in combination with encoders to guarantee the accuracy of measurements [N. Abdelmagd, 2002]. The data obtained from the encoders via BNC 2120's are compared for analysis and control purposes using LabVIEWTM programs. The next section, 5.2 discusses the details of LabVIEWTM programs developed for online data acquisition and communication with hardware.

5.2 NI LabVIEW™ program development and dynamic data acquisition

To implement the functioning of the laboratory set-up and log required data, an interface had to be designed. The interface should implement the following requirements.

- The design and transfer of an input signal
- Plots of input and output data
- Data acquisition and logging.

5.2.1 LabVIEW™

The software used for implementing the interface is National Instruments (NI) LabVIEW™. LabVIEW™ is a graphical program designed to make interfacing with any measurement hardware.

NI LabVIEW™ is used for data acquisition, system modeling, identification, and control throughout the research. LabVIEW™ has several interesting features like simulation of signals, interface with data acquisition devices, front panel instrument blocks, etc. Moreover, LabVIEW™ doesn't require a script or program chart to make the files work. It requires only the connection of "real" devices in the block diagram. Applications created with LabVIEW™ are referred to as virtual instruments (VIs) created as block diagrams. Input and output interfacing with the VI is performed in another window called the front panel. The front panel helps to view and manipulates the results/ devices in the block diagram through various graphical charts, displays and switches. LabVIEW™ also enables to interface directly to instruments, sensors and actuators. These signal transfers are done using the analog inputs/ outputs of the NI DAQ device. LabVIEW™ can create applications which can be used to collect, analyze and share data with

ease and with higher accuracy. LabVIEW™ make it connect to I/O and integrate with software which makes it easier to compare data from a process with the theoretical models.

The LabVIEW™ virtual instrument (VI) block diagrams are developed for the data acquisition and processing from the incremental encoders. The entire block diagram is attached in Appendix 3.

5.3 Sensors used in the laboratory set up

This section details the sensors used in the laboratory set up, and the data acquisition procedure using them.

5.3.1 Incremental encoders

An incremental encoder converts the angular position of rotating shafts to digital code. This digital code is programmed to get the angular velocity data. Figure 5.7 plots the number of revolutions taken by the upper rotary and lower drill bit when excited by a voltage of 2.5 volts. Due to non synchronous movement of the upper rotary and drill bit, a twist or torsion arises in the drill string. The difference in the angular position is called the torsion angle.

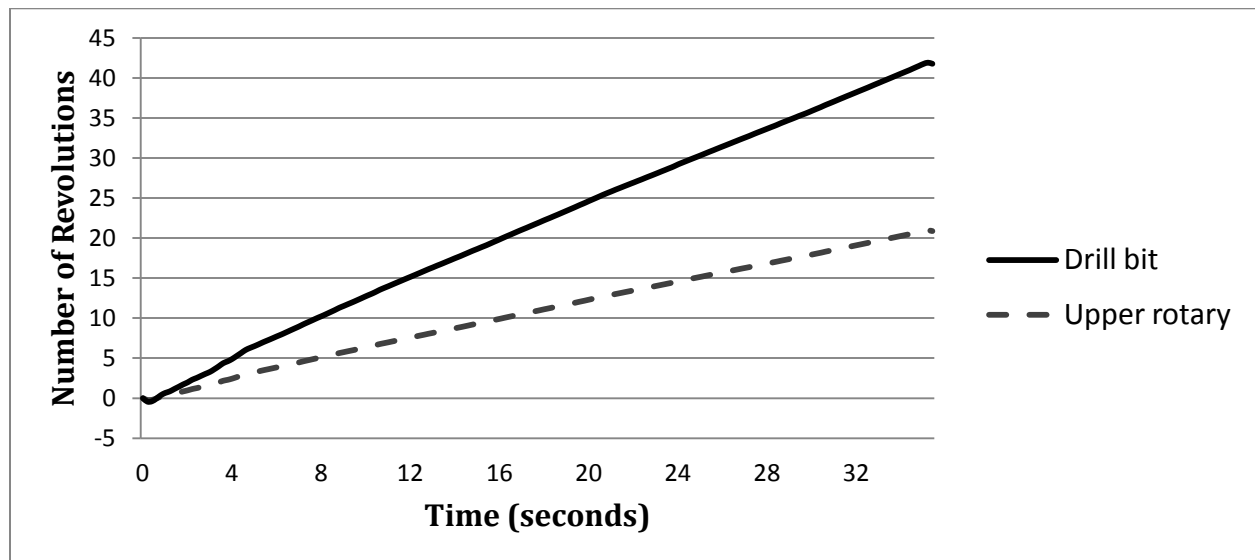


Figure 5.7: Revolutions taken by the upper rotary and drill bit

The presence of torsion increases due to the added effects of friction from the environment (drill bit and earth) and due to the loss of transmitted power from the upper rotary table to the drill

bit in the joints in drill strings. The drill string set-up in the lab does not take into account the bottom-hole friction and also does not have the many attached sections of drill string. Nevertheless, it can be seen the presence of torsion in the near ideal case set-up in the lab. It can hence be seen that the torsion angle will only increase with real time drilling in the presence of friction and loss of transmitted power. The torsion angle is the main cause behind the stick slip and major vibrations leading to failure which can be noticed in the drilling field. The time response of the system is also studied. The response of the upper flywheel to the command speed is studied in Figure 5.8 to analyze the step response of the system. Analyzing the step response gives major insights to the system behavior such as steady state following, stability, and settling time. The system is seen to be stable, fast response time (0.5s), and slightly large settling time (5s).

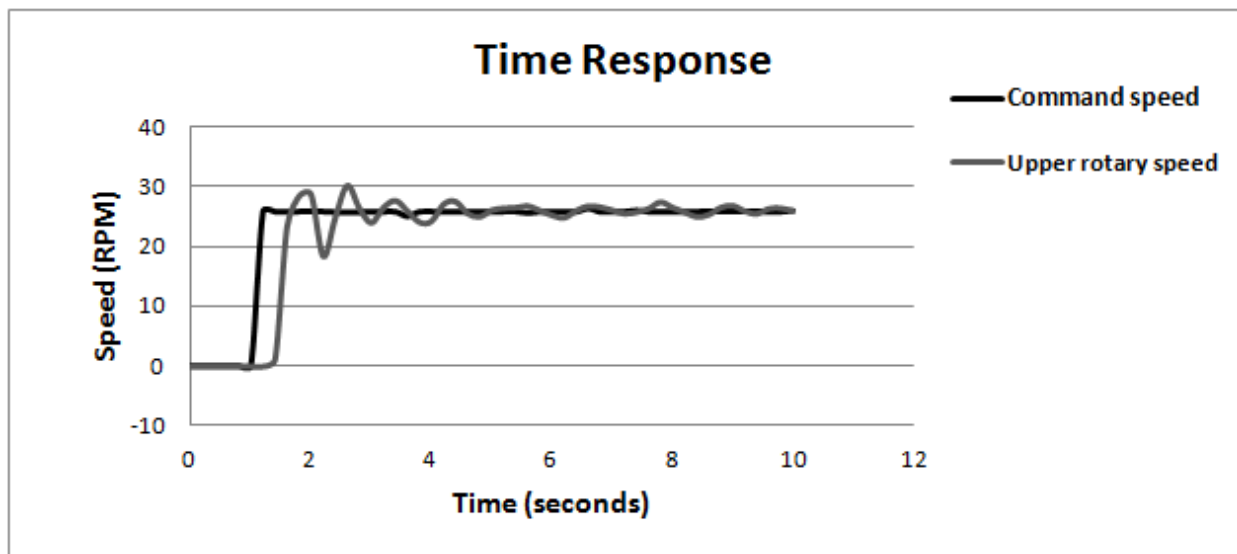


Figure 5.8: Step response of the upper rotary to command speed of 26RPM.

The incremental encoders provided noise free, good quality speed data from the system. In Figure 5.11, the system response is compared with the required operational angular velocity by the system (referred as the command speed) input as a voltage to the motor for low, average, and high drilling speeds at a sampling frequency of 5 samples/second. Observation of the plot displays some vibrations at speeds around 8 RPM which could indicate resonance; i.e., the first mode of vibration and exciting frequency are close to each other. The average drilling speed is about 40 RPM. It was noticed that the response of the drill string system lags behind the command speed input at low speeds; however, as the speed is increased the lag is reduced. This deficiency at low speeds can be attributed to power dissipation in the elements. It is seen that the drill string upper rotary follow the command signal (depicted as corresponding speed in RPM) more closely at higher angular velocities.

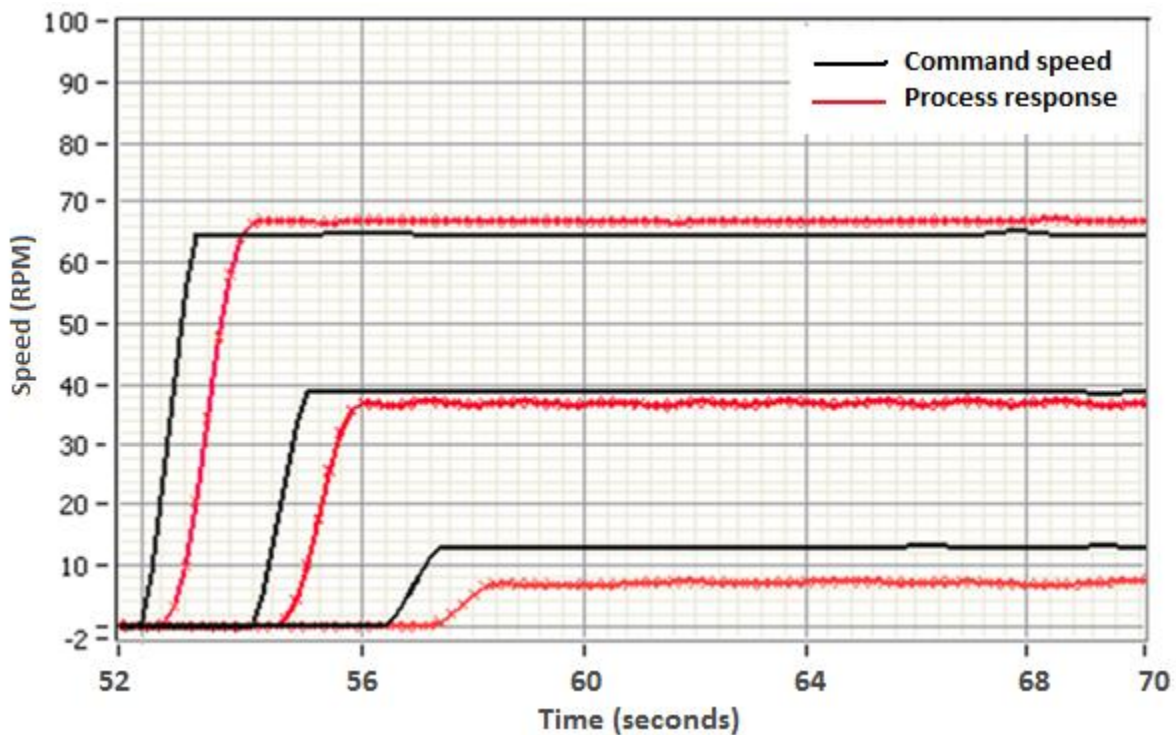


Figure 5.11: Plot of Command speed and process response for various speeds (configuration 1).

As the speed is increased further to 65 RPM, near the high speed range for the actual drilling, the power dissipation is less compared to the input power. Due to inertial effects the drill bit follows a slightly higher speed to the command speed input.

5.3.2 Three-axis vibration detection and logging using Kionix accelerometer

The accelerometer used to detect and log the vibration data was a Kionix 3 axis accelerometer. An accelerometer evaluation board was used to enable fast and reliable data processing. The board was placed on the incremental encoder by a plank mechanism. The laboratory arrangement is shown in Figure 5.12. The sensor board was screwed on to the plank by metal screws. The mounting holders of the encoder onto which the plank is screwed did not have any linear accelerations in the XYZ axes. Hence, the placing of the sensor in such a manner ensures that the accelerometer stayed connected like a singular piece of the drill string and captured all its vibrating accelerations about the three axes. The mounting holders of the incremental encoder (Figure 5.13) enabled the mounting of the aluminum plank. Aluminum was chosen for its lightness in weight and strength.

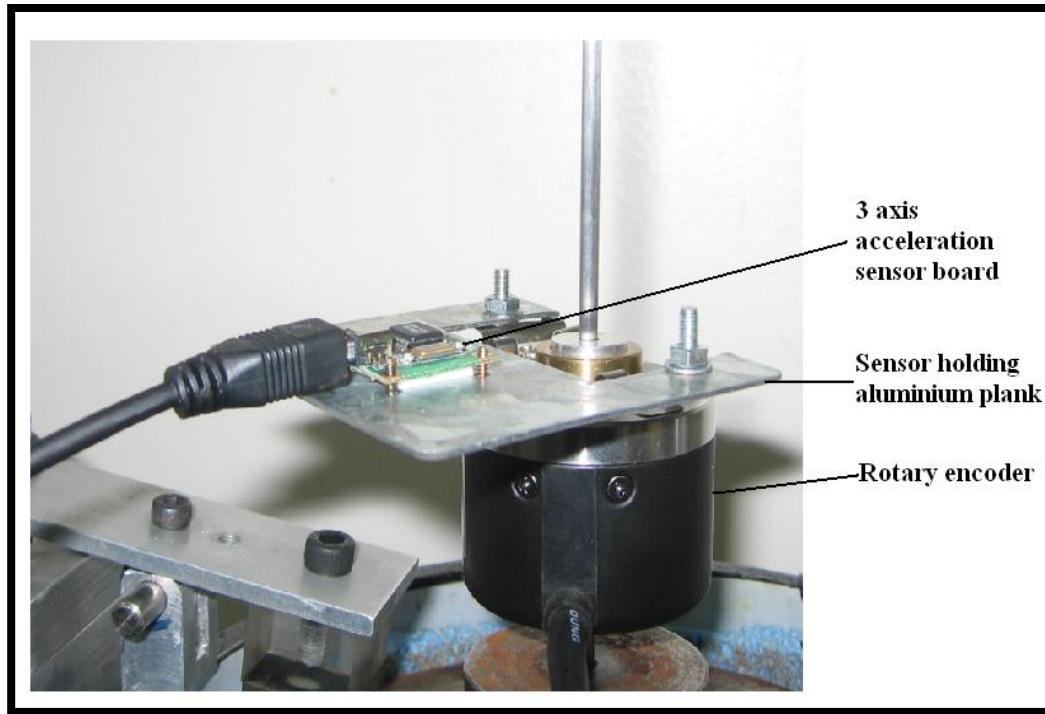


Figure 5.12: Laboratory arrangement of the acceleration sensor mounted on the incremental encoder.

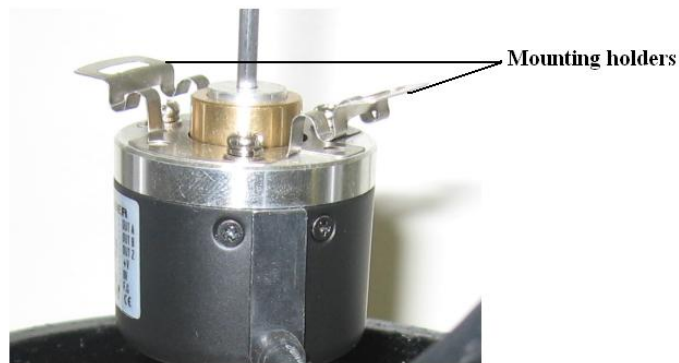


Figure 5.13: Mounting holders of the incremental encoder.

In order to analyze and log correct acceleration data, the sensor was initially configured. Configuration ensured the axes were correctly positioned in accordance with the device's placement. The device was placed where required and 'calibrate' was pressed on the 'Configuration palette' (Figure 5.14) to accept the required settings.

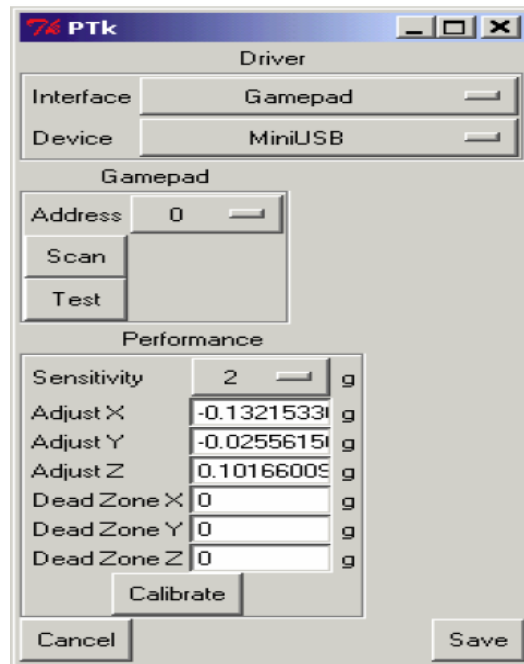


Figure 5.14: Configuration palette for the 3 axes acceleration sensor.

The acceleration data was logged using the 'data logger'. The 'data logger' window displayed the acceleration data about all three axes and the logging of data can be set to start and stop manually.

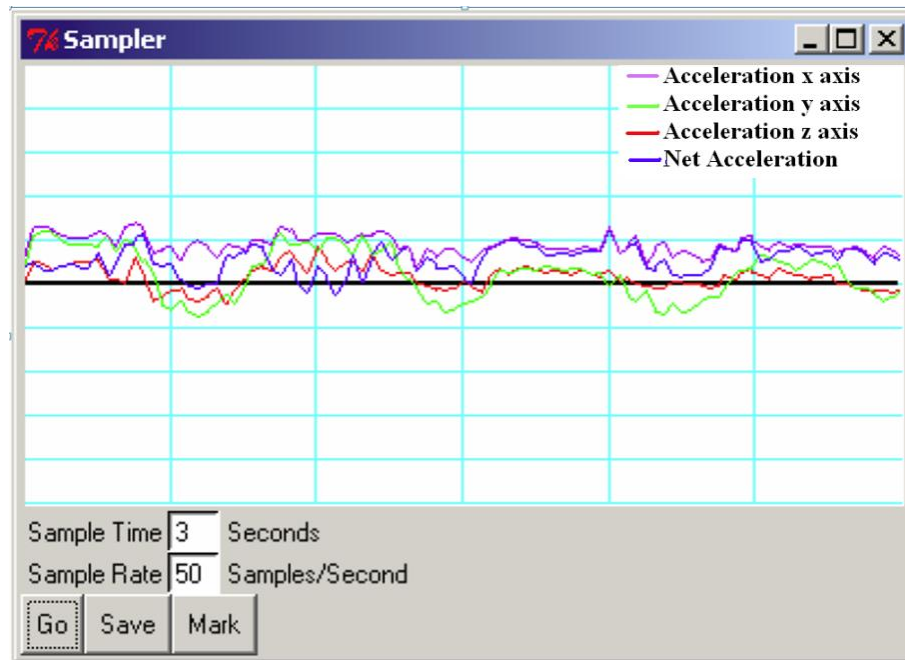


Figure 5.15: Data logging panel of the 3 axes accelerometer

Figure 5.15 displays the online logging of acceleration data. The data logger took a constant stream of readings from the device and graphed them in real-time to the screen. The sampling rate can also be adjusted by setting the time and the rate. The data logger displayed the acceleration about all three axes in various colors to ease distinction, and the median is also displayed. Hence 4 data lines are seen in the panel. The data once logged could be saved as text file for use by LabVIEW™, MATLAB®, etc. for data processing.

Chapter 6. Laboratory set-up configurations and analysis of dynamics

This chapter discusses three new configurations of the laboratory set up. These configurations are introduced to analyze various dynamics of the drill string. Configurations 2 and 3 analyzes external effects like the effect of hard brake, borehole friction and configuration 4 analyzes internal physical or inherent effects like unbalanced drill bit and critical speeds on the rotary drilling dynamics.

6.1 Analysis of drill string dynamics when effected by a hard brake

This study is concerned with analyzing the outset of torsional vibrations in a rotary drilling system.

6.1.1 Configuration 2: Hard brake implemented on laboratory set up

Torsional vibrations in drill strings have been analyzed using humped friction models by Jansen J.D and van den Steen L., (1995), Serrarens. A.F.A. et al., (1998), Navarro E. M. and R. Suarez, (2004), etc. These models represented self excited torsional vibrations present in drill string systems due to the friction between drill bit and borehole. Jansen J. D., (1995), van den Steen L., (1997) and Liene R. I., (2000) have stated that torsional vibrations in drill-string systems can be modeled using the friction model with the Stribeck effect. Mihajlovic et al. (2003) and de Bruin J.C.A. et al. (2007) have implemented experimentally the stribeck effect using a hard brake system as depicted schematically by Mihajlovic et al., (2003) in Figure 6.1.

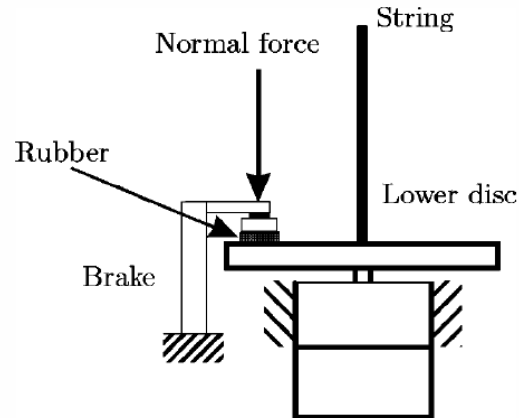


Figure 6.1: Applied normal force at the drill bit [Mihajlovic et al., (2003)].

To analyze firsthand the conclusions of the above researches, a hard brake is implemented on the laboratory set-up. Initially, a schematic of the braking arrangement was designed. The schematic also reflects the principles of implementation of the brake (Figure 6.2).

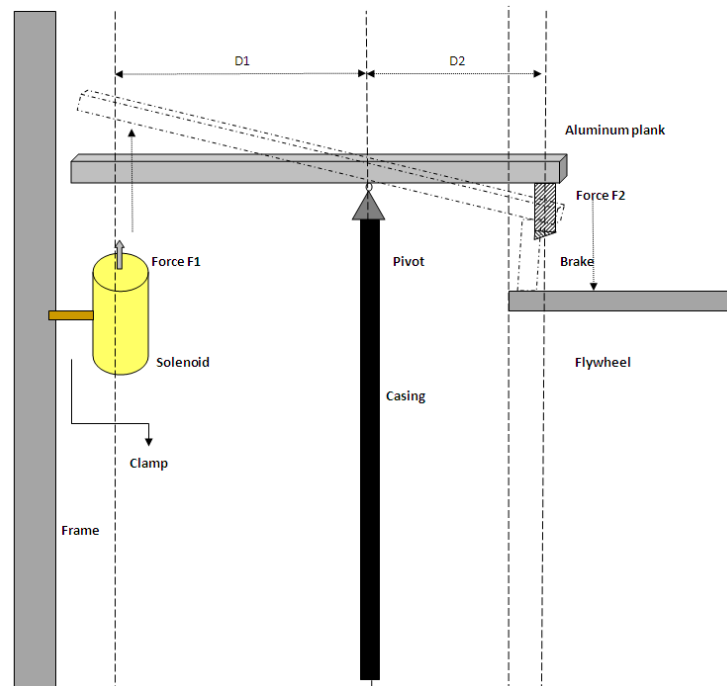


Figure 6.2: Schematic of braking arrangement.

The implementation of the hard brake required a mechanical pivot system, a linear solenoid and an accurate calculation of the braking force required to be applied. The mechanical pivot arrangement was designed and manufactured at the machine shop. The amount of the force which will induce limit cycling, the length of the metal plank, and the dimensions of the brake shoe were calculated and determined by a number of trial runs and tests. Finally, the laboratory arrangement of the hard brake was implemented as in Figure 6.3. The linear solenoid is connected to a DC power source and it gets activated and pushes the plank of the pivot arrangement up when excited over 12 volts and remains so until the excitation voltage is lowered. The position of the solenoid clamp onto the metal frame is crucial and its determination depended on the length of the brake shoe, the solenoid length and the voltage applied to it. All the experiments in this chapter are recorded at a sampling frequency of 5samples/second.



Figure 6.3: Laboratory arrangement of implementing hard brake on lower flywheel.

6.1.2 Observed dynamics: Configuration 2

This section discusses the data recorded when the hard brake is effected on the rotating drill bit. The experiments are recorded for two speeds of rotation (23 RPM and 53 RPM). The tests recorded clear limit cycling (Figure 6.4). The brake induces friction induced limit cycling and torsion in the system; however no stick slip is observed. The Figure 6.4 displays the upper rotary speed (black) and the drill bit speed (red), for the two speeds of operation. The blue and purple signals represent the difference in the upper and lower flywheel speeds. The tests conclude that the limit cycling effect induced by a hard brake do not differ much in magnitude for lower and higher speeds of rotation, assuming there is no friction between the drill bit and borehole. The tests also indicate that hard / sudden obstacles by itself are not the cause of stick slip phenomena in rotary drilling.

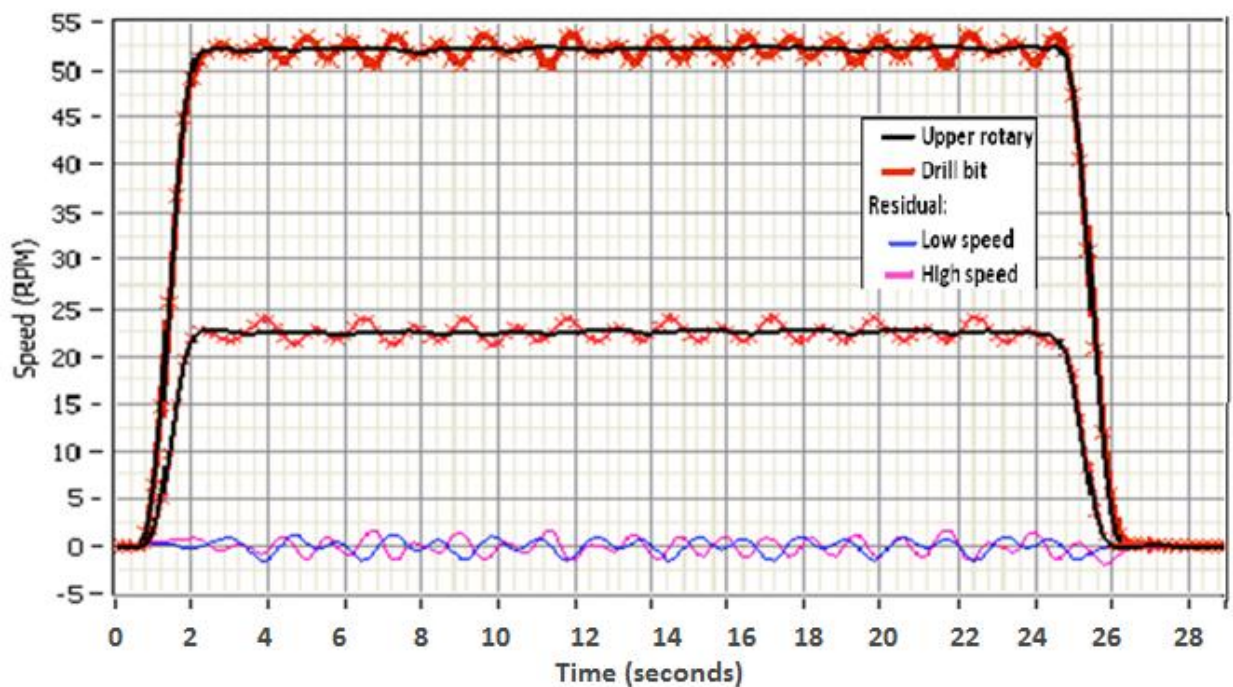


Figure 6.4: Results of hard brake tests (configuration 2).

6.2 Analysis of drill string dynamics in presence of borehole friction

This section details the observations on experiments with rubber sponge lining used to represent bore-hole friction. In the previous experiment, the borehole is assumed to impart no friction on the lower flywheel representing the drill bit. The experiments on analyzing the limit cycling dynamics are extended in this section to include the presence of borehole friction.

6.2.1 Configuration 3: Borehole friction

A rubber sponge is added as a lining to the casing surrounding the lower flywheel to represent the ‘borehole’ mud effect. The cylindrical casing with the lining is depicted in Figure 6.5. The laboratory set-up is once again operated as discussed in the previous section, with the hard brake applied by triggering the linear push solenoid. The experimental data recorded from the fly wheels are plotted in Figure 6.6 (a – d). The experiments are conducted at various operational speeds, Figure 6.6a is recorded while operating at 23 RPM. Figure 6.6b is recorded at 53 RPM. Figures 6.6c and 6.6d are recorded while operating the system at 62 and 78 RPM, respectively.



Figure 6.5: The cylindrical casing lined with rubber sponge.

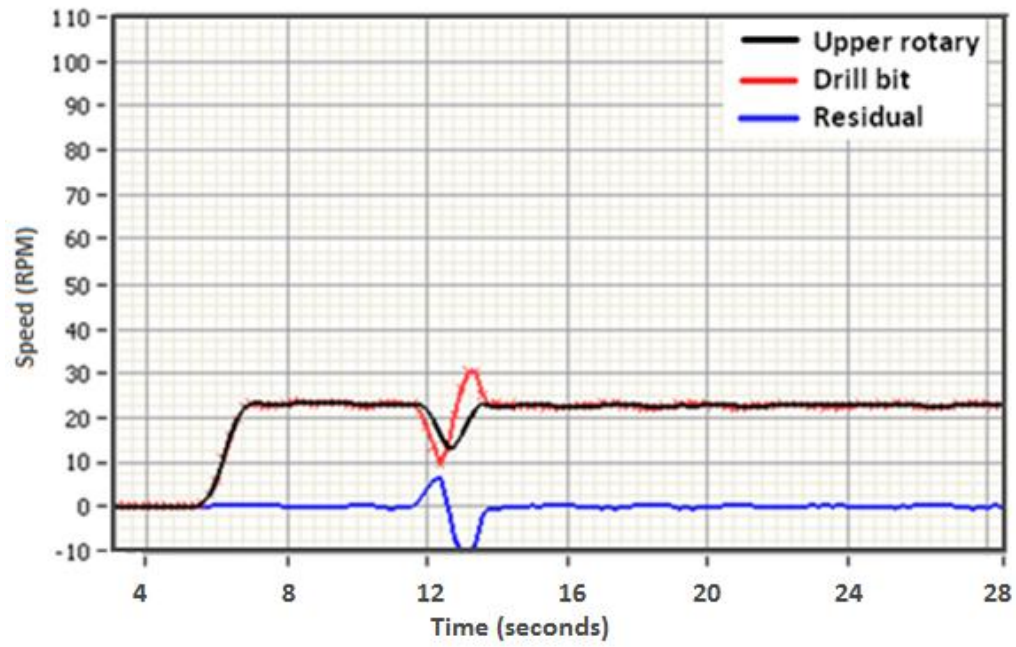


Figure 6.6a: Configuration 3 drill bit experimental response at 23 RPM.

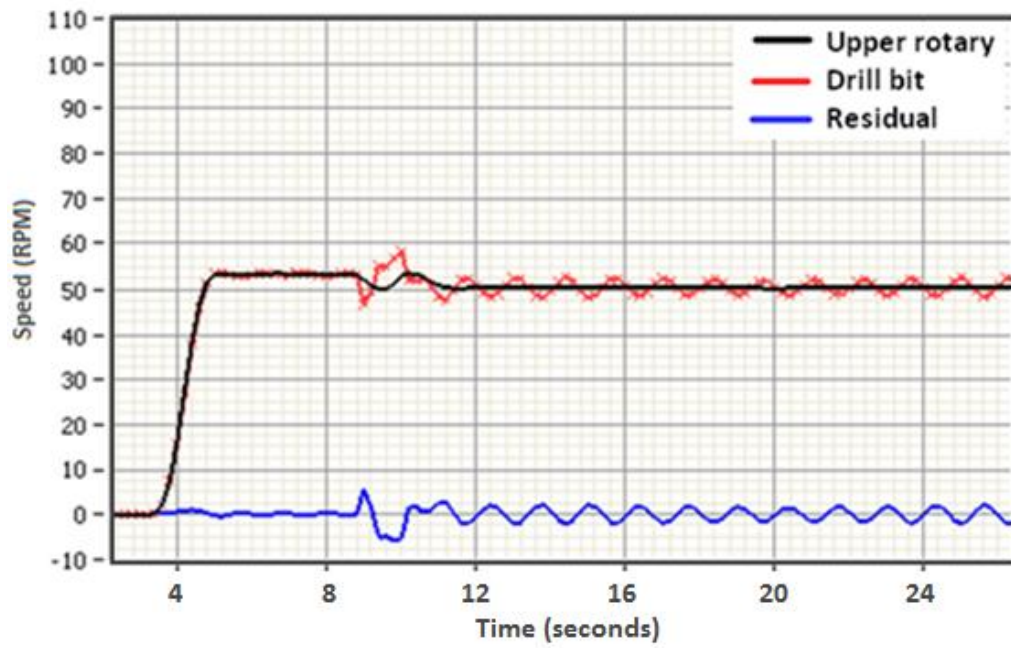


Figure 6.6b: Configuration 3 drill bit experimental response at 53 RPM.

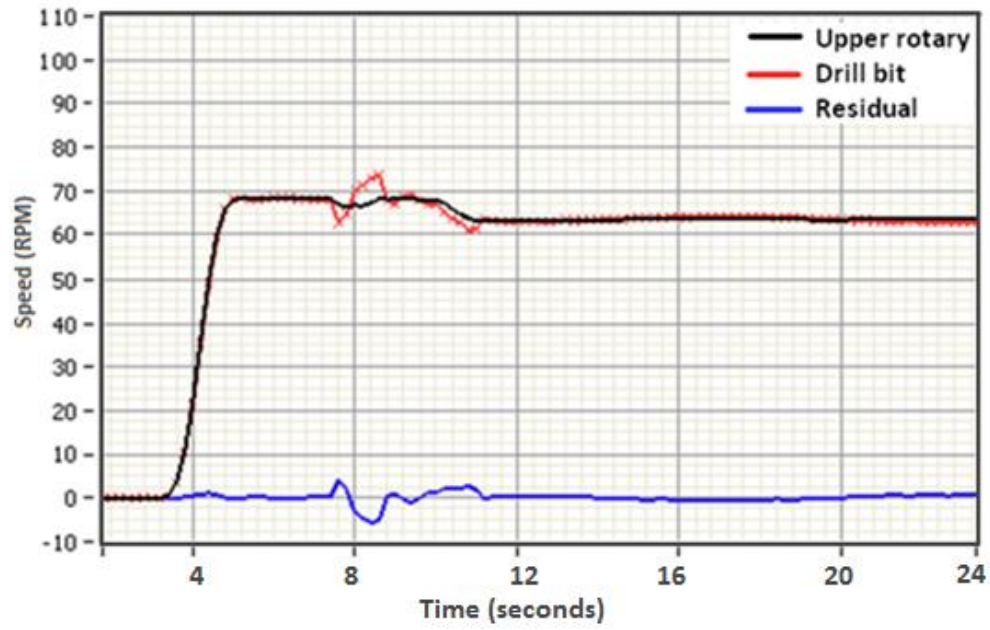


Figure 6.6c: Configuration 3 drill bit experimental response at 69 RPM.

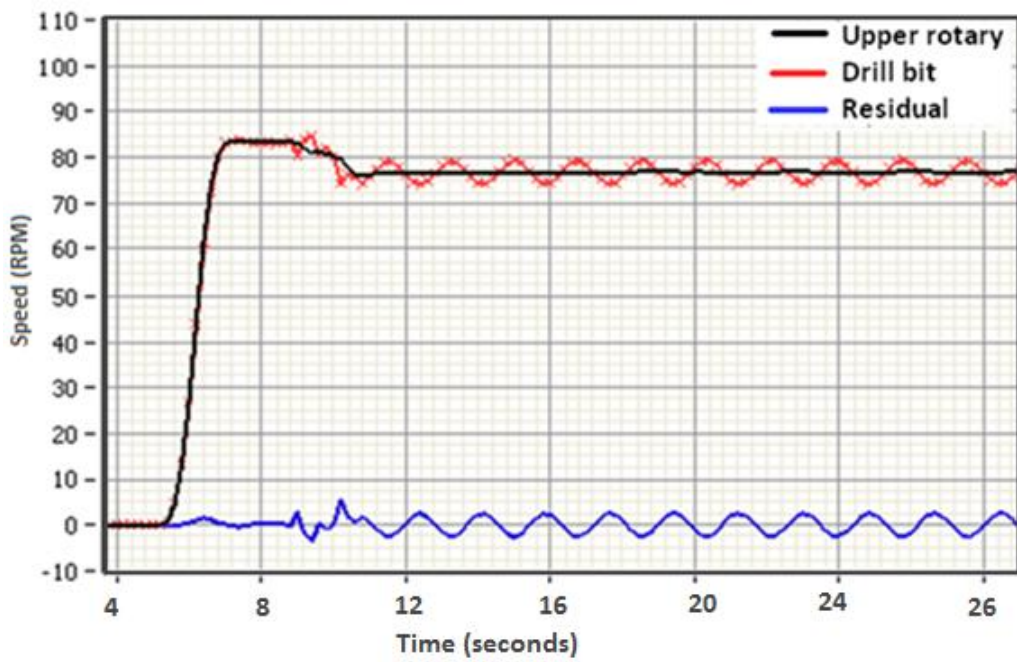


Figure 6.6d: Configuration 3 drill bit experimental response at 83 RPM.

The data recorded and displayed in Figure 6.6 (a-d) are analyzed and discussed below. The upper flywheel angular velocity is depicted in black in the plots. The lower flywheel angular velocity is depicted in red. The blue signal is the difference between the angular velocities of the upper and lower flywheels. It is noted that the limit cycling is present and noticeable at 53 and 78 RPM. However they are not visible in the 23 and 62 RPM plots though the lower flywheel was visibly whirling due to the friction effect imposed by the rubber sponge lining on the casing. Some very important remarks are noted from these experiments.

1. The limit cycling of drill bits induced due to a hard object will be present with the presence or absence of borehole friction.
2. The magnitude of the torsional vibrations resulting from limit cycling remains unaffected in the presence of borehole friction. However, lateral vibrations are aggravated in presence of borehole friction.
3. The torsional vibrations disappear at certain velocities, even though whirling of the drill bit is present. In other words, lateral and torsional vibrations of the drill bit can co exist or separate.
4. The presence of critical speeds of operation which aggravate vibrations are confirmed by these experiments.

6.3 Analysis of lateral vibrations & bit whirl

This section analyzes lateral vibrations and drill bit whirl induced by configuration 4. In the literature review, it was noted that the lateral vibrations of the drill bit are the most destructive type of vibrations affecting rotary drilling [Schlumberger, (2010), R. Mathur, (2009), J. Zare, (2011)]. They result in a phenomenon called bit whirl. This chapter investigates the causes leading to high lateral vibrations and bit whirl.

Bit whirl causes reduction of drilling efficiency, drill pipe bending and well bore hole enlargement. Hence it is the most destructive phenomenon associated with rotary drilling assemblies due to its effects of drill collar damage and borehole enlargement and resultant drastic reduction of fatigue life [Helios Spanos, (1999)].

Drill bit whirl can be due either to: (a) bend drill string or (b) an unbalanced drill bit. An inhomogeneous borehole can aggravate the conditions of whirling. The two different causes produce a similar phenomenon i.e.; the bit whirl. This chapter analyzes the drill bit whirl dynamics caused due to both the above reasons. Experimental tests are conducted and analyzed to understand the bit whirl phenomenon at various speeds.

Jansen , (1991) stated that the bit whirling phenomenon occurs when drill bits have an imbalance in the drill bit design during manufacture or when there is a slight bend in the drill collars due to high lateral vibrations. Both of these imperfections cause the lateral vibrations to be predominant and cause bit whirl at higher operational ranges [Brett et al., (1990)].

Most commercially available bits have imbalances in the range of 2 to 10 % with the 2% only for a very high commercially graded bit [Thomas Warren, (1990)]. An imbalance on the bit due to manufacture or borehole effect causes it to stray away from its center of rotation during drilling.

This will lead to high centrifugal force to be developed which increases the side loading of the bit. This results in hole enlargement and bit whirling.

Jansen, (1991) also suggested that the dynamics of a bend drill string in forward whirl can be demonstrated by an unbalanced mass on the lower bit.

The following sections demonstrate and discuss the analysis of the bit whirl dynamics. Bit whirl is induced in the laboratory arrangement by utilizing the research review presented above.

6.3.1 Configuration 4: Unbalanced Drill bit

This section discusses the data recorded during experiments on bit whirling due to an unbalanced mass on the drill bit. In the laboratory set up , an additional mass is placed on the drill bit, however, in rotary drilling rigs the commercially available drill bits have a manufacturing imbalance between 2% -10%. The drill string in the laboratory arrangement is vertical, about 1m long, and is made of carbon steel to ensure the material properties are as close as possible to the actual rig. An unbalanced mass is added to the flywheel representing the drill bit (Figure 6.7). Unbalanced rotors are used to represent an eccentric drill pipe in the research of Dykstra, (1996) and Liao, (2008).

Dykstra et al., (1996) conducted tests on drill collars and studied the effects of lateral shocks and backward whirl. The discussion was based on the fact that the source of vibration is the bit and hence the centrifugal forces developed when an unbalanced drill string is rotated can be one of the major sources of vibrations. Liao et al., (2009) developed a reduced order model for a drill string system with a mass imbalance on the rotor. The tests were focused to analyze the trajectory of the bit for various mass and angular velocities while displaying bit whirl and stick slip characteristics.

In order to analyze the above discussions on lateral vibrations, various tests with different WOBs and operational velocity of the rotary table were conducted. Further to suggestions by Warren, T., (1990) on drill bit imbalance presented earlier, tests are conducted with various unbalanced mass conditions.

Figure 6.8 (a-c), displays the plots of the command speeds applied to the system, the angular velocity data of the upper rotary and lower bit for the three unbalanced mass cases discussed below. The angular velocities are displayed and analyzed in contrast to angular positions, because the vibration information is clearer and the behavior of the drill string at the lower bit in the x-y plane can be better analyzed in this manner.



Figure 6.7: Laboratory set-up configuration 4 with unbalanced mass.

Case1: Ideal (no unbalance) condition

Initially the drill string system is allowed to rotate freely (zero unbalanced mass). In this state the system can be compared to the state when the drill string rotates and there is no unbalance on the drill bit. At operational speeds of around 8 RPM, there existed some vibrations (Figure 6.8a). These can be termed as self excited vibrations, which arise in rotary drilling at very low speeds. However it can be noted that when the speed is increased to around 36 RPM, the self

excited vibrations disappear and vibrations similar to limit cycling appear. At a speed of 51 RPM, the drill string now rotates smoothly with lesser limit cycling and self excited vibrations.

The average speed of the drilling is at 50 – 60 RPM. Analyzing the graphs for case 1 angular velocity data, it is noted that the drill string system lags behind the command speed required to be followed at lower speeds of 8 RPM and almost reaches up to the command speed at 51 RPM. This deficiency at low speeds can be attributed to power dissipation in the elements. It is seen that the drill string upper and lower velocities followed the command speed more closely at higher speeds due to the fact that the power received by the system is much higher than the power dissipated in the system.

Case 2: Small Unbalanced Mass Condition

Based on research conclusions in Jansen, (1991) and Warren T., (1990), an unbalance of 2.6% of drill bit mass (28g) is added to the lower rotor to represent an unbalanced drill bit. During experiments, it was observed that the drill string upper and lower velocities follow the command speed better than in the ideal condition (Figure 6.8). It was also noted that the self excited vibrations appear similar to case 1 when rotated at low speeds, but they were less prominent due to the higher mass of the bit. The increased unbalanced mass on the drill bit forced the drill bit from rotating away from the center of rotation, and vibrations of the self excited type were minimized. This could provide an explanation for the use of drill collars in the drilling rig to provide increased weight for the bit. As the operational speed was increased to 50 RPM, the system now rotated at a speed slightly higher than the command speed, this could be attributed to the increase in nonlinear properties (discussed in following section 6.3.2) of the drill string with an unbalanced mass addition.

Case 3: High unbalance condition

The unbalanced mass added to the lower rotor was further increased to 5.2% and now a 56 g mass rested on the bit. The drill string followed the command speed closer at a speed of 39 RPM, but rotated at higher speeds when operated at speeds of 50 RPM- this could be due to increased nonlinearity (section 6.3.2). Limit cycling vibrations were more prominent, and whirling was noticed at higher speeds (Figure 6.8). This whirling could change to stick slip in presence of increased friction between the well bore and lower bit.

The next section briefly analyzes some characteristic nonlinear properties exhibited by the system with unbalanced mass.

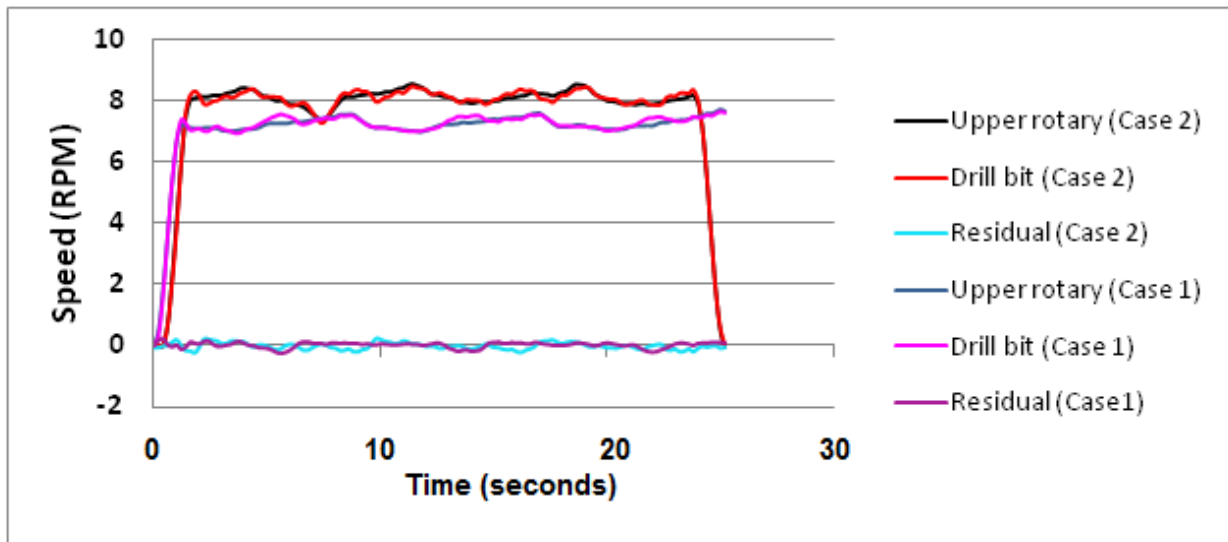


Figure 6.8a: The command speeds and the responses of the laboratory set up configuration 4 at low speed of operation.

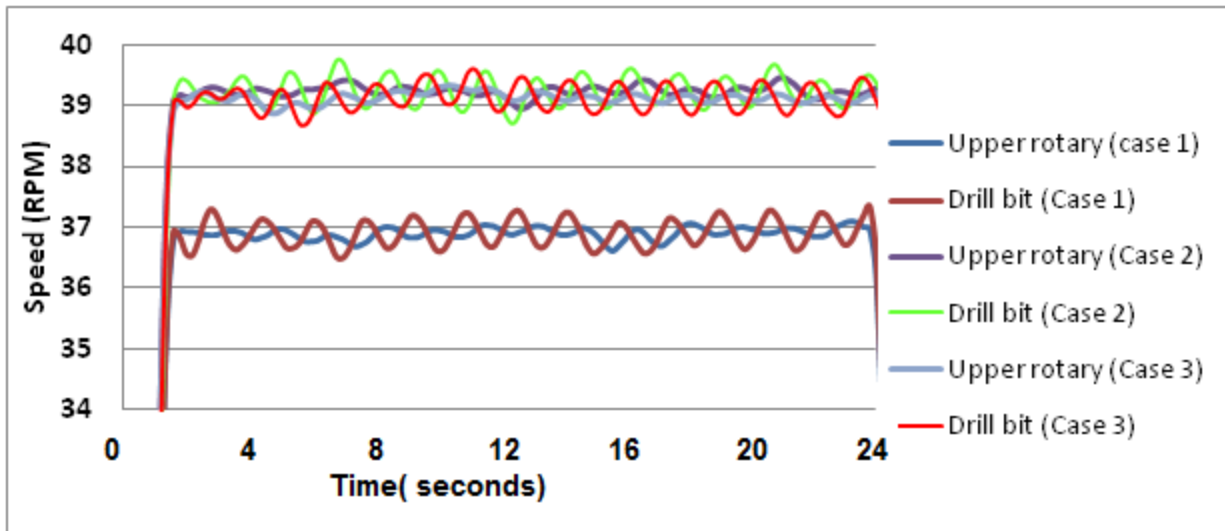


Figure 6.8b: The command speeds and the responses of the laboratory set up configuration 4 at average speed of operation.

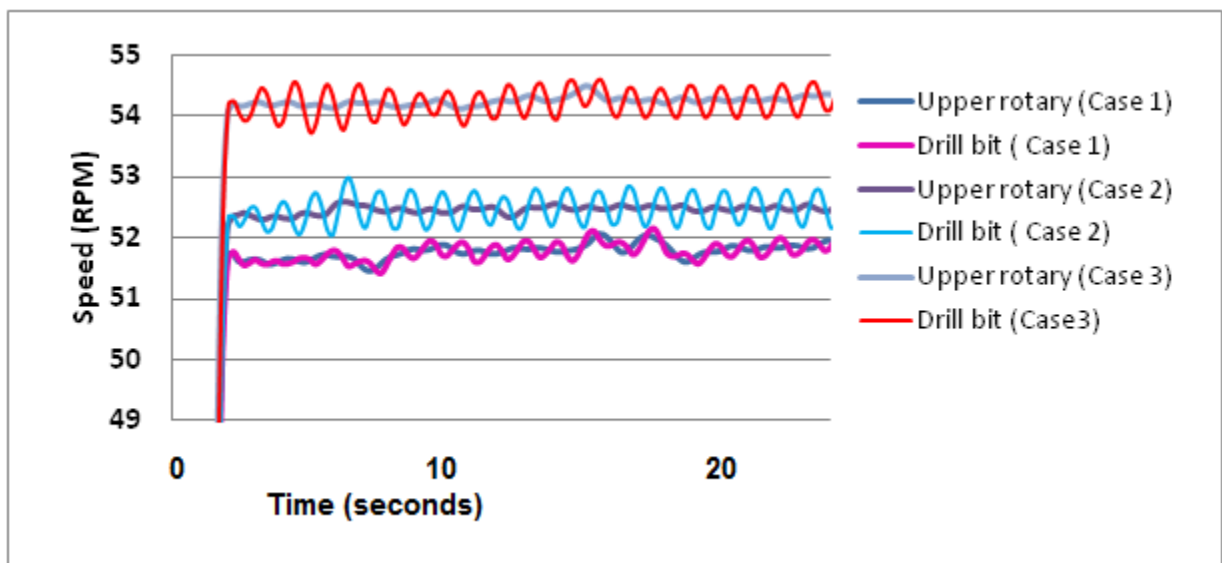


Figure 6.8c: The command speeds and the responses of the laboratory set up configuration 4 at high speed of operation.

6.3.2 Analysis of the nonlinear characteristics presented by laboratory set up configuration 4.

This section details the analysis of non linear properties exhibited by the laboratory system with unbalanced mass addition. Nonlinear characteristics of the system are analyzed to get a thorough understanding of the system for model identification and controller design purposes.

Case 1: Minor Change In Initial Condition: Frequency

This section presents analysis of the system behavior for a minor change in input frequency signal for ideal and unbalanced mass conditions. Figure 6.9a displays the system input to observe system response when affected by a change in the frequency of applied input signal under zero mass unbalance condition. The residual signal from the system is plotted in Figure 6.9b. It was noticed that there was no major erratic behavior displayed by the system in this case. The pattern of vibration was the same and there was only a slight change in the magnitude of the residual.

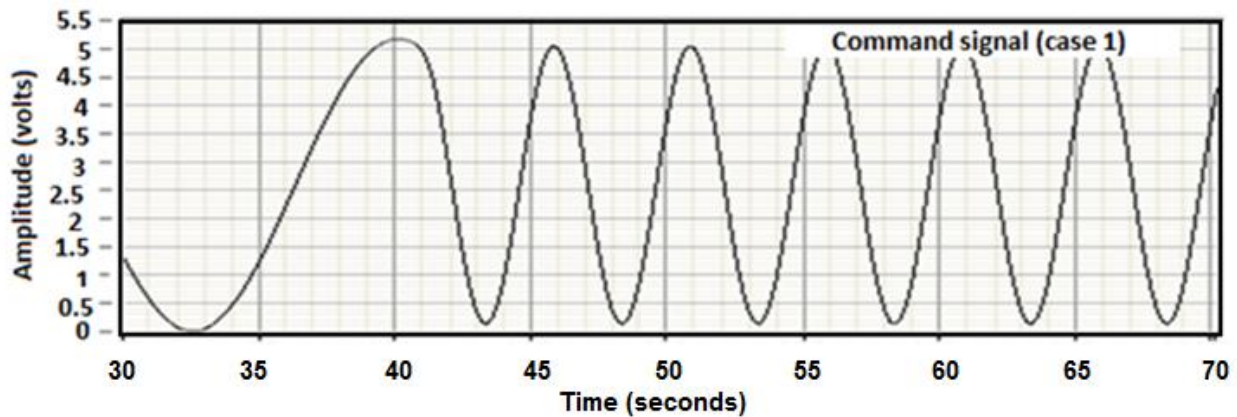


Figure 6.9a: Command signal applied to test configuration 4 laboratory set-up for nonlinear characteristics. (Case 1)

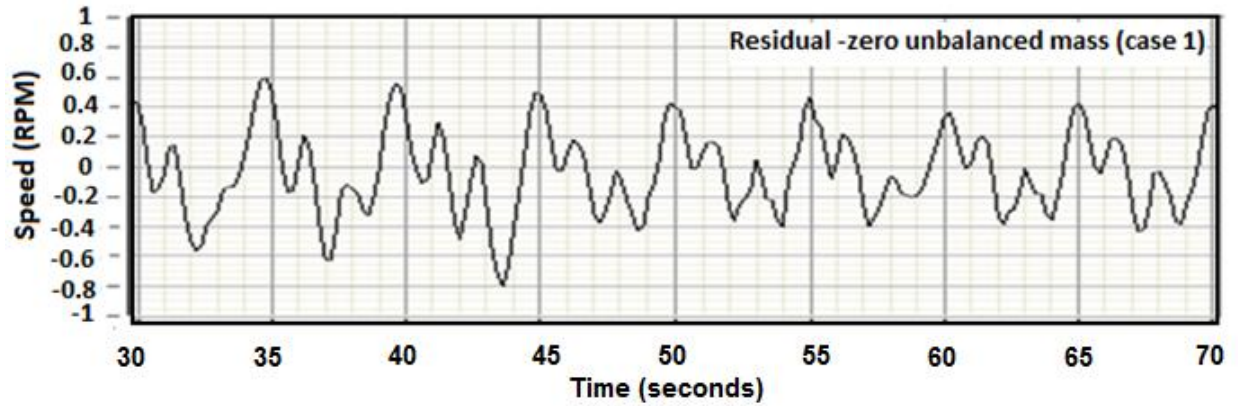


Figure 6.9b: Residual signal under zero unbalanced mass on drill bit.(Case 1)

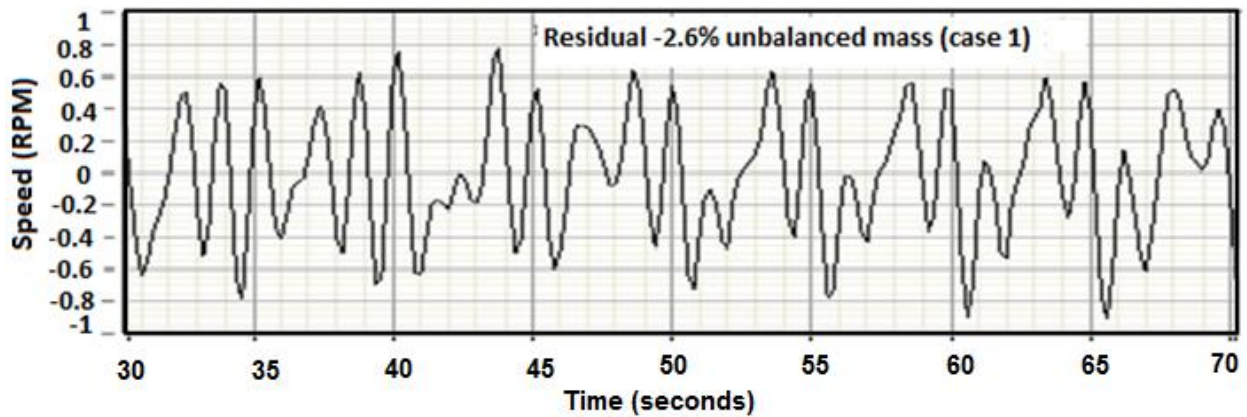


Figure 6.9c: Residual signal obtained with 2.6% unbalanced mass on drill bit. (Case 1)

Figure 6.9c displays the residual signal plot for the system when the input signal frequency is changed under a mass unbalanced condition. It was noted here, that now the pattern of the residual signal had changed with a slight change in magnitude. This implied that the vibration pattern of the lower bit when compared to the upper rotary has changed. This change in residual implied the increase of nonlinear properties exhibited by the drill string in the presence of the unbalanced mass. Drilling with unbalanced drill bit lead to in-homogenous boreholes and this will lead to higher eccentric paths and increased nonlinear characteristics of the drill string as drilling progressed.

Case 2: Minor Change In Initial Condition: Magnitude

This section presents an analysis of the drill string system behavior under ideal and unbalanced mass conditions, when a slight change in magnitude is made to the input command signal. Figure 6.10a displays the input signal to the system to analyze system response to a magnitude shift of the applied input signal. A command speed of 50 RPM was applied to the drill string system, and a shift to 52 RPM was made at a time approximately 21st second. The residual signal obtained from the system under zero unbalanced mass on drill bit condition is plotted in Figure 6.10b. It was noticed that the residual initially decreased in magnitude slightly, but returned to the original magnitude soon and there was no evident change in vibration pattern.

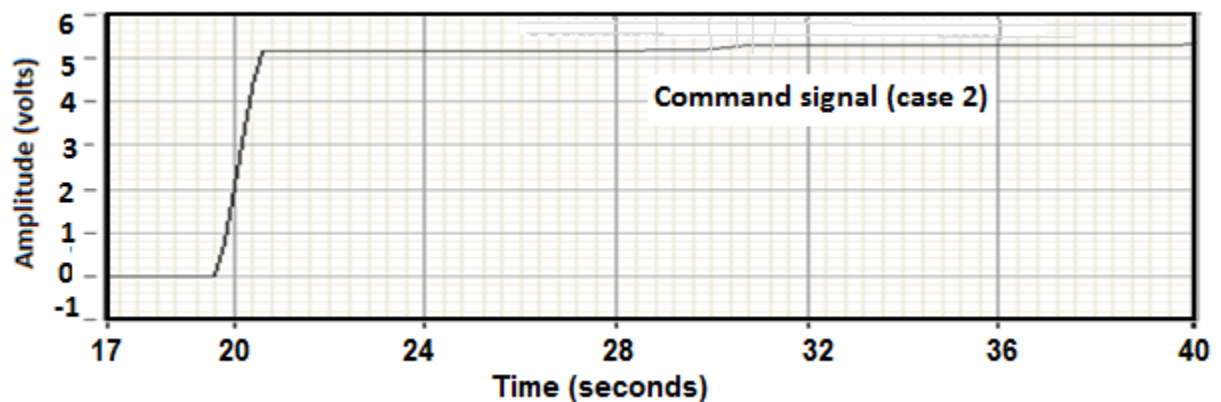


Figure 6.10a: Command signal applied to test configuration 4 laboratory set up for analyzing nonlinear characteristics (Case 2)

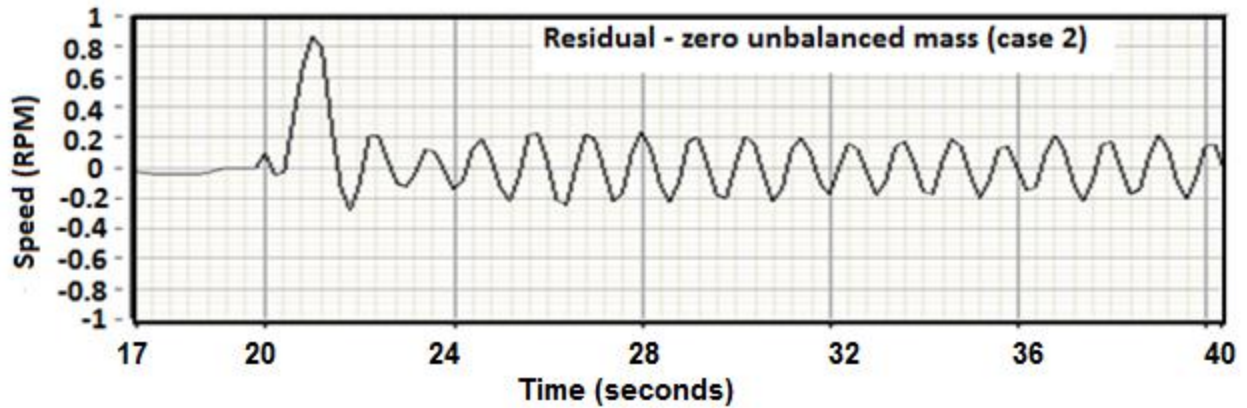


Figure 6.10b: Residual signal obtained under zero unbalanced mass condition (case 2)

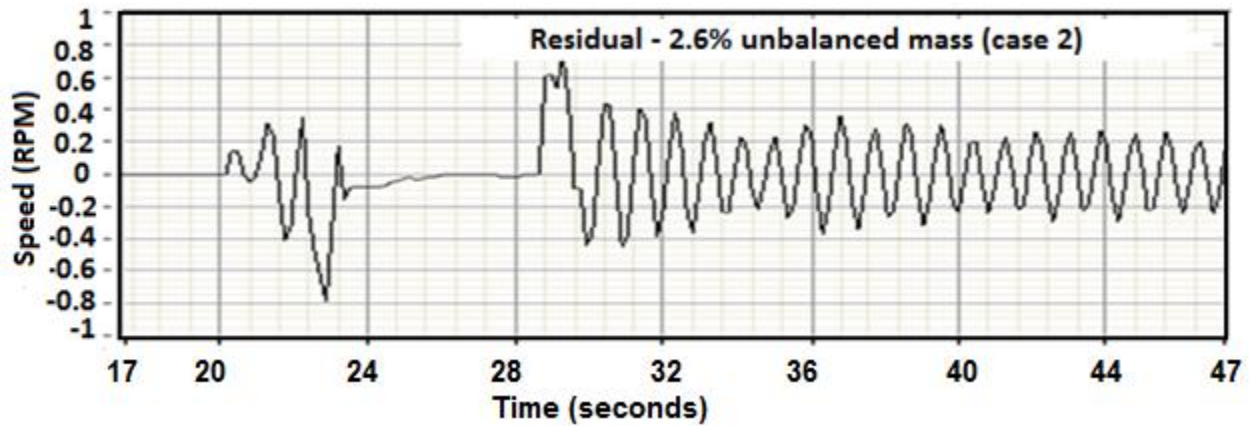


Figure 6.10c: Residual signal obtained under 2.6% unbalanced mass condition (case 2)

The command signal and the residual plots for the system when the input signal magnitude was changed slightly under unbalanced mass condition are plotted in Figure 6.10c. Analyzing the residual plot (Figure 6.10c), it was seen that following a delay of around 6 s to follow the command, the residual signal displayed a slight decrease in magnitude and did not return to the previous magnitude or pattern of vibration. These experiments proved the onset of nonlinear properties in the laboratory configuration with the addition of unbalanced mass on the drill bit.

Chapter 7. Identification of mathematical model:

Configuration 1

The mathematical model of any system or process is a set of mathematical equations which efficiently describe the behavior of the system /process. The better mathematical model should be simple and yet incorporate the major features of the process. There are two major methods well known in literature for defining the mathematical model of any system. They are:

Analytical modeling: Development of a mathematical model for a system using equations of physics and laws of motion. This process involves a number of assumptions to simplify the physics involved.

System identification: Identifies the mathematical model of the system using the input output data and fits a predefined model structure to the data.

A combination of the above: some mathematical models are developed using a part of the system developed analytically and a part identified and combined to get the overall model.

Since the physics involved in rotary drilling is inherently non-linear, recourse to modeling is inevitable to compensate for the lack of detailed dynamic information available on the drill string dynamics. Most of the models developed for representing drill string dynamics and similar laboratory set-ups, have been based on assumptions. The numerical simulations of the developed models are mostly validated by experimental data. Hence, the lack of a coherent model in the literature that is free from unwarranted assumptions makes it difficult to accurately assess the nature of drill string vibrations and thereby to get a clear overview of the applicability of the control options available. This chapter develops a mathematically identified dynamic model that

permits control of the approximations involved, is not computationally over expensive and has the potential to accommodate the many complexities of a realistic drilling assembly.

Most of the researchers in drill string dynamics modeling have depended on mathematical models derived by analytical modeling [E.M.Navarro, (2005), J. D. Jansen et al., (1995) and Jansen and van den steen, (1995)]. But the analytical modeling method has the disadvantage of many assumptions. The model will eventually fail to capture all the modes of the system and hence leads to less accurate models on which to base the further researches and experiments. N. Mihajlovic, (2004) used the method of parameter estimation to arrive at the model. They have used angle data to derive the model, and there is no detailed explanation of how to predefine a model structure, the process of identifying the selected model, and the criteria used for it.

In this chapter, an auto regressive moving average exogenous model of the drill string (ARMAX) is identified by the least squares based parameter estimation approach of system model identification. The identification method is also known as Black box modeling. The method of Black box modeling presented here is void of assumptions and dependent only on actual process data and the method can be extended easily to any physical or real process. Section 7.1 presents an overview of the system identification process and its major steps. Section 7.2 gives a brief description of the ideal drill string dynamics presented by configuration 1. Section 7.3 describes the procedure to develop the mathematical model by the system identification method. Section 7.3 is divided into various subsections which explain each of the stages of model identification of configuration 1 are laid out briefly in section 7.1 with experimental results, tables, and plots. The identification for non linear system, represented by configuration 4 set-up is discussed in the following chapter 8.

7.1 System identification Method

Every identification process consists of a series of basic steps.

1. Collecting information about the system.

Relevant information from the system required for the identification process are its input and output data. All the system modes should be excited to get data which reflects the system well. A pseudo random binary sequence (PRBS) or Swept sine wave is normally used to excite all the system modes. Once the data are obtained, it should be cleared of all the mean values and de-trended. Any noise present in the data should be filtered out.

2. Selecting a model structure to represent the system.

A choice should be made within all the possible mathematical models that can be used to represent the system. There are many types of models:

- **Parametric versus nonparametric models:**

In a parametric model, the system is described using a limited number of characteristic quantities called the parameters of the model. In a nonparametric model, the system is characterized by measurements of a system function at a large number of points. Examples of parametric model are the transfer function of a filter described by its poles and zeros and the equations of motion of a piston. An example of a nonparametric model is the description of a filter by its impulse response at a large number of points.

- **White box models versus black box models:**

In the construction of a white box model, physical laws whose availability and applicability depend on the insight and skills of the experimenter can be used (Kirchhoff's laws, Newton's

laws, etc.) Specialized knowledge related to different scientific fields may be brought into this phase of the identification process. The Black box approach extracts the coefficients for the pre defined model structure from the data. Instead of making a detailed study and developing a model based upon physical insight and knowledge, a mathematical model is proposed that allows sufficient description of any observed input and output measurements. This significantly reduces the modeling effort.

- **Linear models versus nonlinear models:**

In real life, almost every system is nonlinear. However, nonlinear systems are mostly approximated by linear models, assuming that in the operation region the behavior can be linearized. This kind of approximation makes it possible to use simple models.

Choosing the model parameters – Model development.

The model parameters like model order, model coefficients, etc are chosen by application of methods like least squares, pole zero graphs, correlation graphs, etc.

3. Validating the selected model.

Model validation is an important part of good modeling. Usually model validation is done by comparing the identified model simulations and experimental system responses. The developed model is said to be validated if there is a good match between the responses.

If the system needs feedback a controller has to be chosen, too. The available measurements are controller input and output, system input and output, in other words, reference signal, control signal, measured control signal, and all degrees of freedom. The control signal and the measured control signal can differ because of saturations and noise.

7.2 Ideal drill string dynamics (Configuration 1)

The dynamics of a drill string in the presence of well bore friction is highly nonlinear. The nonlinearities of the system usually lead to what is known as limit cycling. Ideally, with no wellbore friction and assuming the drill string remains straight, the drill string system can be modeled as a two degree of freedom linear system. However, in the presence of wellbore friction, curved/inclined boreholes or unbalanced weight on bits (WOB), the dynamics of the system become more complex and the number of degrees of freedom increases to 5. The drill bit centerline will also deviate from the vertical axis under the effect of centrifugal forces causing the drill string to bend. As the first stage of the model identification procedure, the experimental model is an idealized one with no borehole friction (configuration 1).

To investigate the dynamics exhibited by the drill string in an ideal drilling environment, the drill string is made to rotate free. Due to assumption of the non existence of friction between lower disc and casing, this set-up (configuration1) represents an ideal frictionless (between the drill bit and borehole) rotary drilling prototype. Figure 7.1 displays a schematic of the dynamics of the system and Figure 7.2 is a flow chart representation of the system identification procedure. All the experiments are recorded at a sampling frequency of 5samples/second.

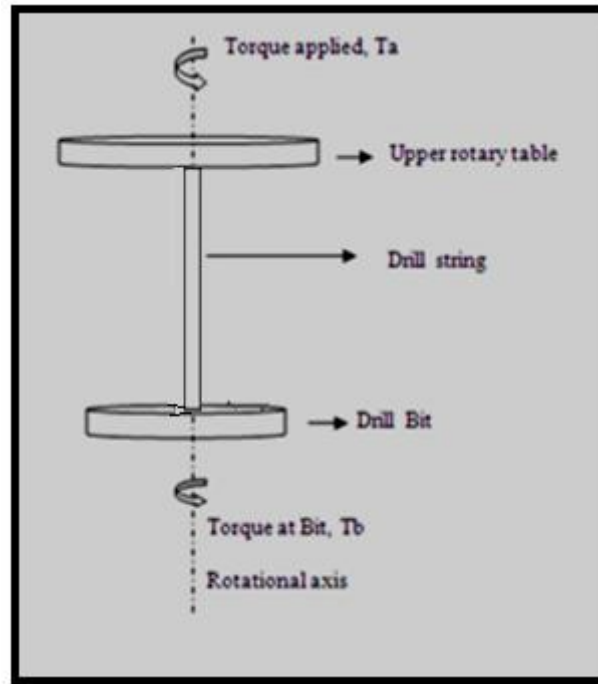


Figure 7.1: Schematic of ideal drill string dynamics

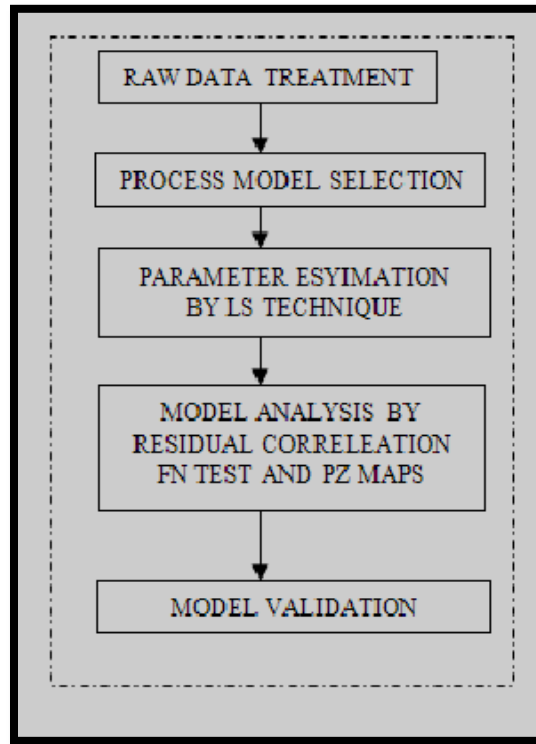


Figure 7.2: Flow chart of the system identification procedure.

The next sections describe and expand the steps discussed above to identify a suitable model for the ideal rotary drilling system. The identification procedure starts with data acquisition (discussed in chapter 5) and is completed with discussion on the identified model validation.

7.3 The Black box model identification of rotary drilling process

System identification is a linear regression technique used in controls theory. It allows a representative model of the system to be developed by systematic selection of model order and using regression analysis to solve for the algebraic coefficients in the model. This approach can be applied online in real time when the drilling operation is being done with the minimal disturbance to the system because this involves exciting the system with a PRBS or white noise input. The method can be easily extended to complex and multiple input multiple output processes without increasing the complexity of the approach. Unlike analytical modeling, this method makes use of very few assumptions and depends on the data directly obtained from the process.

The steps detailed in section 7.1 are followed to identify a model for the process.

7.4 Collecting useful data from the process.

Consider a linear single input single output (SISO) system; the system can be described by the equation,

$$Y(s) = G(s)U(s) \tag{7.1}$$

where $Y(s)$ and $U(s)$ are the Laplace transforms of $y(t)$ and $u(t)$, the output and input respectively to the process at any time t , and 's' is the Laplace variable.

And $G(s) = \frac{B(s)}{A(s)}$, where 'B(s)' and 'A(s)' are the numerator and denominator of the transfer function of the process model $G(s)$. Zero noise /disturbance input is assumed. (Refer schematic in Figure 7.5)

In discrete terms, (1) can be rewritten as:

$$y(k) = \frac{z^{-m}(b_1 z^{-1} + b_2 z^{-2} + \dots + b_n z^{-n})}{1 + a_1 z^{-1} + \dots + a_n z^{-n}} u(k) \quad (7.2)$$

$$y(k) = z^{-m} \frac{B(z^{-1})}{A(z^{-1})} u(k) \quad (7.3)$$

at any sampled instant k .

Here

$$B(z^{-1}) = \sum_{k=1}^n (b_k z^{-k}) \quad (7.4)$$

and

$$A(z^{-1}) = 1 + \sum_{k=1}^n (a_k z^{-k}) \quad (7.5)$$

where n is the process model order and m is the system time delay.

Assuming z^{-p} as a delay operator such that, $z^{-p}u(k) = u(k - p)$; for any constant p ;

Multiplying out equation 7.2 gives;

$$y(k) = b_1 u(k-1) + \dots + b_n u(k-n) - a_1 y(k-1) - \dots - a_n y(k-n) \quad (7.6)$$

Equation (7.6) is now in the form of a difference equation. It relates the process output $y(k)$ at k^{th} sampling instant to the past values of the system inputs u and outputs y and their respective weighting parameters.

The above equations can be represented in matrix form as

$$Y = \Phi \beta \quad (7.7)$$

Where Y is the vector of the output of the process at any instant k ;

Φ is the matrix of the past values of inputs and outputs

$$\Phi = [-y(n), \dots, -y(1); u(n), \dots, u(1)] \quad (7.8)$$

and β is the matrix of the parameters/ weighting coefficients of the past values of outputs and inputs.

$$\beta = \begin{bmatrix} a_1 \\ \cdot \\ \cdot \\ \cdot \\ a_n \\ b_1 \\ \cdot \\ \cdot \\ \cdot \\ b_n \end{bmatrix} \quad (7.9)$$

In order to get good estimates of the model coefficients, the process must be excited by a sufficiently "rich" signal. This ensures that all the modes of the system are excited. Usually a PRBS or a chirp signal is used to excite the system to extract data used for the identification process. These signals are very similar in properties and correlation graphs to white noise. When injected online to a process, they affect the operation of the system minimally and also allow exciting the modes of the system so that no useful information is lost. In this research, a swept sine wave, also known as the chirp signal, with frequency varying from 0-10 Hz is used as the excitation signal. The chirp wave excites all the modes of the system and is ideal for using for system identification purposes. The signal has a frequency variation from 1 Hz to 10 Hz, amplitude of 5 Vp-p, and time span of 3 seconds. The front panel of the LabVIEW™ VI showing the stimulus signal developed in the lab is displayed in Figure 7.3.

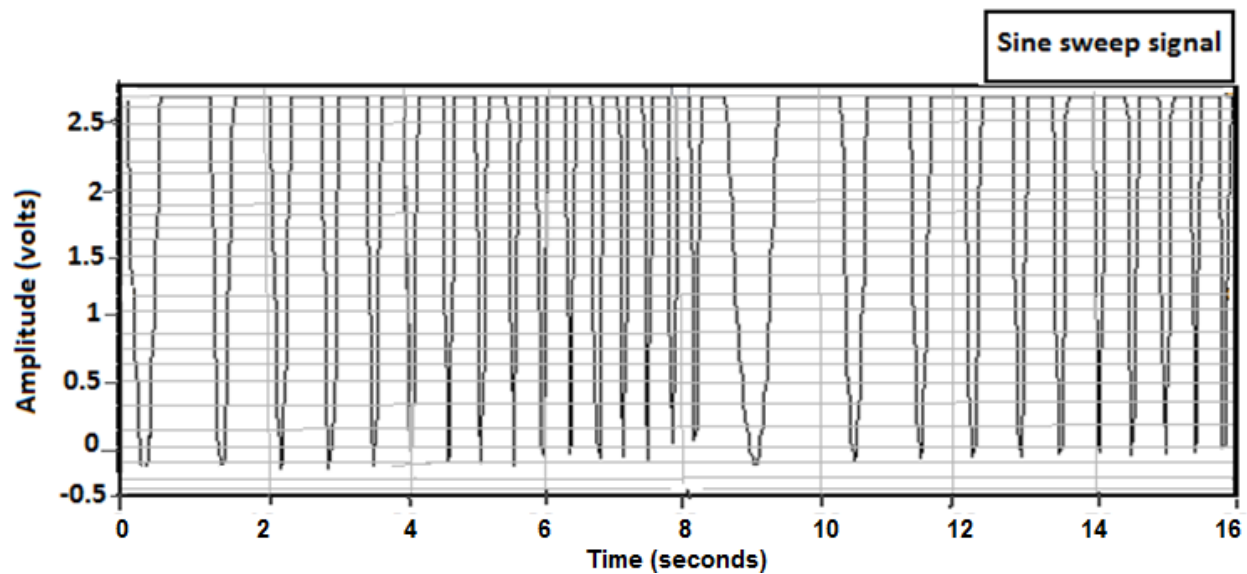


Figure 7.3: Excitation signal applied to the drill string set-up.

As part of data processing for quality data, it has to be checked for mean values, noise, trends, etc. The measured input and output data are raw and need to be normalized and de-trended to ensure quality data to get good estimates.

The mean level can be removed from the raw data by calculating

$$u_m(t) = u(t) - \tilde{u} \quad , \quad (7.10)$$

And

$$y_m(t) = y(t) - \tilde{y} \quad (7.11)$$

Where $u(t)$ and $y(t)$ are the raw input and raw output,

$$\tilde{u} = \frac{1}{N} \sum_1^N u(t) \quad (7.12)$$

And,

$$\tilde{y} = \frac{1}{N} \sum_1^N y(t) \quad (7.13)$$

are the mean of the input and output, and N is the data length.

The input data matrix transpose is,

$$u = [u(1), u(2), \dots, u(N)] \quad (7.14)$$

And the output data matrix transpose is

$$y = [y(1), y(2), \dots, y(N)] \quad (7.15)$$

The data obtained experimentally may have some drift in it. Slight drifts in data could be due to low frequency noise disturbance added to the system during data acquisition. De-trending ensures the data is drift free. It is an essential part of the identification procedure because, data in which there is slight drift can results in unstable models.

The linear trend is removed by the operation as follows;

$$u_d(t) = u(t) - A\theta_u, \quad (7.16)$$

And,

$$y_d(t) = y(t) - A\theta_y \quad (7.17)$$

Where,

$$A = \begin{bmatrix} 1/N & 1 \\ 2/N & 1 \\ \cdot & \cdot \\ \cdot & \cdot \\ \cdot & \cdot \\ (N-1)/N & 1 \\ 1 & 1 \end{bmatrix} \quad (7.18)$$

$A\theta_u$ and $A\theta_y$ are the least squares fits for u and y respectively.

The process of removing the trend from the input and output is also called the remove trend operation. The input and output data are the speeds of the upper disc and lower disc respectively.

7.5 Selecting a model structure to represent the system.

The next step in the identification process is to choose an appropriate model structure. In general, the process can be modeled as consisting of a process model and a noise model. Assuming the added noise is uncorrelated white noise, the noise model will represent any colored noise in the data.

Some of the popular model structures are:

Auto regressive exogenous (ARX) model:

$$y(k) = z^{-m} \frac{B(z^{-1})}{A(z^{-1})} u(k) + \frac{1}{A(z^{-1})} e(k) \quad (7.19)$$

Auto regressive exogenous moving average (ARMAX) model:

$$y(k) = z^{-m} \frac{B(z^{-1})}{A(z^{-1})} u(k) + \frac{C(z^{-1})}{A(z^{-1})} e(k) \quad (7.20)$$

Box Jenkins (BJ) model:

$$y(k) = z^{-m} \frac{B(z^{-1})}{F(z^{-1})} u(k) + \frac{C(z^{-1})}{D(z^{-1})} e(k) \quad (7.21)$$

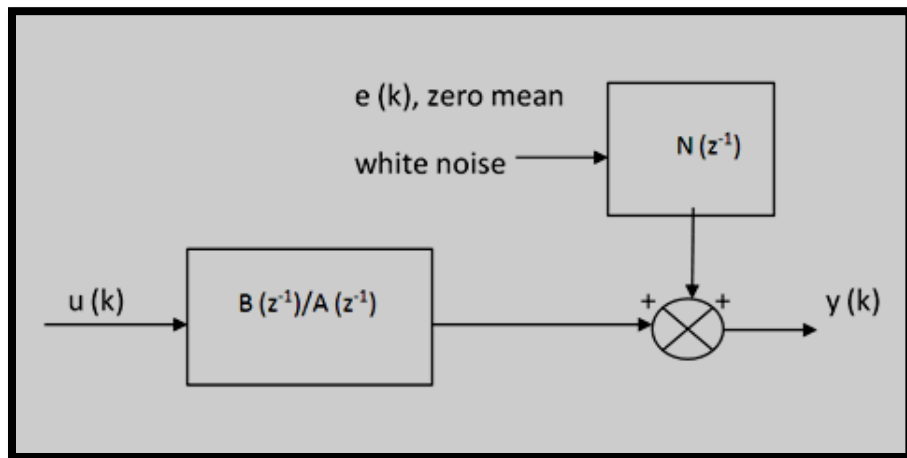


Figure 7.4: Schematic of Process and noise models.

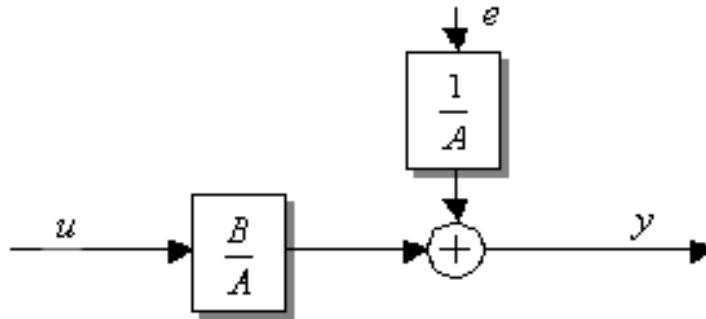


Figure 7.5: Schematic describing ARX model.

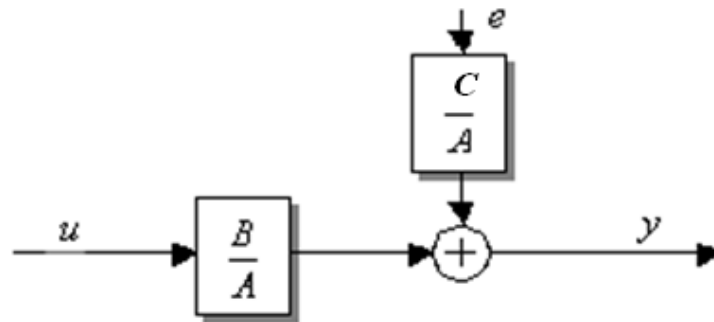


Figure 7.6: Schematic describing ARMAX model.

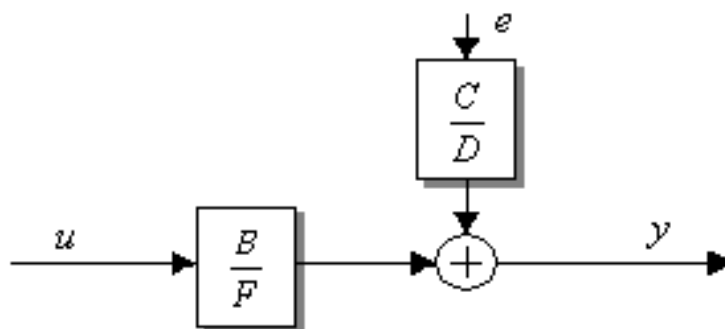


Figure 7.7: Schematic describing Box Jenkins model.

In the above schematics (Figures 7.4 – 7.7), $\{u(k)\}$ and $\{y(k)\}$ are the input and output sequences of the system, respectively, $\{e(k)\}$ is an uncorrelated white noise sequence with zero mean, and $A(z)$, $B(z)$, $C(z)$, $D(z)$ and $F(z)$ are polynomials of known orders (na, nb, nc, nd, nf), while m is the time delay.

The unit backward shift operator z^{-1} implies: $z^{-1} y(k) = y(k-1)$, (7.22)

the polynomials are defined as:

$$A(z) = 1 + a_1 z^{-1} + a_2 z^{-2} + \dots + a_{na} z^{-na} \quad (7.23)$$

$$B(z) = b_1 z^{-1} + b_2 z^{-2} + \dots + b_{nb} z^{-nb} \quad (7.24)$$

$$C(z) = 1 + c_1 z^{-1} + c_2 z^{-2} + \dots + c_{nc} z^{-nc} \quad (7.25)$$

$$D(z) = 1 + d_1 z^{-1} + d_2 z^{-2} + \dots + d_{nd} z^{-nd} \quad (7.26)$$

And,

$$F(z) = 1 + f_1 z^{-1} + f_2 z^{-2} + \dots + f_{nf} z^{-nf} \quad (7.27)$$

Due to the process being linear, an auto regressive moving average exogenous (ARMAX) model structure is selected and used for model coefficient identification. Least squares based iterative algorithms are used to estimate the model coefficients; i.e.; the unknown parameters $(a_i, b_i, c_i, d_i, f_i)$ by using the available input–output measurement data $\{u(k), y(k): k = 1, 2, \dots, K, \dots, N\}$ to improve the accuracy of parameter estimation.

7.6 Choosing the model parameters.

In a parameter estimation approach, the model coefficients are directly obtained from the process or system inputs and output data. In other words, the parameter estimation approach estimates the β parameters of the mathematical model (equation (7.7)) by using the inputs, u , and outputs, y , of the process. The coefficient estimates are identified using the least squares method. The least squares based algorithm converges faster than the gradient based algorithm and the stochastic algorithm used for the identification process. The least squares estimate is found by minimizing the sum of squares of the model errors. Chen, P. and Tang, X., (2010), Wei, H.L., et al. (2010) and Zhao, G. and Wang, Z., (2011) are some examples of the various applications where the least squares principle is applied.

7.6.1 Derivation of least squares estimate

In vector form, using the representations of equation (7.7); assuming the white noise of the system is represented by e , $u(k)$ and $y(k)$ are the input and output of the system/process, respectively. The least squares estimate is found by minimizing the sum of squares of the model errors:

$$Y = \Phi\beta + e \quad ; \text{ (in vector form)} \quad (7.28)$$

If the cost function is defined as, $J = 1/N \cdot \sum (e)^2$; i.e. the sum of squares of model errors for N measurements, the least squares method converges to the solution by minimizing J .

Define, $J = \frac{1}{N} \sum (\text{model errors})^2$ i.e., the sum of squares of model errors for N measurements;

Then in vector form;

$$J = \frac{1}{N} [Y - \Phi \hat{\beta}]^T [Y - \Phi \hat{\beta}]; \quad (7.29)$$

Where $\hat{\beta}$ is the estimated parameter matrix.

$$J = \frac{1}{N} [Y^T Y - Y^T \Phi \hat{\beta} - \hat{\beta}^T \Phi^T Y + \hat{\beta}^T \Phi^T \Phi \hat{\beta}]; \quad (7.30)$$

Note: The size of the variables Y^T is $(1 \times N)$

Φ is $(N \times 2n)$ and β is $(2n \times 1)$. (Hence, $Y^T \Phi \hat{\beta}$ can be transposed and rewritten as $\hat{\beta}^T \Phi^T Y$)

The objective of the least squares method is to minimize the function J ; hence, set $\frac{dJ}{d\hat{\beta}^T} = 0$;

i.e.; from equation (7.30) (Billings, 2004);

$$\frac{dJ}{d\hat{\beta}^T} = 0 - \Phi^T Y - \Phi^T Y + \Phi^T \Phi \hat{\beta} + \Phi^T \Phi \hat{\beta} = 0; \quad (7.31)$$

$$\text{i.e.}; \Phi^T Y = \Phi^T \Phi \hat{\beta}; \quad (7.32)$$

$$\text{Therefore, } \hat{\beta} = (\Phi^T \Phi)^{-1} \Phi^T Y \quad (7.33)$$

is the least squares estimate.

Substituting from (7.28);

$$\hat{\beta} = (\Phi^T \Phi)^{-1} \Phi^T (\Phi \beta + e); \quad (7.34)$$

i.e.;

$$\hat{\beta} = \beta + (\Phi^T \Phi)^{-1} \Phi^T e \quad (7.35)$$

Multiplying by $\Phi^T \Phi$ on both sides;

$$\Phi^T \Phi (\hat{\beta} - \beta) = \Phi^T e \quad (7.36)$$

Taking the Expected value;

$$E[\Phi^T \Phi (\hat{\beta} - \beta)] = E[\Phi^T e] = 0. \quad (7.37)$$

$E[\beta] = \beta$ only if the mean values of the components of the noise vector (e) are zero and if the matrices, Φ , and noise vector are uncorrelated.

In other words, the estimates of the parameters are unbiased if the noise input is assumed to be white and the white noise and data matrix are independent. This is true and the estimates will always be unbiased because in parameter estimation, the noise is always assumed to be white and a moving average (MA) filter is added to represent the colored noise factor.

7.6.2 Model order selection

This section discusses the criteria used and the procedure of selecting the model order for the process. Refer Figure 7.4, $\{u(k)\}$ is taken as a persistent excitation signal sequence with zero mean and unit variance, and $\{e(k)\}$ as a white noise sequence with zero mean and variance σ^2 .

The coefficient matrix Φ is calculated for various model orders using the least squares method. An approximate model order estimate is made by analyzing the number of resonant peaks in the non parametric frequency response function. The identified models are analyzed by analyzing the Akaike's Information criterion (AIC), Akaike's Final Prediction Error Criterion (FPE), and the

Minimum Description Length criterion (MDL) criteria and the residual correlation test results. Each model is tested against the residual function tests and pole/zero (PZ) maps. The results of the criteria and tests are listed in Table 7.1. The final model selection is based on comparing the criteria and PZ plots of the models.

Comparing the FPE, AIC and MDL and the residual correlation test results, an ARMAX model with a model order of 2 is selected. The identification results of the estimated parameters are given in Table 7.2. Figures 7.8 – 7.10 illustrates the auto correlation test of the model residuals and the cross correlation test between the input and the model residual and the prediction error graph.

Unbiased estimates are ensured when the residual signal (also known as prediction error) is reduced to a white noise sequence. If the estimated process or noise model is deficient or biased the residual will be colored.

Table 7.1: Identification test results for ARMAX model structure

Model order n, order of c = 4, Time delay =0.	FPE	AIC	MDL	Auto correlation test (+) : Pass (-) : Fail	Cross correlation test (+) : Pass (-) : Fail
1	0.131	0.130	0.149	+	–
2	0.066	0.065	0.775	+	+
3	0.0679	0.0669	0.0812	+	+
4	0.074	0.0728	0.0906	+	+

The residual can be defined as $E(k) = y(k) - \hat{y}(k/k-1)$. where $y(k)$ is the actual process output at any sampled instant k . $\hat{y}(k/k-1)$ is the estimated response at instant k given data up to and including sampled instant $k-1$.

Table 7.2: Least squares based parameter estimates for ARMAX model

Terms	Parameter estimates	Terms	Parameter estimates
a 1	-0.2418	c1	1.236
a2	0.1217	c2	1
b0	0.9913	c3	0.909
b1	-0.392	c4	0.525
b2	0.113		

7.6.3 Residual error and residual correlation tests on model

Residual signal is the difference between the experimental output data and the model simulated output. In Figure 7.8, the residual signal fluctuates around zero (in the range of ± 0.002) with very small deviations. This indicates that the estimated model displays good prediction.

The Auto Correlation Function (ACF) graph of the model residual (Figure 7.9) resembles white noise ACF and lies within the confidence interval. This indicates that the process and noise model estimates are unbiased. The Cross Correlation Function (CCF) graph (Figure 7.10) denotes the cross correlation between the model input and the residual. It dies out to zero on either side and is bounded within the confidence interval which denotes that the process and noise model are correct and the estimates are unbiased. If the noise or process model is biased then the CCF will not die out to zero, and the estimates will be biased.

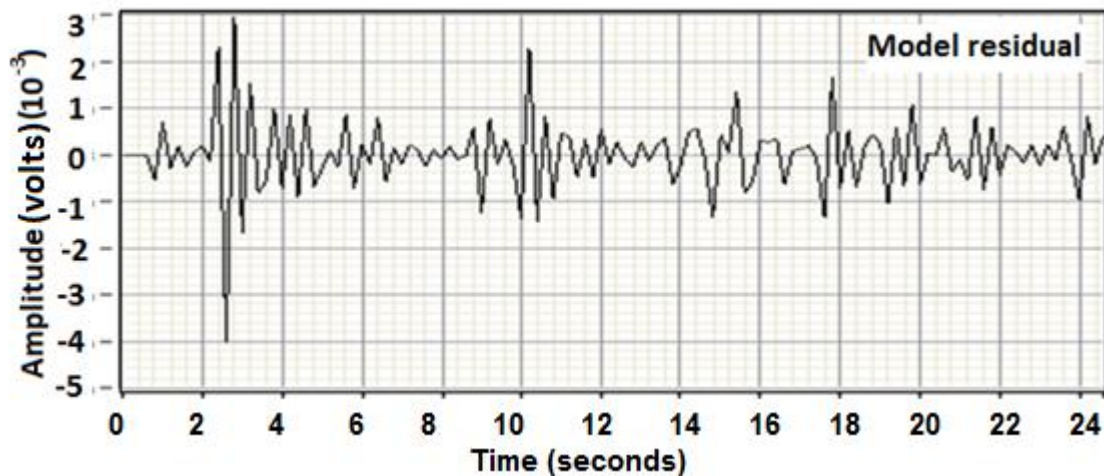


Figure 7.8: Model residual error plot (model order 2).

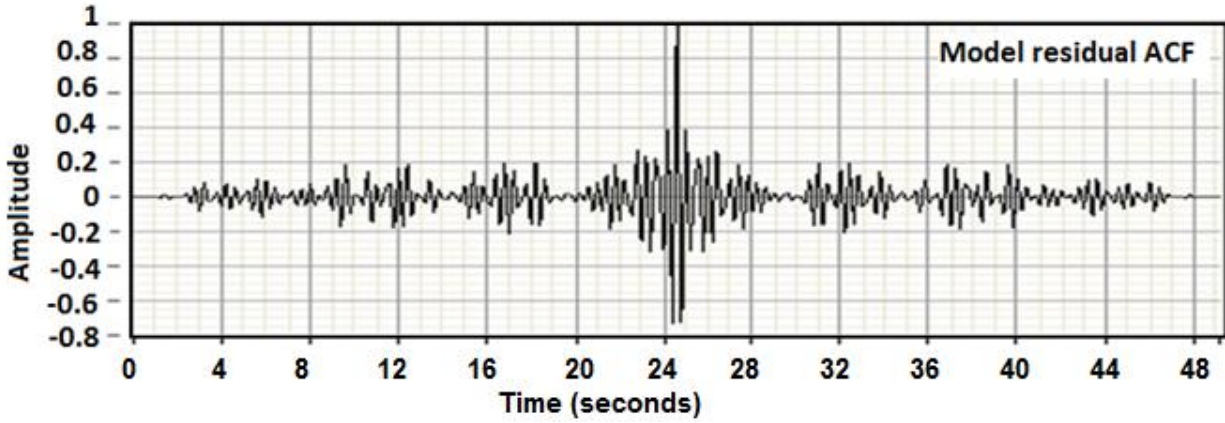


Figure 7.9: Autocorrelation function of the model residual (model order 2).

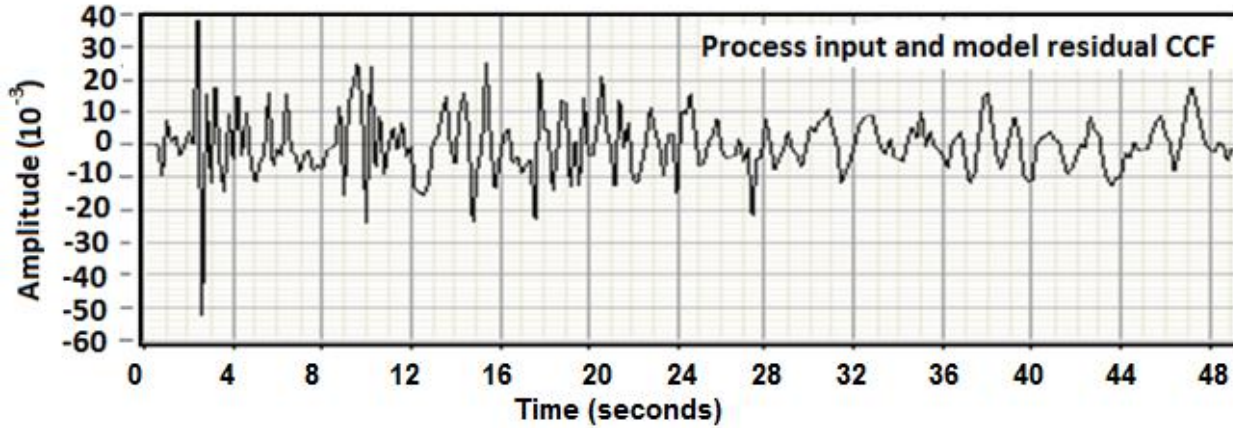


Figure 7.10: Cross correlation function between input and model residual (model order 2).

7.6.4 Model Prediction tests

Model prediction tests are an important part of the identification procedure. The mean squared error (MSE) of the model predictions and the measured outputs determine the accuracy with which model can simulate or predict the system behavior. A comparison of the measured output and the one step and 100 step ahead prediction results from the model are plotted in Figure 7.11 and 7.12. A good match is found in both the cases with the Mean Squared Error levels at 0.00057 and 0.00419 respectively indicating good model performances.

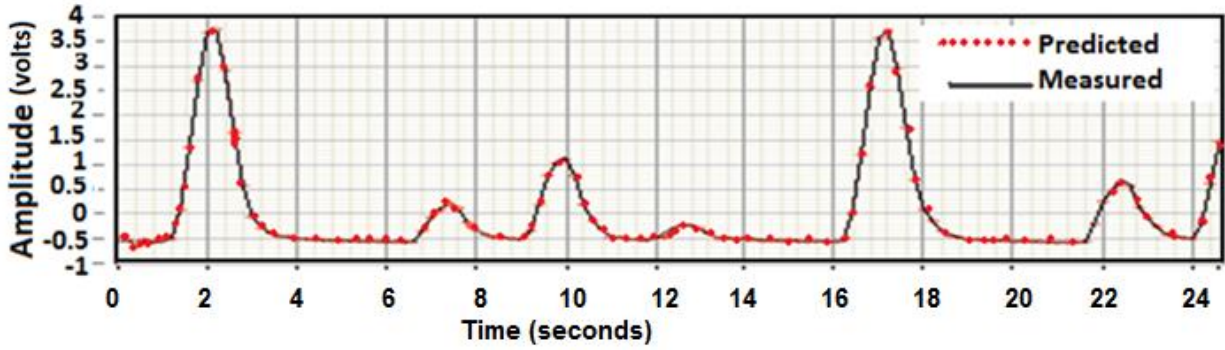


Figure 7.11: One step ahead predicted outputs and measured output (MSE 0.00057).

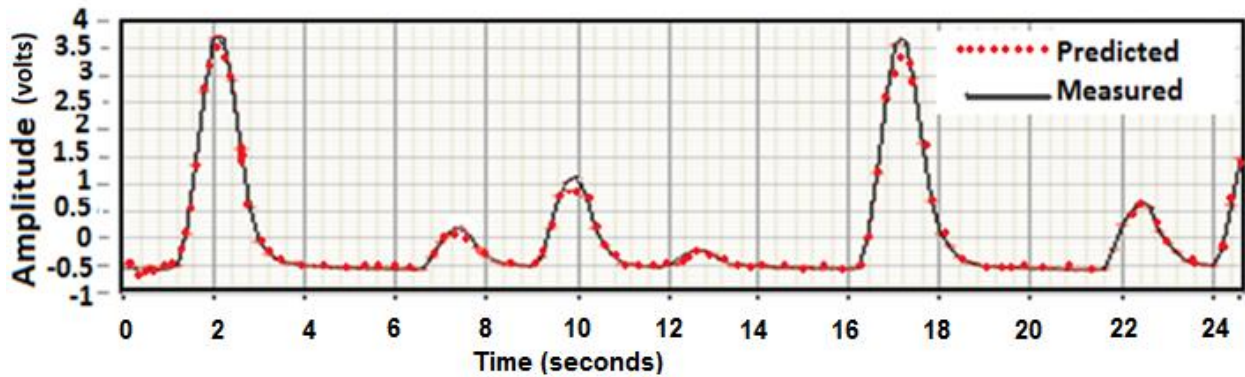


Figure 7.12: 100 step ahead predicted outputs and measured output. (MSE 0.00419)

7.7 Validating the ARMAX model.

The developed model is validated by comparing the model responses with measured responses for various inputs. Figures 7.13, 7.14 and 7.15 compare the model simulated responses with the experimental process response when a chirp, square and ramp input is applied to the model and system respectively. The plots represent the measured output (‘-‘ black) and ARMAX model simulated response (‘*’ red). The close match between the measured response and the model response further validates the correctness of the developed model.

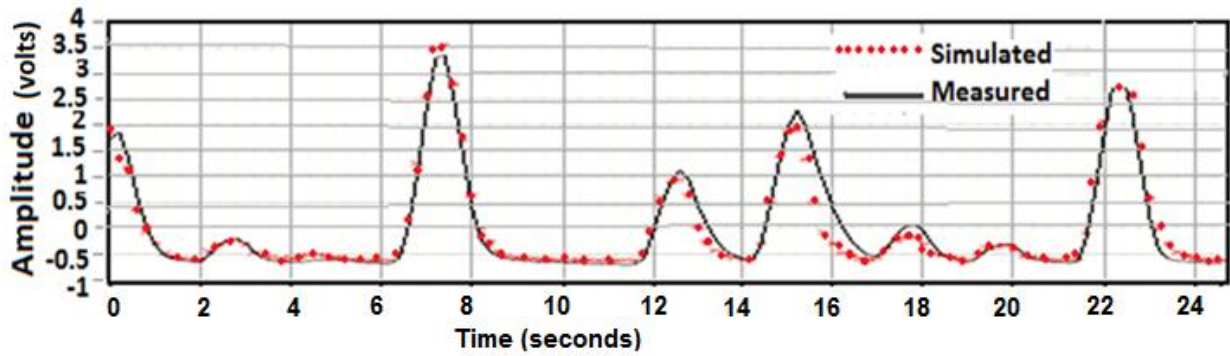


Figure 7.13: ARMAX model validation test for chirp input.

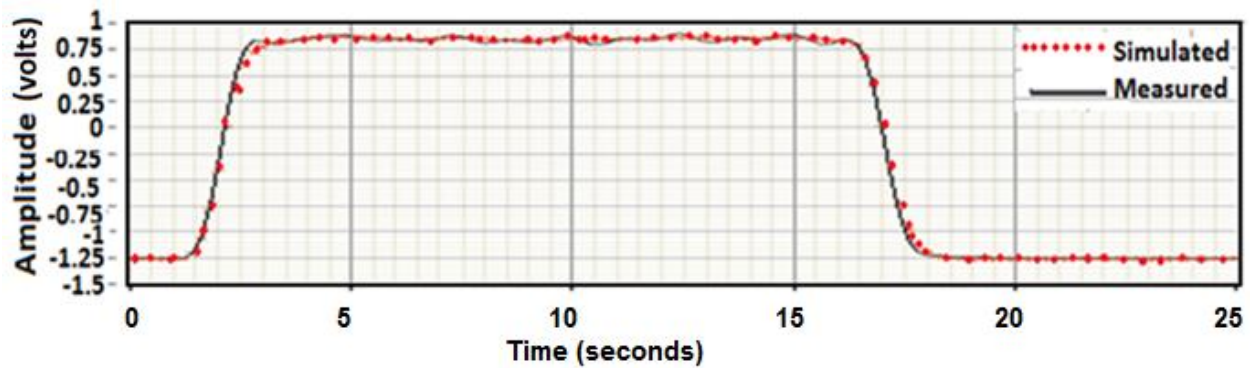


Figure 7.14: ARMAX model validation test for step input.

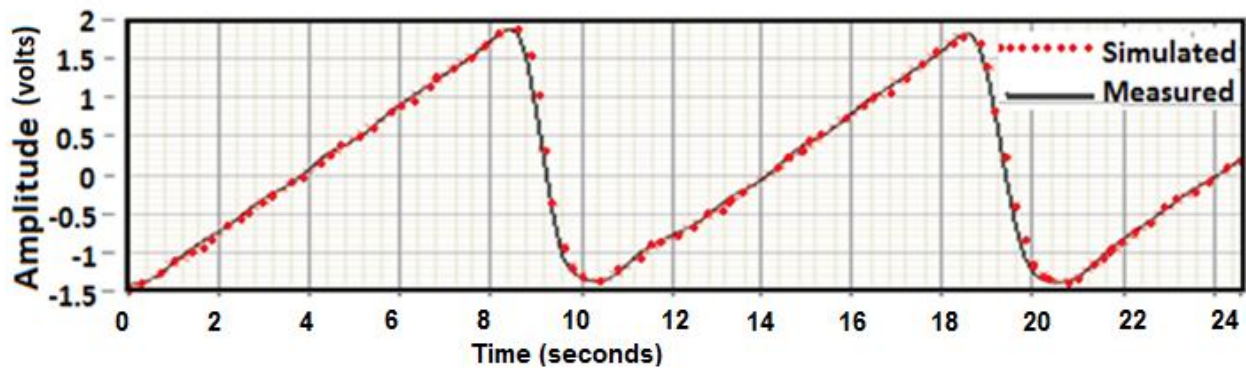


Figure 7.15: ARMAX model validation test for ramp input.

This section completes the ARMAX model identification for configuration 1. The next chapter discusses the model identification of nonlinear system represented by configuration 4.

Chapter 8. Mathematical model identification for configuration 4 laboratory set up.

This chapter discusses the identification of the nonlinear rotary drilling system presented as configuration 4. The dynamics presented by whirling drill bit due to an unbalance in the drill bit mass was discussed in Chapter 6. This chapter is an extension of Chapter 7 where system identification methods were applied to develop a mathematical model of an ideal drill string system used for rotary drilling. Utilizing the discussion in the previous chapters this chapter details the procedure of identifying a mathematical model for a nonlinear drill string system, presenting bit whirl due to drill bit imbalance. The model was identified using the Black box modeling approach of system identification. The Least squares procedure was also used to ensure quality estimates of the model coefficients.

A few research studies have been conducted to model the rotary drilling dynamics using analytical modeling methods in presence of unbalanced drill bit. Navarro Lopez and Suarez, (2004) modeled the drill string torsional behavior as a two degree of freedom torsional pendulum using lumped parameter differential equation. Liao et al., (2011) have developed reduced order models for rotary drilling with unbalanced bit prototype from analytical principles.

The following sections describe the modeling procedure for identification of black box model for the rotary drilling system with an unbalanced drill bit.

8.1 Analyses of the drill string system with unbalanced drill bit

In the presence of drill bit imbalance, the schematic of the system can be depicted as in Figure 8.1. The unbalance of the drill bit was approximated by a small mass fixed on the flywheel representing the drill bit. The driving force was applied to the system at the upper flywheel and it rotated the entire system. Hence the angular velocity of the upper flywheel could be considered to be the ‘input’ for the system. The ‘output’ of the system was the angular velocity at which the lower flywheel rotated.

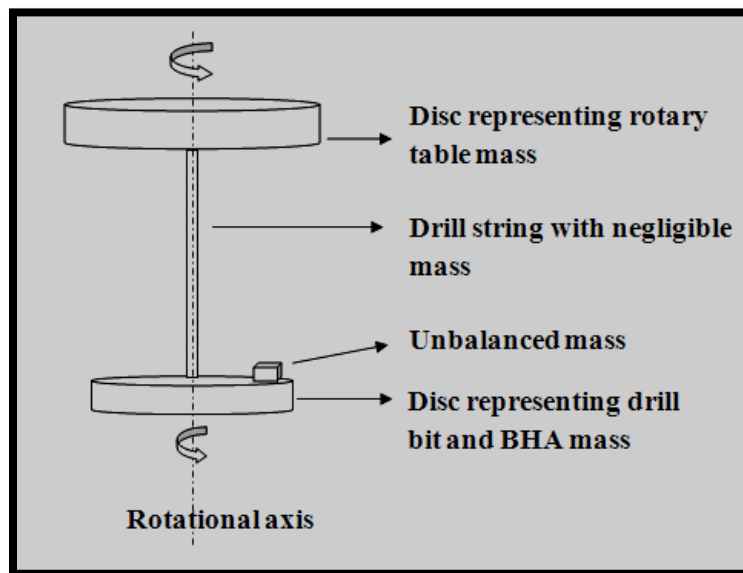


Figure 8.1: Schematic of drill string with unbalanced drill bit

Nonlinear systems are well represented by Auto Regressive eXogenous models (ARX). In the ARX model, a zero noise model was assumed and the model order and coefficients were estimated. However, on detailed analysis of this system, it was easily noticed that the nonlinearities present in the system were added at the output end of the system. In other words, the system could be described as one which has disturbances entering late or near the output end

of the system. In such cases, a Box Jenkins model would be a better fit of the system dynamics than an Auto Regressive eXogenous model [Forssell and Ljung, (2000)]. However, it is imperative to identify an ARX model and use the model coefficient orders to identify the Box Jenkins (BJ) model. The following sections deal with identification and validation of the ARX and BJ model.

8.2 Identifying an ARX model

System identification uses the available measured data to identify the coefficients of a pre defined model structure. The procedure of the system excitation and data collection are similar to the procedure followed in section 7.3.1. The imbalance at the bit was represented by an average scale of imbalance of case 2 in section 6.3 throughout the identification procedure. All the experiments recorded in this chapter are at a sampling frequency of 5 samples/second.

The raw data acquisition procedure is conducted and the data is displayed in Figure 8.2. The raw data are processed by removing the means and de trending (section 7.3.1); it is plotted in Figure 8.3.

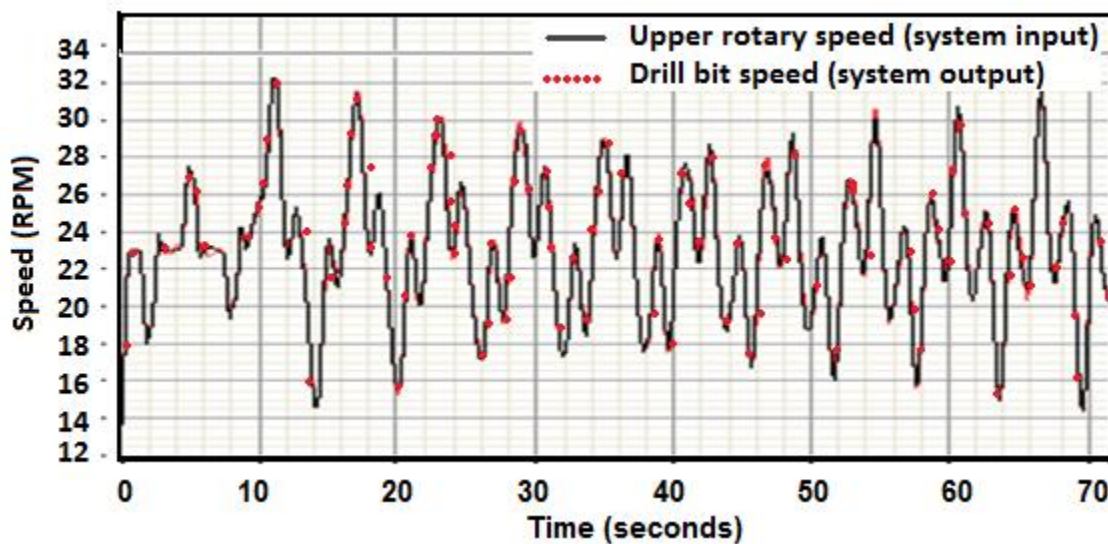


Figure 8.2: Raw input and output data obtained from system.

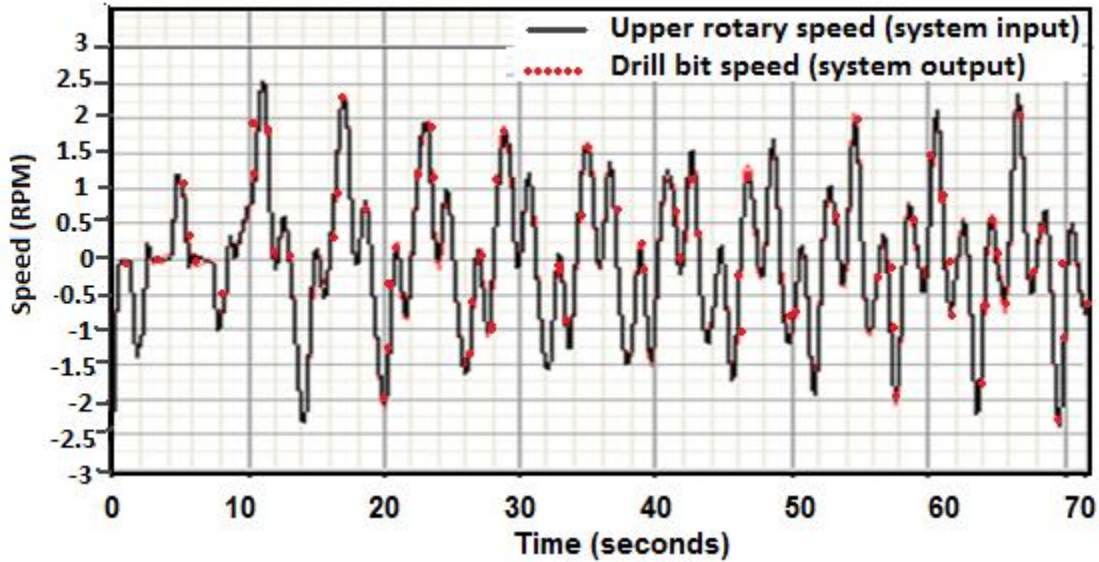


Figure 8.3: Mean removed and detrended system input and output data.

From the processed data, Y and Φ matrices (equation 7, chapter 7) are chosen to estimate the parameters β .

An ARX model consists of the auto regressive exogenous terms and a white noise model. Refer equations 7.19, 7.23 and 7.24 for the model structure.

The next stage of model identification is selection of model order. The model order is selected by analyzing the Akaike's Final Prediction Error (FPE), Akaike's Information Criteria (AIC) and Minimum Description Length (MDL) criteria as well as the residual correlation test results. The AIC, FPE, and the MDL are the criteria used to determine the best model order for the system. As a rule, the lower these values are, the better the model is. Also, to be kept in mind is that if there are only slight changes in these values between the lower and higher order models, the lower

order model is selected taking into account simplicity of the model. The results of the applied criteria and correlation tests are listed in Table 8.1.

Figure 8.4 illustrates the auto correlation test of the model residuals. The cross correlation test between the input and the model residual is plotted as the third plot in Figure 8.4. The cross-correlation tests results are passed when the test graphs are within the confidence intervals and should decay to zero on both ends. The auto correlation graph should have a maximum overshoot in the middle to infinity (ideally) and should decay to zero on both ends. Similar, though not quite the same, results are obtained for above tests on the identified model.

Table 8.1: Identification test results for ARX model structure

Model order n, Time delay =0.	FPE	AIC	MDL	Auto correlation test (+) : Pass (-) : Fail	Cross correlation test (+) : Pass (-) : Fail
2	0.492	0.492	0.512	+	+
3	0.204	0.204	0.216	+	+
4	0.200	0.200	0.216	+	+
5	0.172	0.172	0.190	+	+

Unbiased estimates are ensured when the residual signal (also known as prediction error) is reduced to a white noise sequence. If the estimated process or noise model is deficient or biased, the residual will be colored.

The residual can be defined as

$$E(k) = y(k) - \hat{y}(k/k-1).$$

Where $y(k)$ is the actual process output at any time instant k . $\hat{y}(k/k-1)$ is the estimated response at instant k using data up to and including time instant $k-1$. In the first plot in Figure 8.4, the residual fluctuates around zero (in the range of ± 0.2) with very small deviations. This indicates that the estimated model displays good prediction.

Table 8.2: Least squares based parameter estimates for ARX model

Terms	Parameter estimates	Terms	Parameter estimates
a 1	-0.9614	b0	1.0559
a2	0.6546	b1	-1.1143
a3	0.0759	b2	0.8576

The Auto Correlation Function (ACF) graph of the model residual, (Figure 8.4) resembles white noise ACF and lies within the confidence interval. This indicates that the process and noise model estimates are unbiased. The cross correlation function (CCF) graph (Figure 8.4) denotes the cross correlation between the model input and the residual. It dies out to zero on either side and is bounded within the confidence interval which denotes that the process and noise model are correct and the estimates are unbiased. If the noise or process model is biased then the CCF will not die out to zero, and the estimates will be biased.

Comparing the AIC, FPE, MDL, and the residual correlation test results, an ARX model with a model order of 3 is selected. The basis for the selection is that no major difference is found in the reduction of confidence bands of the cross correlation tests beyond a model order of 3 and the auto correlation test graph is more symmetric on either side of the middle high. The identification results of the estimated parameters are given in Table 8.2.

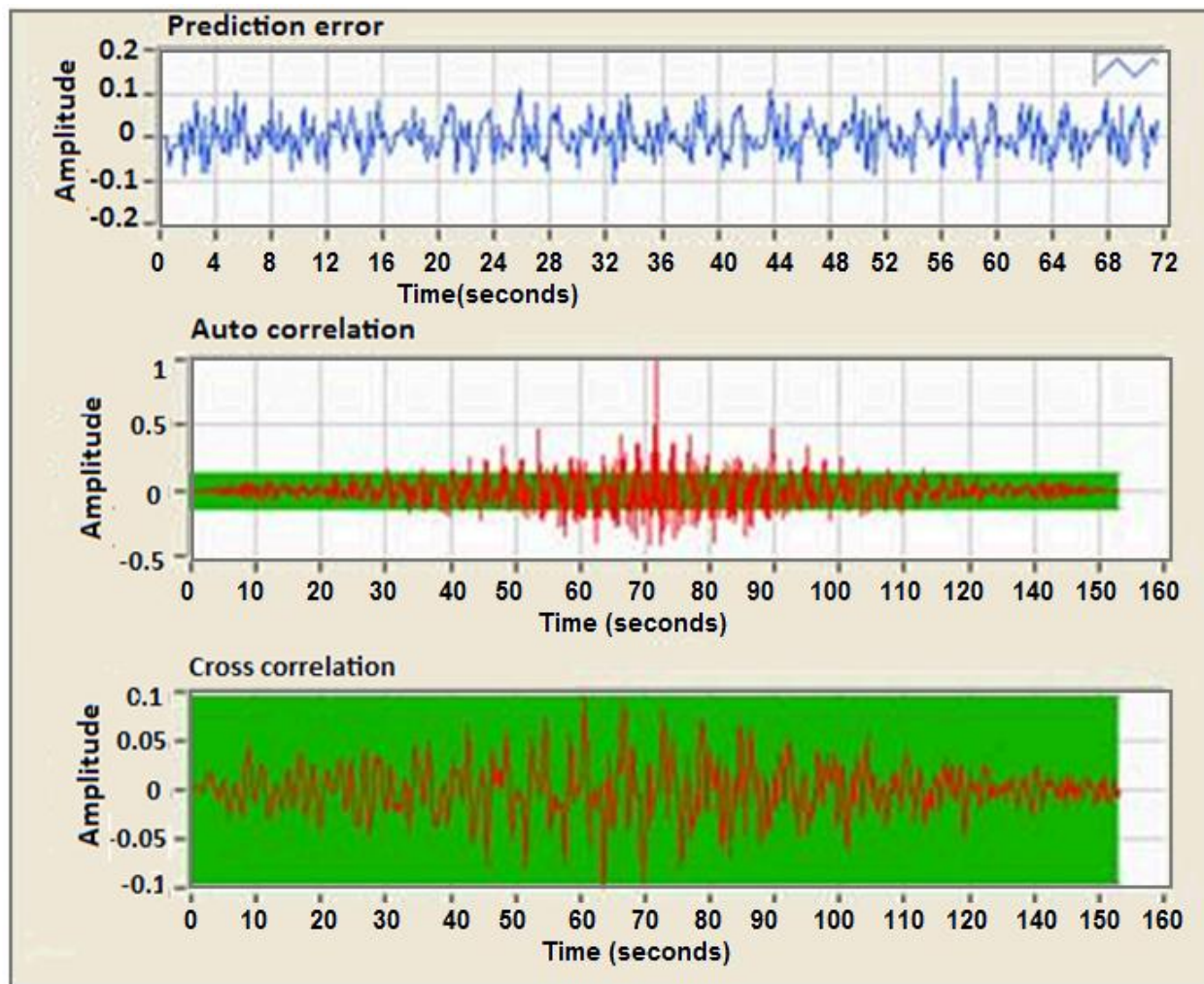


Figure 8.4: Correlation test results and prediction error graph for ARX model.

A comparison of the measured output and the one step and 100 step ahead prediction results from the model are plotted in Figures 8.5 and 8.6. A good match is found in both the cases with the Mean Squared Error levels at 0.00197 and 0.00810 respectively indicating good model performance.

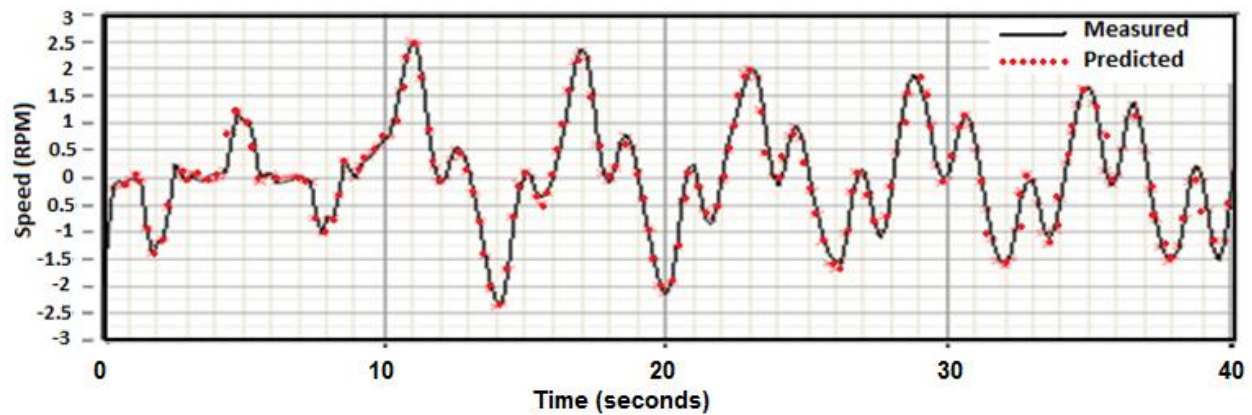


Figure 8.5: One step ahead predicted outputs and measured output. (MSE 0.00197)

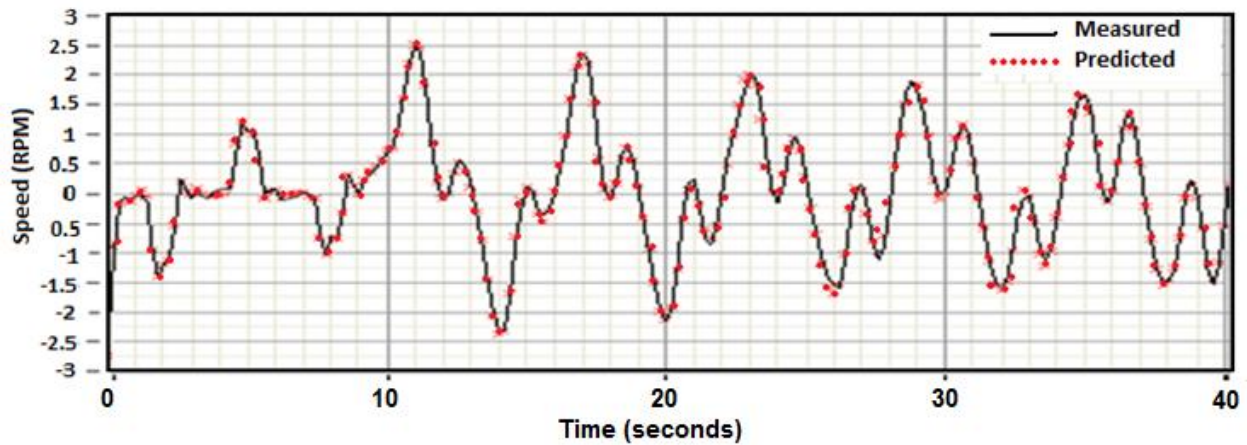


Figure 8.6: 100 step ahead predicted outputs and measured output. (MSE 0.00810)

The parameter estimates of the ARX model were obtained by the method of Least squares to ensure the estimates are unbiased. The least squares estimate is found by minimizing the sum of squares of the model errors (Refer section 7.3.3). The identification results for the ARX structure obtained in this section are used in the next section to identify a Box Jenkins model structure for the same process dynamics.

8.3 Identification of a Box Jenkins model.

The structure of a Box Jenkins (BJ) model is of the form given in equation (7.21), using model coefficient polynomials in Equations (7.24), (7.25), (7.26) and (7.27).

The A and B orders selected for the ARX model are used as the starting orders of F and B in the BJ model identification [Forrsell and Ljung, (2000)]. The noise model is generally selected at orders of range 1 and 2.

In section 8.2 the AIC, FPE, and the MDL as well as the residual correlation test results are compared to obtain an ARX model with a process model order $A=3$, $B=2$. Hence a BJ process model with orders $B=2$, $F=3$, and noise model coefficient orders $C=2$ and $D=2$ is selected. The basis for the selection of the noise model order is that no major difference is found in the reduction of confidence bands of the cross correlation tests beyond a model order 3 and the auto correlation test graph is more symmetric on either side of the middle high. The test criteria obtained for different model orders are laid out in Table 8.3. On analysis, it is seen that the BJ model gives lesser estimation criteria results than the ARX model.

The residual correlation tests in Figure 8.4 for the ARX model show good results and features of a good model. However, when compared to the correlation test results for the BJ model (Figure 8.7); the autocorrelation function for the ARX model tends to out bound the confidence bands more often and is not smooth. The cross correlation function (Figure 8.7) is not symmetric for the BJ model; however, it falls within the confidence bands.

Table 8.3: Residual test and estimation criteria for ARX and BJ model orders

MODEL	ORDER						RESIDUAL TEST		ESTIMATION CRITERIA		
	A	B	F	C	D	DELAY	ACF	CCF	AIC	MDL	FPE
ARX	3	2				0	P	P	0.204	0.216	0.204
	4	3				0	F	P	0.200	0.216	0.200
BJ		2	3	1	1	0	F	P	0.276	0.299	0.276
		2	3	2	2	0	P	P	0.152	0.167	0.152
		2	3	3	3	0	F	P	0.375	0.422	0.375
		3	4	1	1	0	F	P	0.349	0.384	0.349
		3	4	2	2	0	F	P	0.330	0.370	0.330

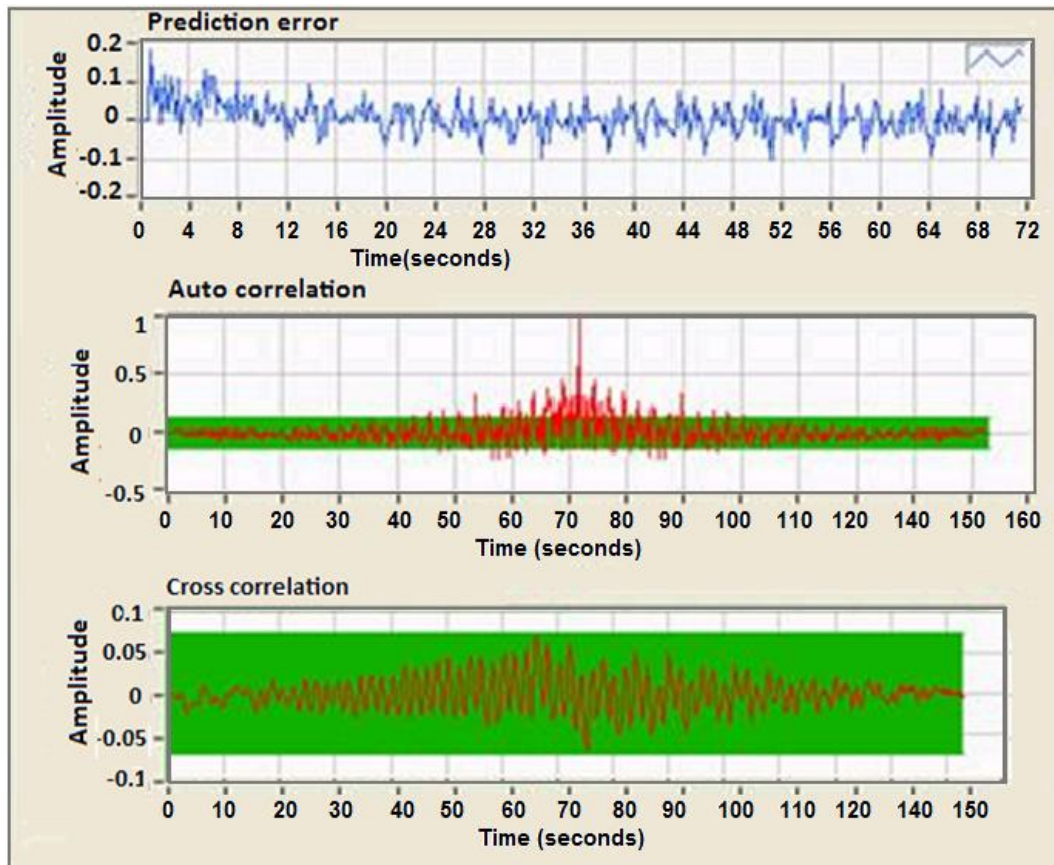


Figure 8.7: Correlation tests results and prediction error graph for the BJ model.

Unbiased estimates are ensured when the residual signal (also known as prediction error) is reduced to a white noise sequence. If the estimated process or noise model is deficient or biased, the residual will be colored. The prediction error graph (Figures 8.4 and 8.7) for both the models shows good ranges and have a white noise pattern; however, the levels of error are less for the BJ model than the ARX model. Based on the above discussion, a BJ model is selected as a better process model structure and analyzed for further validation results.

8.3.1 PZ Map Analysis for Different Model Orders

Further analysis of the model is performed by analyzing the locations of the poles and zeros of the developed model. Pole zero plots of ARX model $A=3$ and $B=2$ with delay = 0 are plotted in Figure 8.8. The model has one marginally stable pole on the imaginary axis. It has two poles and two zeroes which have their confidence intervals overlapping. The position of these poles suggests a stable but oscillatory system. Figure 8.9 displays the pole and zero locations when order of $A=4$, $B=3$ with delay = 0. There is now an extra pole on the imaginary axis indicating stable pole. But the confidence intervals of the complex conjugate poles and zeros now almost coincide/overlap indicating the model order need to be reduced.

For a Box Jenkins model with orders $B=2, F=3$, and noise model $C=2$ and $D=2$, and delay = 0, the PZ plot is shown in Figure 8.10. The pole on the imaginary axis is a stable pole, the poles on the left half circle are inside the circle indicating stability but has an oscillatory response. The BJ model is more stable and less oscillatory than the ARX model. Figure 8.11 presents the PZ plot for a Box Jenkins model with process model orders $B=3$, and $F=4$, noise model orders $C=2$, $D=2$ with delay = 0. The pole zero positions are good and the criteria also has small values; however, in the model simulation tests done for model validation purposes, this model does not provide any

better results for simulation errors when compared to the previous simpler BJ model (2322). The process model coefficients for the selected BJ model are listed in Table 8.4.

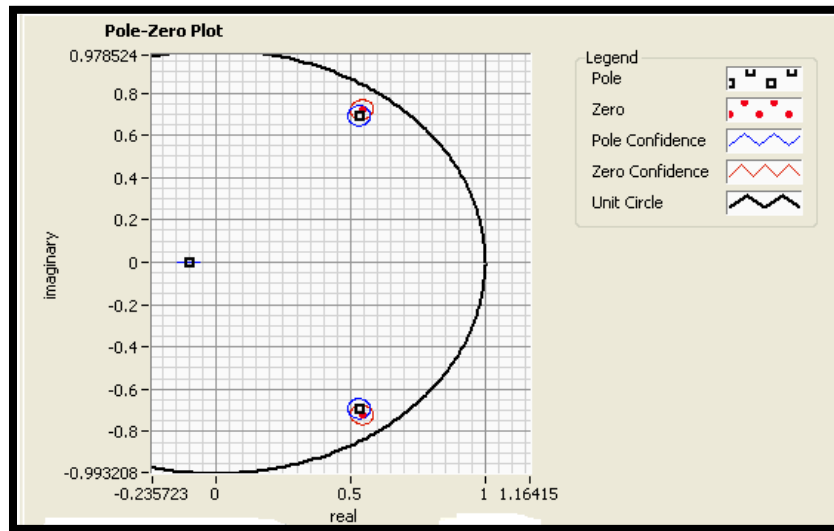


Figure 8.8: Pole zero plot of ARX model with orders $A=3$, $B=2$, delay=0.

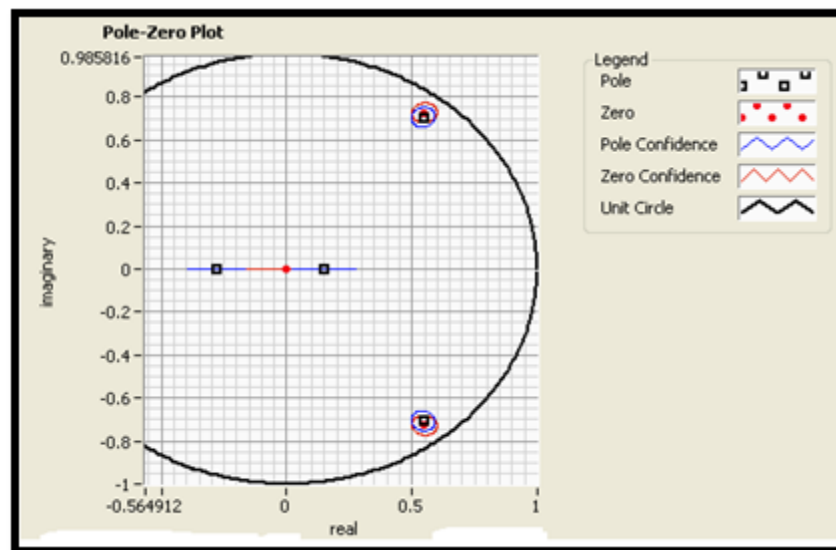


Figure 8.9: Pole zero plot for ARX model with orders $A=4$, $B=3$, delay =0.

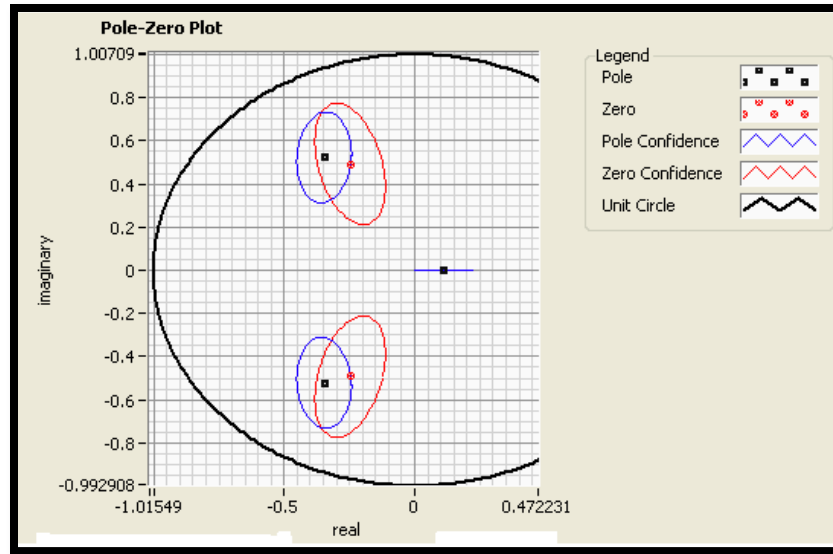


Figure 8.10: Pole zero plot for BJ model with orders B=2, F=3, C=2, D=2, delay = 0.

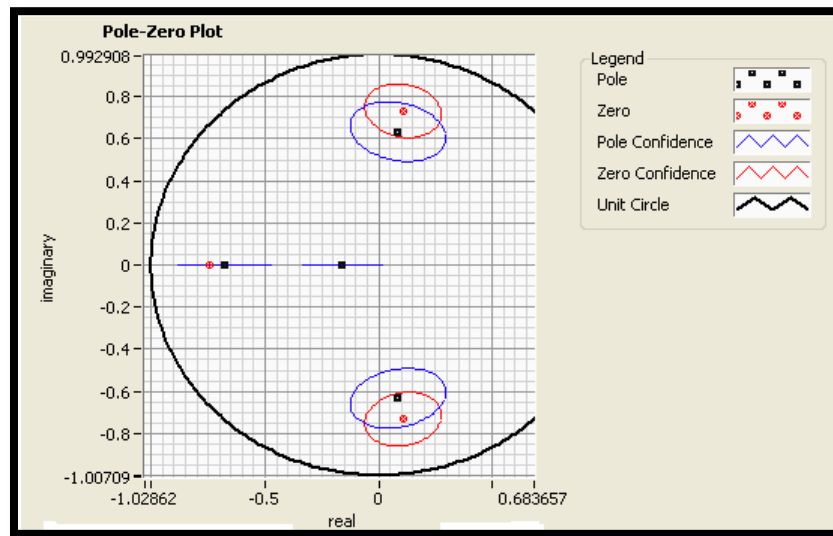


Figure 8.11: Pole Zero plot for BJ model with orders B= 3, F=4,C=3,D=3,delay =0.

Table 8.4: Least squares based parameter estimates for selected Box Jenkins model

Terms	Parameter estimates	Terms	Parameter estimates
b0	1.0345	f3	-0.0442
b1	0.512	c1	-0.2482
b2	0.3147	c2	-0.7141
f1	0.5825	d1	-1.2031
f2	0.3153	d2	0.7316

8.4 Model Validation Tests

To support model validation, two fold results are presented. Model responses and experimental responses are compared under (1) command signal type variation and (2) varying operational speeds.

8.4.1 Command signal type variation

Sinusoidal, ramp and step speed commands are given to the laboratory system. The responses are then compared with the ARX and BJ model simulated responses for same inputs. The signals are plotted in Figure 8.12 a- c respectively. This stage of validation ensures the model and the system responds similarly to different speed variations. On analysis of the plots in Figure 8.12, the ARX model provides a good fit for the experimental data. However on close inspection; it is seen that the residual error of the BJ model has smaller amplitude than the ARX model. Moreover, as discussed in the previous section, the BJ model has a more stable PZ location than the ARX model. The next section discusses the second stage of model validation.

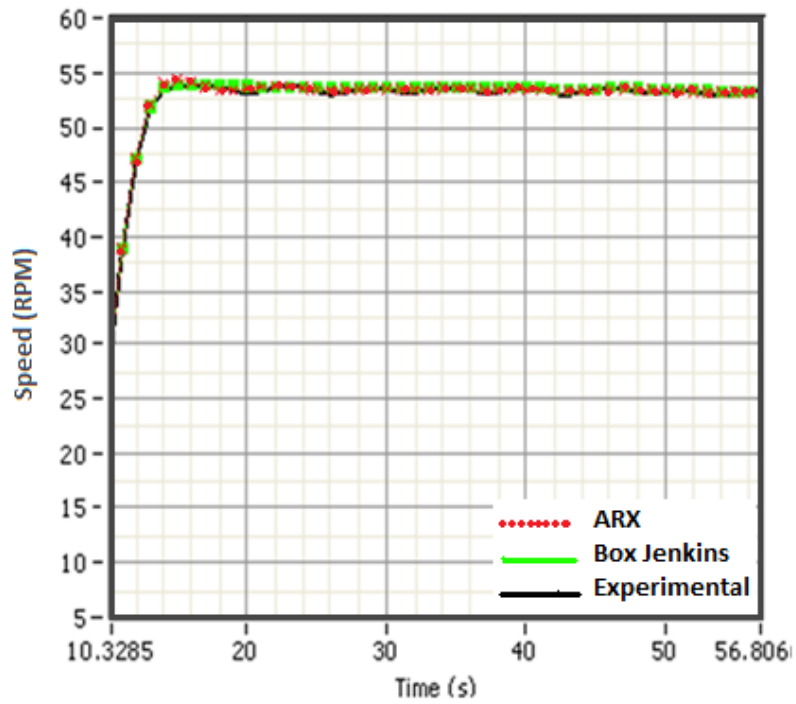


Figure 8.12a: ARX and BJ model validation with square input.

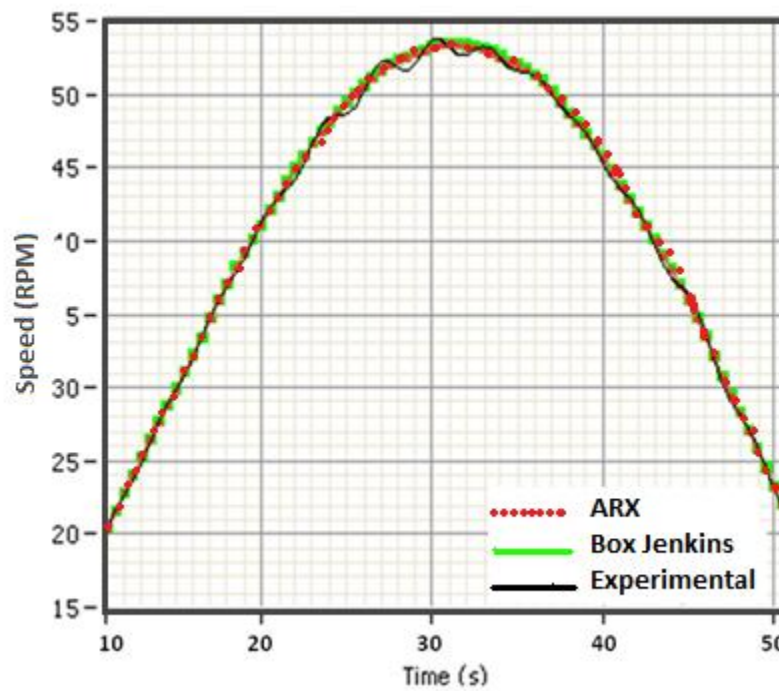


Figure 8.12b: ARX and BJ model validation with sinusoidal input.

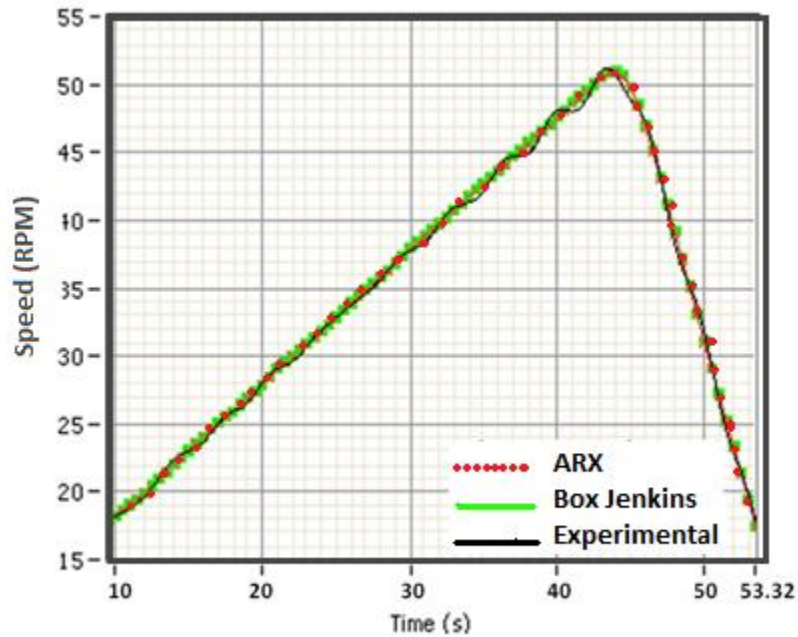


Figure 8.12c: ARX and BJ model validation with ramp input.

8.4.2 Varying operational speeds

The next stage of validation is conducted by operating the model and the drill system at different speed ranges to analyze if the model efficiently captures the nonlinear properties exhibited by the system. For this purpose the process model is subjected to low, average and high speed range inputs for normal drilling operation. The results are plotted and compared in Figure 8.13. It is noticed that the process model accurately simulates the system response and displays the self excited vibrations at low speed. Limit cycling is predominant at the average speed range of 38RPM. The vibrations ease out and limit cycling is less noticed at high speeds of 100 RPM, with the assumption of no further additive frictions affecting the system. This section completes the model validation.

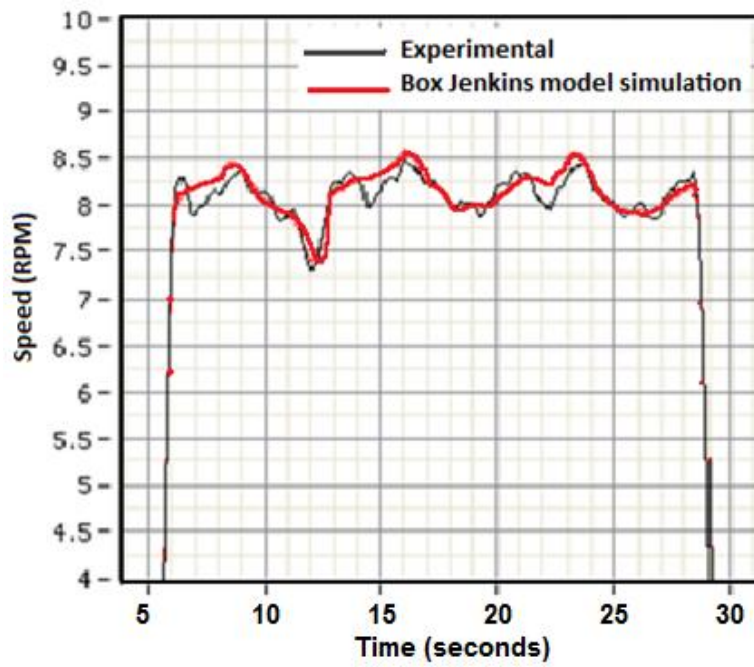


Figure 8.13a: BJ model validation at low speed operation.

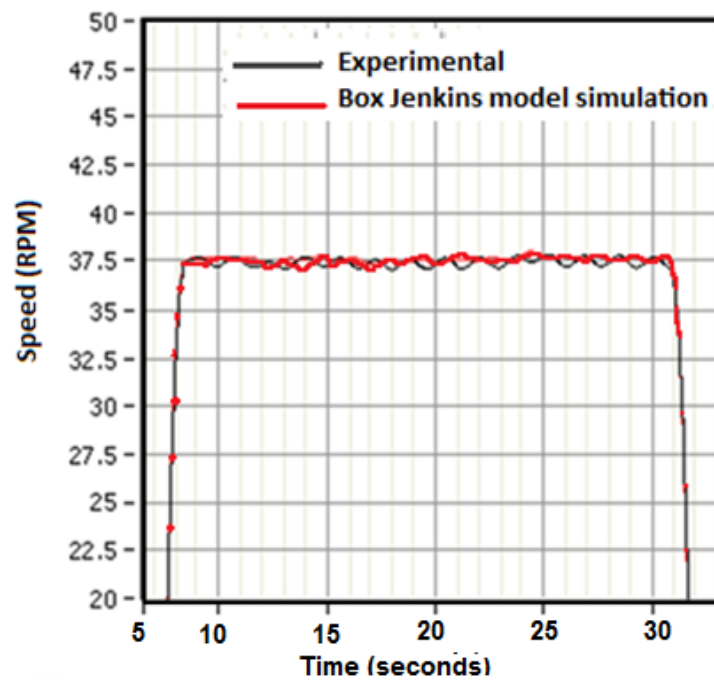


Figure 8.13b: BJ model validation at average speed operation.

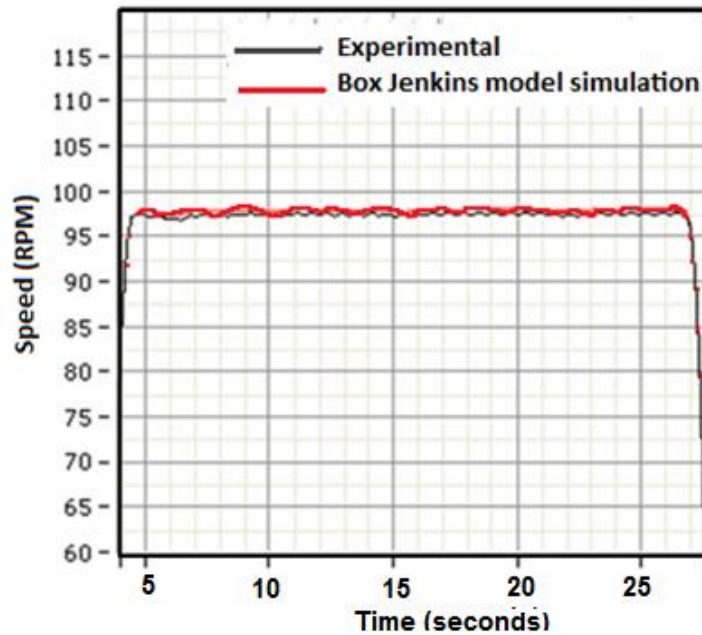


Figure 8.13c: BJ model validation at high speed operation.

8.5 Model robustness analysis

This section discusses the robustness of the identified model (section 8.4).

8.5.1 Residual error and Model error

To analyze model robustness, the laboratory operating speeds are selected to represent the rotary drilling process within its normal operational speed range. Rotary drilling operational speeds are mostly around 35 to 60 RPM. The process is excited by command inputs of 8 RPM, 38 RPM and 52 RPM. The low speed operation is analyzed to understand the drill string behavior in the transient period. The experimental responses of the process are recorded and plotted in Figures 8.14, 8.15 and 8.18. The identified model is seen to have very close response to the process response. The residual signal graph between the process response and model response is seen to be very low with values around 0.180 RPM, Figures 8.16 and 8.17. This suggests that the

model provides a good fit for analyzing the process behavior. However, the presence of the residual and its causes need to be analyzed. These sections discuss the probable sources of error.

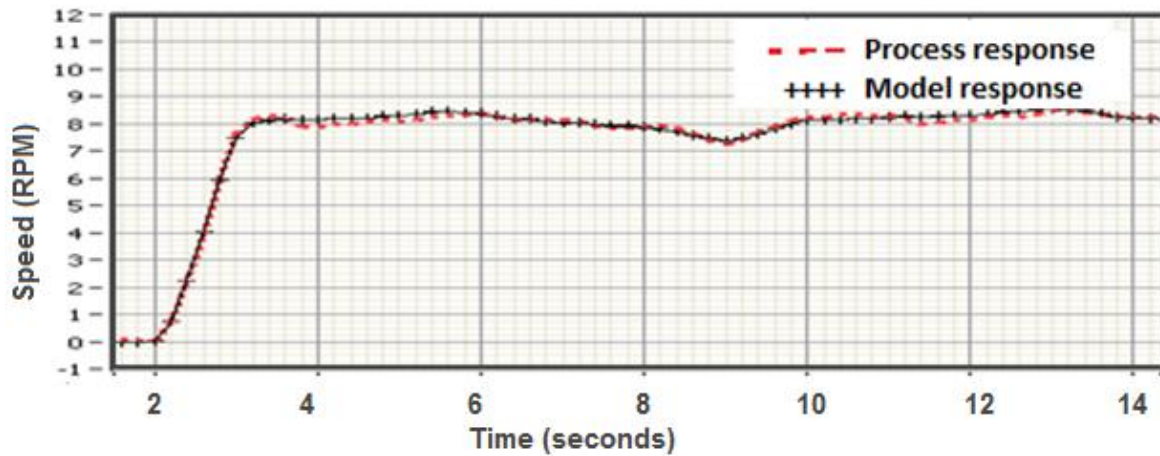


Figure 8.14: Process response and model response for low drilling speed

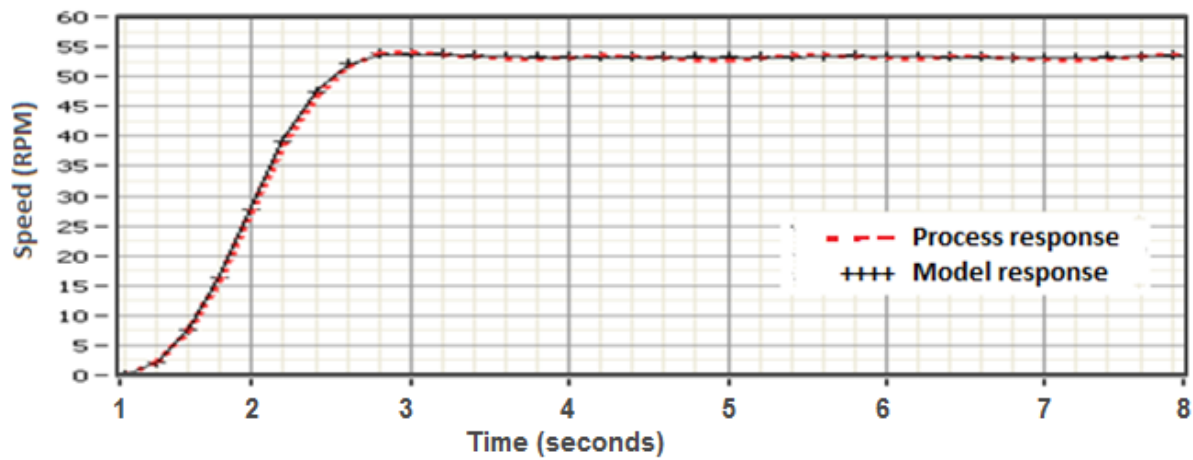


Figure 8.15: Process response and Model response at average drilling speed

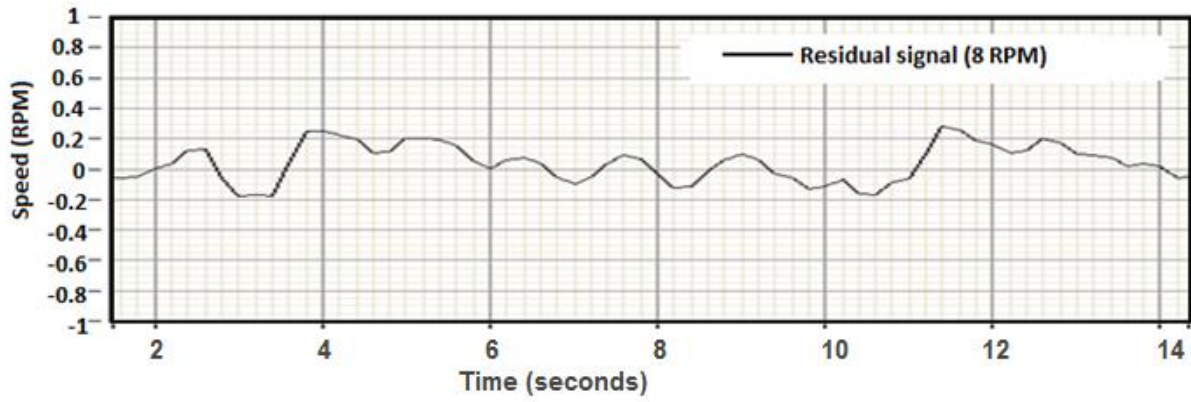


Figure 8.16: Residual signal for low speed analysis

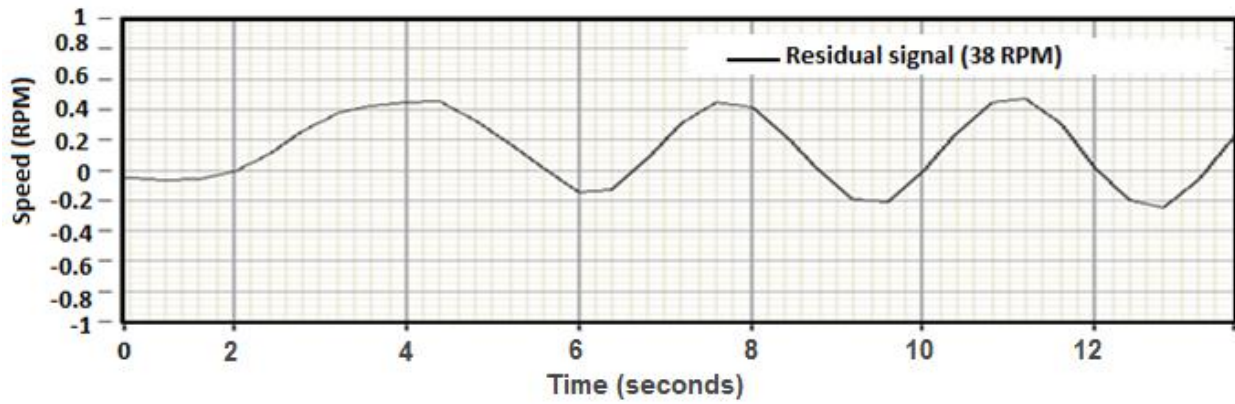


Figure 8.17: Residual signal for average speed analysis

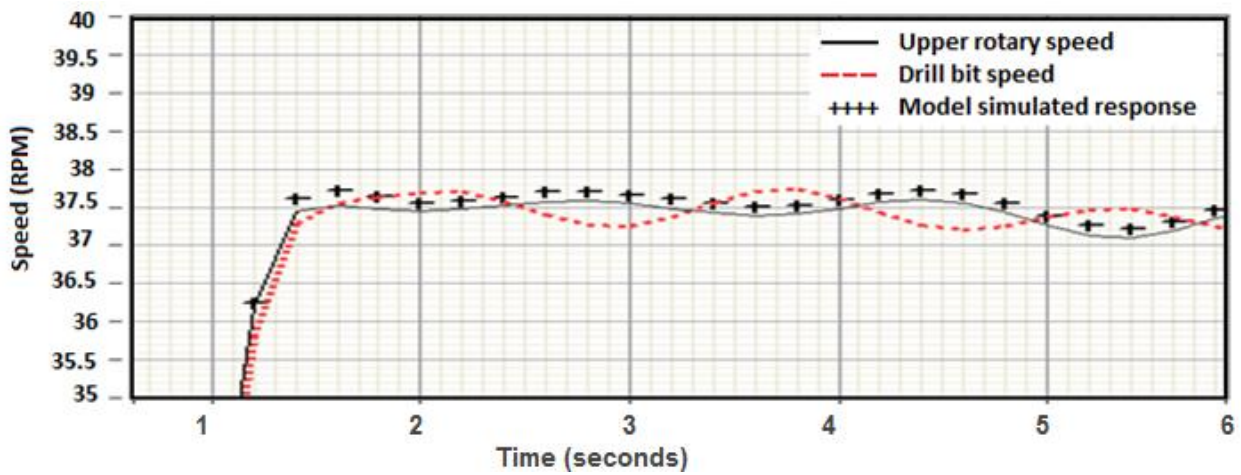


Figure 8.18: Experimental and simulated response at 38 RPM.

In spite of the close match between the simulated and process response, very small vibrations in the speed of the process at the output due to the unbalanced mass are noticeable, Figure 8.18. Here the unbalanced mass was 5.2 % of the mass of the lower rotor representing the drill bit. This mass will represent only a very small bend in the drill string. However, in reality, drill strings when they are bent slightly, present more severe vibrations due to the presence of well bore friction and higher mass of the bottom hole assembly. The black box model of the process was identified in a Box Jenkins model format specifically because the Box Jenkins models are good for processes in which disturbances enter late in to the system.

The residual error, Figures 8.16 and 8.17 presented a model robustness issue which needed to be dealt with. One suggestion is to combine the black box model with a separate model describing the effect of the unbalanced mass using analytical principles and larger degrees of freedom Liao, et al., (2011).

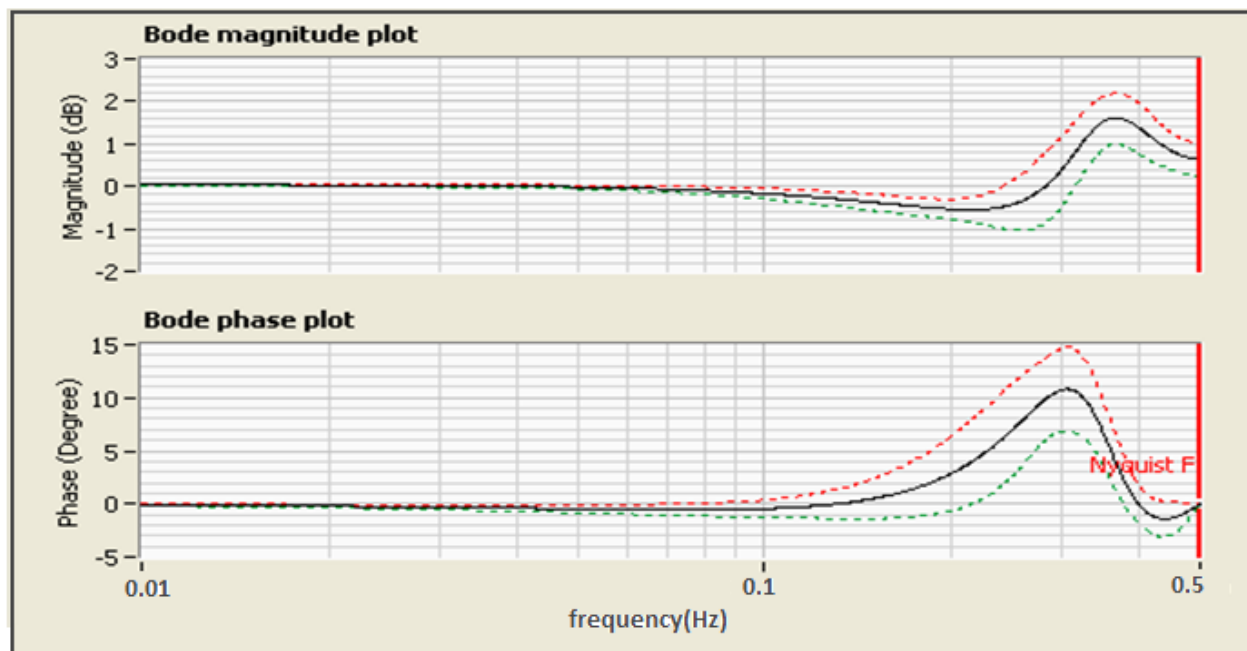


Figure 8.19: Bode plot of the model with lower (green) and upper (red) bounds.

The drilling system prototype concerned here can be seen to be a strictly proper system. In other words, in the bode plot, the gain tends to zero in the limit as frequency tends to infinity, Figure 8.19. This can be attributed to the presence of inertia in the system. The model itself will have robustness errors and they need to be analyzed further by looking for right hand plane (RHP) poles and zeros, cancellations, and analyzing the internal stability of the model. The next section analyzes the probable sources of modeling error.

8.5.2 Modelling error

Real time systems are nonlinear, time varying, infinite dimensional, and very complicated. Modeling error is due to two major reasons.

The model obtained here assumed third order transfer function; this approximation lead to a simpler model and lack of robustness in the model. This was one of the major sources of modeling error. Assuming that the real plant model is $G_p(s)$, and the best model approximation of the plant is $G(s)$; then

$$G_p(s) = G(s) + \Delta G(s) \quad (8.1)$$

Where, $\Delta G(s)$ is the modeling error, or the difference between the real plant model and the best possible plant model.

$$\text{If, } G_p(s) = \sum_{i=1}^{\infty} \frac{N(s)}{D(s)} ; \quad (8.2)$$

$$\text{Then this would imply, } G(s) = \sum_{i=1}^k \frac{N(s)}{D(s)} \text{ and } \Delta G(s) = \sum_{i=k+1}^{\infty} \frac{N(s)}{D(s)} \quad (8.3) \text{ \& } (8.4)$$

Where $\frac{N(s)}{D(s)}$ are the numerator and denominator of the plant transfer function.

Another source of modeling error can be deduced from analyzing the frequency response magnitude; Figures 8.20 and 8.21. The frequency response gains are plotted for two different conditions, for 2.6% mass unbalance and 5.2% mass unbalance. It was noticed that as the frequency increased, the size of the resonant peaks tended to decrease after a certain point ω' . In the frequency response gain plots, the point ω' of the drilling system was seen to be around 150m Hz for the two cases studied. This particular frequency ω' , was noticed to be constant for a particular system and did not vary with added disturbance, here the unbalanced mass. Hence it is safely assumed that for frequencies higher than ω' the magnitude of the frequency response will never exceed the gain at that value.

i.e.;

$$20\log_{10}|\Delta G(j\omega)| = \begin{cases} = 0; 0 \leq \omega \leq \omega' \\ \leq \rho; \omega' < \omega < \infty \end{cases} \quad (8.5)$$

Where ρ is the value of gain at ω' and it represented an upper bound on the magnitude of the frequency response of the modeling error.

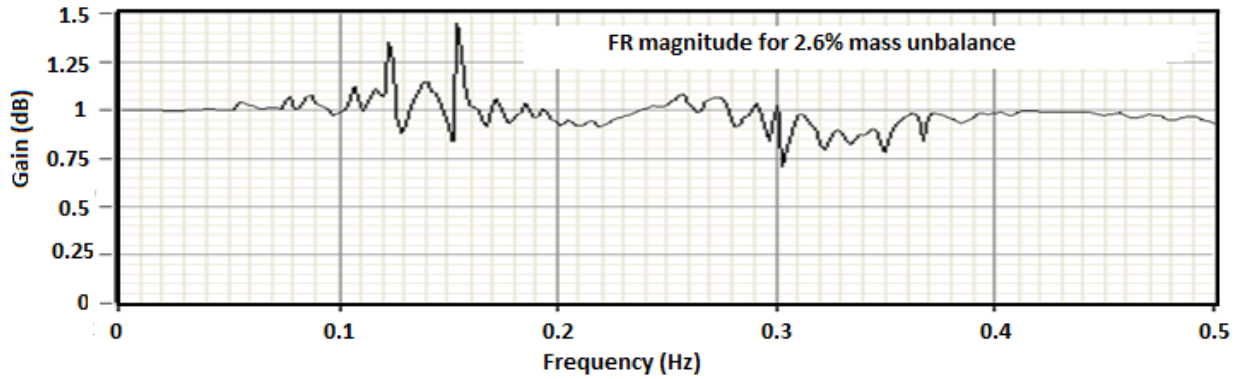


Figure 8.20: Frequency response magnitude plot for small mass unbalance.

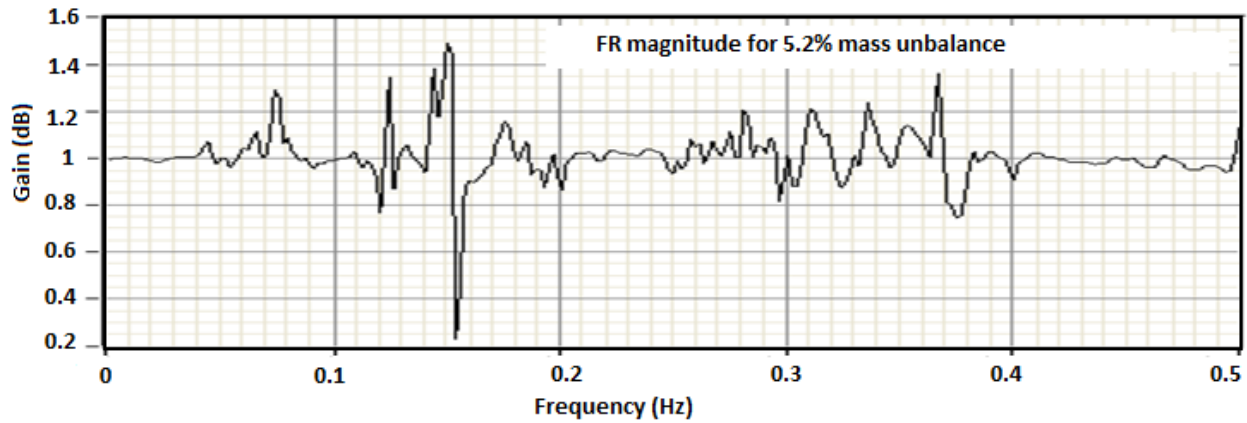


Figure 8.21: Frequency response magnitude plot for large mass unbalance.

Another probable source of error in modeling is from parameter uncertainty. The parameters estimated to obtain the model will have a tolerance associated with their values. Hence at every frequency, the gain and phase response will have an uncertainty associated with its value. These uncertainty bounds are plotted in the bode plot (Figure 8.19) with the upper and lower bound of the magnitude and phase curves.

However, it is concluded that for laboratory scale assessment of vibration and related control the Box Jenkins model can be considered appropriate enough due to residual error values not exceeding 0.2 RPM which is 0.4% of the rotation rate.

The next section will discuss the development of an analytical model to further validate the identified model.

8.6 Validation with analytical model

8.6.1 Analytical model development and simulation

This section presents the development of an analytical model for the rotary drilling system with an unbalanced drill bit (configuration 4). The objective of the model development is to further validate the BJ model by comparing with simulations of an analytically developed model simulations.

The rotary table is represented by a rotating disc with moment of inertia I_1 , the drill string with negligible mass and the drill bit is represented by a rotating disc with moment of inertia I_2 . The entire system is assumed to rotate in an anticlockwise direction about the rotational axis, in the X-Y plane. The unbalanced mass is represented by a mass m_b at a distance 'e' from the rotational axis (known as the eccentricity) placed on the drill bit. The analytical equations for defining the dynamics of the system model were derived using the energy method by Lagrange equations. The derivation of the equations is discussed in the next section.

Four DOF analytical model development

Analytical modeling approach has been used by many researchers for similar dynamical systems. Jansen [1991] modeled the bottom-hole assembly from analytical principles as an unbalanced rotor supported by two bearings. Following this effort, Melakhessou et al. [2003]

developed a four degree-of-freedom (DOF) reduced-order model to study the bending and torsion motions of the drill string as well as the interactions with the outer shell. Liao et al. [2011] developed a four degree-of-freedom model for similar laboratory set-up, and considered contact conditions in detail, which studied bifurcations that arose due to discontinuities in the system. Their model includes the rotary inertia associated with the unbalanced mass. They also developed a five DOF model with the tilt angle of the drill bit as the fifth DOF.

The system discussed in this research work does not include the borehole friction effect, the tilt angle of the drill bit, and the rotary inertia effect due to the unbalanced mass. Hence, the four degree-of-freedom model developed does not take into consideration the contact or friction effects of the borehole on the drill bit.

The Lagrange Equations states that the equations of motion of a multiple degree of freedom vibrating system [Widnall, S. (2009)] can be derived using the equations (8.6-8.9). Φ is called the Lagrangian; and is defined as the difference of the net kinetic energy T and the net energy of deformation U of the system. Further the net kinetic energy is computed for each degree of freedom defined by q_i , using the equation 8.9. Here q is the rotational coordinate for the concerned degree of freedom, i is the n^{th} degree of freedom and δW is the virtual work.

$$\begin{aligned} \frac{d}{dt} \left(\frac{\partial \Phi}{\partial \dot{q}_i} \right) - \frac{\partial \Phi}{\partial q_i} &= T_i; \\ \Phi &= T - U; \\ T_i &= \frac{d(\delta W)}{d(\delta q_i)} \end{aligned} \tag{8.6 -8.9}$$

The system in configuration 4 has four DOFs. These DOF can be represented using the schematic in Figure 8.22. The various DOF are :

- $\dot{\theta}$, the upper rotary speed
- $\dot{\alpha}$, the lower bit speed
- ρ , the displacement of lower disk in radial direction
- φ , the tangential bending angle

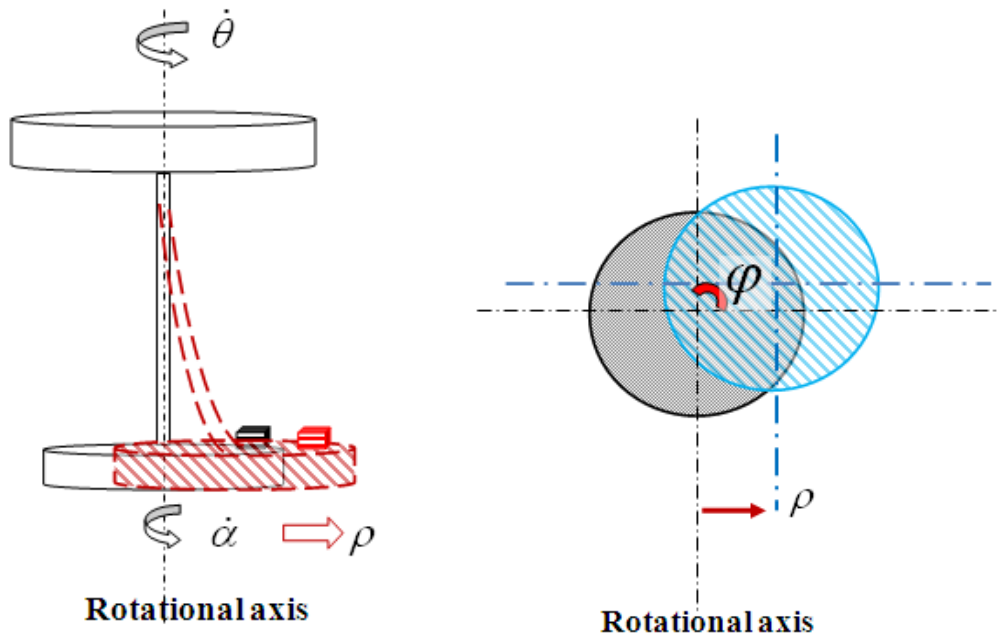


Figure 8.22: Schematic of laboratory arrangement (front and side perspectives) displaying degrees-of-freedom.

In order to derive the Lagrange equations, it is essential to develop the equations for the net kinetic energy, the net energy of deformation and the virtual work.

1. Net kinetic energy:

The net kinetic energy equation for the system consists of the kinetic energy of the upper and lower discs, the kinetic energy associated with the unbalanced mass T_b and the kinetic energy due to the radial displacement of the lower disc V_G .

$$T = \frac{1}{2}I_1\dot{\theta}^2 + \frac{1}{2}mV_G^2 + \frac{1}{2}I_2\dot{\alpha}^2 + T_b \quad (8.10)$$

$$V_G = \dot{\rho}\vec{n} + \rho(\dot{\theta} + \dot{\phi})\vec{t} \quad (8.11)$$

$$T_b = \frac{1}{2}m_b\left(\frac{d}{dt}\vec{OM}_b\right)^2 \quad (8.12)$$

Where \vec{OM}_b is the coordinate of the unbalanced mass.

$$\vec{OM}_b = \begin{bmatrix} \rho\cos(\phi + \theta) + e\cos(\alpha) \\ \rho\sin(\phi + \theta) + e\sin(\alpha) \end{bmatrix} \quad (8.13)$$

Hence the net kinetic energy of the system is:

$$T = \frac{1}{2}I_1\dot{\theta}^2 + \frac{1}{2}m[\dot{\rho}^2 + (\rho(\dot{\theta} + \dot{\phi}))^2] + \frac{1}{2}I_2\dot{\alpha}^2 + \frac{1}{2}m_b e^2 \dot{\alpha}^2 + \frac{1}{2}m_b [\dot{\rho}^2 + (\rho(\dot{\theta} + \dot{\phi}))^2] \\ + m_b e \dot{\alpha} [\rho(\dot{\theta} + \dot{\phi})\cos(\beta) - \dot{\rho}\sin(\beta)] \quad (8.14)$$

$$\text{Where } \beta = \alpha - (\theta + \phi) \quad (8.15)$$

2. The energy of deformation of the drill string is due to three components: bending along radial direction (k_r), tangential direction (k_t), and torsion (k_{tor}) of the rod.

Hence the net energy of deformation is:

$$U = \frac{1}{2}k_r\rho^2 + \frac{1}{2}k_t(\rho\phi)^2 + \frac{1}{2}k_{tor}\beta^2 \quad (8.16)$$

3. The virtual work associated with the system is the external torque (δM) applied at the upper disc to rotate the system. $\delta\theta$ is the change in angular position of upper disc affected by the external torque.

$$\delta W = \delta M_{ext} \delta\theta; \quad (8.17)$$

However, material damping is to be considered and hence an additional term is added; 'c' is the damping coefficient and the energy imparted due to damping is negative because this force is in the opposite direction to δM .

$$\delta W = \delta M_{ext} \delta\theta - c \dot{\alpha} \delta\alpha \quad (8.18)$$

Applying the Lagrange equations 8.6 – 8.9 using 8.14- 8.18;

The equations of motion for the rotational coordinate for the degrees-of-freedom

$q_i = (\rho, \theta, \phi, \alpha)$ are correspondingly:

$$(m + m_b)\ddot{\rho} - m_b e \ddot{\alpha} \sin(\beta) - (m + m_b)\rho(\dot{\theta} + \dot{\phi})^2 - m_b e \dot{\alpha}(\dot{\theta} + \dot{\phi} + 1) \cos(\beta) + k_r \rho + k_t \rho \phi^2 = 0 \quad (8.19)$$

$$I_1 \ddot{\theta} + 2(m + m_b)\rho^2(\ddot{\theta} + \ddot{\phi}) - m_b e \dot{\alpha} \dot{\rho} \sin(\beta) + 4(m + m_b)\dot{\rho}\rho(\dot{\theta} + \dot{\phi}) + m_b e(\ddot{\alpha}\rho + \dot{\alpha}\dot{\rho}) \cos(\beta) - k_{tor}(\alpha - 2(\theta + \phi)) = \delta M_{ext} \quad (8.20)$$

$$(m + m_b)\rho^2(\ddot{\theta} + \ddot{\phi}) - m_b e \dot{\alpha} \rho \sin(\beta) + (m + m_b)2\dot{\rho}\rho(\dot{\theta} + \dot{\phi}) + m_b e(\ddot{\alpha}\rho + \dot{\alpha}\dot{\rho}) \cos(\beta) + k_t \rho^2 \phi = 0 \quad (8.21)$$

$$\begin{aligned}
& I_2 \ddot{\alpha} + m_b e^2 \ddot{\alpha} - \dot{\alpha} m_b e [\dot{\rho} \cos(\beta) + \rho[(\ddot{\theta} + \ddot{\phi}) \sin(\beta)] + m_b e [2\dot{\rho}(\dot{\theta} + \dot{\phi}) + \rho(\ddot{\theta} + \ddot{\phi})] \cos(\beta) \\
& + m_b e [\rho(\dot{\theta} + \dot{\phi})^2 - \ddot{\rho}] \sin(\beta) + k_{tor}(\alpha - (\theta + \phi)) = (-c \dot{\alpha})
\end{aligned}
\tag{8.22}$$

The above equations 8.19- 8.22, represent the dynamic equations of the analytical model for the system in Figure 8.22. The system represents a four DOF rotational drilling process with an unbalance. It represents lateral and torsional dynamics displayed by the drill bit during drilling.

8.6.2 Single DOF model development

Initially only one DOF, α , is considered as unknown. The transfer function model for the single DOF system with unbalanced mass m_b , is developed assuming, $\dot{\theta}$, the upper rotary speed is known, $\dot{\alpha}$ the lower bit speed is unknown, ρ , the displacement of lower disk in radial direction and ϕ the tangential bending angle are zero(neglected). The Lagrange equation for DOF α (equation 8.22) is reduced to apply the above assumptions, to obtain:

$$\ddot{\alpha}[I_2 + m_b e^2] + (\alpha - \theta)k_{tor} = 0 \quad (8.23)$$

In order to simulate the transfer function model, the numerical values of the terms in equation (8.23) are calculated as follows:

1. I_2 is the moment of inertia of lower bit. $2.0016 * 10^{-3} \text{ Kgm}^2$

It is calculated using the well known formula;

$$I_2 = \frac{1}{2} m_2 r^2; \quad (8.24)$$

(m_2 is the mass of lower disc (1.112kg); $r = 60 \text{ mm}$)

2. The second term consists of the unbalanced mass m_b and its eccentricity e .

$$m_b e^2 = 92 * 10^{-6} \text{ Kgm}^2$$

($m_b = 57.5 \text{ g}$; $e = 40 \text{ mm}$)

3. The third term in equation (17) consists of the torsion constant of the drill string, $k_{tor} = 7.742 * 10^{-12} \text{ Nm/rad}$.

The torsion constant is obtained using the formula, $k_{tor} = \frac{GJ_p}{L}$ (8.25)

$$\text{Where the shear constant } G = \frac{E}{2(1 + \mu)}; \quad (8.26)$$

E is the elastic modulus found experimentally for the drill string material to be 193GPa, and the Poisson's ratio, μ is 0.29.

J_p , the polar moment of inertia is $\frac{\pi r^4}{2}$; r is the radius of the drill string 1.49mm, L is the length of the drill string (1m).

Substituting the above values in equation (17),

$$\ddot{\alpha} + (272.316)[\alpha - \theta] = 0 \quad (8.27)$$

To obtain the s domain transfer function, Laplace transform is applied to (21) and zero initial conditions are assumed.

$$\alpha(s) = \frac{272.316}{s^2 + 272.316} \theta(s). \quad (8.28)$$

In the equation (8.23) developed, air damping (or drag) is not considered since the speed is low. However, material damping is significant and is to be included. The amount of material damping is identified experimentally using free vibration. The disc representing the drill bit and BHA mass is spun manually and the observed responses are recorded. The damping ratio is obtained from the decay.

It is found using the formula:

$$\zeta = \frac{\delta}{\sqrt{(2\pi)^2 + \delta^2}}, \text{ where } \delta \cong \ln \frac{x_1}{x_2} \quad (8.29)$$

where x_1 and x_2 are two consecutive maxima in the plot of the under damped oscillating response of the system. The damping coefficient is obtained experimentally (Shear test). It was found to be around 0.995;

The transfer function model is now changed by adding the 0.995s in the denominator. The TF

$$\text{model is: } \alpha(s) = \frac{272.316}{s^2 + 0.995s + 272.316} \theta(s). \quad (8.30)$$

8.6.3 Single DOF Model analysis and validation

MATLAB[®] is used for simulating the analytical model response. The input and output of the transfer function model obtained in equation (8.30) are in radians. However the data obtained experimentally is the speed in RPM. Hence the data is first converted to radians per second and integrated to get the position data in radians. The output of the transfer function model is similarly differentiated and scaled to get the model simulated response in RPM. The MATLAB[®] Simulink block diagram developed for the simulations is displayed in Figure 8.23. In the below block diagram:

The experimental input (upper rotary data; outlined in red block) is fed to the transfer function model (green block) to simulate the model response. The model simulated response is then compared with the experimental output (lower bit data; outlined in blue block) and displayed in the plots in the Figures 8.24 and 8.25.

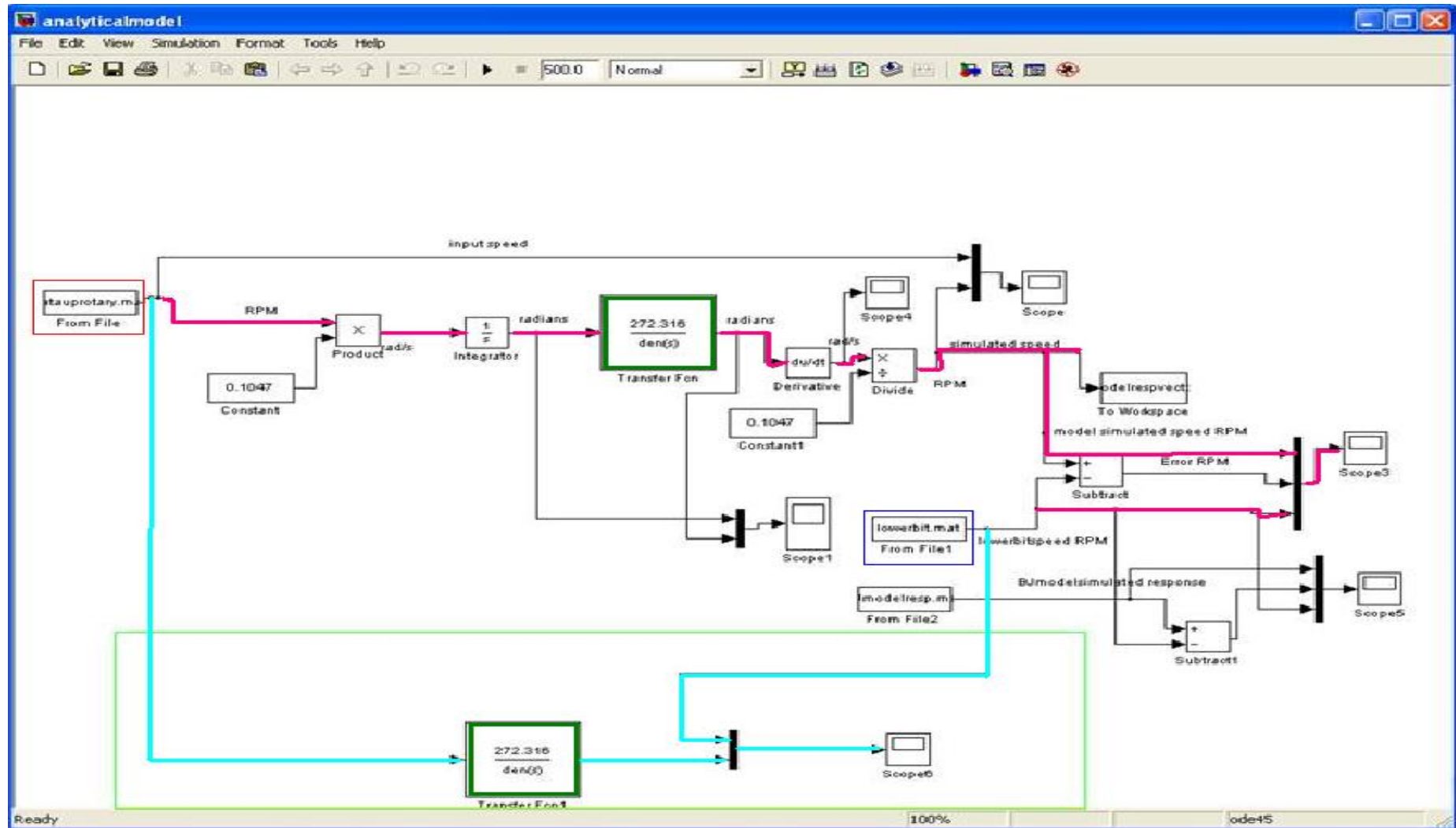


Figure 8.23: MATLAB[®] Simulink block diagram developed for simulating the SDOF model.

The data flow in the Block diagram is explained using color-coded routes for easier understanding.

The Pink line route (method 1): The upper rotary data recorded by the incremental encoders is in RPM, it is converted to radians per second and then to position (radians). The position data is fed to transfer function block. The model response in radians is derivated to radians per second and converted to RPM. The RPM simulated response is compared with the experimental output. The compared plots are displayed in Figure 8.24.

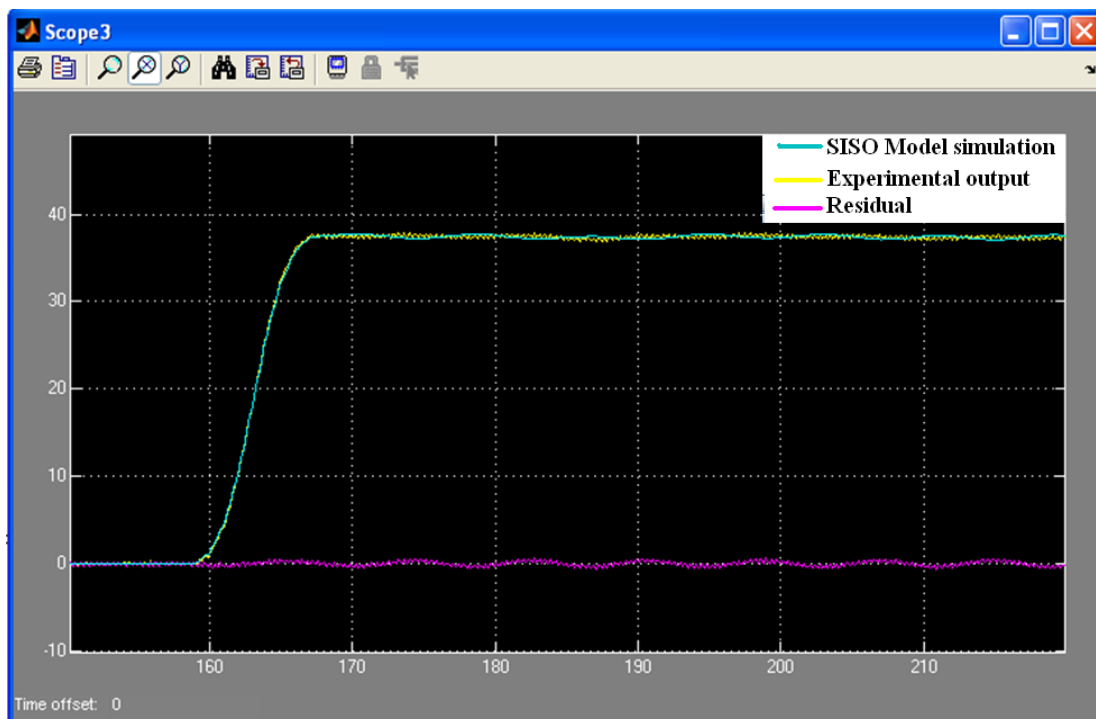


Figure 8.24: Analytical model validation

The Blue line route (method 2): This part is only to compare the simulation of the model response when the angular velocity or position data is input to the model. The upper rotary data is

directly fed to the transfer function block. The model simulated response is compared with the lower bit data and displayed in Figure 8.25.

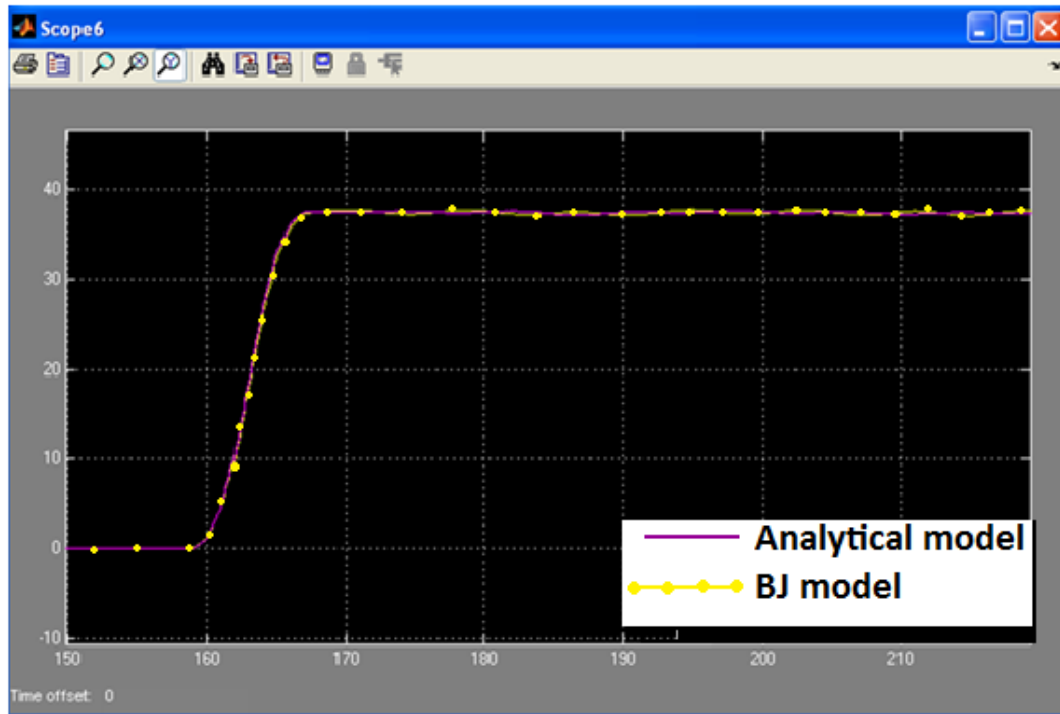


Figure 8.25: Comparing BJ model and analytical model simulations.

Conclusion:

A very good match is obtained between the analytical model and the Box Jenkins model simulated responses. The analytical model is popular and widely used for researches. This further strengthens the accurateness of the identified Box Jenkins model. The next section develops the matrix format for the 4 DOF system dynamic equations. The matrix format representation is widely used to simulate multi DOF systems. A 4 DOF analytical model is also developed for future reference in Appendix 6.

Chapter 9. Analyzing solutions to mitigate drill string vibrations

This chapter presents experiments conducted to determine the natural frequencies of the laboratory set up. The findings of the experiments are evaluated and incorporated in the following chapter 10 to develop controller to mitigate drill string vibrations. A short analysis of vibration controllability challenges when vibrations are induced by unbalanced drill bit or a bent drill string is also presented.

9.1 Vibrations and critical speeds

The experiments in Chapter 6, proved that the vibrations were noticeably higher when operating at some particular speeds. These operational speeds at which vibration intensifies are called critical speeds. Dareing (1984) stated that the various vibrational modes (lateral, torsional and axial) have separate excitation frequencies associated with each of them. When the drilling rig is run at these particular critical speeds, these vibrational modes get excited and aggressive vibrations take place. Hence there is a need for the identification of these critical speeds in order to avoid these speeds during operation. They developed formula which proves a directly proportional relationship between the critical speeds and the natural frequencies of the drill collar. However, the drill collar length changes during the drilling operation as the drill borehole gets deeper. Due to it, the natural frequencies of the drill collar associated with each of the vibrational modes will hence change [Dareing, (1984), Cobern, (2005, 2007)]. The importance of the relation between the critical speeds and operational speed was utilized by Bailey et al., (2008) when they

developed a BHA modeling tool which, for a particular operating range will avoid the critical modes causing resonance.

However, most of the recent technologies have not incorporated the above concept in designing new vibration mitigation active and passive controllers. In the next section, the frequencies of the system and critical speeds are identified and used for developing controller in chapter 10.

9.2 Identifying the presence of natural frequencies

Realizing the important role of natural frequencies and their relation to vibrations in rotary drilling, tests were conducted to detect the natural frequencies of the laboratory set-up. The most common and reliable method to detect the natural frequencies of a system is to find the fast fourier transform (FFT) spectrum of the system output. Here, the FFT of the drill bit angular velocity was computed and plotted using MATLAB[®]. For increased accuracy of the findings the system was operated at three velocities (37, 53 and 98 RPM) within the operating range of rotary drilling rigs. Tests are conducted under configurations 3 and 4 of the laboratory set up.

The laboratory set-up with configuration 4 is operated at three speeds spanning from the low to high operational speed range (30 – 100 RPM) of rotary drilling. The frequency response (FFT) of the drill bit angular velocity is plotted using MATLAB[®] for analyzing and detecting the system natural frequencies. The part of the MATLAB[®] program used for plotting the FFT spectrum is added as Appendix 5.

Figure 9.1 displays the FFT spectrum of the drill bit rotational velocity data while experimenting for the bend drill string dynamics. The laboratory operational velocities are selected such that they are within the operational range of rotary rig operating velocities.

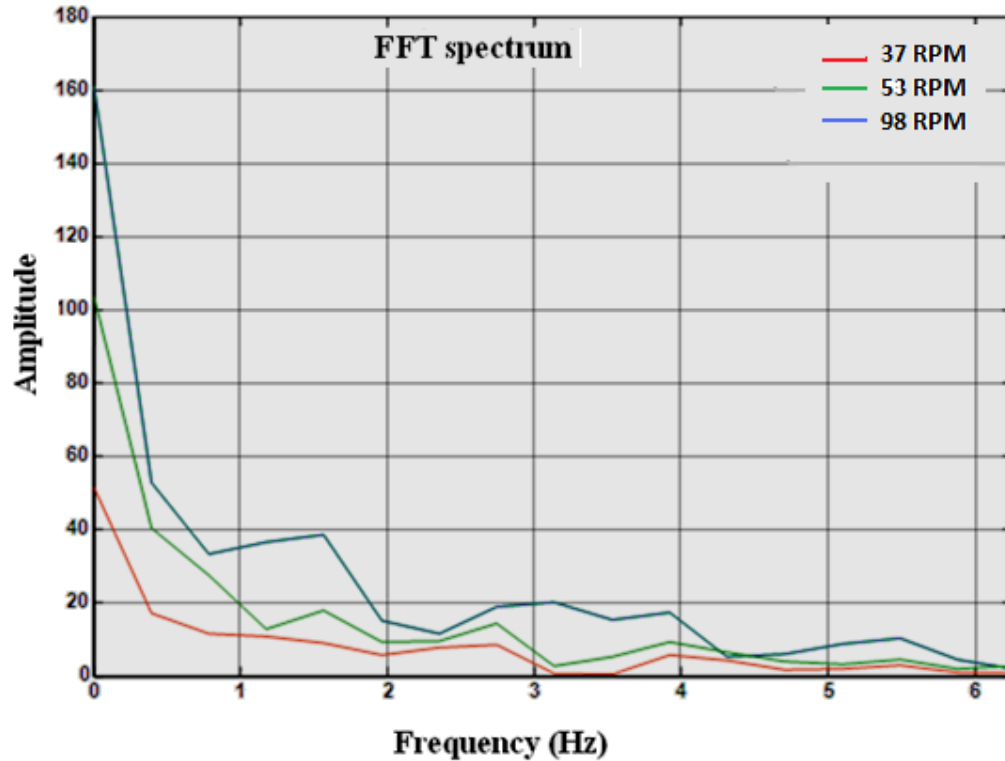


Figure 9.1: FFT spectrum for configuration 4 laboratory set up.

In order to analyze the borehole effect on the drill bit whirl dynamics, the following test is done with configuration 3 and 4 of the laboratory set up together. This combination ensured that well defined prominent vibrations were now present by the system. The FFT spectrum of the output data for the whirling tests under borehole influence was plotted in Figure 9.2. It was noticed that the frequency of the whirling is higher and sharper than the whirling due to the drill bit imbalance. The frequency response plots had sharper spikes and laboratory observations in Figures 9.1 and 9.2, both proved that the vibrations exhibited by the drilling system were aggravated in the presence of borehole friction.

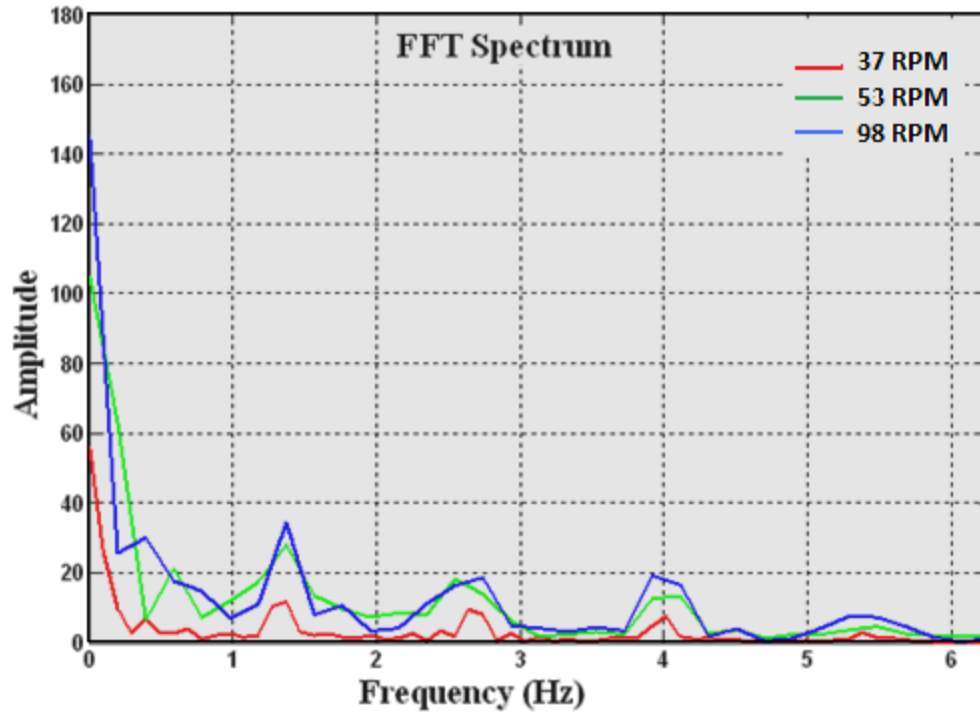


Figure 9.2: FFT spectrum for laboratory set up configuration 3 and 4.

Analyzing the plots, it was noticed that the system had more than one natural frequency, and the resonant frequencies of the system did not vary with the operational speed. Comparing the FFT plots (Figures 9.1 and 9.2), it was noted that the resonant modes are excited and more prominent when the external borehole effect was present. Experimentally, the lateral and torsional vibrations exhibited by the drilling system were noticeably more severe under the borehole friction effect. The laboratory system had 4 degrees of freedom, hence the natural frequencies can be corresponded to this number of degrees of freedom.

Using the data in the frequency response plots, the critical speeds for the system for the various excitational modes (Section 9.1) are calculated using the formulae (equations (10.5), (10.6), (10.7)) developed by Dareing, (1984). If the system was operated at operational speeds near or at the critical resonant frequencies in the plots above, high vibration would be seen. In order to verify

these conclusions, laboratory tests under borehole influence were conducted. The presence of resonant vibrations was reflected in the angular velocities recorded during the above tests with configuration 3. Critical speeds of operation and subsequent high vibrations were noticed at 53 and 83 RPM of operation (Figure 6.6b and 6.6d).

9.3 Controllability of Bit whirl

The preceding analysis of drill bit whirl revealed that the bit whirling phenomenon occurs due to two major causes: (a) Drill bit imbalance and (b) bent drill pipe. It is notable that both the causes are physical. If the cause of the unbalance is manufacturing bit imbalance, the solutions currently available are to design newer and better drill bits [Warren T., (1990), Pastusek, (1992), Chen S.L., et al., (2002), Johnson S., (2008)]. However, if the cause of the bit whirl is an eccentricity in the pipe or a bent drill string this could be a difficult control problem with few, if any solutions, as discussed below.

The drill bit is not directly energized and hence there is lesser number of actuated elements when compared to the degrees of freedom for the rotary drilling system. Thus the drill string system is an example of an under actuated system.

Realizing the drill string as a special under actuated system, it now follows to investigate the possibility of applying control principles of under actuated system control (Chapter 3, section 3.2) to the drill string set-up.

9.3.1 Conclusion on applying under actuated control laws to bend drill string dynamics

Under actuated control objective is to control the position or a specified movement. But not velocity and position control together which is the control objective. In the swing up control of

Jerome, (1991), discussed in section 3.2, the control objective is to make the linearized degree of freedom, link1, to track a suitable trajectory. Here, the controller objective is to control the pendubot only at the equilibrium positions. No external disturbance is affected at link 2. The positions of the links are not synchronized during the control operations.

Moreover the full state feedback controller is designed by initially linearizing the model in the required or set equilibrium positions. Thus control principle can only be applied to simple linearized models of the drill system, and cannot be proven practically on a nonlinear laboratory set-up. Moreover, the problem is to set two trajectories to be followed in the presence of unexpected disturbance. Also, the control is achieved in case study 1 for only a short period of time. Control can be well said to be near impossible to be achieved in the drilling system, which is operated in a highly unpredictable environment for an extended period of time.

The flatness based control solution of case study 2 (section 3.2) is used to model a rest to rest maneuver. It should be noted that external friction/ damping force is not affecting the under actuated disc. Here again, the positions and velocities of the actuated and under actuated parts are not synchronized and are widely different at the time of application of the control law. Such a situation in the rotary drilling will induce torsional vibration because of the friction developed at the drill bit by the bore hole and could result in more severe phenomena like backward whirl.

From the above analysis, it can be concluded that the physical causes inducing drill bit whirl can be overcome only by using other physical solutions; like new drill bit designs or dampers near the BHA. However, the effect of borehole friction and critical speeds of operation could be minimized by using controllers.

Chapter 10. Control methodology and implementation

This chapter discusses the control design law development and implementation on the laboratory set up under configuration 3 . Previously, it was concluded that the control strategy which would minimize the vibrations affecting the drill string and stabilize it would have to ensure that the drill string set-up is operated at a velocity away from its critical speeds of rotation.

It is known that the drill string natural frequencies and critical speeds vary during the drilling process as the well deepens and the drill string length changes. This posed a challenge to have a method to identify the critical speeds of the system during drilling operation. However, new tools which were developed like the BLACKBOX down hole dynamics data recorder, can log dynamic data, and researchers have identified methods for online detection of natural frequencies for complex nonlinear systems [K.J.Kim et al., (1984), M. Bodruzzaman, et al., (1994), X. Xu, (2003)]. The controller developed should adapt its control output to effectively stabilize the system based on the identified natural frequencies and critical speeds. The complete control system has four objectives: to detect the vibration of the system above an acceptable threshold value, to force the system to operate at a stable operating speed away from the system's critical speeds, to pull / free the axially displaced drill bit from the fluid /mud forces to a point near its center of rotation, and to resume normal operating speeds as soon as the vibration decreased below the threshold.

The point of the control law is that the rotary drilling system is a stable system, affected by external disturbances which make the system unstable. So the control law effectively returns the system to its initial stable dynamics by helping the system to free itself from the de stabilizing forces and forcing the system to operate in its stable region.

10.1 Self tuning adaptive control:

As per the definition, an adaptive control changes or adapts the design of the control algorithm to accommodate changes in the plant or its environment. There are two major types of adaptive control: self tuning and model reference. This research used self tuning adaptive control. Model reference control requires a reference model. Because the drill string length changes as rotary drilling progresses, the model for the system would also change. This would imply the necessity of using an additional system to identify the model for the system continuously and developing the controller based on its performance. This would unnecessarily complicate things further, because as detailed earlier it is important to detect online the natural frequencies of the system to generate an efficient control law. Model reference control applied here would then necessitate a twofold online identification system: online identification of process model and process natural frequencies. Adaptive control applied to complex systems itself is quite complex and requires good data synchronization. Based on the fact that it's better to simplify where possible without losing quality results, this research developed an adaptive control law which was also proven experimentally.

Self tuning control of a plant has three major parts: feedback control law, a control design, and an online identifier. The feedback control law should be designed to give control performance based on the data from the online identifier. The online identifier should provide good estimates of the data required to form the control law. The control design algorithm uses the estimate of the online identifier to update the feedback control law.

For the current research system the above three parts are defined as following: the adaptive control signal served as the feedback control law, the synchronization of the flow of data using a

vibration detector, the command signal selector and signal generation as the control design algorithm, and the online natural frequency identifier served as the online identifier.

The adaptive controller developed for the research was a combined application of minimum variance and gain scheduling algorithms.

10.2 Controller development and implementation

Developing a minimum variance control law:

Consider a discrete process model

$$y(t) = \frac{z^{-k}B(z)}{A(z)}u(t) + \frac{C(z)}{A(z)}n(t); \quad (10.1)$$

where $y(t)$ is the output, $u(t)$ the input and $n(t)$ is white noise at any sampled instant t and k is the process delay. For schematic and details of the equation (10.1), please refer section 7.5.

$$E[n(t)n(s)] = \begin{cases} 0, s \neq t \\ \sigma^2, s = t \end{cases} \quad (10.2)$$

[Assume $k \geq 0$; and

Then the control law for minimal output variance is obtained as

$$u(t) = \frac{-G(z)}{B(z)F(z)} y(t) \quad (10.3)$$

$$\text{by solving for: } C(z) = A(z)F(z) + z^{-k}G(z). \quad (10.4)$$

However, the rotary drilling system is an under actuated system (chapter 2) with the drill bit being the under actuated part [F. Abdul Majeed (2011)]. It is also the part affected by external disturbances and the source of nonlinear phenomena such as bit whirl, stick-slip, etc. The under actuation of the drill bit posed a serious problem to the results which could be obtained practically by the application of any control law. This is because the control objective was to minimize the vibrations of the under actuated part. Moreover, the control objective is more complicated by the fact that the under actuated part was affected by unpredictable and uncontrollable external disturbances (like well bore hole friction, hard rocks, etc). However, application of control

technology is proven in simulations and this has been widely demonstrated in numerous publications [Eva.M & D.Cortes, (2007), Shi Fubin, et al., (2010), Li. L, et al., (2011), etc].

Here, in order to achieve the control objectives practically a new control mechanism based on gain scheduling was applied. Research suggestions from [Dareing, (1984), Cobern, (2005, 2007)] were carefully considered and incorporated. They suggested the importance of avoiding the critical speeds during rotary drilling operation as the better predictable method of minimizing the drill bit vibrations. Dareing, (1984) had developed equations relating the critical speeds of resonance to the natural frequencies of the rotary drilling system.

$$N = 60.f_n; \quad (10.5)$$

i.e.; for a natural frequency f_n (Hz) of the drilling system, the critical speed of operation of the drilling process to excite it will be N (RPM).

However, the natural frequency is inversely related to the length of the drill string [Dareing, (1984)] and hence the natural frequencies corresponding to different modes of vibrations will change continuously as drilling progresses.

The natural frequency of the fundamental drill collar longitudinal mode is:

$$f_{na} = \frac{1}{4L} \sqrt{\frac{E}{\rho}}; \quad (10.6)$$

And the natural frequency of the fundamental drill collar torsional mode is:

$$f_{n\theta} = \frac{1}{4L} \sqrt{\frac{G}{\rho}}; \quad (10.7)$$

Where E and G are the compression and shear constants of drill string material, ρ is the material density and L is the length of the drill string.

The above equations were used for developing a control law which selected the appropriate speed of operation for the drilling system based on gain scheduling the natural frequencies of the process obtained by an online identification procedure. An example online procedure of obtaining the natural frequencies is detailed in Appendix 6.

The applied control law is:

$$u(t) = 60.f \sin 2\pi nt; \quad (10.8)$$

where f is a frequency (Hz) in the low frequency of operation of the drilling process which is also not near any of the natural frequencies of the system and n is the original frequency (Hz) of operation of drilling. This frequency f was selected using equation (10.5) so as to avoid all the critical speeds of resonance. The selected f was taken up by the adaptive controller which produced the control signal as defined by the control law in equation (10.8). The controller is termed adaptive, due to its necessity of adapting the operational frequency according to drill string length variation. The next section describes the simulation of the plant model in configuration 3 with the controller. Testing of the controller on laboratory set up is provided in following sections.

10.3 Simulation of Closed loop control

This section presents the simulation results of the controller developed in the last section. The laboratory set-up is operated with configuration 3. In order to model the system dynamics, a chirp input is applied to the laboratory set-up, the data are recorded and a Box Jenkins (BJ) model is estimated using the Lab VIEW System identification tool kit (detailed in Chapter 7 and 8).

A fourth order Box Jenkins model is estimated using the tool kit for configuration 3. The transfer function and the pole-zero plot obtained for the model are displayed in Figure 10.1. The poles and zeros for the estimated BJ model are seen to be inside the unit circle and well placed in the left half plane, indicating a stable model. The response of the model is plotted as the 'estimated BJ model response' in the plot. The external effect induced by the rubber sponge lining is modeled separately using signal generation functions and added to the estimated model. The complete model (the estimated model with the external effects modeled) is termed 'BJ model'. The response of the 'BJ Model' is simulated and validated by comparing the simulated response to the process response (Figure 10.1). The objective of the simulation is to analyze the controller effect in mitigating vibrations.

The developed model is simulated in closed loop with the controller developed in the last section. The closed loop simulation showed good vibration mitigation results. The programs were developed using LabVIEW™ control and simulation module. The results obtained are plotted in Figure 10.2. Analyzing the plot in Figure 10.2, it was noticed that the controller detected the vibrations in a matter of seconds, injected the control signal and resumed normal operation by switching control in around 5 seconds.

However, as discussed in the earlier chapters, the rotary drilling system being a special case of under actuated system, the control law applied can only be verified if the simulations are proven experimentally. The next sections discuss the data communication interfacing and deployment of the control law on the laboratory arrangement.

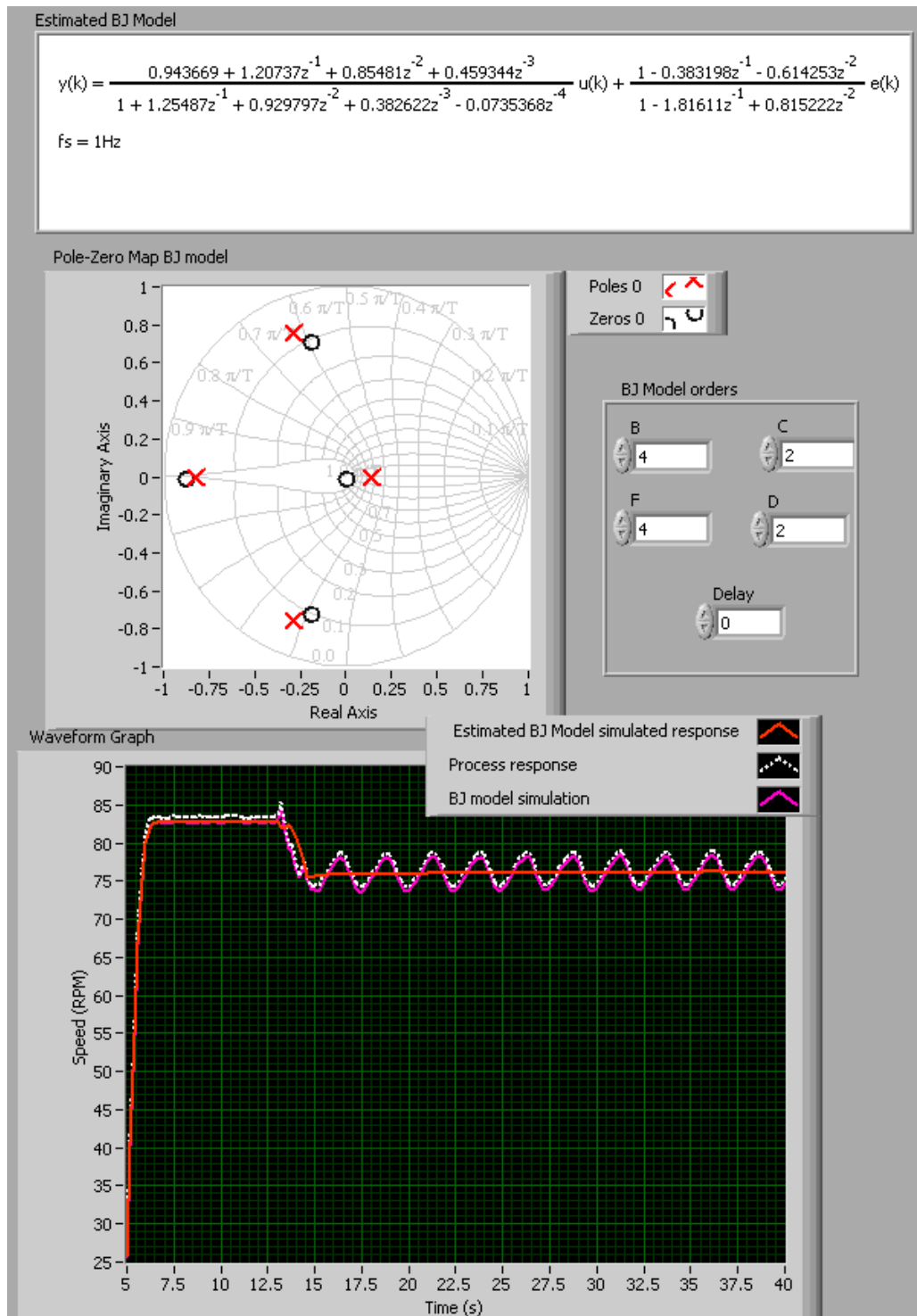


Figure 10.1: Estimated model and open loop model simulations.

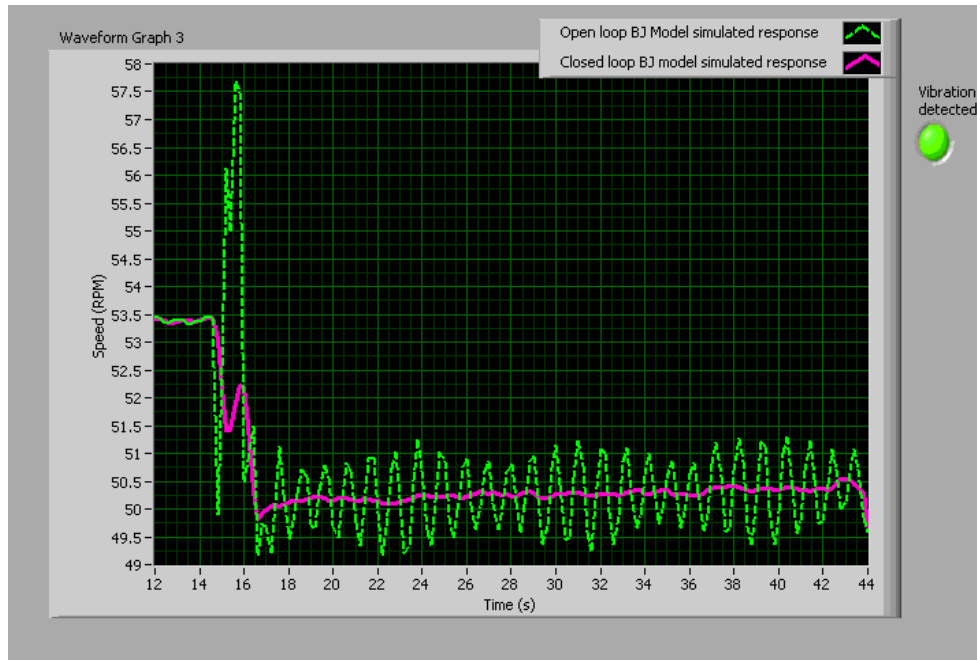


Figure 10.2: Open loop and closed simulation results.

10.4 Closing the loop - Laboratory Data synchronization using LabVIEW™

The control objectives detailed in section 10.2 were met by a complex synchronization achieved between the operating command signal, the developed adaptive controller signal (section 10.2) and the laboratory rotary drilling set-up. Figure 10.3 displays the schematic of the flow of data between the software and hardware parts of the closed loop system. The various parts synchronizing to apply the self tuning adaptive control law is also displayed in the Figure 10.3. The angular velocities of the upper rotary and drill bit are the data used by the vibration detector and the online natural frequency identifier. The data are measured by incremental encoders and logged using LabVIEW™ programs. The vibration detector plays an important part in deciding the level of vibrations. It is also responsible for switching the motor excitation signal between the operating speed and control signal. The threshold value is determined by the amount of vibration levels the system could withstand and will vary depending on the system. The amplitude of the control signal is selected by the adaptive controller using the system natural frequency data to operate the system at a speed away from system critical frequency. The control signal is designed to be sinusoidal so that the system can force itself out of any friction or holding force at the drill bit end. The vibration detector is responsible for the switch back of the excitation signal to normal operating speed to resume normal operation once the vibration level is reduced and maintained below threshold level for a specific time. The next section describes the recording and logging of vibration data about all the three axes.

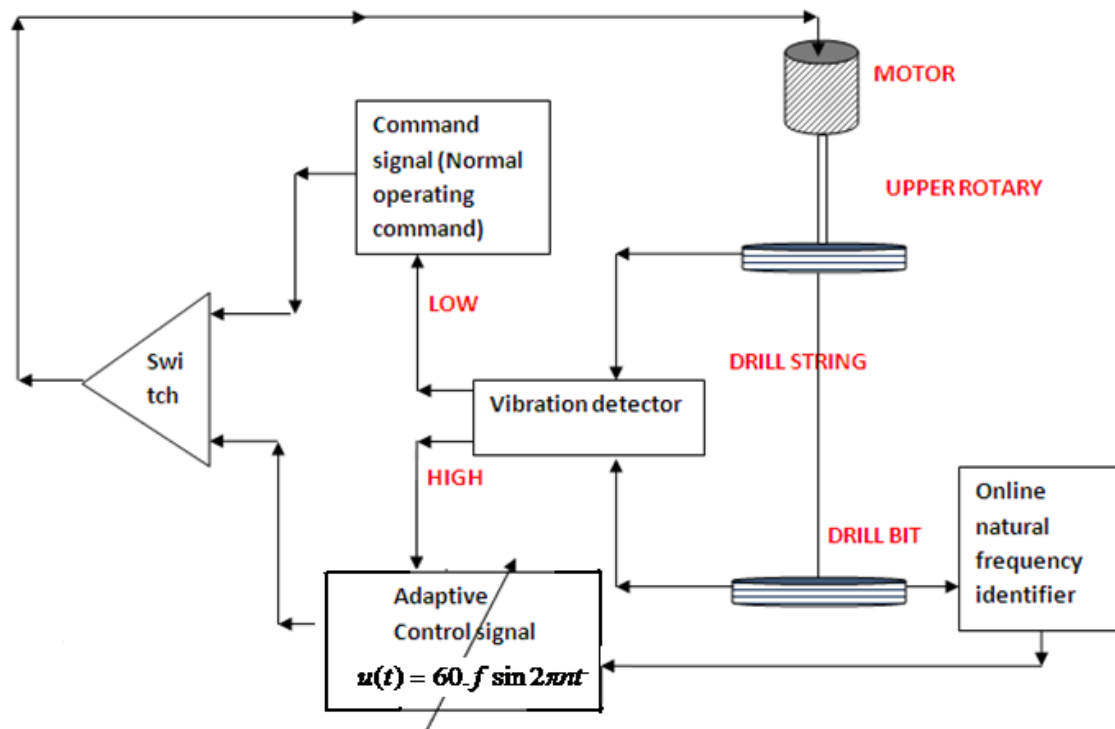


Figure 10.3: Schematic of flow of data during synchronization of the operating command signal and adaptive control signal.

10.4.1 Experimental closed loop configuration 3 observations

The controller discussed in the previous section was implemented using LabVIEW™ on the laboratory drilling arrangement. The block diagram and front panel view of the developed LabVIEW™ VI are given in Appendix 4. The closed loop of the control scheme (Figure 10.3) applied experimentally to the configuration 3 laboratory set up. In Figure 10.4, the laboratory set-up configuration 3 was operated at 54 RPM. The drill bit angular velocity was recorded and plotted in the Figure. The drill bit was seen to rotate with no major vibrations. Whirling vibrations are introduced by affecting the drill bit with the braking system (section 6.1). Under open loop operation, the drill bit was observed to be in prolonged whirling condition (green signal). However, when operated in closed loop (red signal), the adaptive controller detected the increased vibration levels, and started closed loop control action. When the vibration persisted above the threshold value for a specified time, the vibration detector switched the command to the controller. The controller took over the operation of the system and forced the upper rotary to rotate according to the control law in equation (10.8). This initialization of control action is depicted by the sudden dip, (Figures 10.4, 10.7 and 10.8) which is induced by the control signal to minimize the vibration. The control signal produced by the controller was observed to force the drill bit to equilibrium by operating it such that it is taken away from its resonant modes of frequency. The vibration detector now detected the vibration levels of the drill bit to have come down and remained within the threshold value. The switch is then switched back to the command signal to resume normal operation.

The blue and purple signals (Figure 10.4) are the differences in angular velocities of the upper rotary and drill bit during the open and closed loop tests respectively. On observing these signals it is noticed that the upper rotary and drill bit are operating at different magnitude and phase

during the vibrations. This indicated the presence of lateral and torsional vibrations at the same time.

During closed loop operation, the controller minimized both the vibration effects and the residual signal (purple) was seen to be stable and near zero. This is further strengthened by monitoring the vibrations using a Kionix 3 axis accelerometer during the tests. The accelerometer recorded the linear vibrations in all three axes during open loop bit vibrating condition as plotted in Figure 10.5. The acceleration data recorded during closed loop operation was plotted in Figure 10.6. The plots proved the presence of vibrations in all the 3 axes and the minimizing of the vibrations about all the 3 axes by the controller in closed loop operation.

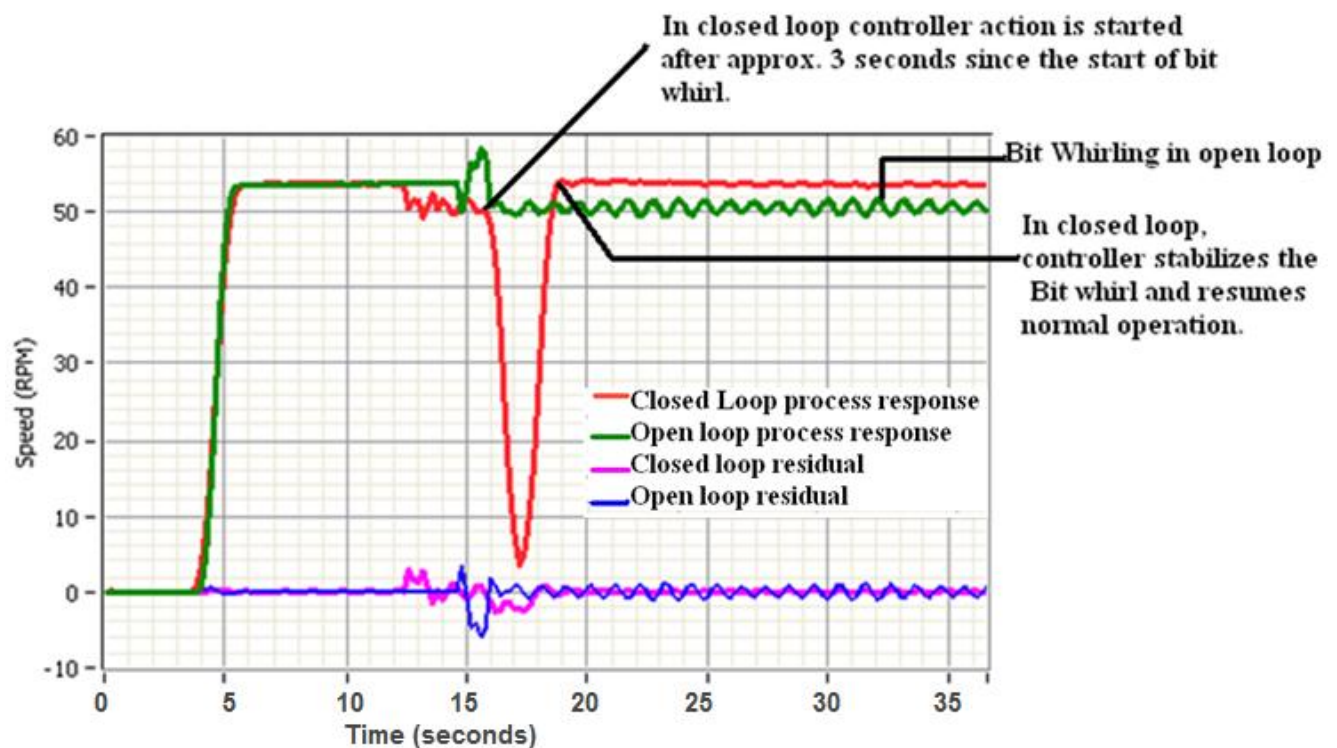


Figure 10.4: Experimental open and closed loop observations at 54 RPM operation.

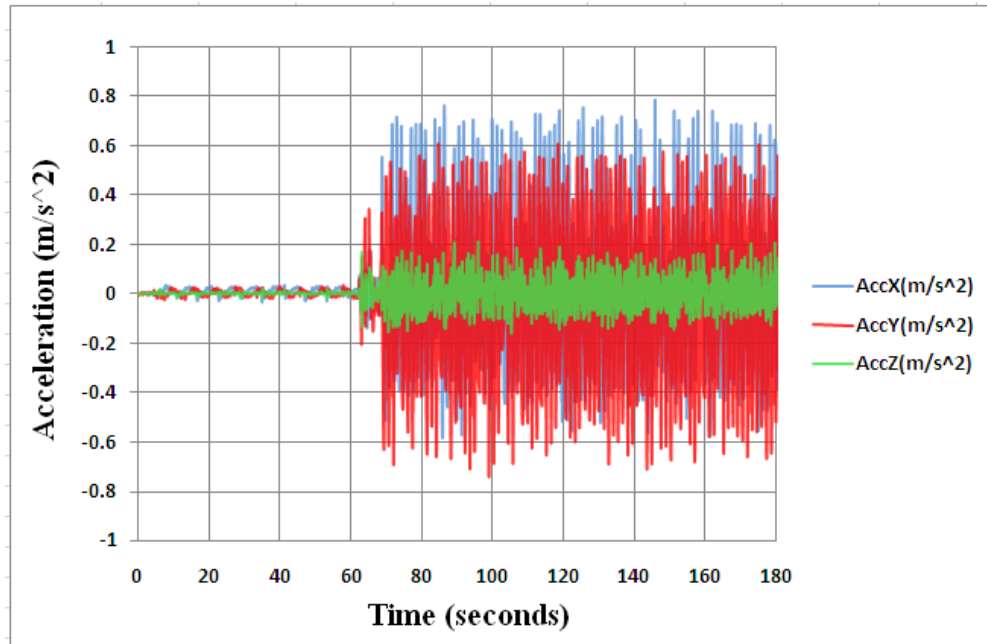


Figure 10.5: Three axes acceleration data of the drill bit whirl control in open loop.

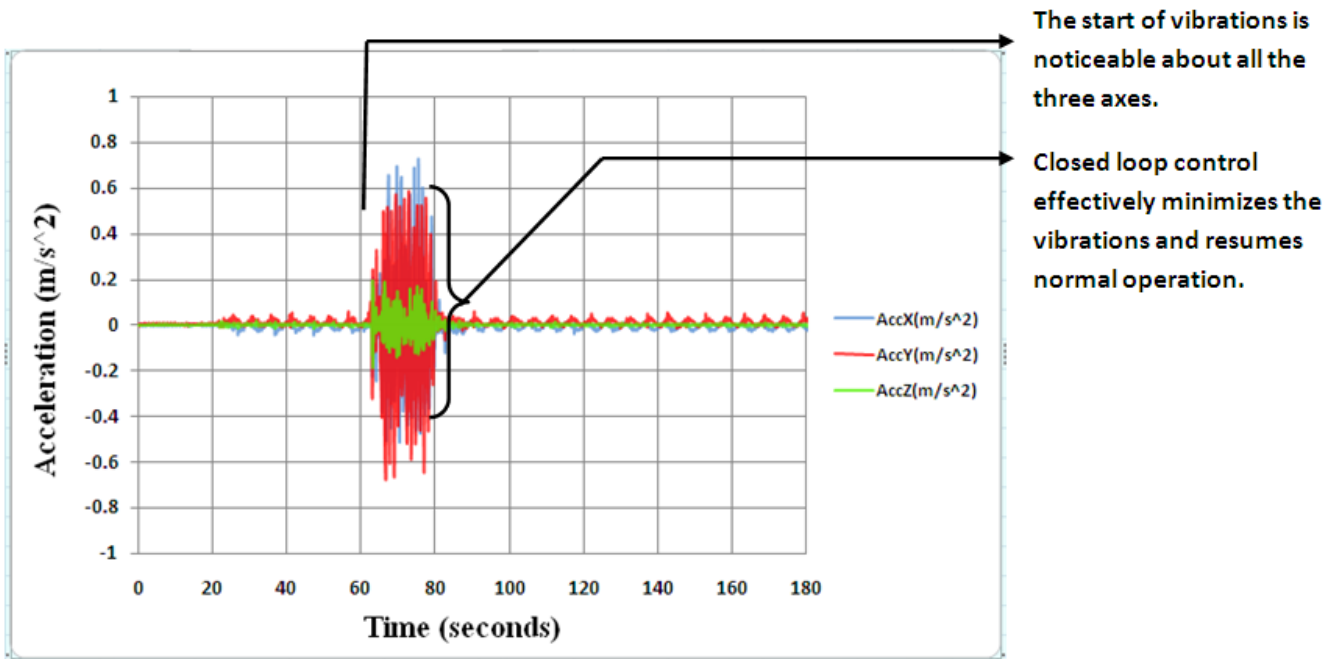


Figure 10.6: Three axes acceleration data of the drill bit whirl control in closed loop.

Figure 10.7 displays the plot of the open and closed loop operation of the system at 84 RPM. Results similar to above discussion were seen. A clear reduction in vibration and fast resuming of the normal operation was achieved by the controller.

It should be noted that during experimentation in laboratory, the controller was effective in minimizing vibrations in a very short time. However, in real system if this control effect gets prolonged due to drill bit borehole friction etc, the controller has been designed to move in opposite direction, thus aiding to retrieve the drill bit from being stuck in the borehole.



Figure 10.7: Experimental open and closed loop observations at 84 RPM.

10.5 Testing controller on configuration 4 laboratory set-up

This section presents results when the developed controller is tested on the laboratory set-up configuration 4. An unbalanced of 5.2% was added to the drill bit (Chapter 6). However, due to the smaller scale of vibrations displayed in this case, the vibration detector was tuned to a vibration threshold value of 0.5 RPM. The set-up was operated in open and closed loop conditions. Small vibrations were noticed under open loop conditions due to the presence of the unbalanced mass. Under closed loop operation, a slight disturbance was induced as previously by the braking arrangement to increase the vibration levels to levels which could be detected by the controller. The controller immediately detected the vibrations, minimized the effect and resumed normal operation as can be observed from the experimental data recorded in Figure 10.8. The Figure 10.9 displayed the residual signal between the upper rotary and drill bit speeds, the vibration level and closed loop vibration minimization are clearly visible in the plot.

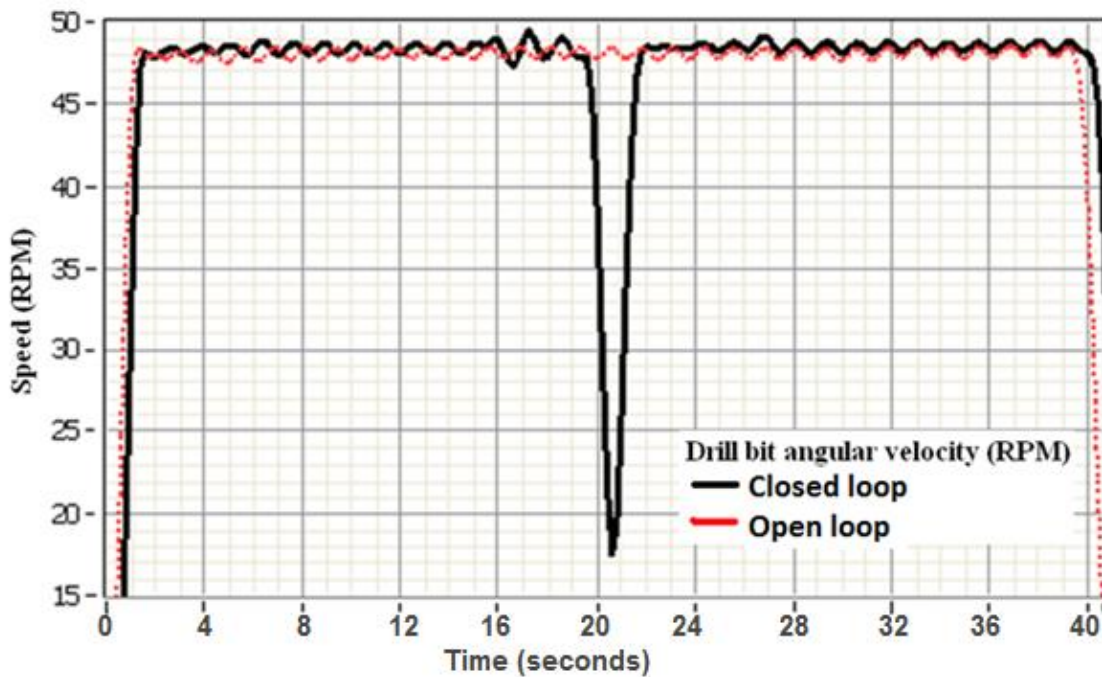


Figure 10.8: Drill bit angular velocity in open and closed loop configuration 4 operation.

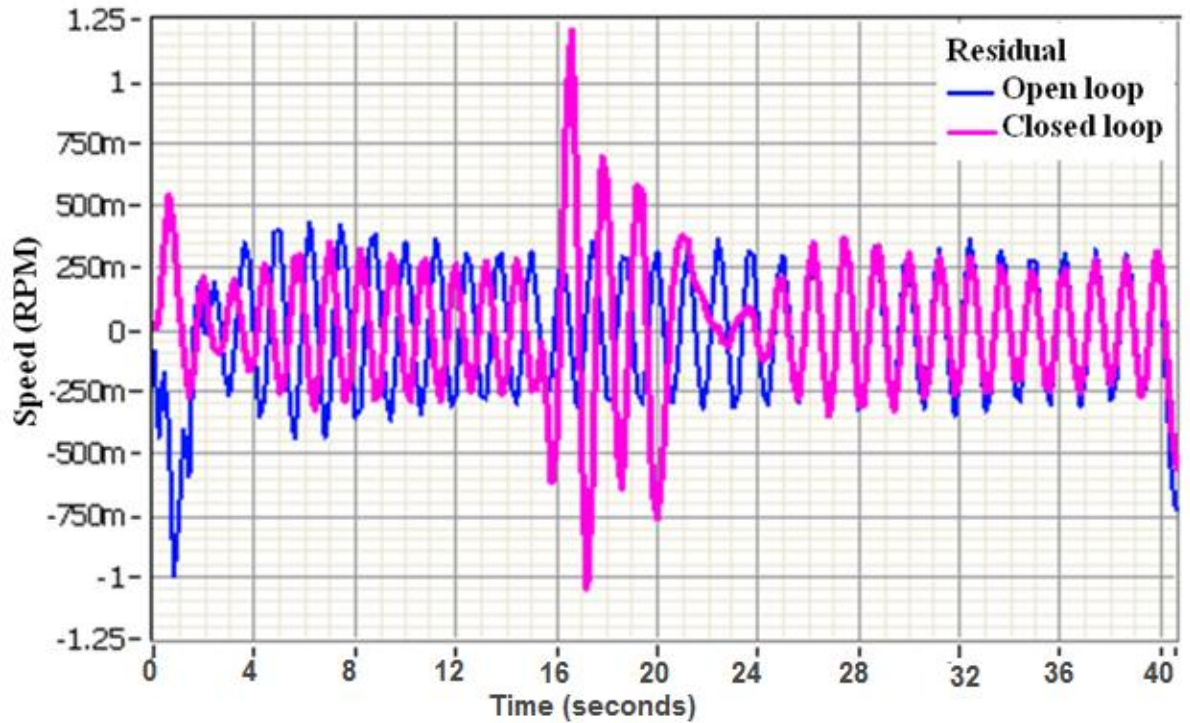


Figure 10.9: Residual signals in open and closed loop operation.

The experiments proved that the controller actively mitigated the effect of the added disturbance inducing high vibrations in a very short time of 6 s. However the controller could not affect the vibrations caused due to the unbalanced mass. These vibrations were present in the system and were visible even after normal operation was resumed by the controller. This further verified the conclusions drawn in section 9.3 that the vibrations induced by the physical causes can be overcome only by using other physical solutions; like new drill bit designs or dampers near the BHA. The next section compares the results obtained in this section to other researches which have applied control technologies to mitigate drill string vibrations.

10.6 Comparison to other experimental research

Much research has been conducted in the field of drill string vibration mitigation. However, most of the attempted control schemes have used simulations to prove their predictions. Previously, the drill string in rotary drilling was discussed in chapter 3 as a special case of an under actuated system. The upper rotary table being the actuated part, with its actuation derived from the electric generator. The drill bit however, is kept in the drill bore hole by ensuring a narrow bore hole and the drill collars which provide heavy weight on the bit. Thus the drill bit is positioned on the borehole and its actuation is done by conducting the driving torque provided by the electric generator through the upper rotary table. The drill bit thus forms the under actuated part; i.e., not directly actuated. Most of the power imparted to the upper rotary is lost during transmission to the drill bit at the tool joints and as heat. The drill bit is also the most subjected part of the process to external influences and thus forms the source of all damaging vibrations. Due to this, the drill bit performance cannot be accurately simulated.

Simulations of any system response will be accurate only if the driving force applied is directly coupled to the system and the external disturbances are well known. Here, the drill bit, the ‘output’ of the system concerned is neither directly coupled to the upper rotary (due to the transmission loss and deflection freedoms of the tool joints, J.Gallagher et al. 1994), nor are the bore hole effects on the drill bit completely known or predictable. Hence, for control purposes, a control model in closed loop simulation of the drill string is never an alternative or even a predictable result for its robustness in even a laboratory scale assessment. However, the control methods used by simulations are worthy to be noted as new control approaches; and should be verified only after practical demonstrations. Hence the next section presents a conclusion on

comparative study to experimental verifications of vibration mitigation in rotary drilling, discussed section 3.4.

10.6.1 Conclusions of the comparative study

On analysis of the experimental control strategies discussed in section 3.4, it can be inferred that damping at the drill bit or tuning the upper rotary torque are by far the only practical means of minimizing drill string vibrations. J. Gallagher, (1994) and Jansen, (1995) have used damping technology to mitigate the drill string vibrations. Jansen 1995 have implemented the active damping technique and proven by field tests its applicability. The H-infinity controller proposed by Serrarens et al., (1998) used active tuning of upper rotary to cure stick slip phenomenon occurring at angular velocities of <10 RPM. Pavkovic et al., (2011) have also used active tuning of upper rotary. Their control objective was to mitigate stick slip and back spinning problems. However their major drawback was that the drill bit has to be lifted off the borehole bottom during the auto tuning, and its time and efficiency is not clear.

This research work has concentrated on developing control methodology which will actively tune the upper rotary torque. The significance of the research lies in the fact that the control law developed uses and automatically updates according to the drill string natural frequencies. The research has ensured that control law adapts itself so that the destructive vibrations are detected and the critical speeds are avoided to restore normal operation in as less time as possible. The technologies required by the research like online natural frequency identification and switching from operating command to adaptive control signal and vice versa are available, simple and easy to implement. The research also stands out in many other factors listed below.

It was stated earlier on, that many other researchers have used similar laboratory arrangements for rotary drilling system analyses. However, the laboratory arrangement used in the research is

unique in that, a universal joint connects the upper rotary to the drill string and drill bit, which gives the lower parts, their flexibility to move in any of the directions such that a complete picture of torsional and lateral vibrations are obtained. Moreover, careful analyses and research was made so that the operating speeds are as close as possible to the actual rig operational velocities. The research has only relied on corresponding measurements of the available to log measurements from the drilling rig for implementing and updating the adaptive self tuning controller. The controller has experimentally proven its effectiveness to control a drill bit lateral and torsional vibrations and resume normal operation within less than 10 seconds time (section 10.4).

Chapter 11. Conclusions and future work

The major contributions of the research are divided into three categories: Black box modeling using system identification procedures, analyzing rotary drilling dynamics in presence of lateral and torsional vibrations and in the field of application of control techniques.

In the field of system identification, the research developed Box Jenkins model of the rotary drilling system by black box method of system identification. This model represented unbalanced drill bit dynamics. A two-fold validation procedure was used to verify the accurateness of the model. Further verification of the model was done by comparing the model simulations with a single degree-of-freedom analytical model. A four degree-of-freedom model was developed to facilitate the online natural frequency identification method discussed in Appendix 6 and for future dynamics analysis of the various states.

The analysis of rotary drilling dynamics: The research experimentally analyzed the dynamics presented by the rotary drilling while drilling with an unbalanced drill bit. These are the major reasons for the outset of lateral vibrations, causing bit whirl, known as the most destructive phenomenon in rotary drilling. The research findings were in accordance with the control solutions in literature, i.e., to minimize the drill bit whirl by designing new drill bit models or adding dampers near the bottom hole assembly (BHA).

This research also analyzed control solutions applied in under actuated systems, to control drill bit dynamics. The study was concluded with the findings that the rotary drilling objectives cannot be synchronized with the objectives of under actuated system controllers. However, this is a vast field requiring further analysis; and this research suggests elaborating the studies by combining current physical methods like active damping technology with under actuated control solutions.

The research analyzed and demonstrated how borehole friction and critical speeds of operation aggravated the lateral and torsional vibrations during drilling. The research observations verified and confirmed the literature studies. The research also developed and implemented a controller to mitigate the effect of these causes.

The application of modern control techniques: The research was successful in developing a self tuning adaptive controller which could mitigate the vibration aggravating causes. The controller automatically detected the vibrations and developed control signals to minimize the vibrations and resume normal operation. The effectiveness of the controller was proven by simulations and verified experimentally. The automatic controller developed in this research proposed the use of a torsional vibration information detector and online natural frequency identifier to adapt the control output to suit the systems' changing characteristics. The vibration detector developed in this research could be extended to detect the vibrations about the x, y, and z axes. It could then be implemented in conjunction with an online identifier to develop a control law aimed at minimizing specific axis vibrations. This could be beneficial, because the various vibrations cause specific phenomena such as stick-slip due to torsional vibrations, bit whirl due to lateral vibrations, etc., and these phenomena occur at different operational speeds. Hence the controller will then be able to detect and address specific phenomena separately.

Literature study has also revealed that very few researchers were able to practically demonstrate stick-slip phenomena and the drill bit-well borehole friction dynamics. A very wide research potential lies in analyzing laboratory demonstration of stick-slip and drill bit-well borehole friction dynamics. This will facilitate the experimental verification of the many control solutions for stick-slip available in literature.

References

- [1] Aadnøy, B. S.: “Transversal Vibrations in Stabilized Drilling Assemblies,” *Energy Sources* (1986) 8, No. 4, 305.
- [2] Aarrestad, T. V. and Kyllingstad, A.: “Measurements and Theoretical Models on Rig Suspension and the Effect on Drill string Vibrations,” paper SPE 19553 presented at the 1989 SPE Annual Technical Conference and Exhibition, San Antonio, Oct. 8-11.
- [3] Kyllingstad, A. and Nessjøen, P. J., (2009), “A New Stick-Slip Prevention System”, SPE/IADC Drilling Conference and Exhibition, 17-19 March 2009, Amsterdam, The Netherlands.
- [4] Balachandran, B. , Liao, C. , Karkoub, M. , and Abdel Magid, Y. (2008), “Drill string Dynamics”, Paper presented at The Twelfth Conference on Nonlinear Vibrations, Dynamics, and Multibody Systems, Blacksburg, VA, USA. June 1-5.
- [5] Basu, S.Nagarajaiah and A.Chakraborty, Online Identification of Linear Time-varying Stiffness of Structural Systems by Wavelet Analysis, *Structural Health Monitoring* Vol. 7(1) 2008, Pp. 21-36.
- [6] Berlioz, A. , DerHagopian, J. , Dufour, R. and Draoui, E.(1996) , “Dynamic behavior of a drill string: Experimental investigation of lateral instabilities”, *J of Vibration and acoustics*, Vol. 118, pp.292-298.
- [7] Besaisow, A. A. and Payne, M. L.: “A Study of Excitation Mechanisms and Resonance Inducing Bottom hole Assembly Vibrations,” *SPE Drilling Engineer* (March 1988) 93.
- [8] Billings, S.A. (2004),”Lecture notes in System Identification, MSc Eng. Course in Control systems Engineering”, University of Sheffield.

- [9] Brett, J F; Warren, T M; Behr, S M;1990 Bit Whirl - A New Theory Of PDC Bit Failure ; SPE Drilling Engineeringv5, N4, Dec 1990, P275–280
- [10] C.M. Liao, B. Balachandran, M. Karkoub, Y. Abdel Magid, Drill-String Dynamics: Reduced-Order Models and Experimental Studies, Journal of Vibration and Acoustics, 2011,vol.133. pp. 041008.1-8.
- [11] Canudas-de Wit, F. Rubio, and M. A. Corchero. D-OSKIL: A new mechanism for controlling Stick-Slip Oscilations in oil well drillstrings. IEEE Trans. Control Sys. Tech., 16:1177–1191, November 2008
- [12] Chen, P., Tang, X., (2010),” Study on parameters self-tuning of speed servo system based on LS_SVM model”, Int. J. of Modelling, Identification and Control, Vol. 10, No.1/2, pp. 12 – 18.
- [13] Christoforou, A. and Yigit, A.(1997) , “Dynamic modeling of rotating drill string with borehole interactions”, J. sound and vibration, Vol.206, pp.243-260.
- [14] Christophe Gerday, Nathan Van de Wouw, Henk Nijmeijer, and Rodolphe Sepulchre, 2009 Nonlinear Drillstring Dynamics Analysis, SIAM J. Applied Dynamical Systems, 2009
- [15] C-Min Liao, B. Balachandran, M. Karkoub, Drill String Dynamics: Reduced Order Models, ASME International Mechanical Engineering Congress and Exposition, Nov. 13-19, 2009, Lake Buena Vista, Florida, USA.
- [16] D.J. Block, Mechanical design and control of the pendubot, MSc Thesis, University of Illinois, 1991.
- [17] Dareing, D., et.al (1997), “Effect of Torsion on Stability, “Dynamic Forces, and Vibration Characteristics in Drillstrings”, J. of Energy Resources Technology, Vol. 119, pp.111-19.

- [18] Dareing, D W; 1984, Drill Collar Length Is A Major Factor In Vibration Control 1984 Journal Of Petroleum Technology, SPE ; Vol 36 No:4, Pp 637-644
- [19] Doris, Output-feedback design for non-smooth mechanical systems: Control synthesis and experiments, PhD Thesis, Technische Universiteit Eindhoven, 2007.
- [20] Dunayevsky, V., Abbassian, F. and Judziz, A. and Mills, H.(1993) , “Dynamic stability of drill-strings under fluctuating weight on bit”, SPE Drilling and Completion,,Vol.8, pp. 84- 92.
- [21] Dykstra, M., Christensen, H., Warren, T. , and Azar, J.(1996) , “Drill string component mass imbalance: A major source of drill string vibrations”, SPE Drilling and completion,Vol.11, pp.234-241.
- [22] Dykstra, M.W., 1996. Nonlinear drill string dynamics. PhD Thesis, The University of Tulsa
- [23] E.M. Navarro-Lopez, R. Suarez-Cortez, Practical Approach To Modelling And Controlling Stick-Slip Oscillations In Oilwell Drillstrings, Proceedings Of The 2004 IEEE International Conference On Control Applications, Taipei, Taiwan, 2004, Pp. 1454–1460.
- [24] Elsayed, M. A., and Dareing, D. W.(1994), “Coupling of Longitudinal and Torsional Vibrations in a Single-Mass Model of a Drillstring,” Developments in Theoretical and Applied Mechanics, Vol. XVII, University of Arkansas, Fayetteville, AR, pp. 128–139.
- [25] Eva M. Navarro-López & D.Cortés, Sliding-mode control of a multi-DOF oil well drillstring with stick-slip oscillations ,Proceedings of the 2007 American Control Conference, Pp.3837-3842.
- [26] Eva M. Navarro-López and Eduardo Licéaga-Castro, Non-desired transitions and sliding-mode control of a multi-DOF mechanical system with stick-slip oscillations, Chaos, Solutions and Fractals 41 (2009), Pp. 2035–2044

- [27] F. A. Serrarens, H_{∞} Control as applied to torsional drillstring dynamics. PhD thesis, Eindhoven University of Technology, 2002.
- [28] F. A. Serrarens, M. J. G. V. de Molengraft, J. J. Kok, and L. V. den Steen, “ H_{∞} control for suppressing stick slip in oil well drillstrings,” IEEE Transactions on Automatic Control, vol. 18, no. 2, pp. 19–30, 1998.
- [29] F. Abdul Majeed, H. Karki, Y. Abdel Magid, M. Karkoub, Managing oil drilling efficiency in bend drill pipes – An under actuated system perspective, Proceedings of World Congress on Sustainable Technologies (WCST-2011), IEEE, UK/RI Chapter, Nov.2011, Pp.129-133.
- [30] F. Abdul Majeed, H. Karki, Y. Abdel Magid, M. Karkoub, Modeling by System Identification of a Nonlinear rotor system with an Un Actuated end, Accepted by Global Congress on Science and Engineering to be published in the Journal, Procedia Engineering, (ISSN: 1877-7058, ELSEVIER), Dec 2011, Pp. 494-498.
- [31] F. Abdul Majeed, H. Karki, Y. Abdel Magid, M. Karkoub, Nonlinearity and Spectrum Analysis of Drill Strings with Component Mass Unbalance, Proceedings of World Academy of Science, Engineering and Technology Conference JAN 2011 73 2011, Pp. 459-462
- [32] F. Abdul Majeed, M. Karkoub, H. Karki, Y. Abdel Magid, Identification of a Box Jenkins Model for Rotary Drilling Laboratory Prototype, Submitted Dec 2010, Int. J. of Modelling, Identification and Control, Inder science publications, vol.17, No.4, 2012, Pp.302-314.
- [33] F. Abdul Majeed; H. Karki; Y. Abdel Magid; M. Karkoub, Analyses of the robustness of the mathematical model with the laboratory prototype of the drilling process during simulation

and vibration control experiments, Book Series: WIT Transactions on Modelling and Simulation, Series Volume: 51, Published: 2011, Pp. 307-316.

[34] F. Abdul Majeed; H. Karki; Y. Abdel Magid; M. Karkoub, Analysis of the method of Black box Modelling of Drill string Dynamics by Least Squares method, Proceedings of International Conference on Mechanical and Electrical Technology (Sept 2010) by IEEE, Pp.257-261.

[35] F. Abdul Majeed, H. Karki, Y. Abdel Magid, M. Karkoub, Experimental verification of drill string vibration suppression using adaptive self tuning controller, Int. J. of Acoustics and Vibration, IIAV publishers, vol.8, No.1, March 2013, Pp.20-26.

[36] F. Abdulgalil and H. Siguerdidjane , PID Based on Sliding Mode Control for Rotary Drilling System, EUROCON 2005, Serbia & Montenegro, Belgrade, November, 22-24, 2005, Pp.262- 265

[37] F. Abdulgalil and H. Siguerdidjane, “Input-state linearisation technique and nonlinear control in oil well drillstrings system,” 6th IFAC NOLCOS, Stuttgart, Germany, September 2004.

[38] F. Abdulgalil and H. Siguerdidjane, “Nonlinear friction compensation design for suppressing stick slip oscillations in oil well drillstrings,” 7th IFAC DYCOPS, Massachusetts, USA, July 2004.

[39] F. Abdulgalil and H. Siguerdidjane, Backstepping Design for Controlling Rotary Drilling System, Proceedings of the 2005 IEEE Conference on Control Applications Toronto, Canada, August 28-31, 2005, Pp.120-124

[40] F. Brett, “Genesis of torsional drillstring vibrations,” SPE Drilling Engineering, vol. 7, no. 3, pp. 168–174, 1992.

- [41] F. Ding, Y. Shi, T. Chen, Performance analysis of estimation algorithms of non-stationary ARMA processes, *IEEE Trans. Signal Process.* 54 (3) (2006) 1041–1053.
- [42] G. Lenaers, L. Pelkmans, P. Debal, The realisation of an on-board emission measuring system serving as a R&D tool for ultra low emitting vehicles, *Int. J. of Vehicle Design* 2003 - Vol. 31, No.3 pp. 253 – 268.
- [43] G. Singer, Y. Meashio, A. Mahmood, Modelling and control of a flexible structure, *IEE*, 1996, Pp.911-915.
- [44] G.P.G. Sotomayor, J.C. Placido and J.C. Cunha, Drill string vibration : How to identify and suppress, *SPE Conference*, Brazil 1997, SPE 39002.
- [45] Germy, C. , van de wou, N. , Nijmeijer, H. , and Sepulchre, R. (2009), “Nonlinear drill string dynamics analysis”, *SIAM J. Applied Dynamical systems*, Vol. 8, pp.527-553.
- [46] Gopinath, S.(2010), “Study on electric motor mass imbalance based on vibration monitoring analysis technique”, Paper presented at the International conference on electrical and mechanical technology, *IEEE*, pp.539-542.
- [47] H. B. Petterson, Variable Stability Transfer Function Simulation, MSc Thesis, Virginia Polytechnic Institute & State University, 2002.
- [48] Heisig, M. Neubert, Lateral Drillstring Vibrations in Extended-Reach Wells, 2000, *IADC/SPE Drilling Conference*
- [49] Helio Santos, J.C.R. Plácido, Claudio Wolter 1999 Consequences And Relevance Of Drillstring Vibration On Wellbore Stability; 1999 SPE/IADC Drilling Conference Held In Amsterdam, Holland, 9–11 March 1999.
- [50] http://www.slb.com/~media/Files/drilling/brochures/drilling_opt/drillstring_vib_br.ashx; 2010.

- [51] Inman, D.J. (2001), "Engineering Vibration", Prentice Hall, pp.120-121
- [52] J. Gallagher, M. Waller, J. Ruzska, Performance drilling: a Practical solution to drill string vibration, SPE Drilling conference, 1994, Texas, Pp.961-970.
- [53] J. Zare, S.J. Hashemi, G. Rashed, Finite Element Analysis Of Drillstring Lateral Vibration, Scientific Research and Essays Vol. 6(13), pp. 2682-2694, 4 July, 2011
- [54] J.C.A. Bruin, A.Doris, N. vande wouw, H.Nijmeijer, Experimental results on output feedback control of a non smooth rotor dynamic system, Proceedings of IFAC, 2007
- [55] J.D. Jansen and L. van den Steen. "Active damping of self-excited torsional vibrations in oil well drillstrings." Journal of Sound and Vibration, 174(4):647668, 1995
- [56] J.D. Jansen, L.van den Steen, E. Zachariassen, "Active damping of torsional drill string vibrations with a hydraulic top drive", SPE Drilling and completion Dec 1995
- [57] J.D. Jansen. Nonlinear Dynamics of Oil well Drill strings., PhD Thesis Delft University
- [58] J.K. Vandiver, J.W. Nicholson, R.J. Shyu, Case studies of the Bending vibration and whirling motion of Drill collars, SPE Drilling Engineering, 1990, Pp. 282- 290
- [59] Jansen, J.D. (1991),"Non linear rotor dynamics as applied to oil well drill string vibrations", J. Sound and vibration, 1991, Vol.147, pp.115 -135.
- [60] Juloski, "Observer design and identification methods for hybrid systems: theory and experiments," Ph.D. dissertation, Eindhoven University of Technology, 2004.
- [61] K.J. Kim, K.F. Eman And S.M. Wu, Identification Of Natural Frequencies And Damping Ratios Of Machine Tool Structures By The Dynamic Data System Approach, International Journal Of Machine Tools Design, Vol. 24, No.3, Pp161-169
- [62] Kreuzer and M. Steidl, A Wave-Based Approach to Adaptively Control Self-Excited Vibrations in Drill-Strings, Appl. Math. Mech. 10, 509 – 510 (2010)

- [63] Liao. C et al., “Reduced order models of drill string dynamics”, Paper presented at the Second international energy 2030 conference, UAE (2008).
- [64] Lin Li, Qi-zhi Zhang and Nurzat Rasol, Time-Varying Sliding Mode Adaptive Control for Rotary Drilling System Journal Of Computers, VOL. 6, NO. 3, March 2011,Pp.564-570
- [65] Liu, Y., Wang, D. and Ding.F ., “Least squares based iterative algorithms for identifying Box–Jenkins models with finite measurement data”, Digital signal processing,2010, Vol.20, pp. 1458-1467.
- [66] Lj. Juloski, N. Mihajlović, W. P. M. H. Heemels, N. van de Wouw and H. Nijmeijer, Observer Design for an Experimental Rotor System with Discontinuous Friction, Proceedings of the 2006 American Control Conference Minneapolis, Minnesota, USA, June 14-16, 2006, Pp.2886-2891.
- [67] Ljung, L.: System identification toolbox user’s guide, The Math Works, Inc., Natick, MA(1995) 15.
- [68] Ljung, L.: System identification: theory for the user,Prentice-Hall, Inc., Englewood Cliffs, NJ(1987) 518.
- [69] M. Bodruzzaman, S .S .Devgan, K. D. Mach’ And C. Clay High-Resolution Estimation And On-Line Monitoring Of Natural Frequency Of Aircraft Structure Specimen Under Random Vibration Proceedings Of The IEEE Aerospace And Electronics Conference, 1994.
- [70] M. R. Hatch, Vibration simulation using MATLAB[®] and ANSYS, ISBN 1-58488-205-0, 2001 by Chapman & Hall, CRC Press.
- [71] M. Reyhanoglu, A. van der Schaft, N. Harris McClamroch, and I. Kolmanovsky, Dynamics and Control of a Class of Underactuated Mechanical Systems, IEEE Transactions On Automatic Control, Vol. 44, No. 9, September 1999,Pp.1663-1671

- [72] M. Silveira and Wiercigroch M. Low dimensional models for stick slip vibration of drill strings 2009, Proceedings of the 7Th International conference on modern practice in stress and vibration analysis
- [73] M.W. Spong, P. Corke, R. Lozano, Nonlinear control of the Reaction Wheel Pendulum, Automatica 37 (2001), Pp. 1845-1851.
- [74] Martin Cobern& Mark E Wassell, Laboratory Testing Of An Active Drilling Vibration Monitoring & Control System, AADE National Technical Conference And Exhibition, Houston, Texas, April 5-7, 2005.
- [75] Martin E. Cobern, Carl A. Perry, Jason A. Barbely, Daniel E. Burgess And Mark E Wassell 2007 Drilling Tests Of An Active Vibration Damper SPE/IADC Drilling Conference, 20-22 February 2007, Amsterdam, The Netherlands
- [76] Melakhessou, H. et al.(2003), “A nonlinear well drill string interaction model”, J. Vibration acoustics, Vol.125, pp.46 -52.
- [77] Mihajlovic, N., van Veggel, A. , Nan de Wow and Nijmeijer, H. (2004), “Analysis of friction induced limit cycling in an experimental drill string system”, J. of Dynamic systems, measurement and control, ASME , Vol.126, pp.709-721.
- [78] Mihajlovioc, N. , Van Veggel, A. , Van de Wouw, N. and Nijmeijer, H. (2004) ,”Friction induced torsional vibrations in an experimental drill string system”, Paper presented at the 23rd IASTED international conference on modeling , identification and control, pp.228-233.
- [79] Myklebust, Closed Loop System Identification of a Torsion System, Masters thesis, 2009, The Institute of Technology in Linköping

- [80] N.Abdel Maged, New measurement while drilling surveying technique utilizing sets of fiber optic rotation sensors," PhD thesis dissertation, Department of Electrical and Computer Engineering, University of Calgary, Alberta, Canada, 2002.
- [81] N. Mihajlović, "Torsional and lateral vibrations in flexible rotor systems with friction," Ph.D. dissertation, Eindhoven University of Technology, The Netherlands, 2005.
- [82] N.Mihajlovic, A.A.van Veggel, N. van de Wouw,H.Nijmeijer; "Analysis of Friction induced Limit cycling in an Experimental drill string system", J.of Dynamic systems, Measurement and Control, Dec 2004.126
- [83] Navarro Lopez, E. and Suarez, R.(2004), "Modeling and Analysis of stick slip behavior in a drill string under dry friction", Congresso Annual De La Amca, pp. 330-336, 2004.
- [84] P. Sananikone, O. Karnoshirna, and D.B. White, A Field Method for Controlling Drillstring Torsional Vibrations, 1992 IADCISPE Drilling Conference held in New Orleans, Louisiana, February 18-21, 1992.Pp.443-452.
- [85] P. van Der pols, MSc Thesis, Parameter estimation of a rotary drilling process, Eindhoven technical university, Nether lands, 1992.
- [86] Pastusek, P.E., Cooley, C.H.; Sinor, L.A., Anderson, Mark, Directional And Stability Characteristics Of Anti-Whirl Bits With Non-Axisymmetric LoadingSPE Annual Technical Conference And Exhibition, 4-7 October 1992, Washington, D.C
- [87] Pavkovic, J. Deur, A. Lisac, A torque estimator-based control strategy for oil-well drill-string torsional vibrations active damping including an auto-tuning algorithm, Control Engineering Practice 19 (2011), Pp.836–850.
- [88] Puebla, J. Alvarez-Ramirez, Suppression of stick-slip in drillstrings: A control approach based on modeling error compensation, Journal of Sound and Vibration 310 (2008), Pp. 881–901

- [89] R. B. Jij'on, C. Canudas-de-Wit, S. Niculescu, J. Dumon, Adaptive Observer Design under Low Data Rate Transmission with Applications to Oil Well Drill-string, American Control Conference, Marriott Waterfront, Baltimore, MD, USA, 2010, Pp. 1973 - 1978
- [90] R. Bailey; E. A. O. Biediger; S. Sundararaman; A. D. Carson; W. C. Elks; F. E. Dupriest; 2008 Development And Application Of A BHA Vibrations Model International Petroleum Technology Conference, 3-5 December 2008, Kuala Lumpur, Malaysia
- [91] R. Bishop, R. Learning with LabVIEW 7 Express, New Jersey,
- [92] R. I. Leine, D. H. van Campen, A. de Kraker, and L. van den Steen, "Stick-slip vibrations induced by alternate friction models," *Nonlinear dynamics*, vol. 16, pp. 41–54, 1998.
- [93] R. I. Leine, D.H. van Campen, W. J. G. Keultjes Stick-slip Whirl Interaction in Drillstring Dynamics *Journal of Vibration and Acoustics*. APRIL 2002, Vol. 124 Pp. 209-220
- [94] R. Rommetveit, et.al, Drill tronics: An integrated system for real time optimization of the drilling process, Proc. Of 2004 IADC/SPE Drilling conference, Texas , USA.
- [95] R. W. Tucker and C. Wang, "On the effective control of torsional vibrations in drilling systems," *Journal of Sound and Vibration*, vol. 224, no. 1, pp. 101–122, 1999
- [96] R.I. Leine 2000, "Bifurcations in Discontinuous Mechanical Systems of Filippov-Type," Ph.D. thesis, Eindhoven University of Technology, Eindhoven, The Netherlands.
- [97] R.Mathur, B.Donadieu, Best Practices For Drilling With Rotary Steerable And Realtime Drilling Optimization Service, Proc. Of AADE 2009 NTCE-05-03.
- [98] S. Johnson, A New Method Of Producing Laterally Stable PDC Drill Bits SPE Drilling & Completion, Volume 23, Number 3, September 2008, Pp. 314-324

- [99] S. M. Shahruz and S. Behtash, "Design of controllers for linear parameter-varying systems by the gain scheduling technique," J. Mult. Anal. Appl. , vol. 168, no. I, Pp. 195-217, 1992.
- [100] S. Widnall, Lecture notes on Dynamics; Fall 2009; 16.07 MIT Open Course ware.
- [101] S.Hara, Adaptive Nonstationary Control Using Solutions of Time-Varying Riccati Equations—Its Application to Positioning Control of Vibration Systems, ICARCV 2006, IEEE.
- [102] S.L. Chen, K. Blackwood; E. Lamine; Field Investigation Of The Effects Of Stick-Slip, Lateral, And Whirl Vibrations On Roller-Cone Bit Performance SPE Drilling & Completion Volume 17, Number 1 March 2002pg 15-20
- [103] Schlumberger Brochure on Drilling vibrations
- [104] Shi Fubin, ShaLinxiu, Li Lin, Zhang Qizhi Adaptive PID Control of Rotary Drilling System with Stick Slip Oscillation 2010 2nd International Conference on Signal Processing Systems (ICSPS), IEEE, Vol.2 Pp.289-292
- [105] Silviera, M. and Wiercigroch, M. (2009), "Low dimensional models for stick slip vibration of drill strings", J. of Physics, Conference series, Vol. 181.
- [106] Suleiman A.H. Modelling Of Stick – Slip Drillstring Vibration In Oilwell Drilling Operation;2006, Bachelors thesis, Universiti Teknologi Mara (Uitm) Nov 2006
- [107] T. Ioki, et.al., On Vibration Control of Flexible Pipes in Ocean Drilling System, Proceedings of the Sixteenth (2006) International Offshore and Polar Engineering Conference.
- [108] T.L. Hein, Development of a three degree of freedom vibration control test facility, BSc and MSC thesis, MIT, May 1994.
- [109] T.Myrwold & M. Johannesen, Stick-Slip Prevention of Drill Strings Using Nonlinear Model Reduction and Nonlinear Model Predictive Control, Masters thesis,2010, NTNU.

- [110] Theron, A., de.Langre, E. and Putot, C.(2001) , “The Effect of Dynamical Parameters on Precession in Rotary Drilling”, J. of Energy Resources Technology, Vol.123, pp.181-186.
- [111] U. Forssell and L. Ljung, Identification of Unstable Systems Using Output Error and Box–Jenkins Model Structures, IEEE Transactions On Automatic Control, Vol. 45, No. 1, January 2000, Pp. 137- 141.
- [112] Van den Steen, L., 1997, “Suppressing Stick-Slip-Induced Drill-String Oscillations: A Hyper Stability Approach,” Ph.D. thesis, University of Twente, Enschede, The Netherlands.
- [113] W. Blajer, K. Dziwiecki, K. Kołodziejczyk, Z. Mazur, Inverse dynamics of under actuated mechanical systems: A simple case study and experimental verification, Commun Nonlinear Sci Numer Simulation, Elsevier Dec 2010
- [114] W.D. Aldred and M.C. Sheppard, Drillstring Vibrations: A New Generation Mechanism and Control Strategies, 67th Annual Technical Conference and Exhibition of the Society of Petroleum Engineers held in Washington, DC, Octobe; 4 -7, 1992, Pp.353- 363.
- [115] Warren, T M; Brett, J F; Sinor, L A ;1990 Development Of A Whirl-Resistant Bit : SPE Drilling Engngv5, N4, Dec 1990, P267–274
- [116] Wei, H.L., Billings, S.A., Liu, J.J., (2010),” Time-varying parametric modelling and time-dependent spectral characterisation with applications to EEG signals using multiwavelets”, Int. J. of Modelling, Identification and Control, Vol. 9, No.3, pp. 215 – 224.
- [117] XiuzhongXu , Zhiyi Zhang, Hongxing Hua, Zhaoneng Chen, Identification Of Time-Varying Modal Parameters Using A Time-Varying Autoregressive Approach, 2003 Imac-Xxi: Conference & Exposition On Structural Dynamics.
- [118] Y. Bing, Research on Drill String Failure in Gas Drilling Based on Statistical Learning Theory, 2010 International Conference on Computational and Information Sciences, Pp.396- 398

- [119] Y.Y. Kho, S. Hashim, C.F. Soon, Vital physiological signs monitoring, Int. J. of Computer Applications in Technology 2004 - Vol. 21, No.1/2 pp. 58 – 64.
- [120] Zhao, G., Wang, Z., (2011),” Time-frequency analysis for non-stationary signal from mechanical measurement of bearing vibration”, Int. J. of Modelling, Identification and Control, Vol. 13, No.3, pp. 190 – 194.

Appendix 1: Major equipment specifications:

The specifications of the equipment used and their purpose are briefly explained in this section. The function of each equipment is explained in detail in Chapter 5 when the experiments are described.

DC Motor:

It is a Steel geared DC motor, 147RPM, 24V. This motor acts as the top drive of the drill system.



Figure 1: DC Motor used as top drive.

DC motors are popular in the industry, mainly in the control area, because they have high torque and response characteristics and are easy for linear control.

Incremental encoder:

The incremental encoder is an electro-mechanical device that converts the angular position of a shaft or axle to an analog or digital code. A incremental encoder gives the speed data. The encoder used gives totem pole output and is used for measuring angular velocity of the shafts.



Figure 2: Incremental encoder

The incremental encoder used is the E40H 12- 3600 – T – 24. Here E 40 is the name of the encoder model, H stands for hollow type, 12 is the diameter in mm of the inner bore, 3600 is the sensitivity in pulses per revolution, T stands for totem pole output, and 24 is the maximum voltage rating for the product. A totem pole output circuit, has 2 transistors and can both source current (drive the output high) and sink current (pull an output low). The incremental encoders are connected to the counter input of the BNC 2120. The data are then converted to speed by the LabVIEW™ program.

I/O Card - NI DAQ BNC 2120:

The I/O card is a multi function Data Acquisition (DAQ) device. The BNC 2120 Front panel is shown below.

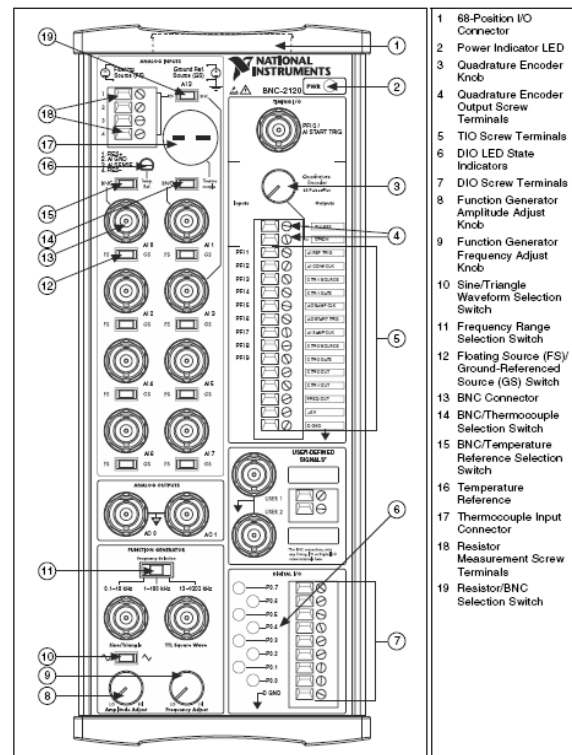


Figure 3: NI BNC 2120 used for data communication between encoder and LabVIEW™.

The encoders are connected to the digital/analog ports and counters of the BNC 2120. These data are called by the DAQ assistants in LABVIEW. The gray coded data are then converted to angle data in the program. The incremental encoders are connected to the BNC 2120 using the counter inputs. The data are similarly converted to speed data by the LABVIEW program. The BNC is also used for closing the loop with PID control when the command/reference signal generated by the function generator has to be modified to get the

desired control output before being fed to the pulse-width-modulation (PWM) amplifier and motor.

Amplifier:

The amplifier used is a brush type PWM servo amplifier. It is used for amplifying the signals to act as a stimulus signal to the top drive of the drill system.



Figure 4: Amplifier used for exciting the top drive.

The function generator or the LabVIEWTM can generate any signal required to drive the motor. But they will not have the sufficient current output to drive the motor. Hence the signals from the function generator are fed to a PWM amplifier before being used to drive the motor.

Linear push solenoid



Figure 5: Linear push solenoid.

The linear solenoid is a 25MM PUSH SOLENOID 24V DC. A linear push solenoid is used for providing the thrust required during the hard brake arrangement for the hard brake effect analysis experiments. When the DC voltage is above a specific threshold voltage, the solenoid pushes the shaft outside and remains so until the voltage is lowered below the threshold value.

Kionix Accelerometer and inclinometer evaluation board



Figure 6: Three axes accelerometer used to detect and analyze vibration.

KXPA4-2050 is a 3-axis $\pm 2g$ accelerometer that detects and transforms motion changes into multiplexed analogue output. This sensor is used in the research to detect the accelerations of the drill bit in all three axes. It helped provide accurate vibration data about all three axes.

Appendix 2: Data Sheets

1. Dc Motor

Data Pack B

Issued November 1996

1502297616



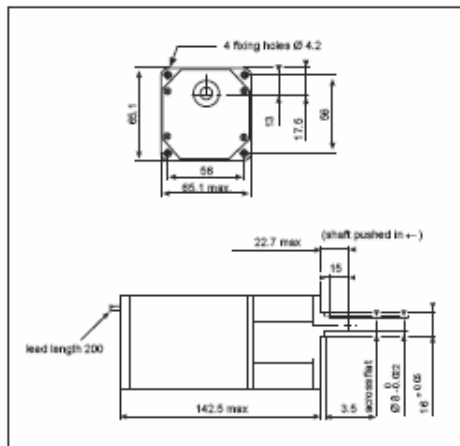
dc geared motor 63mm diameter

Data Sheet

RS stock numbers 224-3647, 224-3653, 224-3596,
224-3625, 224-3603, 224-3619

Introduction

These motors have been designed and manufactured for incorporation into equipment or machines and are considered to be component parts of a larger system. The design and construction has taken in to account the provisions of the appropriate European Legislation for these items.



Technical data

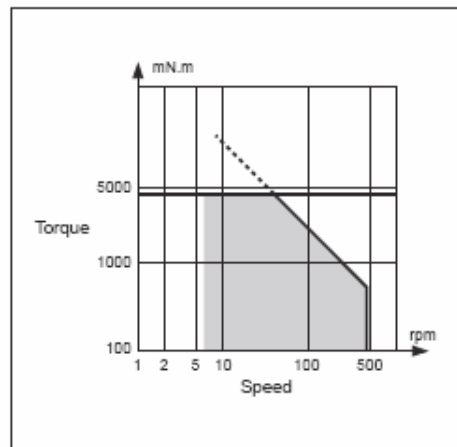
Motor supply voltage (Vdc)	12	24
Nominal output power (W)	27	27
Nominal current (A)	3.6	1.9
Starting torque (mNm)	600	600
Starting current (A)	12	6.2
Resistance (Ω)	1	3.9
Inductive (H)	1.4	6.4
Life (h)	5000	5000
Maximum gearbox torque (Nm)	5	5
Axial load (dynamic) (daN)	6	6
Radial load (dynamic) (daN)	6	6
Gearbox temperature rise (°C)	50	50
Protection rating	IP20	IP20
Weight (g)	1540	1540

12Vdc - Geared motor

RS stock no.	Ratio	Final Speed (rpm)
224-3647	24.5:1	73
224-3653	38.28:1	47

24Vdc - Geared motor

RS stock no.	Ratio	Final Speed (rpm)
224-3596	12.25:1	147
224-3625	24.5:1	73
224-3603	61.25:1	28.4
224-3619	122.5:1	14.7



2. Incremental encoder

E40 Series

Diameter ϕ 40mm Shaft type/Hollow type/Built-in type Incremental Rotary encoder

■ Features

- Easy installation at narrow space
- Small moment of inertia
- Power supply : 5VDC, 12~24VDC \pm 5%
- Various output types

 Please read "Caution for your safety" in operation manual before using.



■ Ordering information

E40	H	8	5000	3	N	24	
Series	Shaft type	Hollow type	Pulse/1 Revolution	Output phase	Output	Power supply	Cable
S: Shaft type	External	Inner		2: A, B	T: Totem pole output	5 : 5VDC \pm 5%	No mark: Normal type
H: Hollow type		6: ϕ 6mm	Refer to resolution	3: A, B, Z	N: NPN open collector output	24: 12~24VDC \pm 5%	(*) Cable outgoing connector type
HB: Hollow built-in type	6: ϕ 6mm 8: ϕ 8mm	8: ϕ 8mm 10: ϕ 10mm 12: ϕ 12mm		4: A, \bar{A} , B, \bar{B} 6: A, \bar{A} , B, \bar{B} , Z, \bar{Z}	V: Voltage output L: Line driver output(*)		

*Standard : E40S6 - PULSE - 3-N-24
E40H8 - PULSE - 3-N-24
E40HB8 - PULSE - 3-N-24

*Standard A, B, Z *The power of Line driver is only for 5VDC

*Cable length : 250mm

■ Specifications

Item	Diameter ϕ 40mm shaft/hollow shaft/built-in type of Incremental rotary encoder	
Resolution (P/R)	(Note1) *1, *2, *5, 10, *12, 15, 20, 23, 25, 30, 35, 40, 45, 50, 60, 75, 100, 120, 150, 192, 200, 240, 250, 256, 300, 360, 400, 500, 512, 600, 800, 1000, 1024, 1200, 1500, 1800, 2000, 2048, 2500, 3000, 3600, 5000 (Not indicated resolution is customizable.)	
Electrical specification	Output phase	A, B, Z phase (Line driver : A, \bar{A} , B, \bar{B} , Z, \bar{Z} phase)
	Phase difference of output	Phase difference between A and B : $\frac{T}{4} \pm \frac{T}{8}$ (T=1 cycle of A phase)
	Control output	* Low \Rightarrow Load current: Max. 30mA, Residual voltage : Max. 0.4VDC * High \Rightarrow Load current: Max. 10mA, Output voltage (Power supply 5VDC) : Min. (Power supply - 2.0)VDC, Output voltage (Power supply 12~24VDC) : Min. (Power supply - 3.0)VDC
		NPN open collector output
		Voltage output
		Line driver output
	Response time (Rise/Fall)	Totem pole output : Max. 1 μ s NPN open collector output : Max. 1 μ s Voltage output : Max. 1 μ s Line driver output : Max. 0.5 μ s
		Max. Response frequency
		300kHz
		Power supply
		+5VDC \pm 5% (Ripple P-P: Max. 5%) *12~24VDC \pm 5% (Ripple P-P: Max. 5%)
Mechanical specification	Current consumption	Max. 80mA (disconnection of the load), Line driver output: Max. 50mA (disconnection of the load)
	Insulation resistance	Min. 100M Ω (at 500VDC mega)
	Dielectric strength	750VAC 50/60Hz for 1 minute (Between all terminals and case)
	Connection	Cable outgoing type, 200mm cable outgoing connector type
	Starting torque	Shaft Type : Max. 40gf \cdot cm (0.004N \cdot m), Hole Type : Max. 50gf \cdot cm (0.005N \cdot m)
	Rotor inertia	Max. 40g \cdot cm ² (4 \times 10 ⁻⁴ kg \cdot m ²)
	Shaft loading	Radial : Max. 2kgf Thrust : Max. 1kgf
	Max. allowable revolution	(Note2) 5000rpm
	Vibration	1.5mm amplitude at frequency of 10 ~ 55Hz in each of X, Y, Z directions for 2 hours
	Shock	Max. 50G
Ambient temperature		-10 ~ 70 $^{\circ}$ C (at non-freezing status), Storage: -25 ~ 85 $^{\circ}$ C
Ambient humidity		35~85%RH, Storage: 35~90%RH
Protection		IP50 (IEC standard)
Cable		ϕ 5mm, 5P, Length : 2m, Shield cable (Line driver output : ϕ 5mm, 8P)
Accessory		* Shaft type: ϕ 6mm coupling standard, ϕ 8mm coupling (Sold separately) * Hole type: Bracket
Unit weight		Approx. 160g
Approval		CE (Except for Line driver output)

*(Note1) "+" pulse is only for A, B phase (Line Driver output is for A, \bar{A} , B, \bar{B} phase)

*(Note2) Max. allowable revolution \geq Max. response revolution [Max. response revolution (rpm) = $\frac{\text{Max. response frequency} \times 60 \text{ sec}}{\text{Resolution}}$]

3. I/O Card – NI DAQ BNC 2120

Specifications

This section lists the specifications of the BNC-2120. These specifications are typical at 25 °C unless otherwise specified.

Analog Input

Number of channels (default) 8 differential

Field connections (default)..... 8 BNC connectors

Protection No additional protection provided. Consult your DAQ device for specifications.

Optional inputs

Input	Description
AI 0	Temperature sensor
AI 1	Thermocouple
AI 3, AI 11	Resistor measurement (requires RSE configuration)

Optional connections

Thermocouple Uncompensated miniature connector, mates with 2-prong miniature or subminiature connector

Resistor 2 screw terminals

Resistor measurement range 100 Ω to 1 M Ω

Resistor measurement error $\leq 5\%$

Screw terminals..... 4 positions, no larger than 24 AWG wire

Switches

Floating source/grounded source ... 8

BNC/temperature reference IC 1

BNC/thermocouple connector..... 1

BNC/resistor screw terminals 1

Analog Output

Field connection2 BNC connectors

Digital Input/Output

Screw terminals9 positions, no larger than

24 AWG wire

LED state indicators8, 1 each for lines P0.<7..0>

Protection (DC max V)

Powered off ± 5.5 V

Powered on+10/-5 V

Drive

Vol0.6 V, 8 mA

1.6 V, 24 mA

Voh4.4 V, 8 mA

4 V, 13 mA

Drive capability

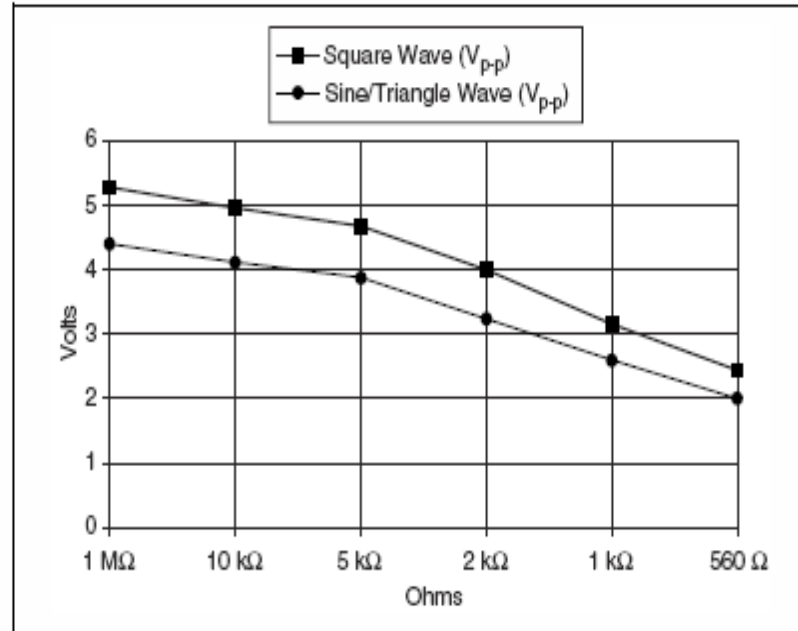


Figure 3. Typical Maximum Voltages versus Load Impedances

Timing Input/Output

Screw terminals.....	14 positions, no larger than 24 AWG wire
BNC connector.....	1, for PFI 0/AI START TRIG
Protection (DC max V)	
Powered off.....	± 1.7 V
Powered on	+6.7/-1.7 V

Quadrature Encoder

Screw terminals.....	2
Output signals	
CLK	96 pulses/revolution
UP/ $\overline{\text{DN}}$	High for clockwise rotation, low for counterclockwise rotation
Pulse width.....	1 μs

4. Amplifier



Analog Servo Drive

30A8

Description	Power Range
<p>The 30A8 PWM servo drive is designed to drive brush type DC motors at a high switching frequency. A single red/green LED indicates operating status. The drive is fully protected against over-voltage, under voltage, over-current, over-heating and short-circuits across motor, ground and power leads. Furthermore, the drive can interface with digital controllers or be used stand-alone and requires only a single unregulated DC power supply. Loop gain, current limit, input gain and offset can be adjusted using 14-turn potentiometers. The offset adjusting potentiometer can also be used as an on-board input signal for testing purposes.</p>	Peak Current 30 A
	Continuous Current 15 A
	Supply Voltage 20 - 80 VDC



Features

- ▲ Four Quadrant Regenerative Operation
- ▲ DIP Switch Selectable Modes
- ▲ Adjustable Current Limits
- ▲ High Switching Frequency
- ▲ Differential Input Command
- ▲ Digital Fault Output Monitor
- ▲ On-Board Test Potentiometer
- ▲ Offset Adjustment Potentiometer
- ▲ Adjustable Input Gain
- ▲ Drive Status LED
- ▲ Current Monitor Output
- ▲ Directional Inhibit Inputs for Limit Switches

MODES OF OPERATION

- Current
- Tachometer Velocity
- Voltage
- IR Compensation

COMMAND SOURCE

- ± 10 V Analog

FEEDBACK SUPPORTED

- Tachometer

COMPLIANCES & AGENCY APPROVALS

- UL
- cUL
- CE Class A (LVD)
- CE Class A (EMC)
- RoHS

Release Date:
2/27/2009

Revision:
0.00

Advanced Motion Controls • 3805 Calle Tecate, Camarillo, CA, 93012
ph# 805-389-1935 • fx# 805-389-1165 • www.a-m-c.com

SPECIFICATIONS

Power Specifications		
Description	Units	Value
DC Supply Voltage Range	VDC	20 - 80
DC Bus Over Voltage Limit	VDC	86
Maximum Peak Output Current ¹	A	30
Maximum Continuous Output Current	A	15
Maximum Power Dissipation at Continuous Current	W	60
Minimum Load Inductance (Line-To-Line) ²	μH	200
Switching Frequency	kHz	22
Control Specifications		
Description	Units	Value
Command Sources	-	±10 V Analog
Feedback Supported	-	Tachometer
Commutation Methods	-	External
Modes of Operation	-	Current, IR Compensation, Tachometer Velocity, Voltage
Motors Supported	-	Brushed, Voice Coil
Hardware Protection	-	Over Current, Over Temperature, Over Voltage, Short Circuit (Phase-Phase & Phase-Ground)
Mechanical Specifications		
Description	Units	Value
Agency Approvals	-	CE Class A (EMC), CE Class A (LVD), cUL, RoHS, UL
Size (H x W x D)	mm (In)	186.7 x 111.7 x 25.4 (7.4 x 4.4 x 1)
Weight	g (oz)	680 (24)
Heatsink (Base) Temperature Range ³	°C (°F)	0 - 65 (32 - 149)
Storage Temperature Range	°C (°F)	-40 - 85 (-40 - 185)
Form Factor	-	Stand Alone
P1 Connector	-	16-pin, 2.54 mm spaced, friction lock header
P2 Connector	-	4-contact, 11.10 mm spaced, tri-barrier terminal block

Notes

- Maximum duration of peak current is ~2 seconds.
- Lower inductance is acceptable for bus voltages well below maximum. Use external inductance to meet requirements.
- Additional cooling and/or heatsink may be required to achieve rated performance.

5. Linear Push Solenoid

Ledex® Tubular Solenoids Selection

Tubular solenoids are available in seven sizes. The three STA Series sizes are available in both push and pull types.

Use the selection overview chart to determine which size offers the desired performance and mechanical specifications.

Refer to the individual size specification pages for complete performance and mechanical data.

Tubular Selection Overview

Size	Solenoid Type	Package Dimension (in)		Max Stroke (in)	Nominal Stroke (in)	Force (lbs) @ Nominal Stroke and Specified Duty Cycle			
		Dia.	Length			100%	50%	25%	10%
STA ½" x ½"	Pull	0.52	0.55	0.10	0.05	0.18	0.30	0.50	1.0
STA ½" x ½"	Push	0.52	0.55	0.10	0.05	0.08	0.18	0.25	0.6
STA ½" x 1"	Pull	0.52	1.05	0.50	0.10	0.19	0.31	0.55	1.00
STA ½" x 1"	Push	0.52	1.05	0.50	0.10	0.13	0.25	0.48	0.94
STA ¾" x 1½"	Pull	0.77	1.56	0.70	0.20	0.50	1.00	1.63	2.69
STA ¾" x 1½"	Push	0.77	1.56	0.70	0.20	0.38	0.80	1.50	2.75
STA 1" x 2"	Pull	1.02	2.05	0.70	0.30	0.90	1.75	3.00	5.20
STA 1" x 2"	Push	1.02	2.05	0.70	0.30	0.75	1.88	2.90	5.20
1½" x 2 ¼"	Pull	1.25	2.25	0.75	0.40	1.00	2.00	4.00	6.50
1½" x 2 ½"	Pull	1.50	2.50	0.75	0.40	1.00	2.50	5.20	9.80
1½" x 4 ¾"	Pull	1.75	4.71	2.50	1.00	1.25	2.50	3.75	6.50

All data is at 20°C coil temperature. Force outputs degrade with elevated temperatures. All specifications subject to change without notice.

LINEAR Tubular

How to Use Tubular Performance Charts

1. Select one of the four columns which provides the appropriate duty cycle. (For example 50%.)
2. Reading down this column provides a variety of performance and electrical data including maximum on time, watts, and amp turns.
3. Following down the column further into the VDC ratings, select the voltage which most closely matches your supply voltage. (For example, 11.5 for a 12 VDC power supply.)
4. Read across (to the left) to select the awg suffix. (In this example, 32 awg is required, thus to order, specify: 195203-232. Note that the digit preceding the awg refers to the plunger configuration and anti-rotation flat selected. Review the STA plunger section on page E3 and on the individual specification page to select the appropriate plunger configuration.

Note: The size 125, 150 and 175 standard models do not use this plunger configuration and anti-rotation flat suffix system.

Performance

Maximum Duty Cycle	100%	50%	25%	10%
Maximum ON Time (sec) when pulsed continuously	∞	50	5	2
Maximum ON Time (sec) for single pulse	∞	140	30	8
Watts (@ 20°C)	4	8	16	40
Ampere Turns (@ 20°C)	497	706	994	1573

Coil Data						
awg (000)	Resistance (@20°C)	# Turns	VDC (Nom)	VDC (Nom)	VDC (Nom)	VDC (Nom)
27	1.43	306	2.4	3.4	4.8	7.6
28	1.95	342	2.8	3.9	5.6	8.8
29	3.84	508	3.9	5.5	7.8	12.4
30	5.29	572	4.6	6.5	9.2	14.5
31	9.56	795	6.2	8.8	12.4	19.6
32	16.54	1048	8.1	11.5	16.3	25.7
33	22.60	1194	9.5	13.4	19.0	30.0
34	37.41	1547	12.2	17.3	24.0	39.0
35	60.71	1976	15.6	22.0	31.0	49.0
36	96.19	2475	19.6	28.0	39.0	62.0
37	149.93	3060	24.5	35.0	49.0	77.0

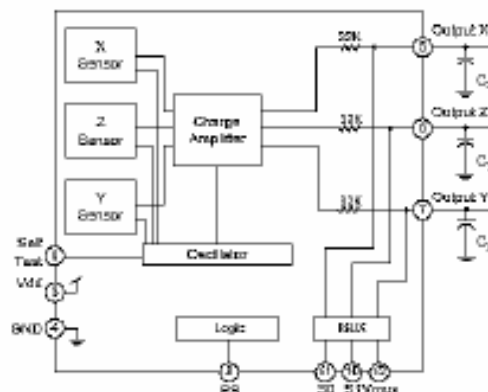
6. Kionix Accelerometer and inclinometer evaluation board

	<p style="text-align: center;">± 2 g Tri-Axis Analog Accelerometer Specifications</p>	<p>PART NUMBER: KXPA4-2050 Rev 4 Mar 07</p>
---	---	---

Product Description

The KXPA4-2050 is a tri-axis, analog output, silicon micromachined accelerometer with a full-scale output range of $\pm 2g$ (19.6 m/s^2). The sense element is fabricated using Kionix's proprietary plasma micromachining process technology. Acceleration sensing is based on the principle of a differential capacitance arising from acceleration-induced motion of the sense element, which further utilizes common mode cancellation to decrease errors from process variation, temperature, and environmental stress. The sense element is hermetically sealed at the wafer level by bonding a second silicon lid wafer to the device using a glass frit. A separate ASIC device packaged with the sense element provides signal conditioning and self-test. The accelerometer is delivered in an $5 \times 5 \times 1.2\text{mm}$ Dual Flat No-lead (DFN) plastic package operating from a 2.6 - 5V DC supply. The KXPA4 also features an integrated 3-channel multiplexer. This feature reduces system MCU requirements to only 1 ADC and 2 digital I/O's.

Functional Diagram





± 2 g Tri-Axis Analog Accelerometer Specifications

PART NUMBER:

KXPA4-2050

Rev 4
Mar 07

Product Specifications

Table 1. Mechanical

(specifications are for operation at $V_{dd} = 3.3V$ and $T = 25^{\circ}C$ unless stated otherwise)

Parameters	Units	Min	Typical	Max
Operating Temperature Range	$^{\circ}C$	-40	-	85
Zero-g Offset	V	1.55	1.65	1.75
Zero-g Offset Variation from RT over Temp.	mg/ $^{\circ}C$		± 1.0	
Sensitivity	mV/g	640	660	680
Sensitivity Variation from RT over Temp.	%/ $^{\circ}C$		± 0.015	
Offset Ratiometric Error ($V_{dd} = 3.3V \pm 5\%$)	%	-	0.3	1.5
Sensitivity Ratiometric Error ($V_{dd} = 3.3V \pm 5\%$)	%	-	0.5	1.5
Non-Linearity	% of FS		0.1	
Cross Axis Sensitivity	%		2.0	
Self Test Output change on Activation	g	2.2 (xy) 0.7 (z)	2.7 (xy) 1.1 (z)	3.2 (xy) 1.6 (z)
Bandwidth (-3dB) ¹	Hz		3300 (xy) 1700 (z)	
Noise Density (on filter pins)	$\mu g / \sqrt{Hz}$		175	

Notes:

1. User definable with external capacitors. Maximum defined by the frequency response of the sensors.

Table 2. Electrical

(specifications are for operation at $V_{dd} = 3.3V$ and $T = 25^{\circ}C$ unless stated otherwise)

Parameters		Units	Min	Typical	Max
Supply Voltage (V_{dd})	Operating	V	2.7	3.3	5.25
Current Consumption	Operating	mA	0.6	1.1	1.5
	Standby	μA	-	-	10
Analog Output Resistance(R_{out})		k Ω	24	32	40
Power Up Time ¹		ms	-	5 $\cdot R_{out} \cdot ^\circ C$	-

Notes:

1. Power up time is determined by 5 times the RC time constant of the user defined low pass filter.

Appendix 3: List of Publications

- [1] **F. Abdul Majeed**, H. Karki, Y. Abdel Magid, M. Karkoub, Managing oil drilling efficiency in bend drill pipes – An under actuated system perspective, Proceedings of World Congress on Sustainable Technologies (WCST-2011), IEEE,UK/RI Chapter, Nov.2011, Pp.129-133.
- [2] **F. Abdul Majeed**, H. Karki, Y. Abdel Magid, M. Karkoub, Modeling by System Identification of a Nonlinear rotor system with an Un Actuated end, Accepted by Global Congress on Science and Engineering to be published in the Journal, Procedia Engineering, (ISSN: 1877-7058, ELSEVIER), Dec 2011,Pp. 494-498.
- [3] **F. Abdul Majeed**, H. Karki, Y. Abdel Magid, M. Karkoub, Nonlinearity and Spectrum Analysis of Drill Strings with Component Mass Unbalance, Proceedings of World Academy of Science, Engineering and Technology Conference JAN 201173 2011,Pp. 459-462
- [4] **F. Abdul Majeed**, M. Karkoub, H. Karki, Y. Abdel Magid, Identification of a Box Jenkins Model for Rotary Drilling Laboratory Prototype, Submitted Dec 2010, Int. J. of Modelling, Identification and Control, Inder science publications, vol.17, No.4, 2012,Pp.302-314.
- [5] **F. Abdul Majeed**; H. Karki; Y. Abdel Magid; M. Karkoub, Analyses of the robustness of the mathematical model with the laboratory prototype of the drilling process during simulation and vibration control experiments, Book Series: WIT Transactions on Modelling and Simulation, Series Volume: 51, Published: 2011, Pp. 307-316.

- [6] **F. Abdul Majeed**; H. Karki; Y. Abdel Magid; M. Karkoub, Analysis of the method of Black box Modelling of Drill string Dynamics by Least Squares method, Proceedings of International Conference on Mechanical and Electrical Technology (Sept 2010) by IEEE, Pp.257-261.
- [7] **F. Abdul Majeed**, H. Karki, Y. Abdel Magid, M. Karkoub, Experimental verification of drill string vibration suppression using adaptive self tuning controller, Int. J. of Acoustics and Vibration, IIAV publishers, vol.8, No.1, March 2013, Pp.20-26.

Selected Published Papers

1. **Identification Of A Box Jenkins Model For Rotary Drilling Laboratory Prototype.**

Identification Of a Box Jenkins Model for Rotary Drilling Laboratory Prototype.

Abstract – Conventionally, analytical modeling is used to analyze the dynamics of complex nonlinear processes. This paper presents identification of mathematical models by the Black box modeling method for nonlinear systems. The nonlinear system concerned in this work is a laboratory prototype of a rotary drilling rig. The system concerned is distinguished for its additive nonlinearity at the output end. The step by step analysis of the procedures and criteria used to select an accurate model for a nonlinear process by the black box identification method is explained. The model identified in the paper is a Box Jenkins model. The model selection procedure uses least squares method, pole zero plots and residual analysis. Accurate simulation results with less than 0.05% error are obtained. The identified Box Jenkins model is validated by a twofold validation procedure.

Keywords: Modeling; system identification; nonlinear process; drill string; least squares; Box Jenkins model.

Introduction and scope of research

Increase in demand for oil and gas leads to an increase in drilling activities. Poor drilling performance and drill string failures cost oil and gas companies hundreds of millions of dollars every year and became a significant factor in the rise of production cost. A major cause of poor drilling performance is drill-string vibrations and high shock loads. Significant improvements in overall drilling performance can be achieved by taking a proactive approach to the prevention or reduction of destructive downhole mechanical forces. Vibrations affecting drilling can be classified into torsional, axial, lateral, or combined vibration modes. The various vibrations affecting the drilling process and its causes are briefly discussed below. Table 1 lists the major phenomena associated with the vibration modes and their effect on the drilling process.

Axial/longitudinal vibrations arise due to interaction between the drilling bit and borehole [Melakhessou, H. et al. (2003) and Theron, A. et al., (2001)]. These interactions are also known as precession. Precession limits the performance of drilling and often endangers the safety of the operation. Bit bounce is another common phenomenon resulting from axial vibrations. It causes damage to drill bit cutting structure, bearings and seals.

Bending/ lateral vibration occurs due to pipe eccentricity; it is also known as drill string whirl (particularly forward and backward whirl). Bit whirl leads to ledges in the bore hole as the soft rocks will be enlarged to a greater diameter than the hard rocks. A detailed study of drill collar whirling and the linear coupling between the weight on bit fluctuations and bending vibration of an initially curved BHA (Bottom

Hole Assembly, i.e. drill bit and down hole equipments) are discussed in Liene, R.I. et al. (2002) and Berlioz, A. et al. (1996) Lateral shocks leading to washouts (Figure2) and parametric resonance causing borehole enlargement are common phenomena associated with lateral vibration.

Torsional vibrations are mainly caused by the inherent flexibility of the drill string which is increased due to the nonlinear interactions between the bit and the rock or the drill string with the borehole. During torsional vibration, the upper rotary angular speed and position are not synchronized with the angular velocity and position of the drill bit [Dareing, D.W. et al., (1997)]. This results in the piling up of inertial energy within the drill bit causing sudden backward movement of the drill bit possibly leading to damage to the drill bit and down hole electronics. This phenomenon is better known as torsional resonance. Stick slip is another possible reason for drill pipe damage during which the BHA sticks to the borehole. The drill bit revolves in the drill hole sticking and slipping at the borehole wall thus causing a sudden decrease in the lower Rate of Penetration (ROP) which could lead to stalling and damaging the PDC (poly diamond crystalline) bit [Elsayed, M.A. and Dareing, D.W. (1994) and Leine, R.I. et al.,(2002)].

The coupling of axial and transverse vibrations result in two types of bending: Linear and parametric coupling. Parametric coupling between axial forces in the drill string and bending vibrations is discussed in Dunayevsky, V. et al. (1993). Linear coupling is easily visualized and does not occur in any perfectly straight beam with axial loads. The main source of linear coupling is the initial curvature of the BHA. Modal coupling is another effect of the three major vibrations resulting in BHA and downhole tool failure.

Many factors affect the nature of vibration of drill-strings like hole angle, drilling fluid types, rig electrical system, heave, bit type, bit-lithology interaction, lithology, borehole size, BHA stabilization, and back reaming with excessively high rpm. Two examples of drill pipe failures are shown in Figure 1.

It is important to carefully model the various vibrations in order to analyze complex phenomena like stick slip, bit whirl, bit bounce, etc. Figure 2 displays the schematic of a typical rotary drilling rig. To facilitate research, the important features of the rig are incorporated in a laboratory prototype (Figure 3). Similar prototypes have been used by other researchers for analyzing drilling vibrations. The prototype used for this research stands out due to the presence of a universal joint connecting the drill string to the upper rotary disk. The joint provides an additional 2 degree of freedom movement to the drill string and the lower rotating components. Hence, the set-up is more similar in dynamics and degrees of freedom to the actual drilling process.

Some recent researches in rotary drilling vibration analysis and their modeling methods are discussed briefly below. Mihajlovic [Mihajlovic, N. et al. (2004)] used experimental prototype to analyze stick-slip vibrations and limit cycling. They have used analytical modeling from first principles and then used parameter estimation to estimate the drill string model coefficients. They also developed a separate friction model analytically for the well borehole friction. The nonlinear properties are analyzed using bifurcation diagrams and a constant braking force is applied to the set-up. However, the type of model obtained or the procedures of model selection are not discussed. It is also worthy to note that they have operated the setup at very low velocities. Navarro Lopez and Suarez [Navarro Lopez, E. and Suarez, R. (2004)] modeled the drill string torsional behavior as a two degree of freedom torsional pendulum using lumped parameter differential equation. Gernay [Gernay, C. et al. (2009)] have also used lumped parameter models to represent the drill string and their contribution is a new approach to modeling the stick slip phenomenon as a result of axial and torsional vibration coupling. Liao [Liao, C-M. et al. (2011)] have developed reduced order models for rotary drilling prototype from analytical principles.

This paper identifies a model for an experimental rotary drilling prototype using Black box identification method. The method of system identification is the modern modeling tool and is used for a wide range of applications [Elkhalil, M., et al. (2010), Gao, Y., et al. (2011), Khaddaj, S.I., et al. (2011)]. The purpose of the work is to provide a detailed analysis of the model identification method so that the procedure can be applied to identify models of similar nonlinear systems easily.

Initially, the nonlinear properties exhibited by the drill string system when a mass imbalance is added (Figs.3 and 4) are analyzed experimentally. Then, a mathematical model is identified for the nonlinear system using the Black box identification method. This model identification method is distinguished from other methods in that it requires no prior information about the process.

The paper is organized as follows. Section 1 gives the description of the experimental set-up in the laboratory. Experimental tests conducted to analyze the effect of varying unbalance mass under varying rotor speeds are also discussed. Section 2 details the theory of the black box identification method using the parameter estimation procedure and the proof for the unbiased nature of the estimates of model coefficients. The step by step procedure of identifying the mathematical model, selection of model structure, model order etc. are detailed in Section 3. Sections 4 and 5 compares two identified models for the system and presents a twofold validation results for the better fit model. Finally, some concluding remarks are presented in Section 5.

1. EXPERIMENTAL SET-UP

The dynamics of a drill string in the presence of well bore friction is highly nonlinear. The nonlinearities of the system usually lead to what is known as limit cycling. Under the assumptions of no wellbore friction and a straight drill string, the drill string system can be modeled as a two degree of freedom linear system. However, in the presence of wellbore friction, curved/inclined boreholes or unbalanced WOBs (weight on bits), the dynamics of the system become more complex and the degrees of freedom of the drill string and drill bit system increases. The friction causes the drill bit centerline to deviate from the vertical axis and the lateral and torsional vibrations to appear. This results in high bending stresses in the drill string which could finally result in a bent drill string.

To investigate the effects of the nonlinear behavior exhibited by the drill string, a laboratory set-up (Figs. 3 and 4) featuring the major components involved in the drilling process is designed and built in our laboratory. A DC motor is fixed to the upper platform of a cubical frame and provides the torque necessary for simulating the drilling motion. A disc representing the rotary table is attached to the motor shaft. A flexible wire representing the drill string is connected to the disc via a universal joint. The drill string is made of carbon steel and has similar material characteristics to the actual drill strings used in oil rigs. The universal joint provides the necessary degrees of freedom of movement to the drill string and drill bit. A second disk representing the BHA (drill bit and complementary components) is connected to the end of the drill string and hangs free. A casing is provided surrounding the lower disk to represent the bore hole. Incremental encoders are attached above the disks to measure the angular velocity data.

Initially, the drill rig is set-up with no unbalanced mass on the lower disk and to represent an ideal linear system. However the addition of the unbalanced mass on the lower rotor representing the drill bit introduces and accounts for the nonlinear characteristics in the system. The nonlinear properties of the system introduced by the addition of the unbalanced mass were analyzed by Abdul Majeed et al. [F. Abdul Majeed et al. (2011)]. Unexpected and erratic changes in the system behavior were noticed even for minor changes in the system parameters such as frequency and magnitude of the applied input command.

The addition of the unbalanced mass to the lower rotor was first proposed by Jansen [Jansen, J.D. (1991)]. He studied the causes of self excited vibrations in rotary drilling. Dykstra [Dykstra, M. et al. (1996)] suggested that the source of vibration is the bit and hence the centrifugal forces developed when an unbalanced drill string is rotated could be one of the major sources of vibrations. The tests were focused on drill collars and lateral shocks and backward whirl. Melakhessou [Melakhessou, H. et al. (2003)] modeled the drill string as an unbalanced rotor supported by two bearings and their research was concentrated on a contact

zone between the drill string and the borehole wall. Liao [Liao, C-M. et al. (2011)] developed a reduced order model for similar drill string system with a mass imbalance on the rotor. The trajectory of the bit for various mass and angular velocities was determined displaying bit whirl and stick slip characteristics.

The working of the laboratory arrangement shown in Figure 3 is detailed below. The motor is actuated by a command signal generated by a function generator and amplified by a power amplifier before being fed to the motor. The command signal is designed so as to run the motor shaft at speeds similar to those used with actual oil rigs. The motor shaft rotates the upper disk as well as the rest of the drill string and lower disk representing the drill bit and BHA. In the presence of unbalanced mass, the drill bit is forced to move in an elliptical and somewhat chaotic path at lower speeds. The following sections analyze the dynamics of the laboratory set-up under various unbalanced mass conditions.

Experiment 1: Zero unbalance

Initially, the drill string system is allowed to rotate freely (zero unbalanced mass) condition. Some vibrations were observed at speeds around 8rpm which could indicate resonance; i.e., first mode of vibration and exciting frequency are close to each other (Figure5a). As the speed is increased to above 36 RPM, the amplitude of vibrations is reduced significantly.

The average drilling speed is about 50 – 60 RPM. It was noticed that the response of the drill string system lags behind the command speed input at low speeds; however, as the speed is increased the lag is reduced. This deficiency at low speeds can be attributed to power dissipation in the elements. It is seen that the drill string upper and lower velocities follow the command speed more closely at higher speeds.

Experiment 2: 2.6% unbalanced mass addition

A mass of 28g (2.6%) is added on the lower disk which represents the drill bit and BHA (Figure 4). The amount of mass added represents a typical commercial drill bit manufacture imbalances (2-10%)[Warren T.M., (1990)]. It was noticed that the drill string upper and lower velocities follow the command speed better than in the ideal condition (Figure5a). It is also noted that the self excited vibrations appear similar to Experiment 1 when rotated at low speeds, but they are less prominent due to the higher mass of the bit. The increased mass forces the system to keep close to the center and the self-excited vibrations are minimized. As the speed is increased to 50 RPM, the system now rotates at a speed slightly higher than the command speed; this could be attributed to the increase in the effect of the nonlinear properties of the drill string due to the unbalanced mass.

Experiment 3: 5.1% unbalanced mass addition

The unbalanced mass added to the lower rotor is further increased and now a 56 g (5.1%) mass rests on the lower disk. The drill string follows the command speed closer at a speed of 39 RPM, but faster at speeds of 50 RPM, this may also be due to increased centrifugal force and increased nonlinearity. Limit cycling vibrations are also more prominent, and a type of whirling can be noticed for the lower bit at higher speeds (Figure5b). This whirling will lead to stick-slip when there is increased friction between the well bore and lower bit. It is worth noting here that the unbalanced mass can only represent the effect of constant friction on the lower drill bit. It cannot represent sudden friction or jerks imposed on the drill bit due to unseen hard rocks or obstacles in the drilling path.

Displayed in Figs. 5a, 5b and 5c are the command speed applied to the system to be followed, the angular velocity data of the upper rotary and lower bit for the three experiments. The angular velocities are displayed and analyzed along with the angular positions. The vibration information is clear and the behavior of the drill bit in the x-y plane can be better analyzed using the provided graphs.

2. SYSTEM IDENTIFICATION BY PARAMETER ESTIMATION

In the parameter estimation approach, the model of the system is directly obtained from the process or system inputs and output data. In other words, the parameter estimation approach estimates the parameters β of the mathematical model (Figure 6) by using the inputs u and outputs y of the process.

Consider a linear single input single output (SISO) system; the system can be described by the equation,

$$y(t) = \frac{b(t)}{a(t)} e^{-st} u(t) \quad (1)$$

where $u(t)$ is the input, $y(t)$ is the output at any time t . The $\frac{b(t)}{a(t)} e^{-st}$ part represents the system at any time t .

In discrete terms, (1) can be rewritten as:

$$y(K) = z^{-m} \frac{B(z^{-1})}{A(z^{-1})} u(K) \quad (2)$$

at any sampled instant K .

$$\text{Here } B(z^{-1}) = \sum_{k=1}^n (b_k z^{-k}) \quad (3)$$

$$\text{and } A(z^{-1}) = 1 + \sum_{k=1}^n (a_k z^{-k}) \quad (4)$$

where n is the process model order and m is the system time delay.

Multiplying out and redefining the constants, $k = K+m$;

$$y(k) = \frac{B(z^{-1})}{A(z^{-1})} u(k) \quad (5)$$

$$y(k) = b_1 u(k-1) + \dots + b_n u(k-n) - a_1 y(k-1) - \dots - a_n y(k-n) \quad (6)$$

Equation (6) is now in the form of a difference equation. It relates the process output $y(k)$ at time k to the past values of the system inputs u and outputs y and their respective weighting parameters.

The above equations can be represented in matrix form as

$$Y = \Phi \beta \quad (7)$$

Where Y is the vector of the output of the process at any instant k ;

Φ is the matrix of the past values of inputs and outputs

$$\Phi = [-y(n), \dots, -y(1) : u(n), \dots, u(1)] \quad (8)$$

and β is the matrix of the parameters/ weighting coefficients of the past values of outputs and inputs.

$$\beta = [a_1 \dots a_n b_1 \dots b_n]^T \quad (9)$$

The method of parameter estimation uses Φ and Y to estimate β .

The schematic in Figs. 7a and 7b describes the ARX and Box Jenkins models where $\{u(t)\}$ and $\{y(t)\}$ are the input and output sequences of the system, respectively, $\{e(t)\}$ is a white noise sequence

with a zero mean, and $A(z)$, $B(z)$, $C(z)$, $D(z)$ and $F(z)$ are polynomials of known orders (na, nb, nc, nd, nf) , in the unit backward shift operator z^{-1} [i.e., $z^{-1} y(t) = y(t-1)$], defined by

$$A(z) = 1 + a_1 z^{-1} + a_2 z^{-2} + \dots + a_{na} z^{-na}$$

$$B(z) = 1 + b_1 z^{-1} + b_2 z^{-2} + \dots + b_{nb} z^{-nb}$$

$$C(z) = 1 + c_1 z^{-1} + c_2 z^{-2} + \dots + c_{nc} z^{-nc}$$

$$D(z) = 1 + d_1 z^{-1} + d_2 z^{-2} + \dots + d_{nd} z^{-nd} \quad \text{and}$$

$$F(z) = 1 + f_1 z^{-1} + f_2 z^{-2} + \dots + f_{nf} z^{-nf} \quad (10-14)$$

The objective here is to develop a Box Jenkins model using least squares based iterative algorithms to estimate the unknown parameters $(a_i, b_i, c_i, d_i, f_i)$ by using the available input-output measurement data $\{u(t), y(t): t = 1, 2, \dots, K, \dots, N\}$ to improve the accuracy of parameter estimation.

The equations for the recursive algorithms used for the Box Jenkins model identification and their advantages are discussed in Liu et al. (2010). The least squares based algorithm converges faster than the gradient based algorithm and the stochastic algorithm used for the identification process. Chen, P. and Tang, X., (2010), Wei, H.L., et al. (2010) and Zhao, G. and Wang, Z., (2011) are some examples of the various applications where the least squares principle is applied.

The least squares estimate is found by minimizing the sum of squares of the model errors.

The least squares estimate is obtained as

$$\hat{\beta} = (\Phi^T \Phi)^{-1} \Phi^T Y \quad (15)$$

[Derivation of the least squares estimate is presented in Appendix 1]

Substituting from (7);

$$\hat{\beta} = (\Phi^T \Phi)^{-1} \Phi^T (\Phi \beta + e); \quad (16)$$

i.e;

$$\hat{\beta} = \beta + (\Phi^T \Phi)^{-1} \Phi^T e \quad (17)$$

Multiplying by $\Phi^T \Phi$ on both sides;

$$\Phi^T \Phi (\hat{\beta} - \beta) = \Phi^T e \quad (18)$$

Taking the Expected value;

$$E[\Phi^T \Phi(\hat{\beta} - \beta)] = E[\Phi^T e] = 0. \quad (19)$$

$E[\beta] = \beta$ only if the mean values of the components of the noise vector (e) are zero and if the matrices Φ and noise vector are uncorrelated.

In other words, the estimates of the parameters are unbiased if the noise input is assumed to be white and the white noise and data matrix are independent. This is true and the estimates will always be unbiased because in parameter estimation, the noise is always assumed to be white and a *MA* (moving average) filter is added to represent the colored noise factor.

3. MODEL DEVELOPMENT AND SELECTION

Referring to Figure 7, $\{u(t)\}$ is taken as a persistent excitation signal sequence with zero mean and unit variance, and $\{e(t)\}$ as a white noise sequence with zero mean and variance σ^2 . A flow chart of the data communication between the software and hardware components of the laboratory arrangement and the system identification procedure is shown in Figs. 8a and 8b, respectively. The steps detailed below of the system identification procedure are processed using the National Instruments Lab VIEW Signal Express tool kit. Lab VIEW Signal Express tool kit has all the built in functions required to carry out the identification procedure efficiently once the steps are known. Some recent researchers who have used Lab VIEW are Kho, Y.Y. et al, (2004) and Lenaers, G. et al, (2003).

The measured input and output data are raw and need to be normalized and de-trended to ensure good estimates.

The mean level can be removed from the raw data by calculating

$$u_m(t) = u(t) - \tilde{u} \quad \text{and} \quad y_m(t) = y(t) - \tilde{y} \quad (20)$$

Where $u(t)$ and $y(t)$ are the raw input and raw output,

$$\tilde{u} = \frac{1}{N} \sum_{t=1}^N u(t) \quad (21)$$

and

$$\tilde{y} = \frac{1}{N} \sum_{t=1}^N y(t) \quad (22)$$

are the mean of the input and output, and N is the data length. The input transpose of the data matrix is, $u = [u(1), u(2), \dots, u(N)]$ and the output data matrix transpose is $y = [$

$y(1), y(2), \dots, y(N)]$. The data obtained experimentally may have some drift in it. Slight drifts in data could be due to low frequency noise disturbance added to the system during data acquisition. It is however essential to do the de-trending to ensure the data is drift free. Data in which there is slight drift can results in unstable models.

The linear trend is removed as follows;

$$u_d(t) = u(t) - A\theta_u, \quad (23)$$

and

$$y_d(t) = y(t) - A\theta_y \quad (24)$$

Where,

$$A = \begin{bmatrix} \frac{1}{N} & \frac{2}{N} & \cdot & \cdot & \cdot & \frac{N-1}{N} & 1 \\ 1 & 1 & \cdot & \cdot & \cdot & 1 & 1 \end{bmatrix}^T \quad (25)$$

and $A\theta_u$ and $A\theta_y$ are the least squares fits for u and y respectively. The input and output data are the speeds of the upper disk and lower disk (Figure 6), respectively. The coefficient matrix, Φ , is calculated for various model orders. Each model is tested against the residual function tests and pole/zero (PZ) maps. An approximate model order estimate is made by analyzing the number of resonant peaks in the non parametric frequency response function. The order of the $A(k)F(k)$ term is taken to be twice the number of peaks in the magnitude response. An ARX model consists of the auto regressive exogenous terms and a white noise model.

$$y(k) = z^{-m} \frac{B(z^{-1})}{A(z^{-1})} u(k) + \frac{1}{A(z^{-1})} e(k) \quad (26)$$

The delay order can be estimated visually from the model responses for various delay orders. The delay order which gives the maximum model fit, and minimizes the prediction error is selected. An ARX model is initially modeled for the data. The orders of A and B are finalized by a trial and error method of testing the model responses, the residual error correlation functions, and PZ maps. The test details are listed in Table 2.

On a closer analysis of the process behavior, it can be seen that the non linear properties are introduced into the system at the lower bit end. In other words, the system can be described as one which has disturbances entering late or near the output end of the system. In such cases, it is better to fit a Box Jenkins model rather than an ARX model.

Box Jenkins (BJ) model is of the form:

$$y(k) = \frac{B(z^{-1})}{F(z^{-1})}u(k) + \frac{C(z^{-1})}{D(z^{-1})}e(k) \quad (27)$$

The A and B orders selected for the ARX model can be used as the starting orders of B and F in the BJ model identification. The noise model is generally selected at orders of range 1 and 2.

The model order is selected by analyzing the Akaike's Final Prediction Error (FPE), Akaike's Information Criteria (AIC) and Minimum Description Length (MDL) criteria as well as the residual correlation test results. The AIC, FPE, and the MDL are the criteria used to determine the best model order for the system. As a rule, the lower these values are, the better the model is. Also, to be kept in mind is that if there is only slight changes in these values between the lower and higher order models, the lower order model is selected taking into account simplicity and complexity of the model. The results of the criteria and tests are listed in Table 2.

Comparing the AIC, FPE, and the MDL as well as the residual correlation test results, an ARX model with a process model order $A=3$, $B=2$, and a BJ process model with orders $B=2$, $F=3$, and noise model coefficient orders $C=2$ and $D=2$ is selected (Refer to equations (10-14) for coefficient order details).

The basis for the selection is that no major difference is found in the reduction of confidence bands of the cross correlation tests beyond a model order 3 and the auto correlation test graph is more symmetric on either side of the middle high. However, the BJ model gives lesser estimation criteria results than the ARX model. Figure 9 illustrates the auto correlation test of the model residuals and the cross correlation test between the input and the model residual and the prediction error graph.

Results are only compared for model orders greater than 1 because the system is clearly nonlinear.

The cross correlation tests results are passed when the test graphs are within the confidence intervals and should decay to zero on both ends. The auto correlation graph should have a maximum overshoot in the middle to infinity (ideally) and should decay to zero on both ends. The residual correlation tests in Figure 9a for the ARX model show good results and features of a good model. However, when compared to the correlation test results for the BJ model (Figure 9b), the autocorrelation function for the ARX model tends to transgress the confidence bands more often and is not smooth. The cross correlation function is not symmetric for the BJ model; however, it falls within the confidence bands.

Unbiased estimates are ensured when the residual signal (also known as prediction error) is reduced to a white noise sequence. If the estimated process or noise model is

deficient or biased, the residual will be colored. The prediction error graph (Figs. 9a and b) for both the models shows good ranges and has a white noise pattern; however, the levels of error are less for the BJ model than for the ARX model. Based on the above discussion, a BJ model is selected as a closer process model and analyzed for further validation results.

4. PZ MAP ANALYSIS FOR DIFFERENT MODEL ORDERS

Further analysis of the model can be performed by analyzing the locations of the poles and zeros of the developed model. Pole zero plots of ARX model $A=3$ and $B=2$ with delay = 0 is plotted in Figure 10a. The model has one marginally stable pole on the imaginary axis. It has 2 poles and two zeroes which have their confidence intervals overlapping. The position of these poles suggests a stable but oscillatory system. Figure 10b displays the pole and zero locations when order of $A=4$, $B=3$ with delay = 0. There is now an extra pole on the imaginary axis indicating stable pole. But the confidence intervals of the complex conjugate poles and zeros now almost coincide/overlap indicating the model order need to be reduced.

For a Box Jenkins model with orders $B=2$, $F=3$, and noise model $C=2$ and $D=2$, and delay = 0, the PZ plot is shown in Figure 10c. The pole on the imaginary axis is a stable pole, the poles in the left half circle is inside the circle indicating stability but has an oscillatory response. The BJ model is more stable and less oscillatory than the ARX model. Figure 10d presents the PZ plot for a Box Jenkins model with process model orders $B=3$, and $F=4$, and noise model orders $C=2$, $D=2$ with delay = 0. The pole zero positions are good and the criteria also has small values. However, in the model simulation tests, this model does not provide any better results for simulation errors when compared to the previous simpler BJ model ($A=2$, $B=3$, $C=2$, $D=2$). The process model coefficients for the selected BJ model are listed in Table 3.

5. MODEL VALIDATION TESTS

Command signal type variation

To support model validation, ramp and step speed commands are given to the laboratory system. The responses are then compared with the ARX and BJ model simulated responses for same inputs. The signals are plotted in Figure 11. This stage of the validation ensures the model and the system responses are similar for different speed input commands. The analysis of the plots in Figure 11 shows the ARX model provides a good fit for the experimental data. However, on close inspection; it is seen that the residual error of the BJ model has smaller amplitude than the ARX model. Moreover, as discussed in the

previous section, the BJ model has more stable PZ locations than the ARX model.

Varying operational speeds

The next stage of validation is to operate the model and the drill system at different speed ranges to analyze if the model efficiently captures the nonlinear properties exhibited by the system. For this purpose the process model is subjected to low, average and high speed range inputs for normal drilling operation. The results are plotted and compared in Figure 12 below. It is noticed that the process model accurately simulates the system response and displays the self excited vibrations at low speeds. Limit cycling is prominent at the average speed range of 38 RPM. The vibrations ease out and limit cycling is less noticed at speeds around 100 RPM, with the assumption of no further additive frictions affecting the system.

6. CONCLUSION:

This paper analyses and identifies a mathematical model for a laboratory prototype of a rotary drilling rig. The nonlinear characteristics and dynamics presented by the system are briefly described with plots. The step by step procedure for applying black box modeling techniques of system identification using least squares principles are detailed. The data used is collected from an experimental setup and identification is done offline. ARX and Box Jenkins model structures are selected, and compared. The better fit Box Jenkins model is validated by a twofold validation procedure.

7. REFERENCES

- [1] Abdul Majeed, F, Karki, H. , Abdel Magid, Y. , Karkoub, M. (2011), "Nonlinearity and Spectrum Analysis of Drill Strings with Component Mass Unbalance", Proceedings of World Academy of Science, Engineering and Technology Conference, January, pp. 459-462
- [2] Balachandran, B. , Liao, C. , Karkoub, M. , and AbdelMagid, Y. (2008), "Drillstring Dynamics", Paper presented at The Twelfth Conference on Nonlinear Vibrations, Dynamics, and Multibody Systems, Blacksburg, VA, USA. June 1-5.
- [3] Berlioz, A. , DerHagopian, J. , Dufour, R. and Draoui, E.(1996) , "Dynamic behavior of a drill string: Experimental investigation of lateral instabilities", J of Vibration and acoustics, Vol. 118, pp.292-298.
- [4] Billings, S.A. (2004),"Lecture notes in System Identification, MSc Eng. Course in Control systems Engineering", University of Sheffield.
- [5] Chen, P., Tang, X., (2010)," Study on parameters self-tuning of speed servo system based on LS_SVM model", Int. J. of Modelling, Identification and Control, Vol. 10, No.1/2, pp. 12 – 18.
- [6] Christoforou, A. and Yigit, A.(1997) , "Dynamic modeling of rotating drill string with borehole interactions", J. sound and vibration, Vol.206, pp.243-260.
- [7] Dareing, D., et.al (1997), "Effect of Torsion on Stability, "Dynamic Forces, and Vibration Characteristics in Drillstrings", J. of Energy Resources Technology, Vol. 119, pp.111-19.
- [8] Dunayevsky, V., Abbassian, F. and Judiz, A. and Mills, H.(1993) , "Dynamic stability of drill-strings under fluctuating weight on bit", SPE Drilling and Completion,,Vol.8, pp. 84- 92.
- [9] Dykstra, M., Christensen, H., Warren, T. , and Azar, J.(1996) , "Drill string component mass imbalance: A major source of drill string vibrations", SPE Drilling and completion,Vol.11, pp.234-241.
- [10] Elkhailil, M., Ltaief, M., Ben Abdennour, R., M'Saad, M., (2010)," Multimodel reference model control: an experimental validation on a chemical reactor", Int. J. of Modelling, Identification and Control, Vol. 9, No.4, pp. 350 – 358.
- [11] Elsayed, M. A., and Dareing, D. W.(1994), "Coupling of Longitudinal and Torsional Vibrations in a Single-Mass Model of a Drillstring," Developments in Theoretical and Applied Mechanics, Vol. XVII, University of Arkansas, Fayetteville, AR, pp. 128–139.
- [12] G. Lenaers, L. Pelkmans, P. Debal, The realisation of an on-board emission measuring system serving as a R&D tool for ultra low emitting vehicles, Int. J. of Vehicle Design 2003 - Vol. 31, No.3 pp. 253 – 268.
- [13] Gao, Y., Fang, L., Wei, M., Ma, J., (2011)," Model identification of EMP electromagnetic coupling using Volterra kernel", Int. J. of Modelling, Identification and Control, Vol. 13, No.3, pp. 171 – 177.
- [14] Gernay, C. , van de wou, N. , Nijmeijer, H. , and Sepulchre, R. (2009), "Nonlinear drill string dynamics analysis", SIAM J. Applied Dynamical systems, Vol. 8, pp.527-553.
- [15] Gopinath, S.(2010), "Study on electric motor mass imbalance based on vibration monitoring analysis technique", Paper presented at the International conference on electrical and mechanical technology, IEEE, pp.539-542.
- [16] Jansen, J.D. (1991),"Non linear rotor dynamics as applied to oil well drill string vibrations", J. Sound and vibration, Vol.147, pp.115 -135.
- [17] Khaddaj, S.I., Jaber, R.G., Karamneh, F.N., (2011), "Dynamic models of student performance: a system identification approach", International Journal of Modelling, Identification and Control, Vol. 14, No.1/2, pp. 46 – 59.
- [18] Leine, R.I., van Campen, D.H. , and Keultjes, W. (2002) , "Stick slip whirl interaction in drill string dynamics", ASME J. of vibration acoustics,Vol.124,pp. 209-220.
- [19] Liao, C-M. Liao Balachandran, B., Karkoub, M., Abdel-Magid, Y. (2011), "Drill-String Dynamics: Reduced-Order Models and Experimental Studies," ASME J. Vib. Acoust. Vol. 133, No. 4, pp. 041008-1—8.
- [20] Liu, Y., Wang,D. and Ding,F.(2010) , "Least squares based iterative algorithms for identifying Box–Jenkins models with finite measurement data", Digital signal processing,Vol.20, pp. 1458-1467.
- [21] Melakhessou, H. et al.(2003), "A nonlinear well drill string interaction model", J. Vibration acoustics,Vol.125,pp.46 -52.
- [22] Mihajlovic, N., van Veggel, A. , Nan de Wou and Nijmeijer, H. (2004), "Analysis of friction induced limit cycling in an experimental drill string system", J. of Dynamic systems, measurement and control, ASME , Vol.126, pp.709-721.
- [23] Mihajlovic, N. , Van Veggel, A. , Van de Wouw, N. and Nijmeijer, H. (2004) ,"Friction induced torsional vibrations in an experimental drill string system", Paper presented at the 23rd IASTED international conference on modeling , identification and control,pp.228-233.
- [24] Navarro Lopez, E. and Suarez, R.(2004), "Modeling and Analysis of stick slip behavior in a drill string under dry friction", Congresso Annual De La Amca, pp. 330-336, 2004.
- [25] Silviera, M. and Wiercigroch, M. (2009), "Low dimensional models for stick slip vibration of drill strings", J. of Physics, Conference series, Vol. 181.

- [26] Theron, A., de.Langre, E. and Putot, C.(2001) , “The Effect of Dynamical Parameters on Precession in Rotary Drilling”, J. of Energy Resources Technology, Vol.123, pp.181-186.
- [27] Warren, T. M. , Brett, J. F. , Sinor, L. A. (1990), Development Of A Whirl-Resistant Bit : SPE Drilling Engng, Vol.5, N4, pp.267–274
- [28] Wei, H.L., Billings, S.A., Liu, J.J., (2010),” Time-varying parametric modelling and time-dependent spectral characterisation with applications to EEG signals using multiwavelets”, Int. J. of Modelling, Identification and Control, Vol. 9, No.3, pp. 215 – 224.
- [29] Y.Y. Kho, S. Hashim, C.F. Soon, Vital physiological signs monitoring, Int. J. of Computer Applications in Technology 2004 - Vol. 21, No.1/2 pp. 58 – 64.
- [30] Zhao, G., Wang, Z., (2011),” Time-frequency analysis for non-stationary signal from mechanical measurement of bearing vibration”, Int. J. of Modelling, Identification and Control, Vol. 13, No.3, pp. 190 – 194.

2. Modeling by System Identification of a Nonlinear rotor system with an Un Actuated end,

F. Abdul Majeed, H. Karki, Y. Abdel Magid, M. Karkoub, Accepted by Global Congress on Science and Engineering to be published in the Journal, Procedia Engineering, (ISSN: 1877-7058, ELSEVIER), Dec 2011.

GCSE 2011: 28-30 December 2011, Dubai, UAE

Modeling by System Identification of a Nonlinear rotor system with an Un Actuated end

F. Abdul Majeed^{*1}, H. Karki^a, Y. L. Abdel Magid^b, M. Karkoub^c

^a*Mechanical Engineering Department, Petroleum Institute, Abu Dhabi, UAE*

^b*Electrical Engineering Department, Petroleum Institute, Abu Dhabi, UAE*

^c*Mechanical Engineering Department, Texas A&M, Qatar,*

Abstract

Conventionally the method of analytical modeling is used to analyze the dynamics of complex nonlinear processes. This paper discusses an alternate procedure for converging to the mathematical model of a system by the method of system identification for a nonlinear rotor system with an un actuated end. The experimental set-up for the model identification consists of two rotors connected by a flexible shaft vertically with a mass imbalance at the un actuated rotor end. The mass imbalance on the un actuated rotor can also represent widely the dynamics of systems with added friction near the output. The paper details the procedure and criterions applied to identify an Auto Regressive Exogenous (ARX) model for the process. The criteria for the selection of various parameters like model order and type are also discussed in the paper. The least squares method is used to confirm unbiased estimates for the process model coefficients. Simulation results of the developed model for various inputs are presented to validate the model.

© 2011 Published by Elsevier Ltd. Selection and/or peer-review under responsibility of GCSE
2011

Keywords: MODELING, SYSTEM IDENTIFICATION, NONLINEAR ROTOR SYSTEM, ARX MODEL

1. Introduction and scope of research

This paper describes the identification of a mathematical model which accurately simulates the dynamics of a nonlinear rotor system with an un actuated end by the system identification method using parameter estimation. It is motivated by the need to explain the various steps required to identify a model for a typical nonlinear system by using data from the system. This method of model identification is also known as black box modeling, because no

^{*} Corresponding author. Tel.: +971 26075449; fax +971 26075200.
E-mail address: fmajeed@pi.ac.ae.

priori information is required about a process other than the data going into and coming out from the process. It is the most popular alternate modern means to derive models of complex processes.

2. Experimental set-up

The laboratory set-up (Figure 1) consists of a rotor connected to the shaft of a motor. The DC motor is fixed to the upper platform of a cubical frame. A flexible string is connected to the rotor by a universal joint (possess two degree of rotational freedom). A second rotor with a mass imbalance is connected to the end of the string and hangs free. Similar non linear systems with one actuated and other un actuated end is seen in many physical systems. The mass imbalance at the un actuated end can also be representative of damping caused by friction due to mechanical and environmental reasons. Some examples of similar systems are industrial and domestic robots, turbine blade dampers or drilling rigs [1,2]. [3] presents an analysis of similar experimental model with mass imbalance. They have suggested mass imbalance studies to represent bottom hole friction found in drilling wells and they propose reduced order models to represent such systems. In the laboratory set-up, when the motor is actuated, the shaft rotates the upper rotor. This rotation forces the un actuated lower disc also to rotate. The presence of the mass imbalance forces the lower disc to move in elliptical and unexpected paths of rotation at lower speeds.

3. System Identification

It is essential to develop well defined suitable models to describe the dynamic behavior of nonlinear systems in order analyze the dynamics and develop better controllers.

Analytical modeling has the disadvantage of many assumptions. This will eventually fail to capture all the modes of the system and hence leads to less accurate models on which to base the further researches and experiments. Hence the deficiencies in the model together with the uncertain behavior of nonlinear systems make it all the more complicated.

The System identification method of modeling presented here is void of assumptions and dependent only on actual process data and the method can be extended to any physical or real process easily. The typical non linear system is selected to analyze the validity of modeling non linear systems by this approach. This paper presents an autoregressive exogenous model of the rotor system (ARX). Least squares based parameter estimation approach is used to converge to unbiased process model coefficients. The speed of the upper and lower rotating discs (Figure 1) form the data used for deriving the model. This paper details the process of selection of model order and the criteria and tests required to choose the correct model by the identification procedure.

System identification is a linear regression technique used in controls theory. It allows a representative model of the system to be developed by systematical selection of model order and using regression analysis to solve for the algebraic coefficients in the model. This approach can be applied online in real time when the drilling operation is being done with the minimal disturbance to the system because this involves exciting the system with a PRBS or white noise input. The method can be easily extended to complex and multiple input multiple output processes without increasing the complexity of the approach. The real time drilling process is very complex, nonlinear, and has many outputs and inputs. Unlike analytical modeling, this method makes use of very little assumptions and depends on the data directly obtained from the process.

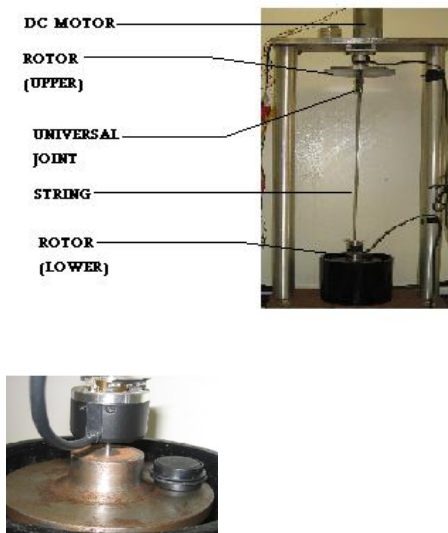


Figure1 : Laboratory experimental set-up (Upper) and unbalanced mass on rotor (Lower)

4. Parameter Estimation Procedure

In parameter estimation approach the model of the system is directly obtained from the process or system input and output data. In other words, the parameter estimation approach estimates the parameters β of the mathematical model (Figure 2) by using the inputs u and outputs y of the process.

Consider a linear single input single output (SISO) system; the system can be described by the equation,

$$y(t) = \frac{b(t)}{a(t)} e^{-st} . u(t) \quad (1)$$

where $u(t)$ is the input, $y(t)$ is the output at any time t . The $(\frac{b(t)}{a(t)} e^{-st})$ part represents the system

at any time t . In discrete terms,(1) can be rewritten as :

$$y(K) = z^{-m} \frac{B(z^{-1})}{A(z^{-1})} u(K) \quad (2)$$

at any sampled instant K .

The polynomials B and A are defined as;

$$B(z^{-1}) = \sum_{k=0}^n (b_k . z^{-k}) \quad (3)$$

and

$$A(z^{-1}) = 1 + \sum_{k=1}^n (a_k . z^{-k}) \quad (4)$$

where n is the process model order and m is the system time delay.

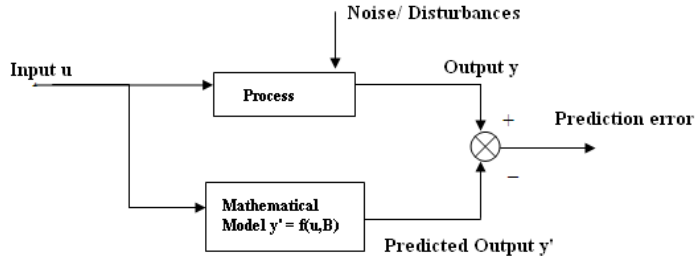


Figure2: Schematic of actual process and its mathematical model

Multiplying out and redefining the constants, $k = K+m$;

$$y(k) = \frac{B(z^{-1})}{A(z^{-1})} u(k) \quad (5)$$

$$\text{i.e.}; y(k) = b_1 u(k-1) + \dots + b_n u(k-n) - a_1 y(k-1) - \dots - a_n y(k-n) \quad (6)$$

This is now in the form of a difference equation. It relates the process output $y(k)$ at time k to the past values of the system inputs u and outputs y and their respective weighting parameters.

The above equation can be represented in matrix form as

$$Y = \phi\beta; \quad (7)$$

where Y is the matrix of the output of the process at any instant k ; Φ is the matrix of the past values of inputs and outputs.

$$\Phi = [-y(n), \dots, -y(1): u(n), \dots, u(1)] \quad (8)$$

and β is the matrix of the parameters/ weighting coefficients of the past values of outputs and inputs.

$$\beta = [a_1 \dots a_n b_0 \dots b_n]^T \quad (9)$$

The method of parameter estimation uses Φ and Y to estimate β . This can be extended for models in which additive noise terms are considered. Theoretically the quality of the estimates can be proved by least squares method. It can also be proved in real time by analyzing the prediction error graph. The prediction error is defined by the schematic in Figure2. The prediction error is also popularly known by the term 'residual'. If the residual plot remains close to zero then it can be said that a good estimate of the parameters is obtained and hence the model is accurate.

4.1. Data Preprocessing

The measured input and output data are raw and needs to be normalized and detrended to ensure quality data to get good estimates.

The mean level can be removed from the raw data by calculating

$$u_m(t) = u(t) - \tilde{u} \quad \text{and} \quad (10)$$

$$y_m(t) = y(t) - \tilde{y} \quad (11)$$

where $u(t)$ and $y(t)$ are the raw input and raw output ,

$$\tilde{u} = \frac{1}{N} \sum_1^N u(t) \text{ and} \quad (12)$$

$$\tilde{y} = \frac{1}{N} \sum_1^N y(t) \quad (13)$$

are the mean of the input and output, and N is the data length.

The input data matrix transpose is , $u = [u(1), u(2), \dots, u(N)]$ and

the output data matrix transpose is $y = [y(1), y(2), \dots, y(N)]$.

Raw data signals will sometimes have linear trends, noticed by a ‘drift’ in the signals with time. The process of removing the trend from the input and output is called the detrending operation.

The linear trend is removed by the operation

$$u_d(t) = u(t) - A\theta_u \text{ and} \quad (14)$$

$$y_d(t) = y(t) - A\theta_y \quad (15)$$

where,

$$A = \begin{bmatrix} 1/N & 1 \\ 2/N & 1 \\ \cdot & \cdot \\ \cdot & \cdot \\ \cdot & \cdot \\ (N-1)/N & 1 \\ 1 & 1 \end{bmatrix} \quad (16)$$

and $A\theta_u$ and $A\theta_y$ are the least squares fits for u and y respectively.

The raw input and output are the speeds of the upper disc and lower disc respectively directly measured from the process by rotary angular encoders placed on the rotors (Fig 3). These form the input (upper disc) and the output (lower disc) data of the system. The mean removed and detrended input (Upper rotary table speed) and output (Lower Bit speed) data are plotted in Figure 4.

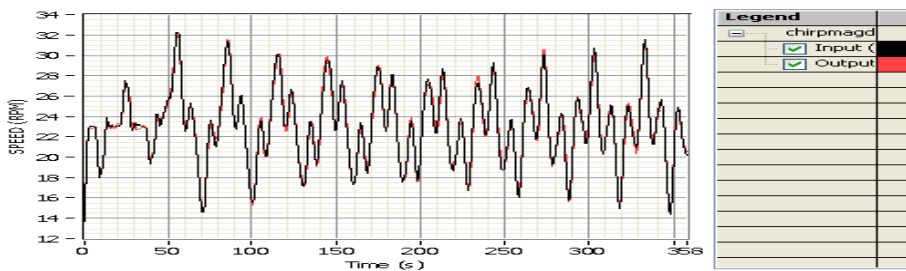


Figure3: Raw input (Black) and output data (Red)

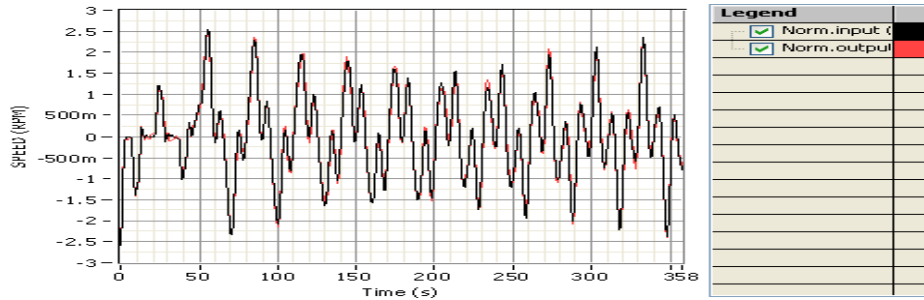


Figure4: Mean removed and detrended input (Black) and output data (Red)

4.2. Fitting a model structure and estimating parameters

From the processed data, Y and Φ matrices (7) are chosen to estimate the parameters β . In nonlinear system modeling, it is better to initially assume a zero noise model and estimate coefficients for an ARX model. An ARX model consists of the auto regressive exogenous terms and a white noise model.

$$y(k) = z^{-m} \frac{B(z^{-1})}{A(z^{-1})} u(k) + \frac{1}{A(z^{-1})} e(k) \quad (17)$$

$$A(z) = 1 + a_1 z^{-1} + a_2 z^{-2} + \dots + a_{na} z^{-na} \quad (18)$$

$$B(z) = 1 + b_1 z^{-1} + b_2 z^{-2} + \dots + b_{nb} z^{-nb} \quad (19)$$

Here $e(k)$ is white noise and 'm' is the time delay. The model order is selected by analyzing the FPE, AIC and MDL criteria and the residual correlation test results. The results of the criteria and tests are listed in Table 1.

Comparing the Akaike's Information criterion (AIC), Akaike's Final Prediction Error Criterion (FPE), and the Minimum Description Length criterion (MDL) and the residual correlation test results, an ARX model with a model order of 3 is selected. The AIC, FPE, and the MDL are the criteria used to determine the best model order for the system. As a rule, the lower these values are, the better is the model. The basis for the selection is that no major difference is found in the reduction of confidence bands of the cross correlation tests beyond a model order of 3 and the auto correlation test graph is more symmetric on either side of the middle high. The identification results of the estimated parameters are given in Table 2. Figure 6 illustrates the auto correlation test of the model residuals and the cross correlation test between the input and the model residual and the prediction error graph.

Results are only compared for model orders greater than 1 because the system is clearly a nonlinear one. The cross correlation tests results are passed when the test graphs are within the confidence intervals and should decay to zero on both ends. The auto correlation graph should have a maximum shoot in the middle to infinity (ideally) and should decay to zero on both the ends.

Unbiased estimates are ensured when the residual signal (also known as prediction error) is reduced to a white noise sequence. If the estimated process or noise model is deficient or biased the residual will be colored.

The Auto Correlation Function of the model residual (Figure5) resembles white noise ACF and lies within the confidence interval. This indicates that the process and noise model estimates are unbiased. The CCF graph (Figure6) denotes the cross correlation between the model input and the residual. It dies out to zero on either side and is bounded within the confidence interval which denotes that the process and noise model are correct and the estimates are unbiased. If the noise

or process model is biased then the CCF will not die out to zero, and the estimates will be biased.

In Figure 7, the residual fluctuates around zero(in the range of $\pm 200a$) with very small deviations. This indicates that the estimated model displays good prediction.

A comparison of the measured output and the one step and 100 step ahead prediction results from the model are plotted in Figure 6 .A good match is found in both the cases with the Mean Squared Error levels at 0.00197 and 0.00810 respectively indicating good model performance.

Table 1. Identification results for nonlinear rotor system dynamics data

Model order n, Time delay =0.	FPE	AIC	MDL	Auto correlation test (+) : Pass (-) : Fail	Cross correlation test (+) : Pass (-) : Fail
2	0.492	0.492	0.512	+	+
3	0.204	0.204	0.216	+	+
4	0.200	0.200	0.216	+	+
5	0.172	0.172	0.190	+	+

Table 2. Least squares based parameter estimates for nonlinear rotor system data

Terms	Parameter estimates	Terms	Parameter estimates
a 1	-0.9614	b0	1.0559
a2	0.6546	b1	-1.1143
a3	0.0759	b2	0.8576

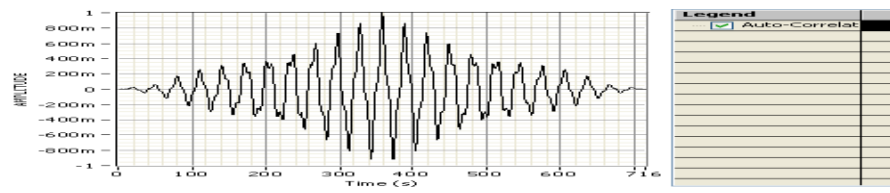


Figure5: Autocorrelation function of the model residual (model order 2)

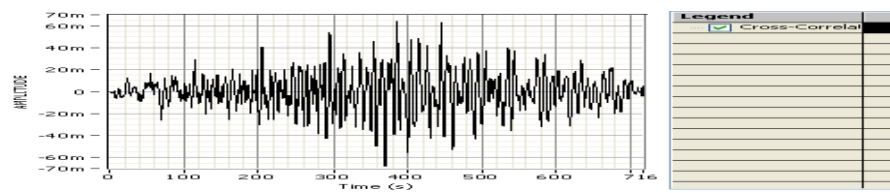


Figure6: Cross correlation function between input and model residual (model order 2)

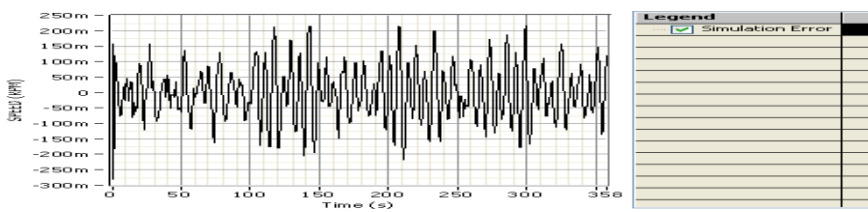
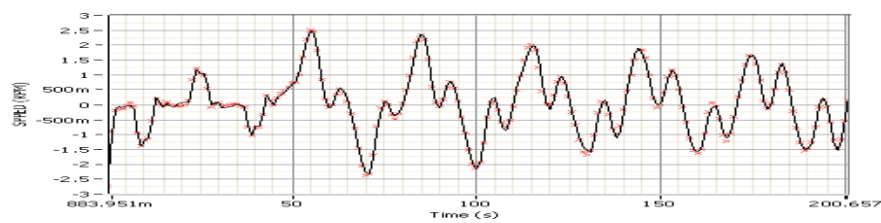
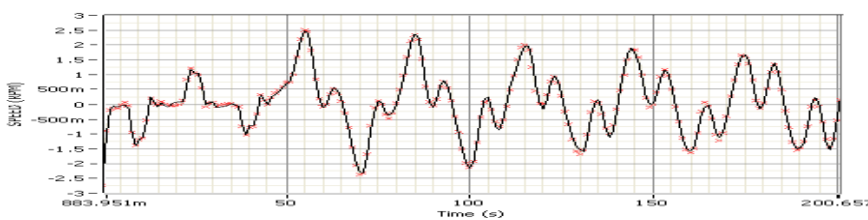


Figure7: Model residual (model order 2)



(MSE 0.00197)



(MSE 0.00810)

Figure8: One step ahead (Upper) and 100 step ahead (Lower) predicted outputs and measured output.

The parameter estimates obtained by the method of Least squares ensures the estimates to be unbiased. The least squares estimate is found by minimizing the sum of squares of the model errors. In vector form, using the representations of equation (7); assuming the error is e ;

$$Y = \Phi\beta + e; \quad (20)$$

Defining cost function J as,

$$J = 1/N \cdot \sum (e)^2; \quad (21)$$

i.e. the sum of squares of model errors for N measurements; least squares method converges to the solution by minimizing. The estimates of the parameters are unbiased if the noise input is assumed to be white and the white noise and data matrix are independent. This is true and the estimates will always be unbiased because in parameter estimation, the noise is always assumed to be white.

5. Model validation

The identified ARX model is validated by comparing the model responses with measured responses for various inputs. This method of validation procedure ensures the model and the system responses similarly to different speed variations. Step and ramp inputs are applied to the laboratory set-up and the responses are recorded. The input signals are also logged and they are input to the identified model using LABVIEW virtual instruments created for the purpose. The model simulated responses are then compared with the logged experimental responses. The compared responses are plotted in Figures 9 and 10. On analysis of these plots, it is noticed that the ARX model provides a good fit for the experimental data. The close match between the measured response and the model response further validates the correctness of the developed model.

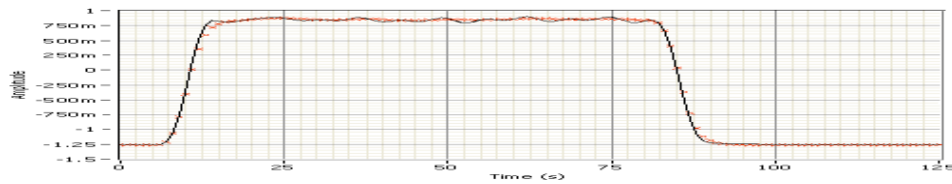


Figure9: Measured output (-) and model response (*) for step input.

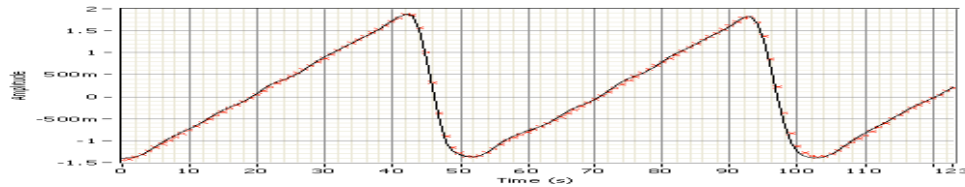


Figure10: Measured output (-) and model response (*) for ramp input.

Conclusion

This paper discusses the method to be followed for selecting the model order for a nonlinear system by the system identification approach of modeling. An Auto regressive exogenous model is initially developed to represent the non linear rotor dynamics by the Least squares based parameter estimation method of system identification. The method initially assumes white noise / disturbance added to the process. Once the model orders are successfully selected, the model can be extended to represent the colored noise / disturbance which accounts for the added nonlinear behavior of the process. The accuracy of the model is proven by residual analysis and validated by subjecting the model to various signals. The experimental set-up featured is a non linear rotary system with a mass imbalance on the unactuated end. The model is characteristic of many similar systems with a friction / imbalance with an un actuated end. The developed model can now be used as a basis for identifying complex nonlinear models for the process which include the colored noise or disturbances which add to the nonlinearity of the system.

References

- [1] A.Lj.Juloski;et al."Observer design for an experimental rotor system with discontinuos friction",Proceedings of 2006 American Control conference,IEEE.
- [2] N.Mihajlovic, A.A.van Veggel, N. van de Wouw,H.Nijmeijer; "Analysis of Friction induced Limit cycling in an Experimental drill string system", J.of Dynamic systems, Measurement and Control, Dec 2004.126
- [3] C.M.Liao; et al."Drill string dynamics: Reduced order models"IMECE 2009-10339.

3. Nonlinearity And Spectrum Analysis Of Drill Strings With Component Mass Unbalance.

F. Abdul Majeed, H. Karki, Y. Abdel Magid, M. Karkoub, Proceedings of World Academy of Science, Engineering and Technology Conference JAN 2011 73 2011, Pp. 459-462

Nonlinearity And Spectrum Analysis Of Drill Strings With Component Mass Unbalance.

Abstract— This paper analyses the non linear properties exhibited by a drill string system under

F. Abdul Majeed, H. Karki, Y. Abdel Magid, M. Karkoub

various un balanced mass conditions. The drill string is affected by continuous friction in the form of drill bit and well bore hole interactions. This paper proves the origin of limit cycling and increase of non linearity with increase in speed of the drilling in the presence of friction. The spectrum of the frequency response is also studied to detect the presence of vibration abnormalities arising during the drilling process.

Keywords— Drill strings, Nonlinear, Spectrum analysis, Unbalanced mass

INTRODUCTION

THE performance of drill string and their effect on drilling performance has been investigated and analyzed by using the latest technologies of the time. The various vibrations affecting drill strings during drilling are mainly classified into three, axial , lateral and torsional. Axial vibrations are caused by sudden bit bouncing and cracks of the drill string. Lateral vibrations (bending) and torsional vibrations are caused by drill bit well bore friction. These vibrations require to be modeled carefully to analyze and understand the important and severe phenomena of stick slip, bit bounce and drill string rupture experienced in the drilling process . Many different models were set-up to analyze drill string vibrations including lateral vibrations (whirl) and mode coupling [1-3]. Other researchers have focused on models which represent torsional vibration and have attempted to suggest methods to avoid stick slip behavior [4,5]. We have set-up a model which works in the same principle as [4]. However taking into consideration recent researches in the field , [6] has modeled the drill string as an unbalanced rotor supported by two bearings .[7] explains that the source of vibration is the bit and hence the centrifugal forces developed when an unbalanced drill string is rotated can be one of the major sources of vibrations.[8] has modeled reduced order models for such a a drill string system with a mass imbalance on the rotor and has analyzed the trajectory of the bit for various mass and angular velocities displaying bit whirl and stick slip characteristics.

This paper intends to analyze the nonlinear properties displayed by the drill string system when a mass imbalance is added to the system. Further the paper also attempts to provide a discussion on the spectrum analysis of the system outputs in the no mass and mass imbalance cases. The discussion is based on the analysis done in [9] where vibration analysis of an electric motor with a mass imbalance is studied to detect abnormalities or cracks.

Description of the laboratory set-up

To investigate the effects of nonlinear behavior exhibited by the drill string a laboratory set-up (Figure 1) is arranged. A DC motor is fixed to the upper platform of a cubical frame, and provides the torque necessary for simulating the drilling motion. A flexible string representing the drill string is connected to a rotary table fixed to the motor shaft by a universal joint (possess two degree of rotational freedom). A second rotor representing the BHA (drill bit and complementary components) is connected to the end of the string and hangs free. An unbalanced mass is added to study and analyse the nonlinear effects of bottom hole friction found in drilling wells. In the laboratory set-up, when the motor is actuated, the shaft rotates the rotary table. This rotation forces the lower disc also to rotate. In the presence of unbalanced mass the lower disc is forced to move in elliptical and unexpected paths of rotation at lower speeds.



Figure 1 Laboratory experimental drill string set-up and mass unbalance on lower rotor

Case 1: Ideal Zero Friction Condition

Initially the drill string system is allowed to rotate freely (0 unbalanced mass) condition. In this state the system can be compared to the state when the drill string rotates and there is no friction (ideal case) between the well bore hole and drill bit. It can be noted here that when the drill string is rotated in the ideal case with no friction at speeds of around 8 RPM, there exists some vibrations (Figure2a). These can be termed as self excited vibrations, which arise in the drilling at very low speeds. However it can be noted that when the speed is increased to around 36 RPM, the self excited vibrations disappear , and vibrations similar to limit cycling appear. At a speed of 51 RPM , the drill string now rotates smoothly with lesser limit cycling and self excited vibrations.

The average speed of the drilling is at 50 – 60 RPM. Analyzing the graphs for case 1 angular velocity data, it is also worthy to note that the drill string system lags behind the command speed required to be followed at lower speeds of 8 RPM and almost reaches up to the command speed at 51 RPM. This deficiency at low speeds can be attributed to power dissipation in the elements. It is seen that the drill string upper and lower velocities are follow the command speed more closely at higher speeds due to the fact that the power received by the system is much higher than the power dissipated in the system.

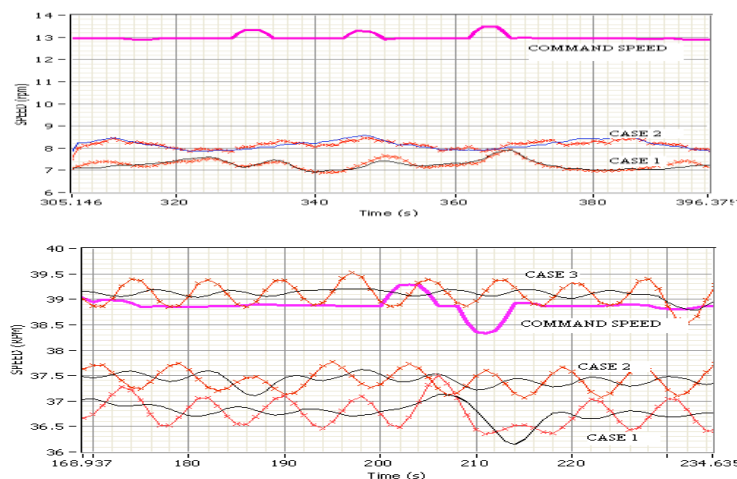
Case 2: Small Unbalanced Mass Condition Representing Low Drill Bit - Well Bore Hole Friction

Utilizing the arguments from [6] and [7], we add a mass of 28gm on the lower rotor which represents the drill bit. Note the casing around the lower rotor in Figure 1, which represents the borehole, so as to study the effects of stick slip and whirling. It is seen that the drill string upper and lower velocities follow the command speed better than in the ideal condition(Figure2). It is also noted that the self excited vibrations appear similar to case 1 when rotated at low speeds , but they are less prominent due to the higher mass of the bit. The increased mass forces the system to keep closer to the center and vibrations of the self excited type are minimized. This can also provide an explanation for the use of drill collars in the drilling rig to provide increased weight for the bit. As the speed is increased to 50 RPM , the system now rotates at a speed slightly higher than the command speed, this could be attributed to the increase in nonlinear properties of the drill string with an unbalanced mass addition.

Case 3: Large Unbalanced Mass Representing Higher Drill Bit – Well Bore Hole Friction

The unbalanced mass added to the lower rotor is further increased and now a 56 gm mass rests on the bit. The drill string follows the command speed closer at a speed of 39 RPM , but higher at speeds of 50 RPM, this may also be due to increased centripetal force and increased nonlinearity. Limit cycling vibrations are also more prominent, and a type of whirling can be noticed for the lower bit at higher speeds (Figure2). This whirling will be changed to stick slip when there is increased friction between the well bore and lower bit. It is note worthy to mention here that the unbalanced mass can only represent the effect of constant friction on the lower drill bit. It cannot represent sudden friction or jerks effected on the drill bit due to unseen hard rocks or obstacles in the path of drilling.

Displayed in the Figure 2a, 2b and 2c are the command speed applied to the system to be followed, the angular velocity data of the upper rotary and lower bit for the three cases. The angular velocities are displayed and analyzed in contrast to angular positions, because the vibration information is clearer and the behavior of the drill string at the lower bit in the x-y plane can be better analyzed in this manner.



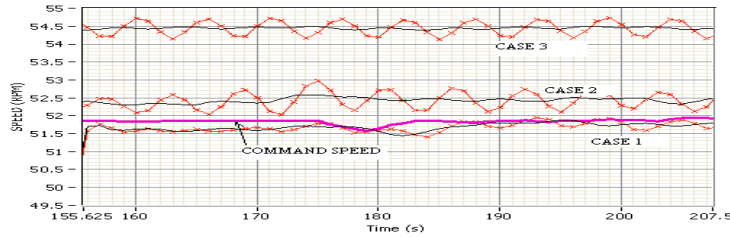


Figure 2 The command speeds and the responses of the drill string system for different unbalanced mass conditions and various speeds.

Nonlinearity analysis: Minor change in initial condition

Case 1: Minor Change In Initial Condition: Frequency

Analysis of the system behavior for a minor change in input frequency signal for ideal and unbalanced mass conditions. Figure3a displays the system response to a change in the frequency of applied input signal for the system under no mass or ideal condition. The residual signal from the system is plotted. It can be noticed that there is no major or erratic behavior displayed by the system in this case. The pattern of vibration is the same and there is only a slight change in the magnitude of the residual.

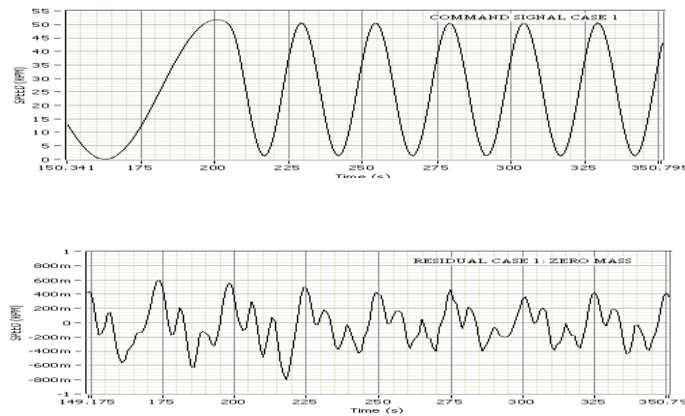


Figure 3a Command signal (upper) and residual signal (lower) for zero mass condition

Figure3b displays the command signal and the residual plots for the system when the input signal frequency is changed under unbalanced mass condition. It can be noted here, that now the pattern of the residual signal has changed with a slight change in magnitude also. This implies that the vibration pattern of the lower bit when compared to the upper rotary has changed. It is interesting to note here that the implication is the increase of nonlinear properties of the drill string in the presence of continuous friction, represented by the unbalanced mass.

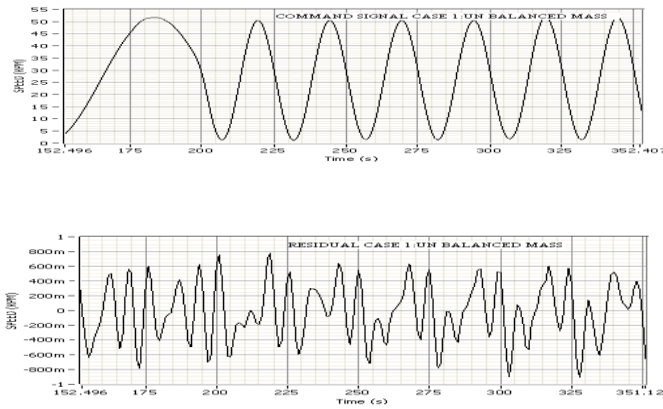


Figure 3b Command signal (upper) and residual signal (lower) for un balanced mass condition

Case 2: Minor Change In Initial Condition: Magnitude

Here, we present an analysis of the drill string system behavior under ideal and unbalanced mass conditions, when a slight change in magnitude is made to the input command signal. Figure 4a displays the response of the system to a magnitude shift of the applied input signal under no mass or ideal condition. A command speed of 50 RPM is applied to the drill string system, and shift to 52 RPM is made at a time of approximately 150s. The residual signal from the system is plotted. It can be noticed that the residual initially decreases in magnitude slightly, but returns to the original magnitude soon and there is no evident change in vibration pattern.

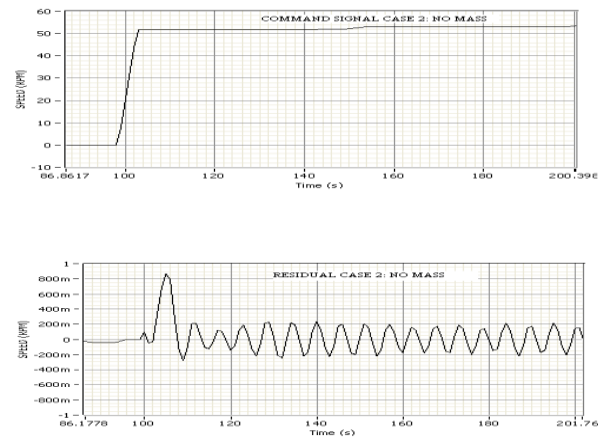


Figure 4a Command signal (upper) and residual signal (lower) for no mass condition

The command signal and the residual plots for the system when the input signal magnitude is changed slightly under un balanced mass condition is plotted in Figure 4b. The shift takes place at approximately 265 s and the magnitude of the command signal is varied from 50RPM to 52 RPM. Analyzing the residual plot, it is seen that following a delay of around 30 s to follow the command, the residual signal displays a slight decrease in magnitude and does not return to the previous magnitude or pattern of vibration. These experiments prove the increase of nonlinear

properties of the drill string in the presence of continuous friction, represented by the unbalanced mass.

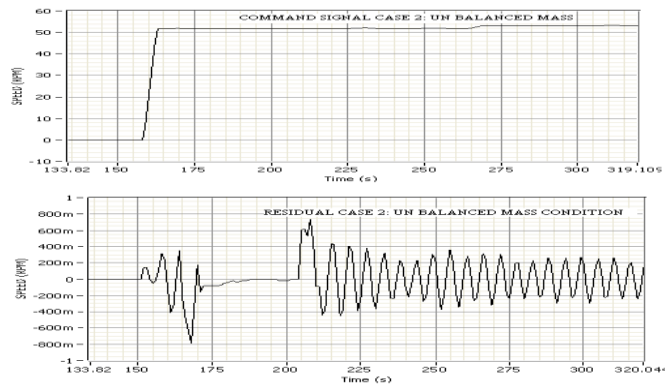


Figure 4b Command signal (upper) and residual signal (lower) for un balanced mass condition

Spectrum analysis

Spectrum analysis of the drill string system in the presence of small mass unbalance and high mass unbalance is discussed below. Referring to [9], where they have identified vibration abnormalities from spectrum analysis, we can see the same pattern in the drill string analysis. Figure5 (upper) shows the frequency response spectrum of the drill string system in the presence of a small un balanced mass on the rotor. Figure5 (lower) plots the frequency response spectrum of the drill string system for a large un balanced mass on the rotor. The ‘high peaks’ in the magnitude of the spectrum for large mass implies the presence of larger vibration in the system. The spectrum analysis of fig 4a also shows that the system initially experienced vibration , but it is trying to overcome it during the rotation. Both the spectrum are taken from readings when a sweeping sine signal is applied to the system under the respective mass unbalance conditions.

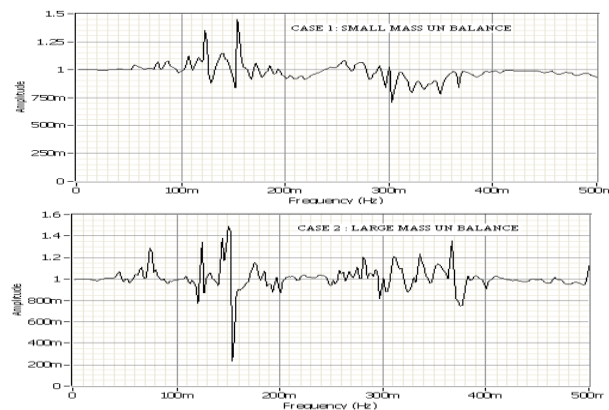


Figure 5 Drill string vibration frequency response spectrum under small mass (upper) and large mass (lower) unbalance.

Conclusion:

This paper analyses the study on the underlying causes for the non linear properties exhibited by drill string when affected by continuous friction. The study proves that the nonlinear properties exhibited by the drill strings increase with increase in the friction between the drill bit and well bore hole interactions. The nonlinearity and the increase in limit cycling tendencies are also proven. Further recommendations are for study of the dynamics under various other friction conditions affecting the drill string .

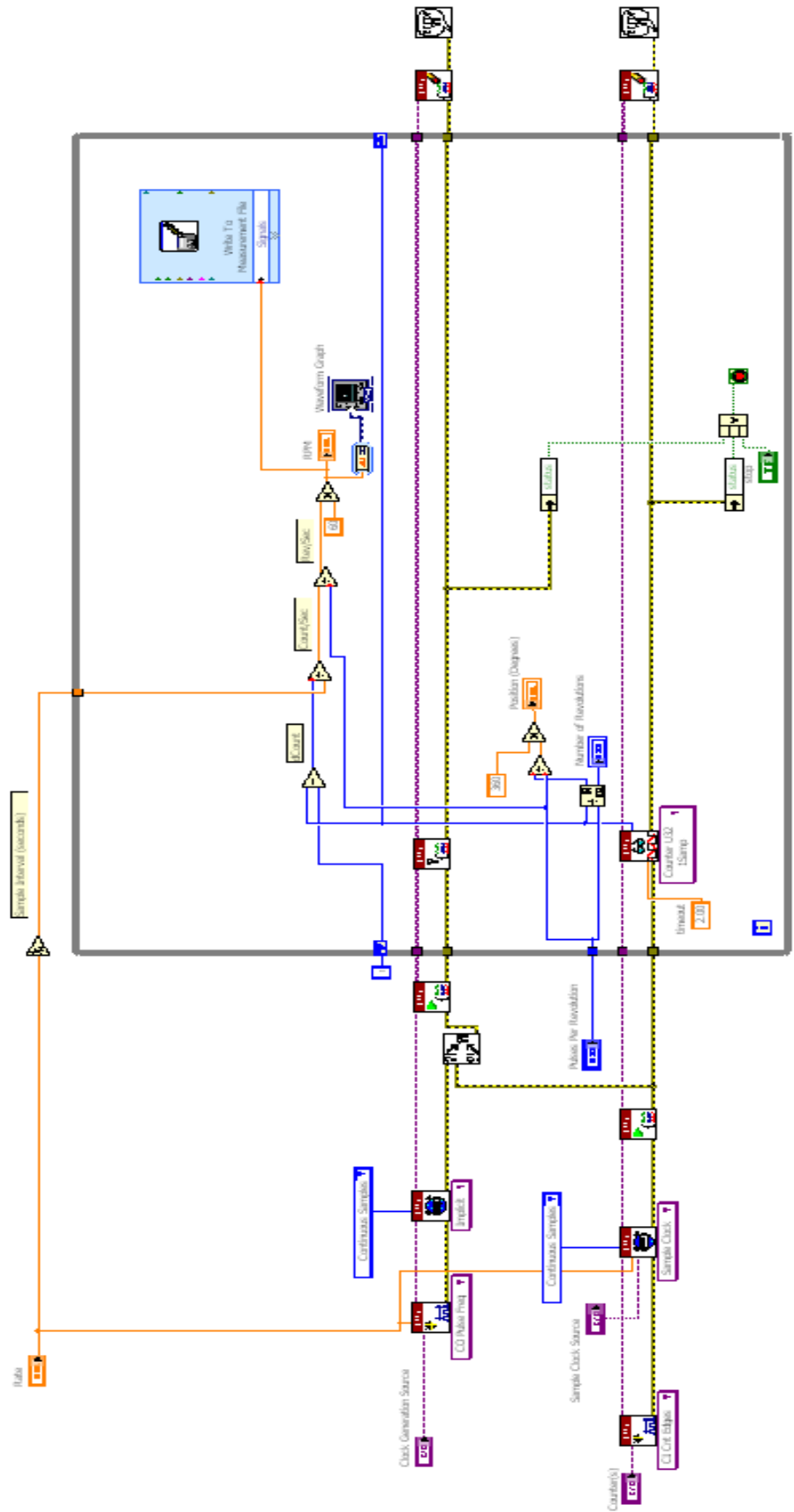
References

- [1] El sayed et al. Coupling of longitudinal and torsional vibrations of a drill string, Dev. \Theory Applied mechanics, 17.
- [2] Christoforou.A and Yigit .A.,1997 Dynamic modeling of rotating drill string with borehole inter\actions, J. sound and vibration, 206
- [3] Leine et al. Stick slip whirl interaction in drill string dynamics, ASME J. of vibration acoustics,124,2002.
- [4] N.Mihajlovioc, et al. Friction induced torsional vibrations in an experimental drill string system,23rd IASTED international conference on modeling , identification and control,pp.228-233
- [5] C.Germay, N. van de wow, H. Nijmeijer, R.Sepulchre, Nonlinear drill string dynamics analtsis,2009 SIAM J. Applied Dynamical systems, Vol .8.
- [6] H.Melakhessou et al., A nonlinear well drill string interaction model, J.Vib acoustics (125) 2003
- [7] M.W.Dykstra, H.Christensen, T.M.Warren, J.J.Azar, Drill string component mass imbalance:A majopr source of drill string vibrations.SPE Drilling and completion Dec 1996.
- [8] C.M.Liao et al., Reduced order models of drill string dynamics, Second international energy conference 2030,U.A.E,2008
- [9] S.Gopinath, Study on electric motor mass imbalance based on vibration monitoring analysis technique, International conference on electrical and mechanical technology,IEEE,2010.

Appendix 4: LabVIEW™ Virtual Instrument Block diagrams

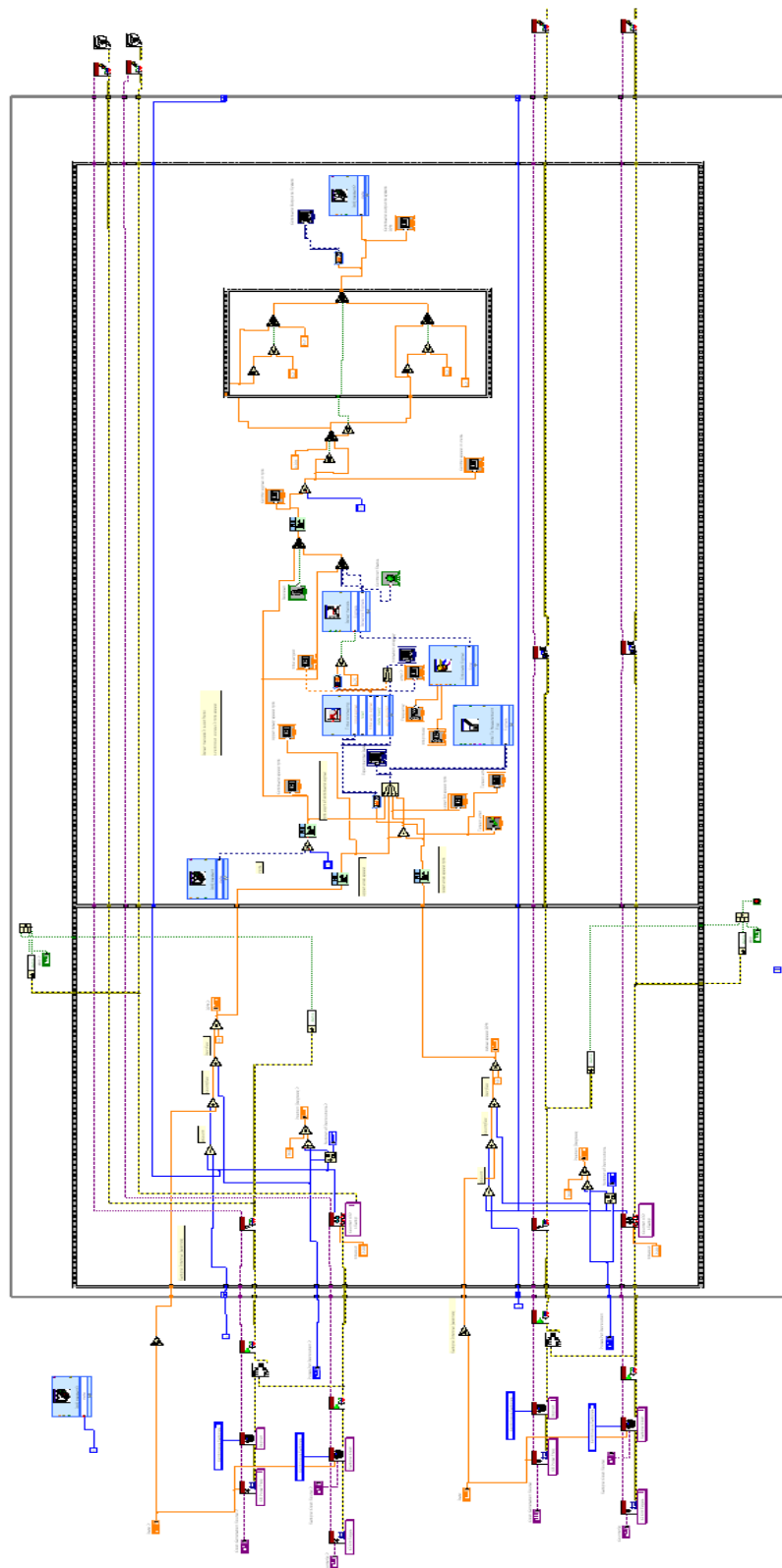
1. Data acquisition using Incremental encoder

Block diagram connection diagram section of LabVIEW™ Virtual Instrument created for facilitating online data acquisition from laboratory set-up using BNC 2120 devices and incremental encoders.



2. Closed loop vibration control using adaptive controller

Block diagram connection diagram section of LabVIEW™ Virtual Instrument created for facilitating open and closed loop control of the laboratory prototype of rotary drilling using adaptive control algorithm, vibration threshold monitor, automatic switching and online data acquisition from laboratory set-up using BNC 2120 devices and incremental encoders.



Appendix 5: The part of the MATLAB® program used for plotting the FFT spectrum.

```
fftmodelresp=fft(modelrespvector);  
length(modelrespvector);  
l=length(modelrespvector);  
ll=2^nextpow2(l);  
y=fft(modelrespvector,ll)/l;  
Fs=200;  
f = Fs/2* linspace(0,1,ll/2);  
plot(f,2*abs(y(1:ll/2)))
```

Appendix 6: 4 DOF analytical model development and Online identification method of natural frequency detection for multi DOF system by wavelet transforms

Four DOF model simulation

The four DOF model can be simulated in MATLAB[®] by rearranging the equations in matrix form.

$$M\ddot{x} + C\dot{x} + Kx = F \quad (1)$$

M, C, K are matrices functions of the state and x is the state vector.

Hence, rearranging these equations, the matrices M, C, K and F are formed.

$$M = \begin{bmatrix} m + m_b & 0 & 0 & -m_b e \sin(\beta) \\ I_1 & 2(m + m_b)\rho^2 & 2(m + m_b)\rho^2 & m_b e \rho \cos(\beta) \\ 0 & (m + m_b)\rho^2 & (m + m_b)\rho^2 & m_b e \rho \cos(\beta) \\ -m_b e \sin(\beta) & M_{42} & M_{43} & I_2 + m_b e^2 \end{bmatrix} \quad (2)$$

$$M_{42} = m_b e \rho (\cos(\beta) - \dot{\alpha} \sin(\beta))$$

$$M_{43} = m_b e \rho (\cos(\beta) - \dot{\alpha} \sin(\beta))$$

$$C = \begin{bmatrix} 0 & C_{12} & C_{13} & -m_b e \cos(\beta) \\ -m_b e \dot{\alpha} \dot{\beta} \sin(\beta) & -m_b e \dot{\alpha} \dot{\beta} \sin(\beta) & 4(m + m_b) \rho \dot{\rho} & m_b e \dot{\rho} \cos(\beta) \\ 0 & 2(m + m_b) \rho \dot{\rho} & 2(m + m_b) \rho \dot{\rho} & C_{34} \\ C_{41} & m_b e \rho \sin(\beta) (\dot{\theta} + 2\dot{\phi}) & m_b e \rho \dot{\phi} \sin(\beta) & c \end{bmatrix} \quad (3)$$

$$C_{12} = -[(m + m_b) \rho \dot{\theta} + m_b e \dot{\alpha} \cos(\beta)]$$

$$C_{13} = -[(m + m_b) \rho (2\dot{\theta} + \dot{\phi}) + m_b e \dot{\alpha} \cos(\beta)]$$

$$C_{34} = m_b e [\dot{\rho} \cos(\beta) - \rho \sin(\beta)]$$

$$C_{41} = m_b e \cos(\beta) [2(\dot{\theta} + \dot{\phi}) - \dot{\alpha}]$$

$$K = \begin{bmatrix} k_r & 0 & k_t \phi & 0 \\ 0 & 2k_{tor} & 2k_{tor} & -k_{tor} \\ k_t \rho \phi & 0 & 0 & 0 \\ 0 & -k_{tor} & -k_{tor} & k_{tor} \end{bmatrix} \quad (4)$$

$$F = \begin{bmatrix} 0 \\ \delta M_{ext} \\ 0 \\ 0 \end{bmatrix} \quad (5)$$

And state variables $x = \begin{bmatrix} \rho \\ \theta \\ \phi \\ \alpha \end{bmatrix}$ (6)

The equations developed in this section are in the matrix format. This can now be simulated to obtain the 4 DOF analytical model responses. Useful references for multi DOF systems simulation using MATLAB® are T. L. Heine (1994), M. R. Hatch (2001) and H. B. Petterson (2002).

Online identification method of natural frequency detection

This section discusses a method of online identification of the natural frequencies of a multi DOF system [B.Basu et al. (2008)] after writing it in the matrix format (refer chapter 10).

A linear MDOF system with m degrees of freedom represented by

$$[M]\{\ddot{X}\} + [C(t)]\{\dot{X}\} + [K(t)]\{X\} = \{R\}f(t)$$

is considered where, [M], [C(t)], and [K(t)] are the mass, time varying damping, and time varying stiffness matrices, respectively; {R} is the influence vector for forces at different degrees of freedom and f(t) is a forcing function. The displacement response vector is denoted by {X(t)}.

If the elements $K_{lj}(t); l, j = 1, \dots, m$ in the stiffness matrix have discontinuities at a finite number of points, then it is possible to divide

the time in several segments with indices arranged as to $t_0 < t_1 < \dots < t_n$ such that all

$K_{lj}(t); l, j = 1, \dots, m$ are continuous function in $[t_{i-1}, t_i]$. Further, it is assumed that the variations of all $K_{lj}(t)$ are slower than the fundamental (lowest) frequency of the system (corresponding to the longest period). It subsequently follows that assuming a variation of $\{X(t)\}$ with slowly varying amplitude $\{\phi(t)\}_i^k$ and slowly varying frequency $\omega_{ki}(t)$ at the k^{th} mode, in the time interval $[t_{i-1}, t_i]$ the displacement vector and its derivatives can be represented by

$$\{X(t)\} = \{\phi(t)\}_i^k e^{i\omega_{ki}(t)t}$$

$$\{\dot{X}(t)\} \approx i\omega_{ki}(t)\{\phi(t)\}_i^k e^{i\omega_{ki}(t)t}$$

$$\{\ddot{X}(t)\} \approx -\omega_{ki}^2(t)\{\phi(t)\}_i^k e^{i\omega_{ki}(t)t}$$

Substitution of Equations (11a)–(11c) in the homogeneous free vibration equation corresponding to Equation (1) leads to the time-varying eigen value problem with eigen values $\omega_{ki}^2(t)$ and eigen vectors $\{\phi(t)\}_i^k; k = 1, 2, \dots, m$. If the system in Equation (1) is assumed to be lightly damped, then using wavelet transformations, the natural frequency corresponding to the k^{th} mode in the j_k^{th} band can be obtained as

$$\omega_{0_{jk}} = \frac{\sigma + 1}{2} \cdot \frac{\pi}{a_{jk}}$$

Where a_{jk} is the discrete parameter used for wavelet transform and $a_j = \sigma^j$ where σ is a scalar.

